



**Politecnico  
di Torino**

Department of Electronics and Telecommunications

Master degree in Electronic Engineering

Master Thesis

# Clocking strategy of Reconfigurable Field-Coupled Nanocomputing circuits

**Supervisors:**

Prof. Gianluca Piccinini

Prof. Mariagrazia Graziano

**Candidate:**

Sara Puglia

October 2021

*A chi c'è sempre stato.  
Grazie, Vostra S.*

# Acknowledgments

Arrivata a conclusione di questo percorso, mi trovo qui, davanti questo foglio bianco, a tirare un pò le somme di questi anni. Anni impegnativi, fatti di sudore, sacrifici, di notti insonni e momenti no. Ma sono stati soprattutto anni di crescita, spinti dalla passione e dalla curiosità, fatti di amici, di risate, divertimento e di tanto amore. Perciò mi sembra doveroso fare un pò di ringraziamenti.

Primi tra tutti ringrazio i professori Gianluca Piccinini e Mariagrazia Graziano, per la fiducia datami, per avermi permesso di entrare in questo progetto e avermi supportato durante lo sviluppo dello stesso.

Grazie a Yuri e Giuliana per essere stati disponibili quotidianamente in questi mesi, in alcuni casi anche durante il fine settimana. Grazie per tutti i consigli fondamentali, senza di voi questo lavoro non sarebbe stato possibile.

E poi ringrazio tutti quelli che ci sono stati, con un abbraccio, un sorriso, una chiamata, un messaggio. Voi che avete affrontato con me questi anni, che mi avete supportato e sopportato. Voi che forse, a volte, ci avete creduto più di me.

Ai miei genitori e i miei fratelli, che siete i miei sostenitori da sempre, mi avete sempre spronato a spingermi sempre oltre, a cercare qualcosa di più e a non fermarmi davanti agli ostacoli.

Ad Ale, nell' ultimo anno sei stato quel vento di aria fresca, pura e piena di amore e dolcezza che mi serviva.

Alla mia Family, che siete così distanti ma sempre così vicini.

Alla mia seconda Family, i miei amici Ligorio, Giorgia A, MQ, Fra, Ila, Sissy, Manu, Rosa, Giorgia P, Desi, Simo, Luana, Gianbo e Nico per esserci sempre.

E poi grazie a te, che forse potrei non aver nominato, ma se stai leggendo ora, allora sei qui con me a condividere la mia felicità per questo percorso ultimato e l'inizio di una nuova avventura che chissà dove mi porterà. Grazie.

*"Possa il vostro cammino essere tortuoso,  
ventoso, solitario, pericoloso e portarvi al  
panorama più spettacolare. Possano le vostre  
montagne elevarsi fino alle nuvole e superarle "*

Edward Abbey.

# Abstract

From 1965, the trends of innovations in electronic applications follow Moore's law, which specified that the number of transistors on a microchip doubles every two years, allowing faster and efficient computational progress, decreasing costs and increasing performance. Nowadays, due to the physical limits of semiconductor-based technology, the increase of miniaturization is approaching saturation. For this reason, alternative technologies became necessary. One of these is "Beyond-CMOS", where the most promising technology is Field-Coupled Nanocomputing (FCN). It is based on the propagation of information on a device using field's interactions. There is no current transport, enabling higher miniaturization and low power dissipation.

In particular, Molecular FCN is the basis of our study. A computing paradigm that implements QuantumDot Cellular Automata (QCA), using bisferrocene molecules, where the electrostatic interaction among molecules allows the information to propagate. The idea of this project is the Reconfigurable FCN, a self-assembled monolayer (SAM), based on a gold substrate above which molecules are located. Vertical electrical fields are generated on molecule cells, inducing them to assume specific logic conditions and propagate the information in the structure by turning on and off electrodes in adjacent areas.

The structural problem of this configuration is the presence of a high number of nanometric and independent electrodes that have to be managed, generating a complex physical realization and clock configuration.

In this study, the aim is the improving of ease manufacturing of RFCN using the interference of light. With the patterns generated by the interference of light coming from a source that hit a screen with slits, it is possible to induce molecules to assume the wanted logic state. An interference model that can properly work on the RFCN is defined, creating patterns that hit the layer, permitting the achievement of correct logic gates as NAND, majority voters, inverters, half adder and full adder. The obtained patterns of interference are used as input to simulate the molecular structure using the Self Consistent Electrostatic Potential Algorithm (SCERPA), a tool that analyses iteratively the molecule interactions. Physical and electrical characteristics are evaluated to define costs in and physical realization: this approach brings a reduction of the operation area and a simplification of the clock configuration with respect to the standard RFCN.

# List of Figures

1.1	Metallic FCN cell . . . . .	14
1.2	1 and 0 configurations of Magnetic FCN cell . . . . .	15
1.3	Molecular FCN logic states . . . . .	16
1.4	Wire propagation . . . . .	16
1.5	FCN majority voter . . . . .	16
1.6	FCN Inverter . . . . .	17
1.7	Electric field generated by the MUT . . . . .	18
1.8	$V_{in}$ and $V_{out}$ between dots . . . . .	18
1.9	Bis-ferrocene molecule [14] . . . . .	19
1.10	Four phase Clock signal waveform . . . . .	20
1.11	Overlapping of clock signals to ensure correct propagation . . . . .	21
1.12	Example of time steps in a wire. . . . .	21
1.13	Physical Implementation of Sinusoidal clock [18] . . . . .	22
1.14	Sinusoidal propagation on a wire [18] . . . . .	22
1.15	Molecular wire implementation with substrate of gold over which the molecules are deposited. . . . .	23
1.16	Clock field obtained by the potential difference between the top electrodes and the gold nanowire at the bottom of the trench . . . . .	23
1.17	Layout of clock implementation on FCN molecular wire . . . . .	24
2.1	Implementation of a logic operation with classical Clock-FCN (a) and RFCN (b) [22]	25
2.2	Representation of hold and reset states [22] . . . . .	26
2.3	Wire RFCN [22] . . . . .	26
2.4	Inverter RFCN propagation steps [22] . . . . .	26
2.5	Majority Voter RFCN propagation steps [22] . . . . .	27
2.6	Containers that are enabled during the logic operation [22] . . . . .	27
2.7	NAND gate in RFCN [22] . . . . .	27
2.8	Time diagram of the micro-clock evolution for inverter operation [22] . . . . .	28
2.9	Sequencer containing the micro-clock information for a standard cell [22] . . . . .	29
2.10	System Clock used to synchronise the operations of all the standard cells [22] . . . . .	29
2.11	NAND gates repetition in the wanted area [22] . . . . .	30
2.12	Space multiplexing requires the enlarging of the area around the NAND [22] . . . . .	31

2.13	Time multiplexing evolution [22] . . . . .	31
2.14	A series of containers that share the same field works together as a single big container [22] . . . . .	32
2.15	Difference of electrode size in case of small containers and a molecular block [22] . . . . .	32
2.16	Shared electrodes model [22] . . . . .	33
2.17	Molecular structure with charge distribution [22] . . . . .	34
2.18	Trans-characteristic variation with clock and molecular distance [22] . . . . .	34
2.19	NAND steps (a) [22] . . . . .	35
2.20	NAND steps (b) [22] . . . . .	36
2.21	NAND steps (c) [22] . . . . .	36
2.22	NAND steps (d) [22] . . . . .	36
2.23	NAND steps (e) [22] . . . . .	37
2.24	NAND steps (f) [22] . . . . .	37
2.25	NAND Area variation depending on block size [22] . . . . .	39
2.26	NAND gate in RFCN and FinFET layout [22] . . . . .	39
2.27	Pin density variation respect block size [22] . . . . .	40
2.28	$P_{NAND}$ variation with respect to Electric field and block size [22] . . . . .	43
3.1	Spectrum of light radiation . . . . .	44
3.2	Boundary condition for normal vector of $\mathbf{B}$ and $\mathbf{D}$ . . . . .	46
3.3	Boundary conditions for tangential vectors of $\mathbf{E}$ and $\mathbf{H}$ . . . . .	47
3.4	Refraction of incident plane wave . . . . .	51
3.5	Wave-fronts representation . . . . .	52
3.6	Two-slit interference . . . . .	53
3.7	$r_1$ and $r_2$ in far-field condition . . . . .	53
3.8	Intensity shape in case of $d \ll \lambda$ and $d \gg \lambda$ . . . . .	55
3.9	Fringes representation on a screen . . . . .	55
3.10	Schematic representation of N-slits configuration . . . . .	56
3.11	Intensity plot in case of N=4 slits . . . . .	57
4.1	Horizontal fringes obtained by 3 slits . . . . .	59
4.2	Vertical fringes obtained by 3 slits . . . . .	60
4.3	Combination of vertical and horizontal fringes obtained by 6 slits . . . . .	60
4.4	Pointing fringes obtained by 9 slits . . . . .	60
4.5	Pointing fringes obtained by 4 slits . . . . .	61
4.6	Schematic representation of the structure: the source, the perforated screen (3 slits) and the generated secondary sources that hit the SAM . . . . .	62
4.7	SAM representation with gold electrode and dielectric substrate $SiO_2$ . . . . .	63
4.8	Buried gold layer in $SiO_2$ dielectric . . . . .	63
4.9	Vertical and Horizontal fringes on SAM . . . . .	64
4.10	Useless molecules in chosen fringes configuration . . . . .	64

---

4.11	Electro beam lithography and plasma ashing processes . . . . .	65
4.12	SAM representation . . . . .	65
4.13	Complete layout of the structure . . . . .	66
4.14	The electrodes on the corner of an intersection work together to maintain the information . . . . .	66
5.1	Molecular distance settled on SCERPA . . . . .	67
5.2	Drivers values over time for NAND simulation . . . . .	68
5.3	Molecular structure description with SCERPA . . . . .	68
5.4	Plot of the Molecular description realized with SCERPA . . . . .	68
5.5	Code of clock evolution . . . . .	69
5.6	Majority voter FCN . . . . .	69
5.7	True table of Majority voter: by fixing $A=0$ or $A=1$ , it is possible obtain the AND or OR logic operations . . . . .	70
5.8	AND and OR implementation with Majority Voter . . . . .	70
5.9	Majority voter in initial reset state . . . . .	70
5.10	Majority voter simulation step 1: Grid fringes . . . . .	71
5.11	Majority voter simulation step 2: Electrodes activations . . . . .	71
5.12	Inverter FCN . . . . .	71
5.13	Inverter simulation in initial reset state . . . . .	72
5.14	Inverter simulation step 1: Horizontal fringes . . . . .	72
5.15	Inverter simulation step 2: Electrodes activation . . . . .	73
5.16	Inverter simulation step 3: Vertical fringes . . . . .	73
5.17	Inverter simulation step 4: Electrodes activation . . . . .	74
5.18	Inverter simulation step 5: Horizontal fringes . . . . .	74
5.19	Inverter simulation step 6: Electrodes activation . . . . .	75
5.20	Inverter simulation step 7: Grid fringes and Electrode . . . . .	75
5.21	Initial reset state . . . . .	76
5.22	Simulation step 1: Horizontal fringes . . . . .	76
5.23	Simulation step 2: Electrodes activation . . . . .	77
5.24	Simulation step 3: Vertical fringes . . . . .	77
5.25	Simulation step 4: Electrodes activation . . . . .	78
5.26	Simulation step 5: Grid fringes and Electrode . . . . .	78
5.27	NAND logic gate and True table . . . . .	79
5.28	NAND in initial reset state . . . . .	79
5.29	NAND simulation step 1: Vertical fringes . . . . .	80
5.30	NAND simulation step 2: Electrodes activation . . . . .	80
5.31	NAND simulation step 3: Grid fringes . . . . .	81
5.32	NAND simulation step 4: Electrodes activation . . . . .	81
5.33	NAND simulation step 5: Vertical fringes . . . . .	82
5.34	NAND simulation step 6: Electrodes activation . . . . .	82

---

5.35	NAND simulation step 7: Grid fringes and Electrode . . . . .	83
5.36	Half Adder logic gate and True table . . . . .	83
5.37	HALF ADDER in initial reset state . . . . .	84
5.38	HALF ADDER simulation step 1 . . . . .	84
5.39	HALF ADDER simulation step 2 . . . . .	85
5.40	HALF ADDER simulation step 3 . . . . .	85
5.41	HALF ADDER simulation step 4 . . . . .	86
5.42	HALF ADDER simulation step 5 . . . . .	86
5.43	HALF ADDER simulation step 6 . . . . .	87
5.44	HALF ADDER simulation step 7 . . . . .	87
5.45	HALF ADDER simulation step 8 . . . . .	88
5.46	HALF ADDER simulation step 9 . . . . .	88
5.47	HALF ADDER simulation step 10 . . . . .	89
5.48	HALF ADDER simulation step 11 . . . . .	89
5.49	HALF ADDER simulation step 12 . . . . .	90
5.50	HALF ADDER simulation step 13 . . . . .	90
5.51	HALF ADDER simulation step 14 . . . . .	91
5.52	HALF ADDER simulation step 15 . . . . .	91
5.53	HALF ADDER simulation step 16 . . . . .	92
5.54	HALF ADDER simulation step 17 . . . . .	92
5.55	HALF ADDER simulation step 18 . . . . .	93
5.56	HALF ADDER simulation step 19 . . . . .	93
5.57	HALF ADDER simulation step 20 . . . . .	94
5.58	HALF ADDER simulation step 21 . . . . .	94
5.59	HALF ADDER simulation step 22 . . . . .	95
5.60	HALF ADDER simulation step 23 . . . . .	95
5.61	HALF ADDER simulation step 24 . . . . .	96
5.62	HALF ADDER simulation step 25 . . . . .	96
5.63	HALF ADDER simulation step 26 . . . . .	97
5.64	Full Adder logic gate and True table . . . . .	97
5.65	FULL ADDER in initial reset state . . . . .	98
5.66	FULL ADDER simulation step 1 . . . . .	98
5.67	FULL ADDER simulation step 2 . . . . .	99
5.68	FULL ADDER simulation step 3 . . . . .	99
5.69	FULL ADDER simulation step 4 . . . . .	100
5.70	FULL ADDER simulation step 5 . . . . .	100
5.71	FULL ADDER simulation step 6 . . . . .	101
5.72	FULL ADDER simulation step 7 . . . . .	101
5.73	FULL ADDER simulation step 8 . . . . .	102
5.74	FULL ADDER simulation step 9 . . . . .	102

---

5.75 FULL ADDER simulation step 10	103
5.76 FULL ADDER simulation step 11	103
5.77 FULL ADDER simulation step 12	104
5.78 FULL ADDER simulation step 13	104
5.79 FULL ADDER simulation step 14	105
5.80 FULL ADDER simulation step 15	105
5.81 FULL ADDER simulation step 16	106
5.82 FULL ADDER simulation step 17	106
5.83 FULL ADDER simulation step 18	107
5.84 FULL ADDER simulation step 19	107
5.85 FULL ADDER simulation step 20	108
5.86 FULL ADDER simulation step 21	108
5.87 FULL ADDER simulation step 22	109
5.88 FULL ADDER simulation step 23	109
5.89 FULL ADDER simulation step 24	110
5.90 FULL ADDER simulation step 25	110
5.91 FULL ADDER simulation step 26	111
5.92 FULL ADDER simulation step 27	111
5.93 FULL ADDER simulation step 28	112
5.94 FULL ADDER simulation step 29	112
5.95 FULL ADDER simulation step 30	113
5.96 FULL ADDER simulation step 31	113
5.97 FULL ADDER simulation step 32	114
5.98 FULL ADDER simulation step 33	114
5.99 FULL ADDER simulation step 34	115
5.100 FULL ADDER simulation step 35	115
5.101 FULL ADDER simulation step 36	116
5.102 FULL ADDER simulation step 37	116
5.103 FULL ADDER simulation step 38	117
5.104 FULL ADDER simulation step 39	117
5.105 FULL ADDER simulation step 40	118
5.106 FULL ADDER simulation step 41	118
5.107 FULL ADDER simulation step 42	119
5.108 FULL ADDER simulation step 43	119
5.109 FULL ADDER simulation step 44	120
5.110 FULL ADDER simulation step 45	120
5.111 FULL ADDER simulation step 46	121
5.112 FULL ADDER simulation step 47	121
5.113 FULL ADDER simulation step 48	122
5.114 FULL ADDER simulation step 49	122

---

5.115FULL ADDER simulation step 50 . . . . .	123
5.116FULL ADDER simulation step 51 . . . . .	123
5.117FULL ADDER simulation step 52 . . . . .	124
5.118FULL ADDER simulation step 53 . . . . .	124
5.119FULL ADDER simulation step 54 . . . . .	125
5.120FULL ADDER simulation step 55 . . . . .	125
5.121FULL ADDER simulation step 56 . . . . .	126
5.122FULL ADDER simulation step 57 . . . . .	126
5.123FULL ADDER simulation step 58 . . . . .	127
5.124FULL ADDER simulation step 59 . . . . .	127
5.125FULL ADDER simulation step 60 . . . . .	128
5.126FULL ADDER simulation step 61 . . . . .	128
5.127FULL ADDER simulation step 62 . . . . .	129
5.128FULL ADDER simulation step 63 . . . . .	129
5.129FULL ADDER simulation step 64 . . . . .	130
5.130FULL ADDER simulation step 65 . . . . .	130
5.131FULL ADDER simulation step 66 . . . . .	131
5.132FULL ADDER simulation step 67 . . . . .	131
5.133FULL ADDER simulation step 68 . . . . .	132
5.134FULL ADDER simulation step 69 . . . . .	132
5.135FULL ADDER simulation step 70 . . . . .	133
5.136FULL ADDER simulation step 71 . . . . .	133
5.137FULL ADDER simulation step 72 . . . . .	134
5.138FULL ADDER simulation step 73 . . . . .	134
5.139FULL ADDER simulation step 74 . . . . .	135
5.140FULL ADDER simulation step 75 . . . . .	135
5.141FULL ADDER simulation step 76 . . . . .	136
5.142FULL ADDER simulation step 77 . . . . .	136
5.143NAND RFCN: 6 standard cells, each made by 9 blocks . . . . .	137
5.144NAND layout in reset state. In evidence the block's dimension . . . . .	138
5.145Majority Voter standard RFCN propagation steps [20] . . . . .	138
5.146Majority Voter with interference propagation steps . . . . .	139

# List of Tables

2.1	Z-matrix of Bis-ferrocene [22] . . . . .	33
2.2	Gain voltage variation depending on clock and molecular distance [22] . . . . .	34
4.1	Field values of horizontal fringes on a screen . . . . .	61
4.2	Field values of vertical fringes on a screen . . . . .	62
4.3	Field values of fringes grid on a screen combination of vertical and horizontal fringes) . . . . .	62

# Acronyms

**FCN** Field-Coupled Nano-computing

**QCA** Quantum-dot Cellular Automata

**SOI** Silicon on insulator

**MoSQuiTo** Molecular Simulator Quantum-dot cellular automata Torino

**AC** Aggregated Charge

**EFGR** Electric Field Generated at the Receiver molecule

**MUT** Molecule Under Test

Vin-Vout transcharacteristic

**VACT** Vin-AC transcharacteristic

**VOM** Vout Map

**MQCA** Molecular Quantum-dot Cellular Automata

**CWZ** Cell Working Zone

**SCERPA** Self-Consistent Electrostatic Potential Algorithm

**RFCN** Reconfigurable Field-Coupled Nano-computing

**SAM** Self-Assembled Monolayer

# Contents

<b>1</b>	<b>Field-Coupled Nanocomputing</b>	<b>14</b>
1.1	Molecular FCN . . . . .	15
1.2	Molecule Modelling . . . . .	17
1.3	Bis-ferrocene Molecule . . . . .	19
1.4	The clock System . . . . .	19
1.4.1	Four-Phase Clock . . . . .	20
1.4.2	Sinusoidal Clock . . . . .	21
1.5	Molecular FCN technology layout . . . . .	22
<b>2</b>	<b>Reconfigurable FCN</b>	<b>25</b>
2.1	Logic Operations . . . . .	26
2.2	Clock . . . . .	28
2.3	Design . . . . .	30
2.4	Technology . . . . .	31
2.5	Simulations . . . . .	33
2.5.1	Simulation flow . . . . .	33
2.5.2	Simulation structure . . . . .	34
2.6	Figure of merit . . . . .	37
2.6.1	Area . . . . .	37
2.6.2	Interconnection Density . . . . .	39
2.6.3	Power . . . . .	40
<b>3</b>	<b>Light's interference</b>	<b>44</b>
3.1	Introduction on Electromagnetic Field . . . . .	44
3.1.1	Boundary conditions . . . . .	45
3.1.2	Energy of electromagnetic field . . . . .	48
3.1.3	Propagation velocity . . . . .	50
3.2	Interference . . . . .	52
3.2.1	Two-slit Interference . . . . .	52
3.2.2	N-slit Interference . . . . .	56

---

<b>4</b>	<b>Study of Interference on RFCN</b>	<b>58</b>
4.1	Definition of Interference's patterns . . . . .	58
4.2	Layout . . . . .	62
4.2.1	Buried gold layer . . . . .	63
4.2.2	Grid shape of SAM . . . . .	63
4.2.3	Electrodes . . . . .	65
<b>5</b>	<b>Logic operations simulation</b>	<b>67</b>
5.1	Simulation Structure . . . . .	67
5.2	Majority Voter . . . . .	69
5.3	Inverter . . . . .	71
5.4	NAND . . . . .	78
5.5	Half Adder . . . . .	83
5.6	Full Adder . . . . .	97
5.7	Summary . . . . .	136
5.7.1	Area . . . . .	137
5.7.2	Clock . . . . .	138
<b>6</b>	<b>Conclusions</b>	<b>140</b>

# Chapter 1

## Field-Coupled Nanocomputing

Field-coupled nanocomputing (FCN) paradigms propose new approaches to allow digital information processing without using transistors or requiring the transport of charge. Instead, they are based on local fields interactions to obtain the wanted computation, reducing the power consumption. This group of devices includes Quantum-dot Cellular Automata logic that can be implemented using nanomagnets, metallic junctions, semiconductors or molecules [1]. In this thesis, the Molecular QCA will be analyzed, which seems the most promising for the future, due to the possibility to work at room temperature [2], very high-density circuits, low power consumption of the switching mechanism [3] and work at frequencies of about 1 THz. Before this, we briefly analyze the other possible implementation of QCA.

- **Metallic FCN**

The Metallic FCN was the first type of fabrication implemented. The fundamental cell is obtained by merging islands and metallic wires to create a tunnel junction that connects the islands.[4] The problem with this technique is the dimension of the islands that can not scale at nanometers. At the same time, what is interesting is that the electron population inside them have analogue behaviour of quantum dot.

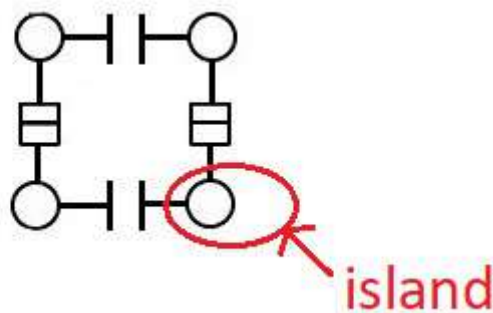


Figure 1.1: Metallic FCN cell

- **Semiconductor FCN**

With semiconductor QCA, advanced CMOS fabrication processes are used to create the dots that contain a mobile charge. The advantage is the well-exploited material. Several fabrication techniques have been exploited to work with semiconductor materials. In this way, using different approaches, it is possible to demonstrate the workability of the Semiconductor QCA structure, as SOI, GaAs, GaAs/AlGaAs technology [5]. Unfortunately, there are issues from a technological point of view that limit the correct functioning with nano-size dimensions.

- **Magnetic FCN**

The Magnetic FCN technology is the most used today. It is based on a nanomagnet standard cell that can assume two logic configurations, depending on the electric field applied. The external field induces the grains of a basic cell to follow the imposed orientation, aligning along the same direction [6].

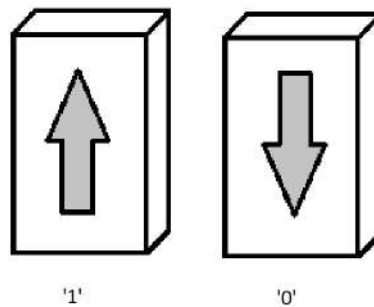


Figure 1.2: 1 and 0 configurations of Magnetic FCN cell

The advantages of using magnets as cells are the low power consumption, high thermal robustness, the possibility of 3D architecture and the memory ability since they maintain at the equilibrium the information until a strong perturbation appears. Moreover, they are feasible and can be integrated using standard technology [4].

## 1.1 Molecular FCN

In the Molecular FCN technology, the molecule works as a container where the information is encoded in the charge distribution in the dots: depending on which of the dot is "filled" by charge and which is "empty", different configurations are obtained.

A molecular cell is realized considering two near molecules, placed as inside a square, to obtain three possible configurations: two associated to logic state 0 and 1 (HOLD), and one associated to the NULL (RESET) state, which enables better control of the cell when there is no logic state assumption [1]. In 0 and 1, charges arrange on a diagonal due to Coulomb repulsion and only two dots have to be occupied, obtaining an equilibrium state for the information.

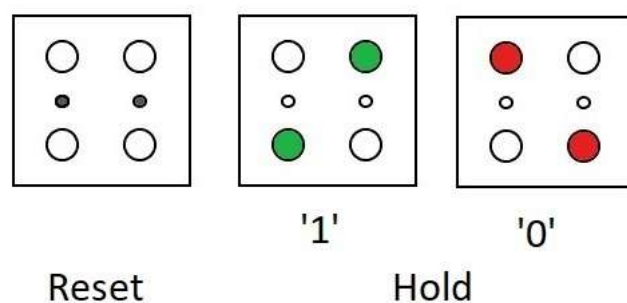


Figure 1.3: Molecular FCN logic states

Considering have containers placed one near to the other at a correct distance, which depends on the technology, they experienced an interaction: a driver cell in one of the possible logic states, with a fixed electrostatic field, will couple with the nearest container field, inducing it to assume the same configuration, to have the lowest possible energy. In this way, the information propagates without charge transfer allowing the realization of many devices, starting from simplest [7] (wires, inverters, AND and OR operations) to reach more complex structures (Half Adder and Full Adder) [8]. The energy needed for the switching of a cell is on the order of  $10 - 20 J$  [9], that compared to a transistor, in which the minimum energy required is  $10^{18} J$  [10] there are two orders of magnitude of difference.

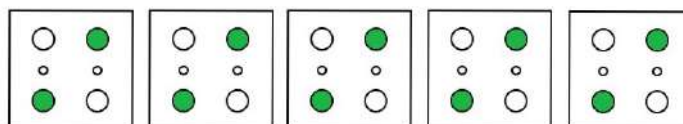


Figure 1.4: Wire propagation

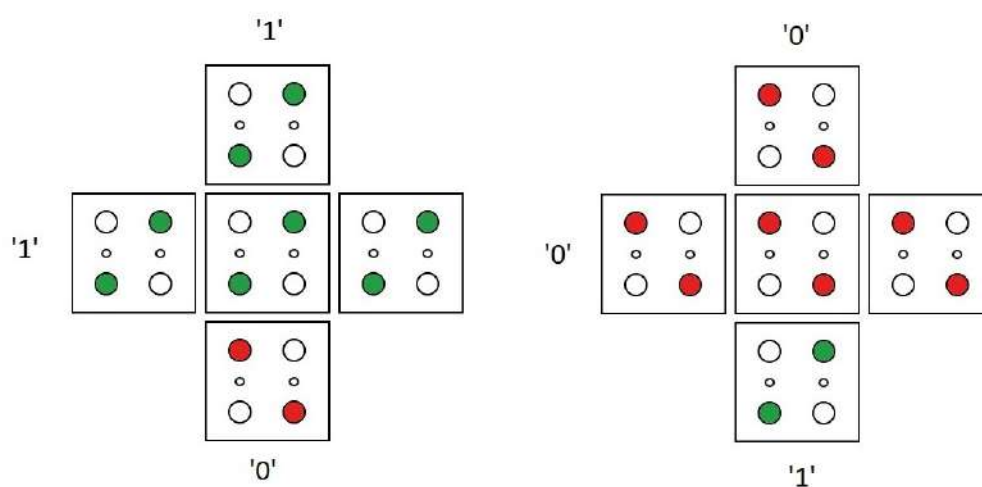


Figure 1.5: FCN majority voter

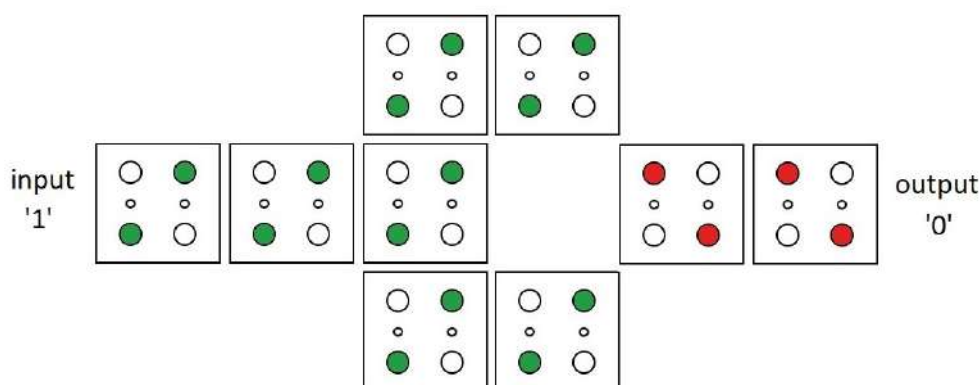


Figure 1.6: FCN Inverter

## 1.2 Molecule Modelling

To realize a Molecular FCN that works properly, the analysis of the molecules is a fundamental step. One approach used is the ab-initio calculation, which allows understanding the physical-chemical behaviour of the molecules. However, the computation is expensive in terms of memory and the obtained results are difficult to be implemented at the device level. For these reasons, the MoSQuiTo (Molecular Simulator Quantum-dot cellular automata Torino) has been developed [11]. It is based on three stages:

- **FIRST STAGE**

Analysis of the molecule with ab-initio simulations. The molecule is described through Z-matrix and the biasing conditions are setted: driver's electric field, the clock signal, presence of other molecules evaluation.

- **SECOND STAGE**

Post-processing and generation of new figures of merit for the device:

- Aggregated charge (AC)

It is preferred to have the information of charges summed in a dot, centred in the point of interest.

- Electric-field generated at the receiver molecule (EFGR)

Each molecule generates an electric field in the space, that can influence a molecule placed at a distance  $d=w$  from the Molecule under test (MUT).

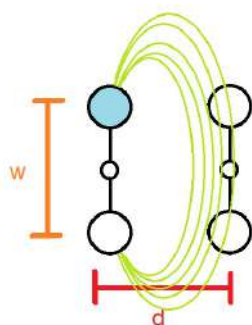


Figure 1.7: Electric field generated by the MUT

$w$  is the distance between two dots.

- Vin-Vout transcharacteristic (VVT)

The field generated by a molecule can be associated with the equivalent voltage, which is the integral of the electric field in a specific path:  $V_{in}$  is between two dots of the MUT, while  $V_{out}$  is the voltage between two dots of the molecule at distance  $d$ .

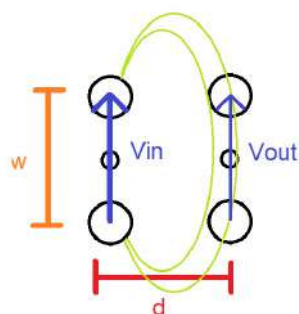


Figure 1.8:  $V_{in}$  and  $V_{out}$  between dots

- Vin-AC transcharacteristic (VACT)

Using the aggregated charge of the MUT instead of the output voltage, and relate it to the input voltage.

- Vout map (VOM)

Input voltage of a molecule placed around the MUT.

- MQCA cell working zone (CWZ)

Definition of the region in which the molecule works correctly.

- **THIRD STAGE**

Circuit simulation, through the implementation of an algorithm, for the evaluation of the technological aspects and the interactions among elements. This algorithm is called Self-Consistent Electrostatic Potential Algorithm (SCERPA) [12]. It consists of an initialization step, in which are defined the information on molecule positions and initial conditions for the charges, drivers and clock. The second step consists of a self-consistent loop: the behaviour of

the molecule is calculated in each step. In the end, there is the evaluation of the final charge distribution.

### 1.3 Bis-ferrocene Molecule

To realize a Molecular FCN that works properly, the correct molecule needs to be implemented. The bis-ferrocene is a molecule synthesized ad hoc for QCA computation purposes [13]. It is formed by two ferrocene units, functioning as redox centres, and a carbazole, the third dot used for the reset state and to connect the two ferrocenes [14]. Moreover, to anchor the molecule on a gold substrate, there is an alkyl chain.

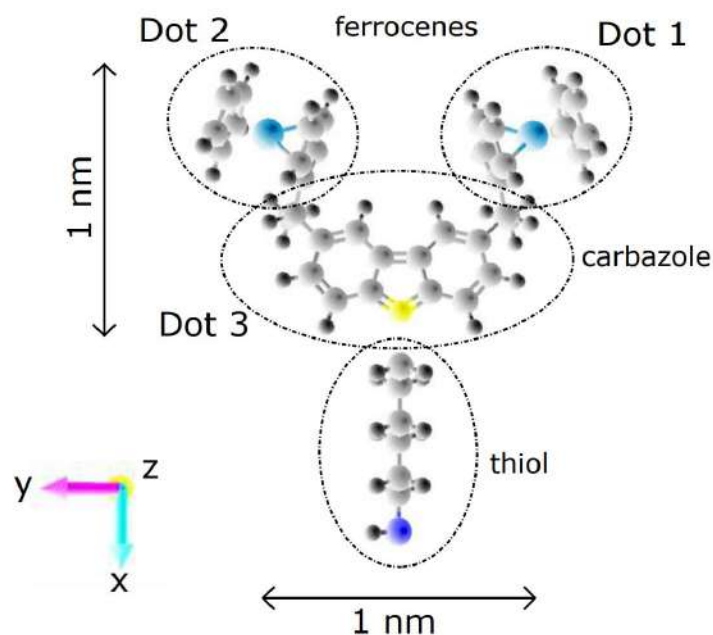


Figure 1.9: Bis-ferrocene molecule [14]

Two bis-ferrocene molecules positioned at a distance of 1 nm make a molecular cell. In this molecule, when a positive electric field is applied, the charge moves in the dots to obtain the hold state; on the contrary, the negative clock field forces induce charge into the reset state [15]. The inhibition of the molecule (RESET) is obtained with an electric field of  $-2 \text{ V/nm}$ , while the molecule is activated at  $+2 \text{ V/nm}$  the molecule.

### 1.4 The clock System

Devices can not work without a clock system due to metastability problems, generated by quantum phenomena and thermodynamics mechanisms. These problems are avoided by applying an external field, therefore the molecule can change its state passing from hold to reset and vice versa [16].

### 1.4.1 Four-Phase Clock

The Four-Phase clock is a clocking mechanism in which the circuit is divided into different clock zones. Each of them is managed by different values of the electric field [17]. The applied clock signal has four phases where the molecule behaves in various ways: switch, hold, release and relax.

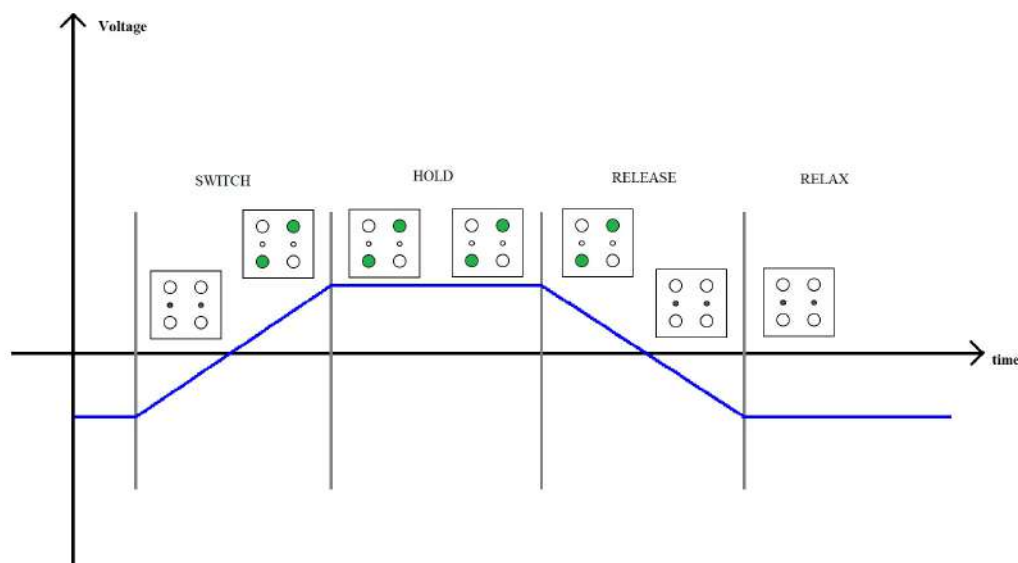


Figure 1.10: Four phase Clock signal waveform

In the switch phase, the electric field passes from a negative to a positive value, the charges leave the reset state, encoding one of the two logical states (0 or 1). With the hold phase, the electric field remains positive and keep stable the logic configuration. The release phase has an opposite behaviour concerning the switch phase, forcing the molecule to the reset state. In the end, the relax phase maintain the molecule in a reset state with a negative electric field.

The electric field switches slowly, avoiding possibility to reach metastable and excited states, called adiabatic switching. In real cases, a single clock zone has more cells, where the number of cells depends on technology. In this way, there is no loss of information and maximization of the performances in frequency. Each zone is associated with a different clock signal. The clock signals are applied in sequence, permitting information propagation as in a pipeline.

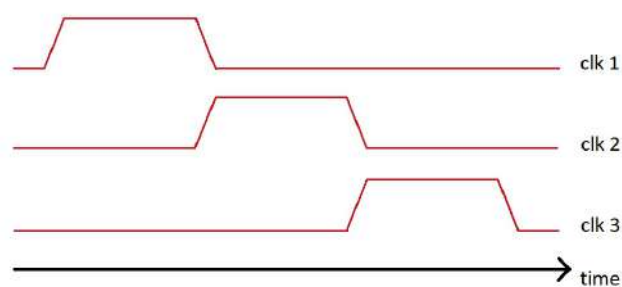


Figure 1.11: Overlapping of clock signals to ensure correct propagation

Moreover, using trapezoidal clock signals, the system works properly even in the presence of a jitter. The overlaps of the clock signals avoid errors in the switching of the cells.

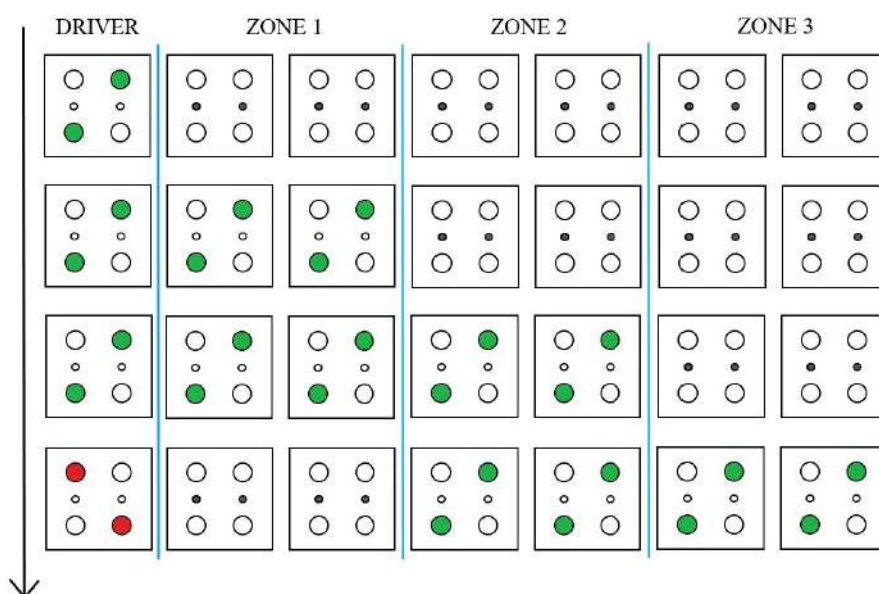


Figure 1.12: Example of time steps in a wire.

### 1.4.2 Sinusoidal Clock

Another mechanism is the Sinusoidal clock. It is characterised by having a single electrode in which a high-frequency signal is applied. Instead of having many electrodes that induce the field on a specific set of molecules, the electrode is made continuous along the wire.[18] It is treated as a transmission line, where the signal generates an electric field that changes concerning the position and time.

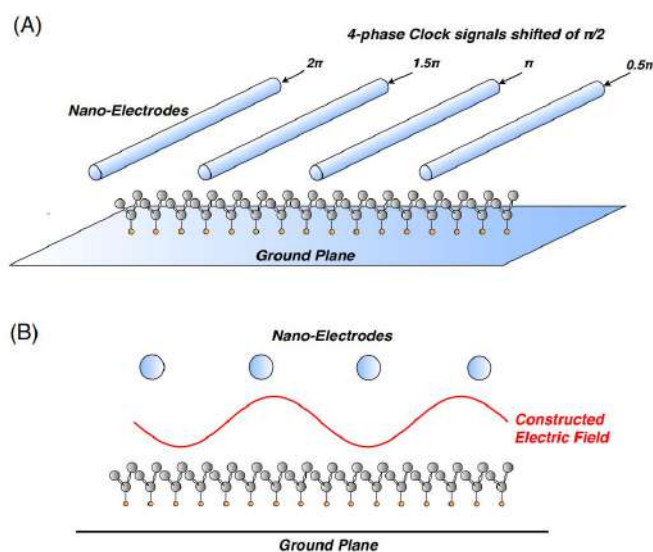


Figure 1.13: Physical Implementation of Sinusoidal clock [18]

In the case of a simple wire, an array of nanoelectrodes is placed above the molecules. In each electrode, the same periodic signal is applied with a phase shift of  $\frac{\pi}{2}$  between one and the other, therefore after four electrodes there is a repetition of the phase difference: for example, the first electrode and the fifth have the same trapezoidal signal, as second an sixth, and so on. The coupling of the electric field generates a "pseudo" sinusoidal clock on the molecules.

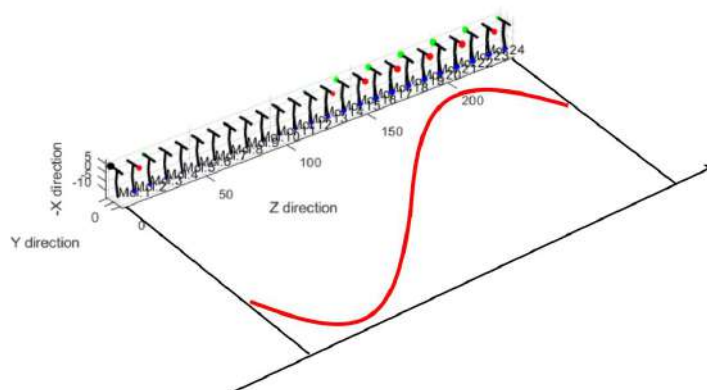


Figure 1.14: Sinusoidal propagation on a wire [18]

## 1.5 Molecular FCN technology layout

The physical implementation of molecular FCN is based on a dielectric substrate used to create a nanometric trench over which gold is deposited.[19] The bisferrocene molecule is anchored to gold through a thiol molecule that ends with a sulphur atom. Gold has a high sulphur affinity enabling the correct deposition of the molecules.

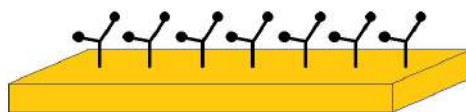


Figure 1.15: Molecular wire implementation with substrate of gold over which the molecules are deposited.

The main problem in the layout is that nanowires need to have the dimensions of the molecules (1-2 nm), but the lithography based technology does not permit it.[20] To avoid it, bigger wires are realized using more lines of molecules. Moreover, in the case of corners, it is difficult to obtain high precision of molecule deposition, which can generate errors in the results of logic operations.

The clock system is obtained by depositing metal electrodes on the substrate on the two sides of the trench. Gold electrode under the molecules is fixed to the ground while the others are connected to a positive or negative voltage. The voltage difference obtained is applied to generate on the molecule an electric field inside the trench.

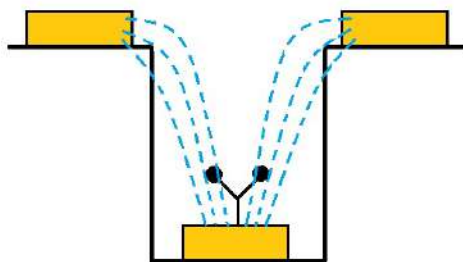


Figure 1.16: Clock field obtained by the potential difference between the top electrodes and the gold nanowire at the bottom of the trench

It is impossible to influence only one molecule because of the dimension of electrodes, so a certain number of molecules are subjected to the generated field. The field is vertically oriented. Each electrode is associated with a different clock zone.[21] In this way, the information propagation is controlled by varying the field applied in each zone.

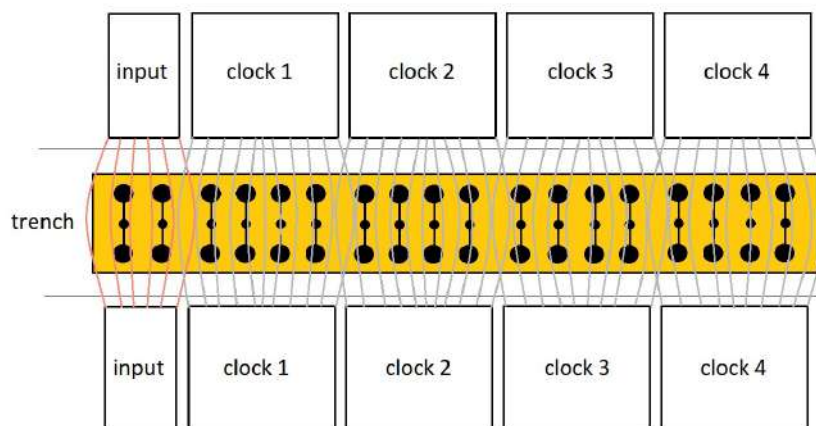


Figure 1.17: Layout of clock implementation on FCN molecular wire

In real systems, neighbouring electrodes interfere with each other, generating an overlapping of fields.[20] This fields' superposition can be useful to solve the problem of the high separation between electrodes: to cover all the molecules with the electrodes, the ideal distance between them should be about  $1\text{ nm}$ , but this is impossible to obtain. When fields overlaps in phase, obtaining a constructive interference, the information is maintained also in the molecules out from electrodes. The presence of overlapped fields in space solves this resolution problem.

## Chapter 2

# Reconfigurable FCN

The Reconfigurable FCN (RFCN) is a new approach developed by Engineer Christian Fabiano in his thesis project in the Polytechnique of Turin [22]. It consists of a regular grid of molecules, grouped in containers (same as standard cell), all placed on the same layer, that are selectively activated similarly to the geometric scheme of the classic FCN. With this technique, any technological implementation is possible and takes advantage of a regular large area patterning and a nano-scale shaping.

In classic FCN there is a pre-defined geometrical scheme, as we can see in Figure 2.1. The space that is not occupied by an FCN container is "empty". Instead, according to the new configuration, the space is "filled" with turned-off containers. In this way, became possible to reconfigure the logic run-time: using electrodes all over the structure, the required containers for a logical operation are turned on and then, in successive steps, the enabled containers can change, activating others, to realize new logic operations.

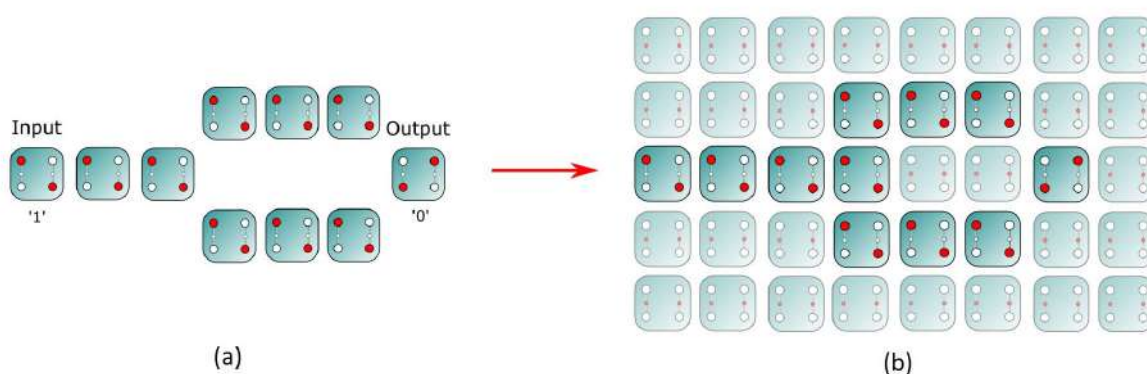


Figure 2.1: Implementation of a logic operation with classical Clock-FCN (a) and RFCN (b) [22]

Molecules are grouped into blocks, acting as containers: each block is subject to an external enable signal coming from a clock electrode. The idea is to have a clock that selectively enables containers, allowing the interaction with neighbours. The enabling imposes the hold state of the molecule, while the inactivation of the container provides the reset state on a molecule.

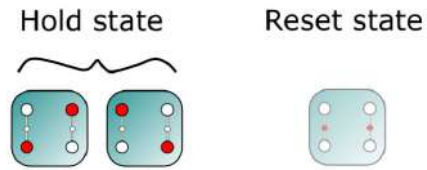


Figure 2.2: Representation of hold and reset states [22]

## 2.1 Logic Operations

An RFCN standard-cell has been defined to perform all the basic logic operations: wire, inverter and majority voter. These operations are carried out correctly using a 3x3 group of containers: wire and majority voter acquires the exact form of its classical FCN version while the inverter is more compact respect classical FCN. Indeed, the operation is obtained through the spatial reuse of containers.

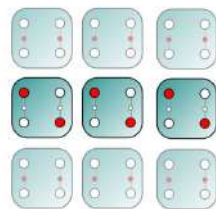


Figure 2.3: Wire RFCN [22]

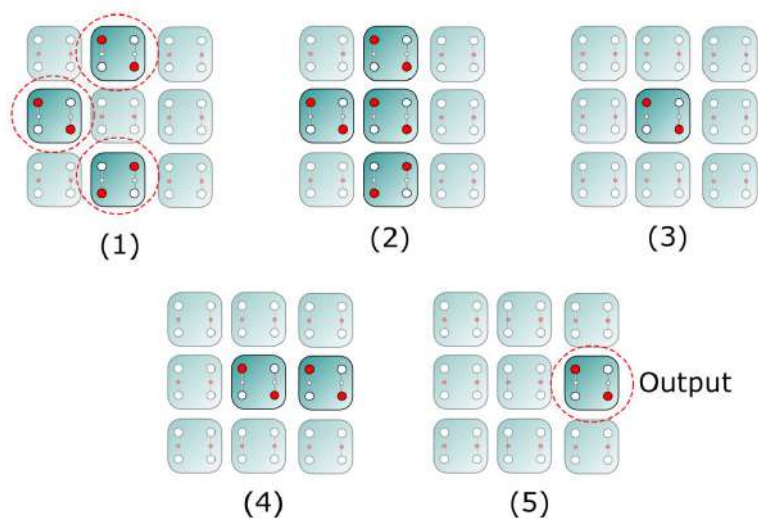


Figure 2.4: Inverter RFCN propagation steps [22]

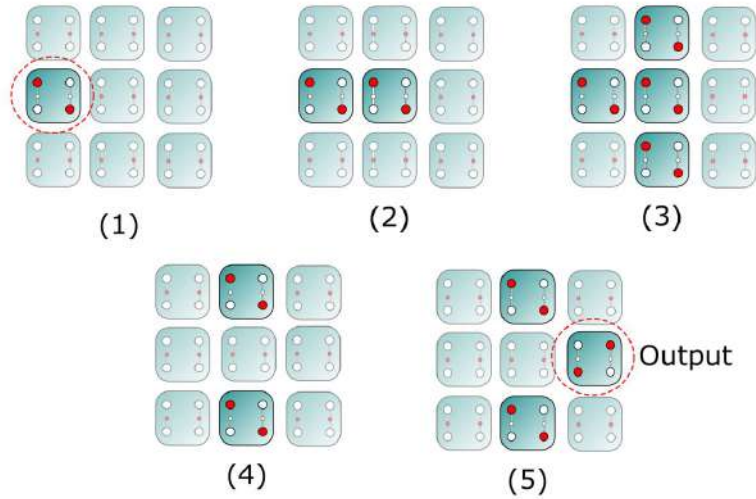


Figure 2.5: Majority Voter RFCN propagation steps [22]

Looking at the steps of the inverter and majority voter evolution, it is possible to note that the containers can switch, passing from reset to hold state and vice versa, while some containers do not switch during the operation and are kept in a reset state, generating the reset islands.

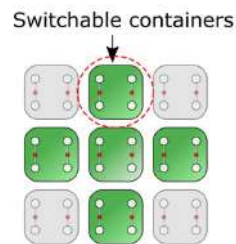


Figure 2.6: Containers that are enabled during the logic operation [22]

This standard cell became the base structure to realize more complex designs, as the NAND. As shown in Figure 2.7, it can be obtained by the union of an inverter and an AND gate.

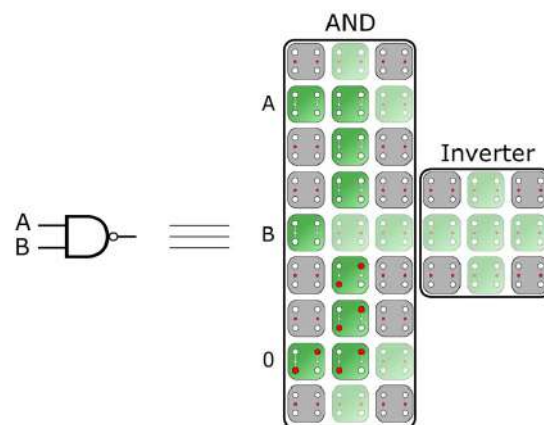


Figure 2.7: NAND gate in RFCN [22]

## 2.2 Clock

In Reconfigurable RFCN, the definition of the clock time is a fundamental point: the clock is used not only to define a time window to execute a combinatorial function but also to set a pre-determined sequence to turn on the containers, permitting correct logic operations. It is a clock with two hierarchical levels:

- **Micro Clock ” $\mu$ -CK”**

It is a ”low level” clock that operates directly within standard cell containers. Considering for example the inverter, the logic operation is divided into small frames, micro-operations, driven by a micro-clock, as shown in Figure 2.8. So the total micro-clock is the sum of all the micro-operations:

$$T_{op} = \sum_i^N T_{\mu op} \quad (2.1)$$

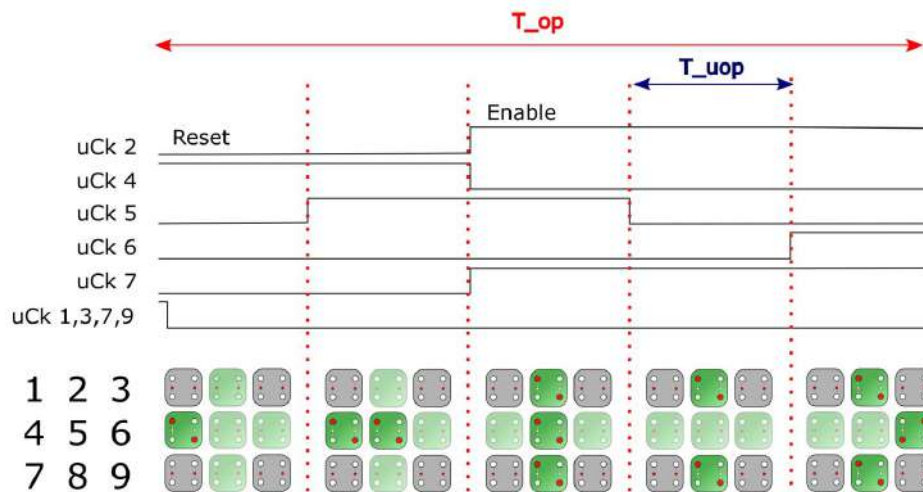


Figure 2.8: Time diagram of the micro-clock evolution for inverter operation [22]

Moreover, to make an operation repeatable the micro-clock is stored into a writable memory, called sequencer.

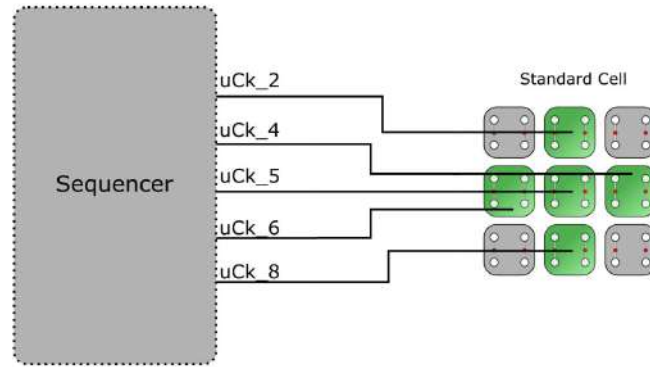


Figure 2.9: Sequencer containing the micro-clock information for a standard cell [22]

- **System Clock**

It is a "high level" clock. As in the CMOS clock, it synchronises operations and data dependency. The system clock defines the order of standard cells that have to be turned on to realize the logic operation. An enable signal on a sequencer allows generating the micro-timing for the containers of the chosen cell.

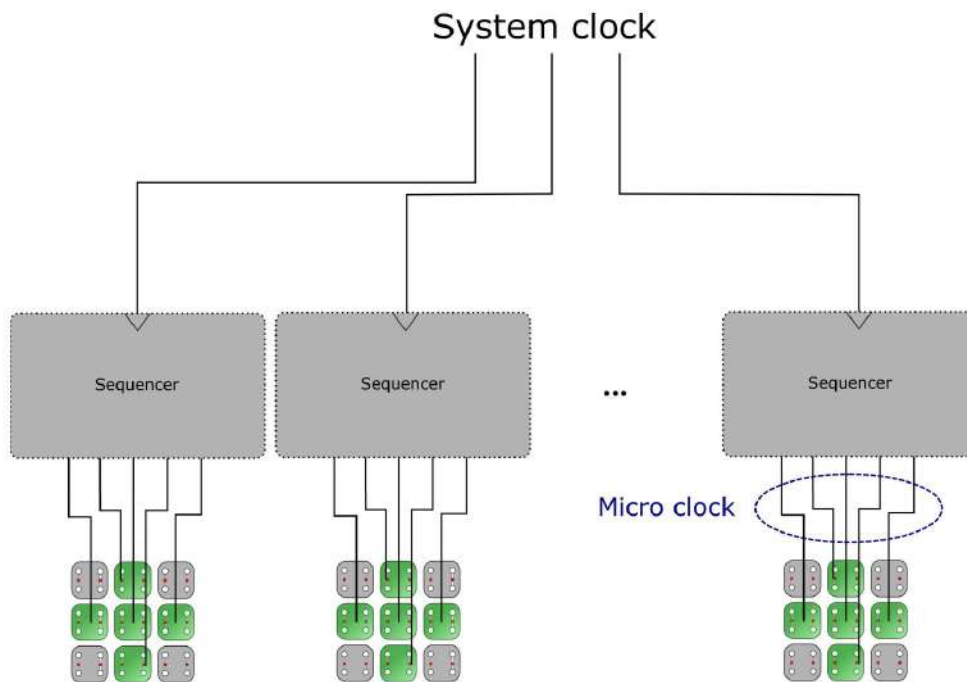


Figure 2.10: System Clock used to synchronise the operations of all the standard cells [22]

It is important to impose the correct period in the system clock: it must be greater than the highest operation duration to make sure having enough time for the logic operation.

$$T_{SCK} > T_{op_{max}} \quad (3)$$

## 2.3 Design

An interesting characteristic of the Reconfigurable FCN is related to the independence of the physical layer from the synthesized operation, permitting different design styles. The operation performed is defined by the micro-clock, with operations memorized in the sequencer. By changing the information inside the sequencer in real-time, a logic operator can change in the consequent SCK cycle.

An example of a possible design is the NAND clusterization. The clusterization permits the creation of custom logic routines, maintaining a repetitive clock scheme.

A delimited area is chosen, enclosing a certain number of containers as in Figure 2.11

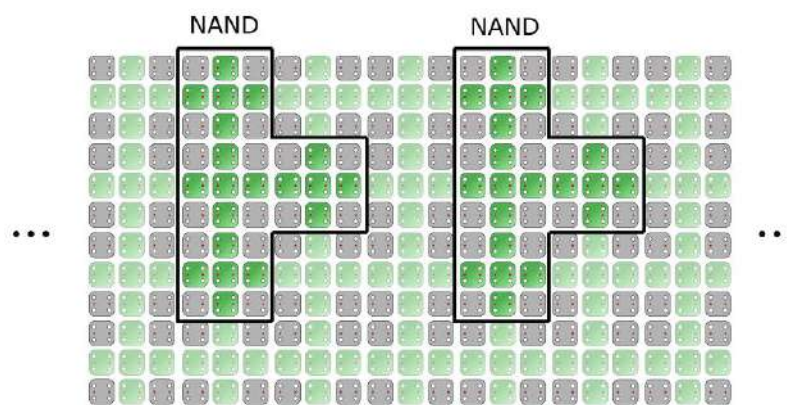


Figure 2.11: NAND gates repetition in the wanted area [22]

In this structure, a portion of the area is reserved for data routing: a predefined number of containers do not perform the logic operation but propagate the logic state from a start to an endpoint. Memory islands are also present to hold precise data.

Collisions can be generated between Memory islands and information propagation: the road of propagation can pass through memory islands, generating the possibility to have errors in the data propagation. There are two alternatives to solve this problem: space and time multiplexing.

- **Space multiplexing**

The area of the blockages is extended, so data propagation paths and memory islands will never collide. At the same time, there is an increase in the occupied area.

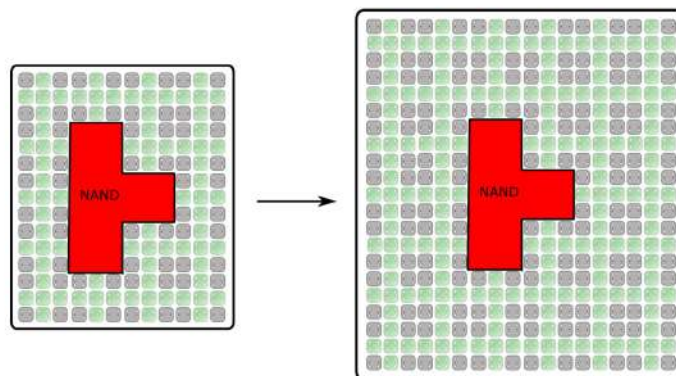


Figure 2.12: Space multiplexing requires the enlarging of the area around the NAND [22]

- **Time multiplexing**

Time multiplexing solution makes possible the propagation along a path with memory islands, providing a backup copy of the data stored in a nearby container. There is a temporary wiping of the data contained in the island that return back when no information has to travel in that zone.

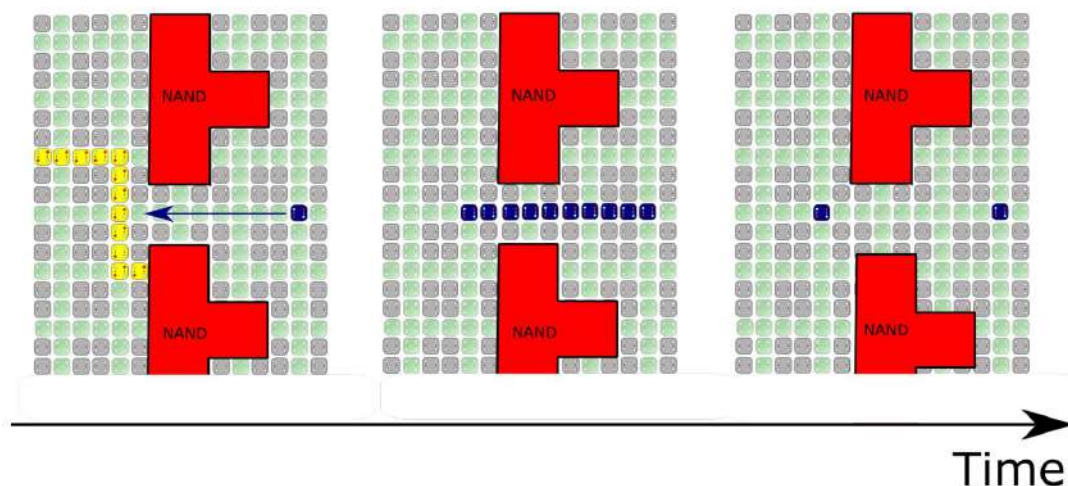


Figure 2.13: Time multiplexing evolution [22]

## 2.4 Technology

A container is made of 2 molecules of Bisferrocene, where the clock field is applied between a gold plate on which the molecules are placed and an electrode lying above the molecules.

Due to the small dimension of the molecules, there are two possible manufacturing issues:

- Clock wires congestion

Each electrode is connected with a clock wire, to enabling the correct propagation of the

information supplied by the micro-clock. The high density of independent electrodes on the SAM area could cause the congestion of the micro-clock wires.

- Electrodes size

A single container has the dimension of  $4 \text{ nm}^2$  and the manufacturing of a so small electrode is very challenging.

A solution that can reduce the electrode manufacturing problem is to consider a container made of more than two molecules, called molecular block: all the molecules that are subjected to the same electric field act in the same way, assuming the same logic configuration. As follows, the dimension of the container increase as the dimension of the electrode.

In Reconfigurable RFCN, the standard cell is made of 9 molecular blocks, each one with N molecules.

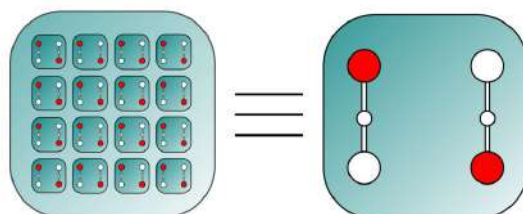


Figure 2.14: A series of containers that share the same field works together as a single big container [22]

Another issue is the high number of independent electrodes that are difficult to manage with time signals.

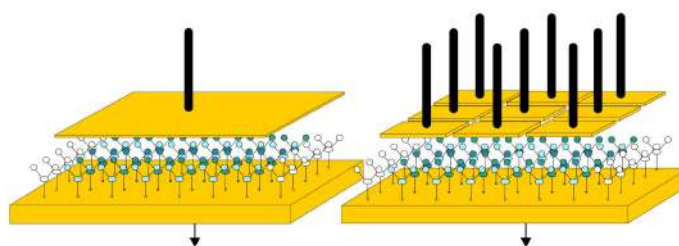


Figure 2.15: Difference of electrode size in case of small containers and a molecular block [22]

A possible simplification is the sharing of electrodes belonging to the same row or to the same column.

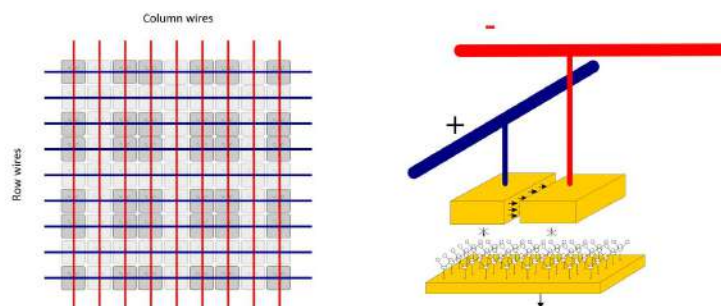


Figure 2.16: Shared electrodes model [22]

Unfortunately, it can not be applied in Molecular RFCN because when a molecule switches to another logic state it passes before to a reset state. The reset state cleans the container's memory before the next hold state. A shared model does not allow to guarantee the needed degrees of freedoms required to mimick the turning-on sequence of the inverter and majority voter.

## 2.5 Simulations

Before realizing the simulations, it is fundamental to evaluate the interaction between molecules. The behaviour of the molecules is understanding through the application of the Molecular Simulator Quantum-Dot Cellular Automata Torino (MoSQuiTo)[11]. After that, the simulations have been developed with Self Consistent Electrostatic Potential Algorithm (SCERPA)[12].

### 2.5.1 Simulation flow

A three-stage algorithm has been applied to evaluate the interaction between molecules:

- **FIRST STAGE:** AB-initio simulation

The Bis-ferrocene molecule is described in a Z-matrix, that take the position of all the atoms of the molecule. During simulation, the molecule under test (MUT) is subjected to different values of an electric field. When the molecule is under field conditioning, the charge aggregates into two-point of the molecule, mimic the driver molecule. The MUT generates an electric field that is used in the second stage[11].

Atom symbol	Atom reference #	Distance [Å]	#	Angle [°]	#	Angle [°]
C	1	1.424				
C	2	1.424	1	108		
C	3	1.424	2	108	1	0
C	4	1.424	3	108	2	0

Table 2.1: Z-matrix of Bis-ferrocene [22]

- **SECOND STAGE:** Aggregated charge model and transcharacteristics

The Aggregation of the charge allows to model the molecules as points with a charge equals

to the average of the charges of the single atoms.

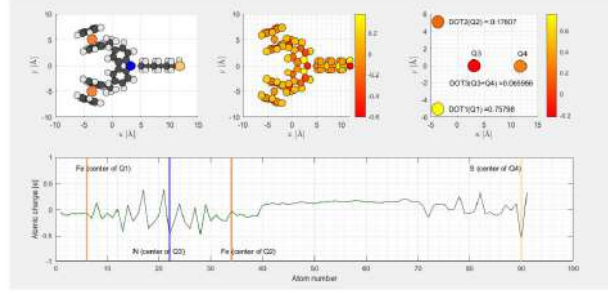


Figure 2.17: Molecular structure with charge distribution [22]

From the results obtained in the first stage, it is possible to carry out the trans-characteristic: it is the gain between the equivalent voltage that the MUT supplies to the near molecule and the voltage that the MUT receives from the same molecule. It depends on the molecular distance and the clock field applied.

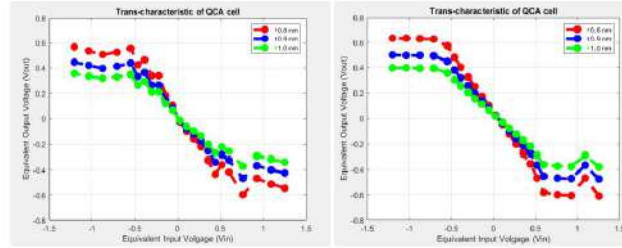


Figure 2.18: Trans-characteristic variation with clock and molecular distance [22]

As shown in table 2.4 an increasing of gain is observed in presence of a clock:

Distance [nm]	Gain with clock +2 V	Gain without clock
1	0.67	0.58
0.9	0.821	0.731
0.8	1.046	0.93

Table 2.2: Gain voltage variation depending on clock and molecular distance [22]

- **THIRD STAGE: Self-Consistent Algorithm**

By using a self-consistent algorithm (SCERPA), the molecule is simulated in the structure, considering the results obtained in the previous steps.

## 2.5.2 Simulation structure

To simulate the structure, the following parameters have been imposed on SCERPA:

- Molecular distance:

The distance used is, according to the expected distance between quantum dots:

$$d_x = 1nm$$

$$d_y = 2nm$$

- Block size:

It is a fundamental parameter because can influence the correctness of the logic operation: a too-small block has not enough molecules for the feedback to take place, resulting in the block not being able to hold the logic state, while a too-large block has a feedback effect that is too intense, therefore the nearby block will not be able to interact with it. The size chosen for the simulation is made of  $N=6$ .

- Clock field strength:

The data extrapolated from the atomistic molecular characterization includes the clock field value from a minimum of  $2Vnm$  (strongest reset state) to a maximum of  $2Vnm$  (strongest hold state)

Here the NAND simulation is reported. It is realized by 6 standard cells of which only 4 are used for the operations. In order to obtain a correct NAND operation, the third input on the majority voter is a binary 0, to impose an AND operation. The other inputs are  $A = 0$   $B = 1$  and the expected output is:

$$Q = AB = 1$$

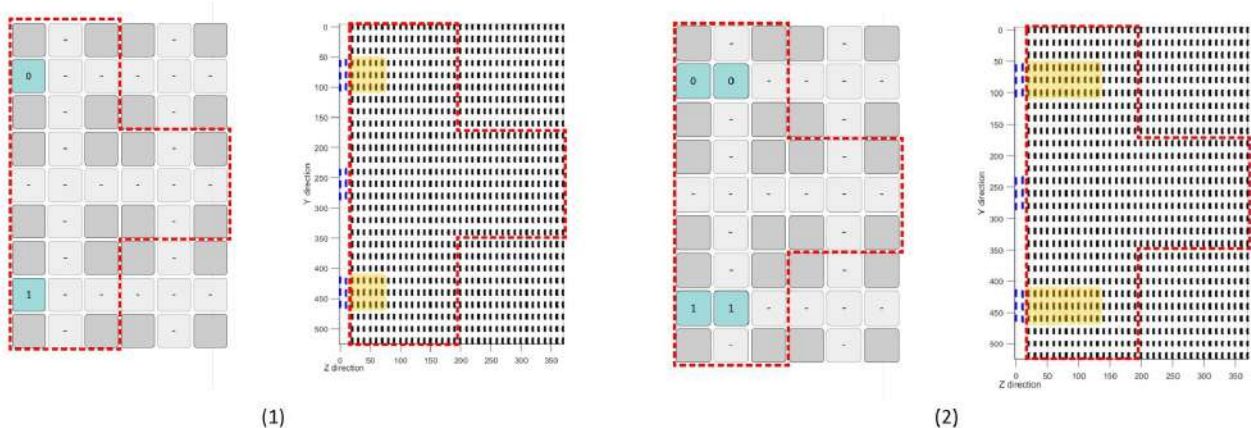


Figure 2.19: NAND steps (a) [22]

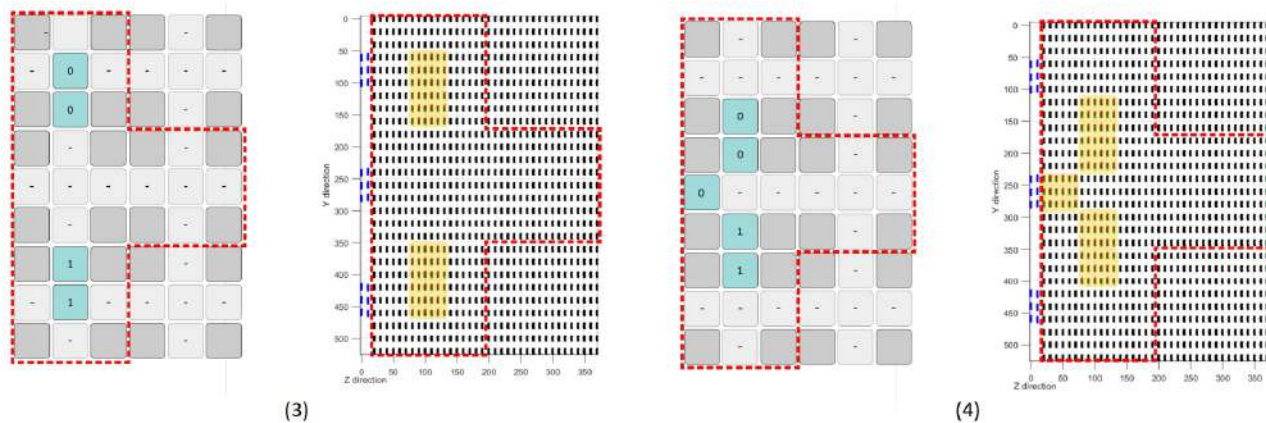


Figure 2.20: NAND steps (b) [22]

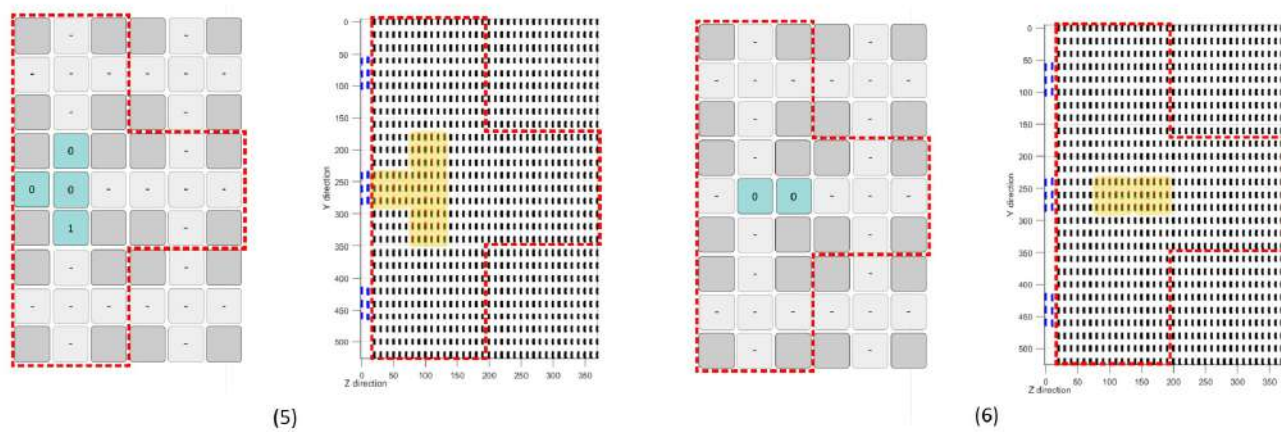


Figure 2.21: NAND steps (c) [22]

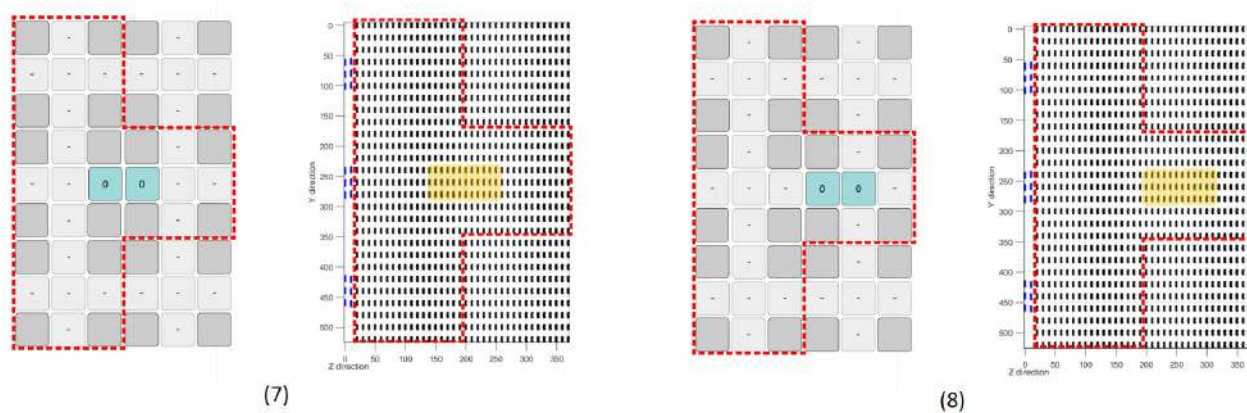
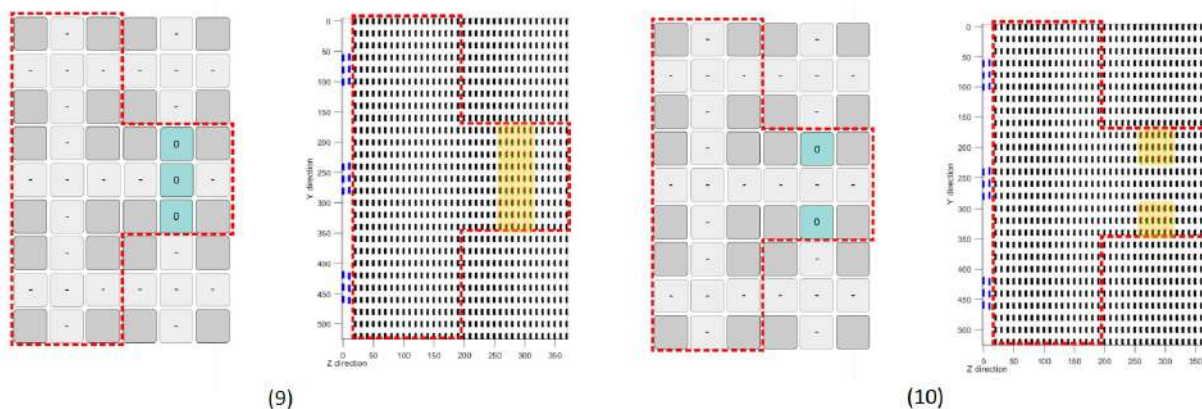


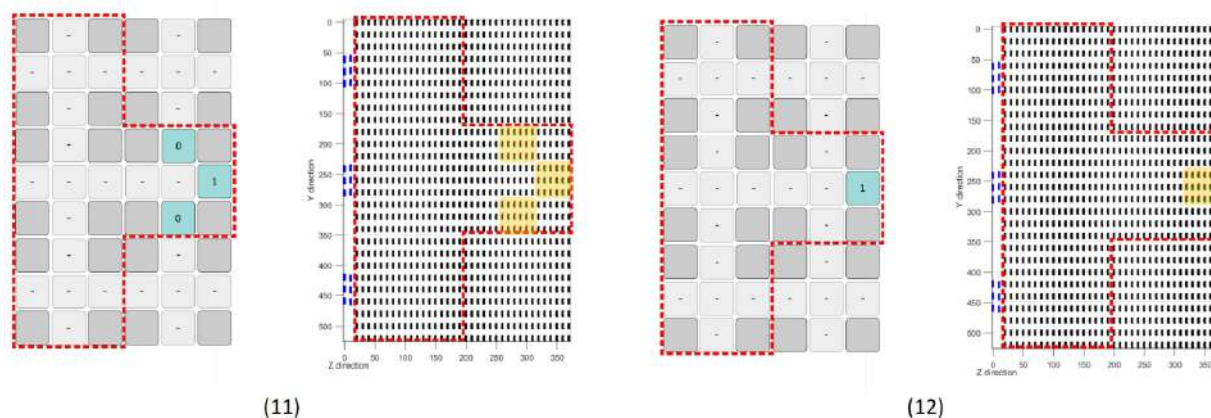
Figure 2.22: NAND steps (d) [22]



(9)

(10)

Figure 2.23: NAND steps (e) [22]



(11)

(12)

Figure 2.24: NAND steps (f) [22]

## 2.6 Figure of merit

The Reconfigurable FCN presents some interesting figures of merit, related to the choice of molecules for the implementation:

### 2.6.1 Area

In Molecular RFCN different areas can be defined.

- Area of the block (Ablock)

Considering the following values for the distance between two molecules in x and y direction:

$$d_x = 1 \text{ nm}$$

$$d_y = 2 \text{ nm}$$

The area of a block of molecules can be calculated: for  $N=6$  molecules, the lateral dimensions of a block and the Area are defined

$$L_x \cong N \cdot d_x = 6 \text{ nm} \quad (2.4)$$

$$L_y \cong \frac{N}{2} \cdot d_y = 6 \text{ nm} \quad (2.5)$$

$$A_{block} = L_x \cdot L_y = \frac{N^2}{2} \cdot d_x \cdot d_y = 36 \text{ nm}^2 \quad (2.6)$$

- Area of the standard-cell (Acell)

A standard cell is made by 9 blocks:

$$A_{cell} = 9 \cdot A_{block} = \frac{9}{2} N^2 \cdot A_{base} = 324 \text{ nm}^2 \quad (2.7)$$

- Area needed for a logic function (Agate)

To realize a NAND operation 6 standard cells are needed: 4 for the AND and inverter operations, and 2 more cells on the sides of inverter, as we can see in the simulation figure 2.17

$$A_{NAND} = M \cdot A_{cell} = M \cdot \frac{9}{2} N^2 \cdot A_{base} \cong 2000 \text{ nm}^2 \quad (2.8)$$

Comparing with a FINFET NAND, which area is shown in formula 2.9, Molecular RFCN technology brings a reduction of the area occupied by the logic gate of 90%.

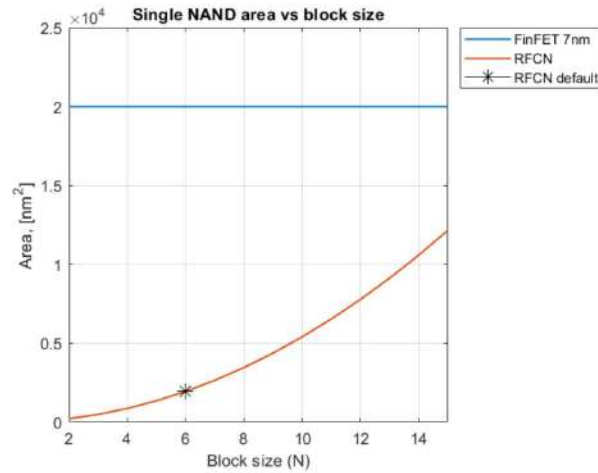


Figure 2.25: NAND Area variation depending on block size [22]

$$A_{Finfet} = 20\,000\,nm^2 \quad (2.9)$$

## 2.6.2 Interconnection Density

In RCFN the elevated number of independent electrodes produces routing congestion: overcrowding of interconnection density inside the same area induce limitations in the manufacturing process.

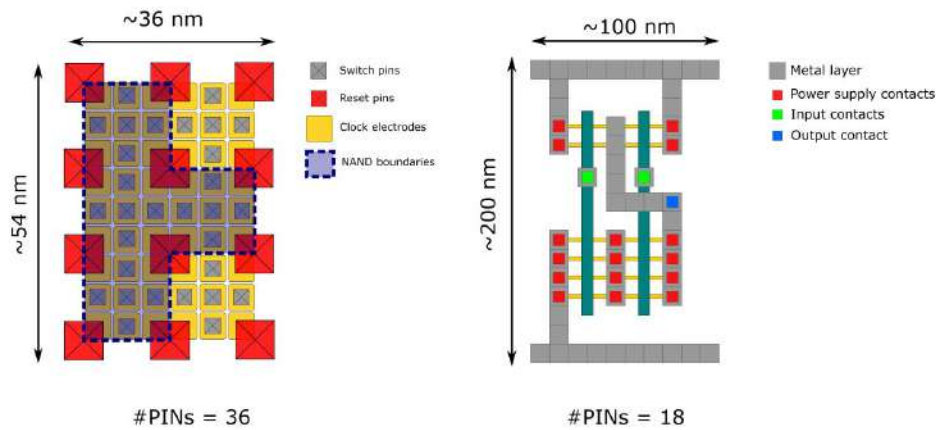


Figure 2.26: NAND gate in RCFN and FinFET layout [22]

Comparing the number of PINs present, per unit area, in a NAND gate implemented in FinFET technology (7nm) and RCFN, the number of PINs per unit area  $p$  is:

$$p_{FinFet} = \frac{PIN}{Area} = 900 \frac{PINs}{\mu m^2} \quad (2.10)$$

$$p_{RFCN} = \frac{PIN}{Area} = 18500 \frac{PINs}{\mu m^2} \quad (2.11)$$

The above numbers suggest that metal wires congestion could be much higher in RFCN when compared to FinFET.

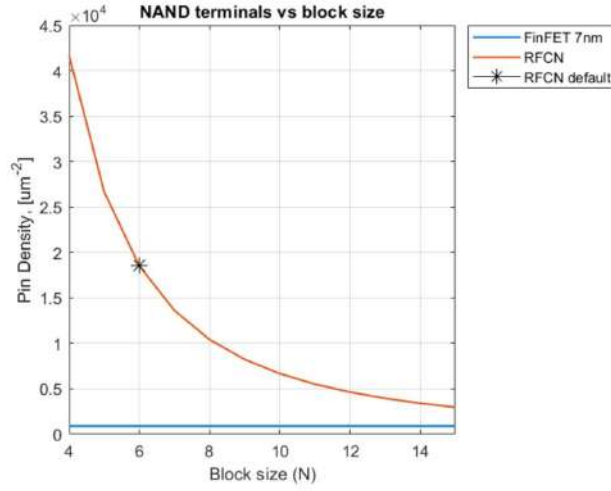


Figure 2.27: Pin density variation respect block size [22]

At the same time, it is necessary to consider that FinFETs are devices that exploit electrical currents to perform operations, therefore the interconnections should be robust enough to supply the high current requested. Instead, RFCN does not need a power supply, so the size of the wires can be much smaller.

### 2.6.3 Power

The dynamic power dissipated from RFCN NAND partially exploit the CMOS formula

$$P_{NAND} = C \cdot V_P S^2 \cdot f \cdot K \quad (2.12)$$

Where K is the number of electrodes that are activated in the NAND operation, f is the frequency of 2.9 GHz.

Moreover, the metal electrodes used to induce an electric field on the molecules induce a capacitance effect.

$$C = C_{main} + C_{lateral} \quad (2.13)$$

The lateral capacitance can be neglect, because the planar area is supposed to be much greater than the sum of the lateral sections, so the capacitance depends only on  $C_{main}$ :

$$C = C_{main} + C_{lateral} = C_{main} \quad (2.14)$$

The capacitance for a parallel plate geometry is given by the following formula:

$$C = \epsilon \cdot \frac{A}{h} \quad (2.15)$$

where  $\epsilon$  is the electric permittivity and  $h$  is the distance between plates: the bisferrocene height is about 2nm, therefore the recommended electrodes distance is 4nm.

$$\epsilon = \epsilon_r \cdot \epsilon_0 \quad (2.16)$$

Considering having air between plates, neglecting the permittivity of the molecules:

$$\epsilon = \epsilon_{air} \cdot \epsilon_0 \quad (2.17)$$

According to the previous values the capacitance of the single electrode is:

$$C = \epsilon \cdot \frac{A}{h} = 0.08 \text{ aF} \quad (2.18)$$

In the end, the power supply voltage  $V_{PS}$  can be defined as:

$$V_{PS} = V_{hold} - V_{reset} \quad (2.19)$$

where:

$$V_{hold} = E_{hold} \cdot h = 2 \frac{V}{nm} \cdot 4nm = 8 V \quad (2.20)$$

$$V_{reset} = E_{reset} \cdot h = -2 \frac{V}{nm} \cdot 4nm = -8 V \quad (2.21)$$

So:

$$V_{PS} = 16 V \quad (2.22)$$

Moreover, the correct behaviour is obtained with a hold field of 0 V/nm and a reset field of -1.5 V/nm, so the power supply voltage needed for this field configuration is :

$$V_{PS} = 6 V \quad (2.23)$$

At the end, the dynamic power has been calculated

$$P_{NAND} = C \cdot V_{PS}^2 \cdot f \cdot K = 166 nW \quad (2.24)$$

Comparing with a NAND Finfet:

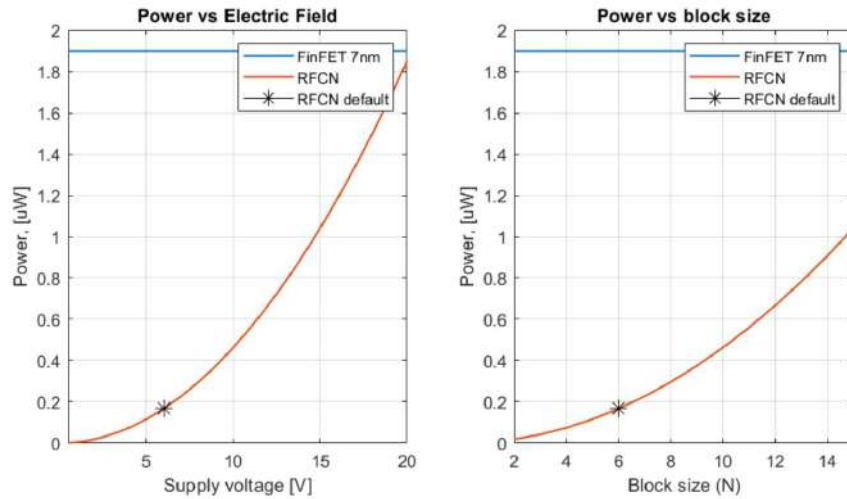


Figure 2.28:  $P_{NAND}$  variation with respect to Electric field and block size [22]

The RFCN technology brings also a reduction of the dynamic power dissipation of 90% on the NAND cell. From Figure 2.26 it is also possible to note an quadratical increasing of the power dissipation with the increasing of the supply voltage due to the higher dissipation on the pull-up/pull-down resistances of the clock network.

# Chapter 3

## Light's interference

Light is electromagnetic radiation, whose spectrum is in a range between low energy radio waves and high energy gamma rays. Electromagnetic radiation describes fluctuations of electric and magnetic fields and their transport of energy.

Light changes its properties when interacting with surrounding elements [23]: everything is composed of atoms, ions or molecules and their interactions with light induce various events that allow understanding the nature of things.

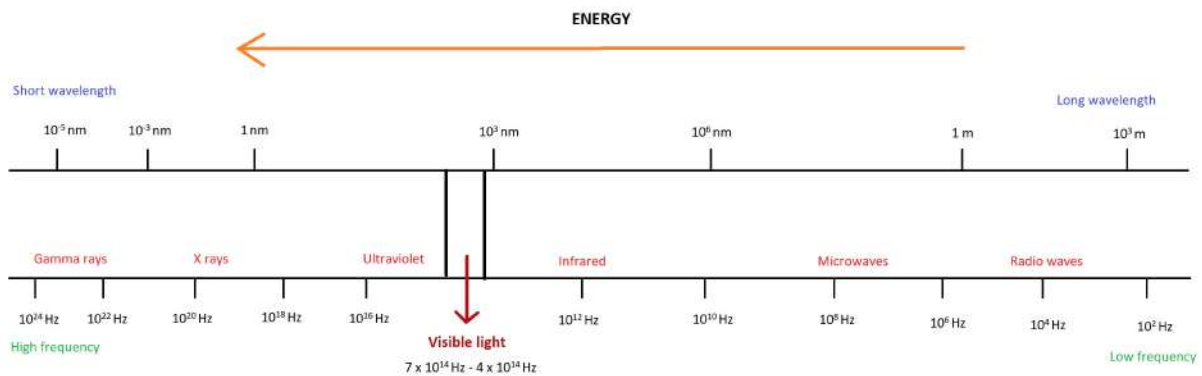


Figure 3.1: Spectrum of light radiation

### 3.1 Introduction on Electromagnetic Field

To describe the effect of the field on objects, it is necessary to introduce Maxwell's equations [24]:

$$\text{curl} \mathbf{H} - \frac{1}{c} \mathbf{D} = \frac{4\pi}{c} \mathbf{j} \quad (3.1)$$

$$\mathit{curl}\mathbf{E} + \frac{1}{c}\mathbf{B} = 0 \quad (3.2)$$

$$\mathit{div}\mathbf{D} = 4\pi\rho \quad (3.3)$$

$$\mathit{div}\mathbf{B} = 0 \quad (3.4)$$

where  $\rho$  is the electric charge density.

$\mathbf{B}$  is the magnetic induction.

$\mathbf{D}$  is the electric displacement.

In the case of interaction with the material, these equations have to describe also the behaviour of the type of material. They are complicated but imposing a time-harmonic field and that bodies are isotropic, the equations became:

$$\mathbf{j} = \sigma\mathbf{E} \quad (3.5)$$

$$\mathbf{D} = \epsilon\mathbf{E} \quad (3.6)$$

$$\mathbf{B} = \mu\mathbf{H} \quad (3.7)$$

where  $\sigma$  is the specific conductivity,  $\epsilon$  is the dielectric constant and  $\mu$  is the magnetic permeability. Depending on the material considered  $\epsilon$ ,  $\mu$  and  $\sigma$  changes, enabling the the field description related to the particular material. For simplicity, the studies are made with substances that the light can penetrate without introducing variations, like air or glass that are transparent and electrically non-conductors.

### 3.1.1 Boundary conditions

Supposing having a surface  $\mathbf{T}$  with certain values of  $\epsilon$  and  $\mu$ . Within this layer is constructed a cylinder, normal to the T layer, with areas on each T side of  $\delta A_1$  and  $\delta A_2$ .  $\mathbf{B}$  may be considered continuous throughout the cylinder, so it is possible to apply the Gaussian Theorem:

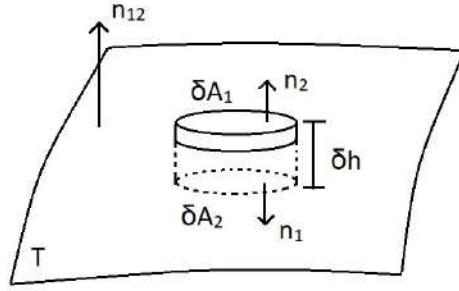


Figure 3.2: Boundary condition for normal vector of  $\mathbf{B}$  and  $\mathbf{D}$

$$\int \text{div} \mathbf{B} dV = \int \mathbf{B} \cdot \mathbf{n} dS = 0 \quad (3.8)$$

where  $\mathbf{n}$  is the unit outward normal.  $\mathbf{B}$  can be considered having constant values on  $\delta A_1$  and  $\delta A_2$  and due to the small dimensions of the areas and the height of the cylinder near to zero (there is no contribution from the walls) the integral became:

$$(\mathbf{B}^{(1)} \cdot \mathbf{n}_1 + \mathbf{B}^{(2)} \cdot \mathbf{n}_2) \delta A = 0 \quad (3.9)$$

Moreover if  $\mathbf{n}_{12}$  is the unit normal pointing in the two media:

$$\mathbf{n}_1 = -\mathbf{n}_{12}$$

$$\mathbf{n}_2 = \mathbf{n}_{12}$$

The equation (9) became:

$$\mathbf{n}_{12} \cdot (\mathbf{B}^{(2)} - \mathbf{B}^{(1)}) = 0 \quad (3.10)$$

Across the surface, the normal component of magnetic induction is continuous.

Similarly, the boundary conditions for the electric displacement  $\mathbf{D}$  can be defined:

$$\int \text{div} \mathbf{D} dV = \int \mathbf{D} \cdot \mathbf{n} dS = 4\pi \int \rho dV \quad (3.11)$$

Imposing that the areas  $\delta A_1$ ,  $\delta A_2$  and the height of the walls sufficiently small:

$$\mathbf{n}_{12} \cdot (\mathbf{D}^{(2)} - \mathbf{D}^{(1)}) = 4\pi\rho \quad (3.12)$$

The normal component of the electric displacement change of about  $4\pi\rho$  across the surface.

To evaluate the boundary conditions for  $\mathbf{E}$  and  $\mathbf{H}$ , the cylinder is substituted with a rectangular area as in Figure 3.3

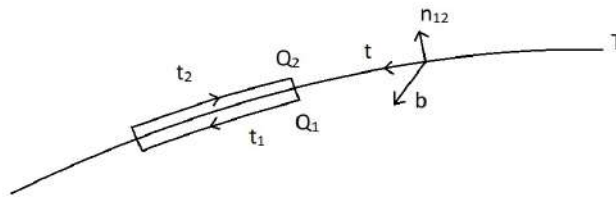


Figure 3.3: Boundary conditions for tangential vectors of  $\mathbf{E}$  and  $\mathbf{H}$

From Stokes' Theorem:

$$\int \text{curl}\mathbf{E} \cdot \mathbf{b}dS = \int \mathbf{E}dr = -\frac{1}{c} \int \mathbf{B} \cdot \mathbf{b}dS \quad (3.13)$$

$\mathbf{b}$  is the unit vector perpendicular to the rectangle.

If  $\delta s_1$  and  $\delta s_2$  are small and the walls tends to zero:

$$(\mathbf{E}^{(1)} \cdot \mathbf{t}_1 + \mathbf{E}^{(2)} \cdot \mathbf{t}_2)\delta s = 0 \quad (3.14)$$

where  $\mathbf{t}$  is the unit tangent across the surface:

$$\mathbf{t}_1 = -\mathbf{t} = -\mathbf{b} \times \mathbf{n}_{12}$$

$$\mathbf{t}_2 = \mathbf{t} = \mathbf{b} \times \mathbf{n}_{12}$$

Considering also the arbitrary of the direction of the rectangle and the vector  $\mathbf{b}$ , the equation became:

$$\mathbf{n}_{12} \times (\mathbf{E}^{(2)} - \mathbf{E}^{(1)}) = 0 \quad (3.15)$$

Across the surface, the tangential component of  $\mathbf{E}$  is continuous.

The same study is applied on the magnetic vector, obtaining:

$$\mathbf{n}_{12} \times (\mathbf{H}^{(2)} - \mathbf{H}^{(1)}) = \frac{4\pi}{c} \mathbf{j} \quad (3.16)$$

The tangential component change across the surface of a quantity of  $\frac{4\pi}{c} \mathbf{j}$

### 3.1.2 Energy of electromagnetic field

From the first two Maxwell's equations [24]:

$$\mathbf{E} \cdot \text{curl} \mathbf{H} - \mathbf{H} \cdot \text{curl} \mathbf{E} = \frac{4\pi}{c} \mathbf{j} \cdot \mathbf{E} + \frac{1}{c} \mathbf{E} \cdot \mathbf{D} + \frac{1}{c} \mathbf{H} \cdot \mathbf{B} \quad (3.17)$$

The term on the left is the divergences of the vector product of  $\mathbf{H}$  and  $\mathbf{E}$ :

$$\mathbf{E} \cdot \text{curl} \mathbf{H} - \mathbf{H} \cdot \text{curl} \mathbf{E} = -\text{div}(\mathbf{E} \times \mathbf{H}) \quad (3.18)$$

As consequence:

$$\frac{1}{c} (\mathbf{E} \cdot \mathbf{D} + \mathbf{H} \cdot \mathbf{B}) + \frac{4\pi}{c} \mathbf{j} \cdot \mathbf{E} + \text{div}(\mathbf{E} \times \mathbf{H}) = 0 \quad (3.19)$$

Applying the Gauss's Theorem:

$$\frac{1}{4\pi} \int (\mathbf{E} \cdot \mathbf{D} + \mathbf{H} \cdot \mathbf{B}) dV + \int \mathbf{j} \cdot \mathbf{E} dV + \frac{c}{4\pi} \int (\mathbf{E} \times \mathbf{H}) \cdot \mathbf{n} dS = 0 \quad (3.20)$$

All the terms are multiplied by  $\frac{c}{4\pi}$  and the resulting last integral take over the boundary, with  $\mathbf{n}$  as normal vector. The equation 3.20 is the consequence of Maxwell's equations: it represent the Energy law on an electromagnetic field. In fact, in case of isotropic material

$$\left\{ \begin{array}{l} \frac{1}{4\pi} (\mathbf{E} \cdot \mathbf{D}) = \frac{1}{4\pi} \mathbf{E} \cdot \frac{\partial \epsilon \mathbf{E}}{\partial t} = \frac{1}{8\pi} \frac{\partial \epsilon \mathbf{E}^2}{\partial t} = \frac{1}{8\pi} \frac{\partial (\mathbf{E} \cdot \mathbf{D})}{\partial t} \\ \frac{1}{4\pi} (\mathbf{H} \cdot \mathbf{B}) = \frac{1}{4\pi} \mathbf{H} \cdot \frac{\partial \mu \mathbf{H}}{\partial t} = \frac{1}{8\pi} \frac{\partial \mu \mathbf{H}^2}{\partial t} = \frac{1}{8\pi} \frac{\partial (\mathbf{H} \cdot \mathbf{B})}{\partial t} \end{array} \right. \quad (3.21)$$

By imposing:

$$w_e = \frac{1}{8\pi} \mathbf{E} \cdot \mathbf{D}$$

$$w_m = \frac{1}{8\pi} \mathbf{H} \cdot \mathbf{B}$$

respectively electric energy density and magnetic energy density of the field, the total energy:

$$W = \int (w_e + w_m) dV \quad (3.22)$$

The equation 3.20 becomes

$$\frac{dW}{dt} + \int \mathbf{j} \cdot \mathbf{E} dV + \frac{c}{4\pi} \int (\mathbf{E} \times \mathbf{H}) \cdot \mathbf{n} dS = 0 \quad (3.23)$$

The energy  $W$  is evaluated in a isolated system, with a certain area  $A$ . The relative variation of the energy during time can be expressed as

$$\frac{dW}{dt} = \frac{\delta A}{\delta t} - Q - \int \mathbf{S} \cdot \mathbf{n} dS \quad (3.24)$$

Q represents the Joule's heat, the resistive dissipation of energy and  $\mathbf{S}$  is the Poynting vector, the energy that cross the area normal to  $\mathbf{E}$  and  $\mathbf{H}$ .

### 3.1.3 Propagation velocity

In an homogeneous medium, the Maxwell's equation can be express as:

$$\nabla^2 \mathbf{E} - \frac{\epsilon\mu}{c^2} \ddot{\mathbf{E}} = 0 \quad (3.25)$$

$$\nabla^2 \mathbf{H} - \frac{\epsilon\mu}{c^2} \ddot{\mathbf{H}} = 0 \quad (3.26)$$

These equations describe the presence of electromagnetic waves that propagates with a velocity:

$$v = \frac{c}{\sqrt{\epsilon\mu}} \quad (3.27)$$

In void the value of the velocity of electromagnetic wave is

$$c = 299792458 \text{ m/s}$$

In materials the velocity is smaller: the value of v inside a material is not determined directly, but only in relation with c, through the law of refraction.

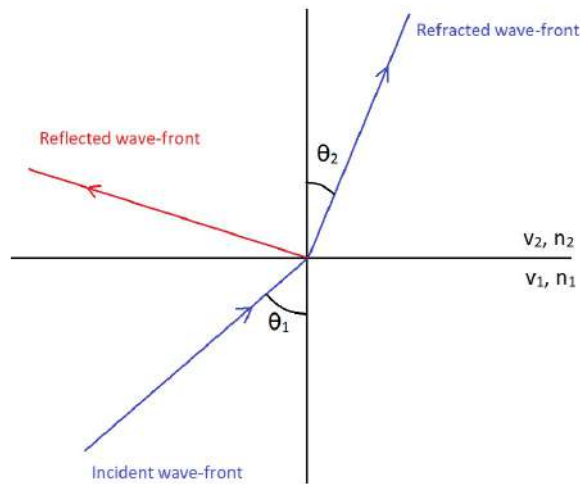


Figure 3.4: Refraction of incident plane wave

$$\frac{\sin\theta_1}{\sin\theta_2} = \frac{v_1}{v_2} \quad (3.28)$$

According to this relation, supposing having an incident wave, with angle of incidence  $\theta_1$ , it passes through a media, generating a transmitted wave with angle of  $\theta_2$ . The relation of two sines angle is equal to the relation of the velocities of propagation in the two media.

$$v_1 = v' \sin\theta_1$$

$$v_2 = v' \sin\theta_2$$

It is possible define also the refractive index  $n$  of a medium:

$$n = \frac{c}{v} \quad (3.29)$$

$$n = \sqrt{\epsilon\mu} \quad (3.30)$$

Generally,  $\mu$  is considered unitary, so the index  $n$  depends on the dielectric constant, which is assumed constant in a material.

## 3.2 Interference

When a source passes through apertures on a screen, the phenomena of diffraction and interference are generated. The passage of a source through the slits induces the diffraction and a series of secondary sources equal to the principal are produced. During propagation, the generated waves superimpose, producing interference. The intensity of superimposition varies between a maximum value and minimum value near to 0, which correspond to the sum and the difference of the intensities. When the beams originate from a single source, they are correlated and partially or completely coherent, depending on correlation. Instead, when the beams came from different sources, they are uncorrelated and incoherent. In this case, the superimposition does not generate interference.[24] The interference of light was firstly demonstrated by the Young's experiment: a monochromatic source hit a holed screen. The holes are equidistant from source and act as secondary in-phase sources, that superimpose generating the interference.

### 3.2.1 Two-slit Interference

As the first assumption, consider having a plane wave, with fronts parallel to a wall, that have very small slits with infinite length in the perpendicular direction to the page [25].



Figure 3.5: Wave-fronts representation

Each slit generates a cylindrical wave due to the no dependence in the perpendicular direction. The two sources are in phase and during the propagation outward from slits, they interfere. As result of the interference phenomena, the sources superimpose generating a constructive interference, when they are in phase, and a destructive interference, when they are out of phase of  $180^\circ$ .

Supposing having a screen parallel to the walls at a distance  $D$ , in a point  $P$  on the screen, the length of the two path, generated by sources  $S_1$  and  $S_2$  at distance  $d$  are  $r_1$  and  $r_2$  as shown in Figure 3.6.

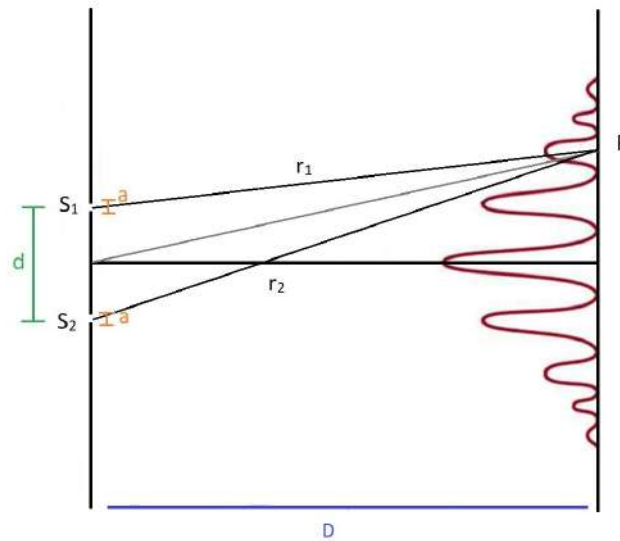
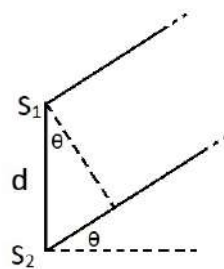


Figure 3.6: Two-slit interference

Moreover, the far-field condition is applied,  $D \gg d$ . This assumption leads two important consequences:

- $r_1$  and  $r_2$  are equal in a multiplicative sense, so the ratio  $r_1/r_2 = 1$ . Indeed, the difference between  $|r_1 - r_2|$  is negligible compared to  $r_1$  and  $r_2$ .
- $r_1$  and  $r_2$  are parallel, so they make the same angle with the normal. the relative difference of paths  $r_2 - r_1$  is defined as  $d \sin \theta$ .

Figure 3.7:  $r_1$  and  $r_2$  in far-field condition

$$k(r_2 - r_1) = kd \sin \theta = \frac{2\pi}{\lambda} d \sin \theta \quad (3.31)$$

Knowing the phase difference, it is possible to define the wave at point P:

$$E_{tot}(P) = A_P e^{i(kr_1 - \omega t)} + A_P e^{i(kr_2 - \omega t)} = A_P (e^{ikr_1} + e^{ikr_2}) e^{-i\omega t} \quad (3.32)$$

To find the total Amplitude, the wave equation can be defined as:

$$E_{tot}(P) = 2A_P \cos\left(\frac{kdsin\theta}{2}\right) e^{i\left(\frac{k(r_1+r_2)}{2} - \omega t\right)} \quad (3.33)$$

So the amplitude

$$A_{tot}(P) = 2A_P \cos\left(\frac{kdsin\theta}{2}\right) \quad (3.34)$$

Noting that:

At  $\theta = 0$ ;  $2A(0)\cos(0) = 2A(0)$ , therefore

$$\frac{A_{tot}(\theta)}{A_{tot}(0)} = \frac{A(\theta)}{A(0)} \cos\left(\frac{kdsin\theta}{2}\right) \quad (3.35)$$

The intensity is related to the amplitude

$$\frac{I_{tot}(\theta)}{I_{tot}(0)} = \frac{A(\theta)^2}{A(0)^2} \cos^2\left(\frac{kdsin\theta}{2}\right) \quad (3.36)$$

Since the propagating wave is cylindrical, the amplitude is proportional to  $1/\sqrt{r}$ , so the intensity became:

$$\frac{I_{tot}(\theta)}{I_{tot}(0)} = \frac{1}{1} \frac{\sqrt{r(\theta)}}{\sqrt{r(0)}} \cos^2\left(\frac{kdsin\theta}{2}\right) = \cos\theta \cos^2\left(\frac{kdsin\theta}{2}\right) \quad (3.37)$$

In term of the distance  $x$  from midpoint to P:

$$\frac{I_{tot}(x)}{I_{tot}(0)} = \frac{D}{\sqrt{x^2 + D^2}} \cos^2\left(\frac{xkd}{2\sqrt{x^2 + D^2}}\right) \quad (3.38)$$

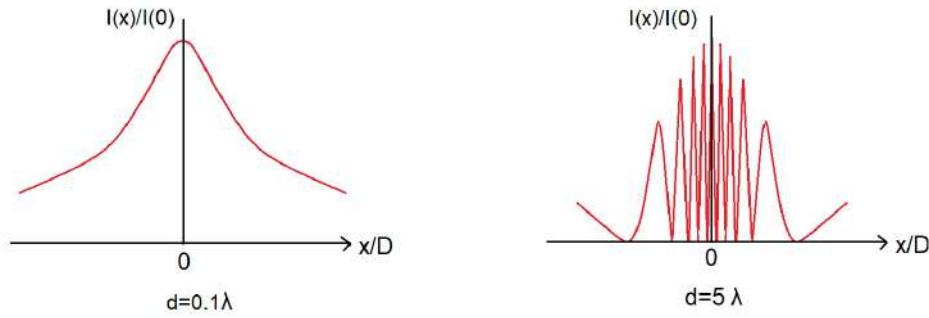


Figure 3.8: Intensity shape in case of  $d \ll \lambda$  and  $d \gg \lambda$

The intensity will be maximum at the midpoint of the screen and decreases as it moves away. Moreover, in these conditions, there is a relation between  $d$  and  $\lambda$ . For  $d \ll \lambda$  the interference is irrelevant because waves can not be out of phase while increasing  $d \gg \lambda$  the interference is noticeable and the maxima occur where the path differ by an integral multiple of the wavelength.

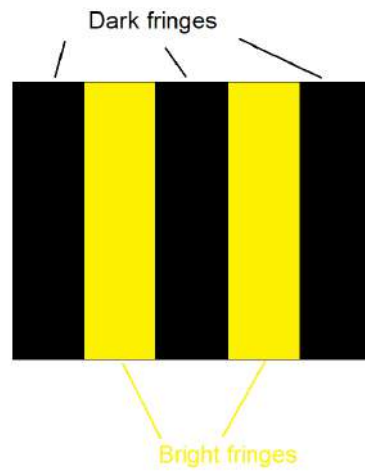


Figure 3.9: Fringes representation on a screen

$$\sin\theta = \frac{m\lambda}{d}; \quad m = 0, 1, 2, \dots \quad (3.39)$$

$$\sin\theta = \frac{(2m + 1)\lambda}{2d}; \quad m = 0, 1, 2, \dots \quad (3.40)$$

### 3.2.2 N-slit Interference

It is possible to extend the previous equations in the case of  $N$  equally spaced slits, called also diffraction grating. In this case, 5 slits are considered:

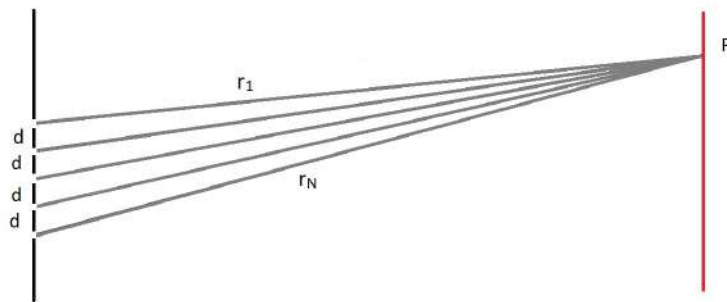


Figure 3.10: Schematic representation of N-slits configuration

In far-field conditions, the distance of to the screen is much higher than  $(N - 1)d$ , total span. The paths to a point P can be considered parallel and with equal amplitudes.

$$r_n = r_1 + (n - 1)dsin\theta \quad (3.41)$$

So the total wave at angle  $\theta$  can be expressed as:

$$E_{tot}(\theta) = \sum_{n=1}^N E_n = A(\theta) \frac{\sin(\frac{1}{2}Ndsin\theta)}{\sin(\frac{1}{2}dsin\theta)} (e^{i(kr_1 - \omega t)} e^{ik((N-1)/2)dsin\theta}) \quad (3.42)$$

with:

$$A_{tot}(\theta) = A(\theta) \frac{\sin(\frac{1}{2}Ndsin\theta)}{\sin(\frac{1}{2}dsin\theta)} = A(\theta) \frac{\sin(N\alpha/2)}{\sin(\alpha/2)} \quad (3.41)$$

$\alpha$  is the phase difference between adjacent paths.

$$\alpha = kdsin\theta = \frac{2\pi dsin\theta}{\lambda} \quad (3.43)$$

As before in midpoint of the screen, where  $\theta = 0$ :

$$\frac{A_{total}(\alpha)}{A_{total}(0)} = \frac{sin(N\alpha/2)}{N sin(\alpha/2)} \quad (3.44)$$

From which we can define the intensity for  $\theta = 0$ :

$$\frac{I_{total}(\alpha)}{I_{total}(0)} = \left( \frac{sin(N\alpha/2)}{N sin(\alpha/2)} \right)^2 \quad (3.45)$$

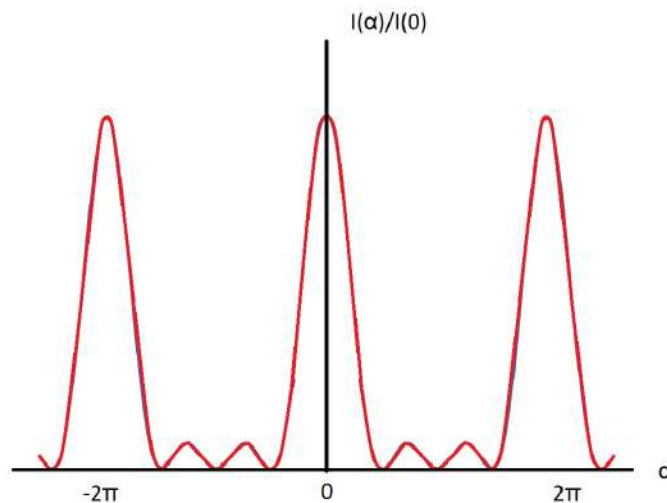


Figure 3.11: Intensity plot in case of  $N=4$  slits

For large angles, the amplitude doesn't affect the locations of maxima and minima, but act on the envelope of the sine function. Moreover, from Figure 3.11 it is possible observe that the maximum in  $\theta = 0$  is 1 and has a period of  $2\pi$ : every  $2\pi$  a totally constructive interference is present. Instead, the zeros of destructive interference are verified for  $N\alpha/2 = m\pi$ , with  $m$  odd numbers. Increasing the number of slits, the side peaks became negligible obtaining the constructive interference only every  $2\pi$ .

## Chapter 4

# Study of Interference on RFCN

This thesis's aim is the implementation of interference of light on Reconfigurable FCN. The main issue of RFCN is the high density of independent and nanometric electrodes needed to induce an electric field on the molecules, enabling the information propagation.

As seen in chapter 3, when a source passes through slits generates secondary sources, equal to the original one, that during propagation interfere. This interference can be constructive, so there is a generation of a field that is equal to the sum of the sources or can be destructive, obtaining a null or quasi null field. Therefore, it is possible to set physical parameters to obtain a specific pattern of interference. The constructive interference is localized in correspondence of the molecules that have to be in a hold state to realize logic operations.

### 4.1 Definition of Interference's patterns

As the first step, the pattern of interference has been realized and made compatible with the grid of molecules of the RFCN. Therefore, considering the dimension of a molecular block, as we can see from equations 2.4 and 2.5, the thickness is about 6 nm. To realize fringes of 6 nm is important to consider the equation that determined the points of bright and dark fringes. For a general N-slit:

bright fringes are located in :

$$\sin\theta = \frac{m\lambda}{d}; m = 0, 1, 2, \dots \quad (4.1)$$

while dark fringes:

$$\sin\theta = \frac{(2m + 1)\lambda}{Nd}; m = 0, 1, 2, \dots \quad (4.2)$$

The distance between fringes  $\Delta x$ , can be defined considering a small angle:  $\sin\theta \cong \theta$

$$\Delta x = \frac{\lambda D}{d} \quad (4.3)$$

where  $D$  is the distance of the slits from the screen;  $d$  is the slits separation and  $\lambda$  is the wavelength. At this point, considering that to obtain the interference effect  $D \gg d \gg \lambda$  and the thickness of the fringes should be  $\Delta x = 6 \text{ nm}$ . Therefore the parameters can be set:

- $d = 9 \text{ }\mu\text{m}$
- $D = 300 \text{ }\mu\text{m}$
- $\Delta x = 6 \text{ nm}$
- $\lambda = \frac{\Delta x \cdot d}{D} = 0.18 \text{ nm}$
- $f = \frac{c}{\lambda} \cong 1.6 \cdot 10^{18}$

With these values the plot of the fringes have been made, considering as source a sinusoidal wave expressed as:

$$E = A \cdot \sin(\omega t + \Phi) \quad (4.4)$$

where  $\omega$  is the angular frequency of the wave equal to  $2\pi f$  and  $\Phi$  is the phase of the wave.

Depending on the number of the slits and their position, different patterns can be obtained:

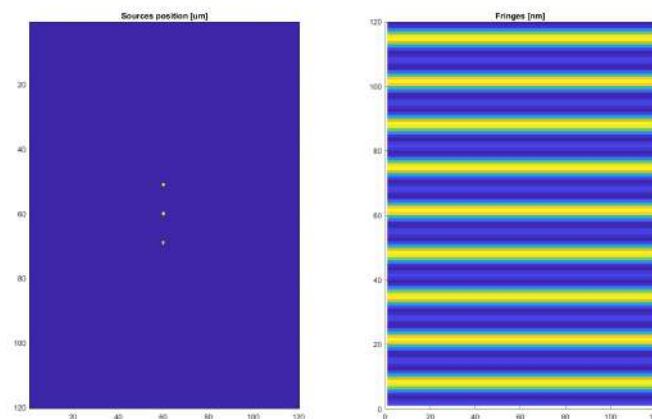


Figure 4.1: Horizontal fringes obtained by 3 slits

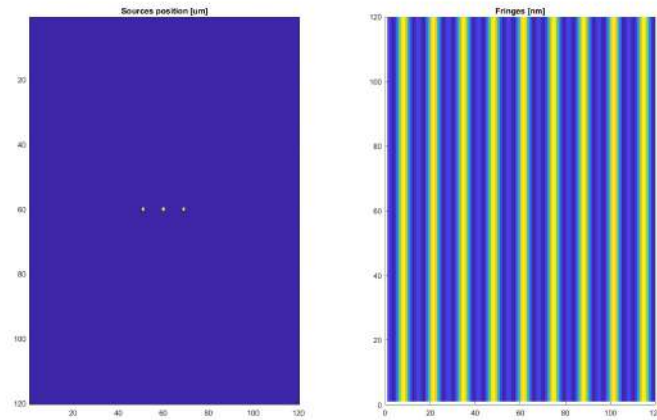


Figure 4.2: Vertical fringes obtained by 3 slits

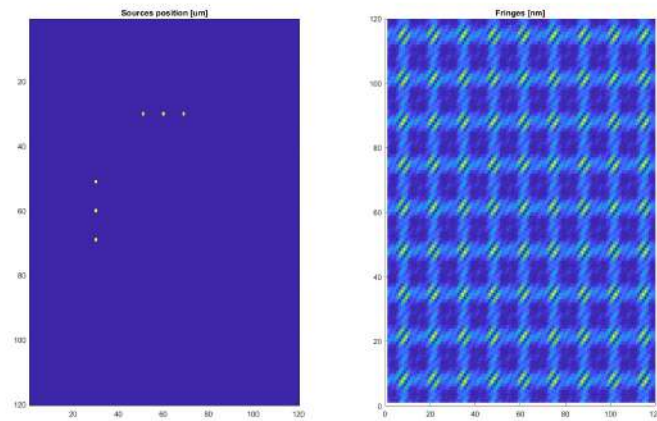


Figure 4.3: Combination of vertical and horizontal fringes obtained by 6 slits  
(Grid)

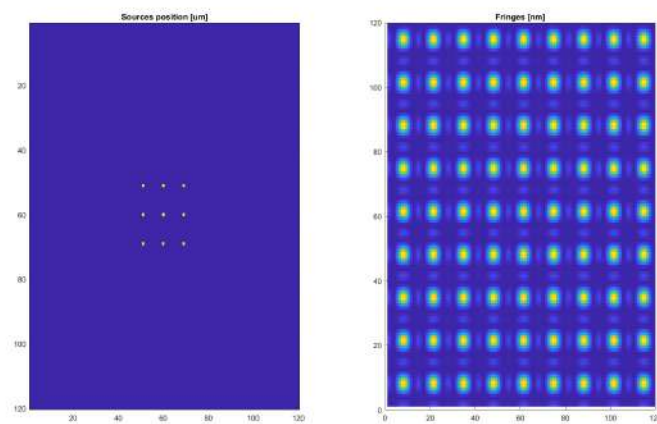


Figure 4.4: Pointing fringes obtained by 9 slits

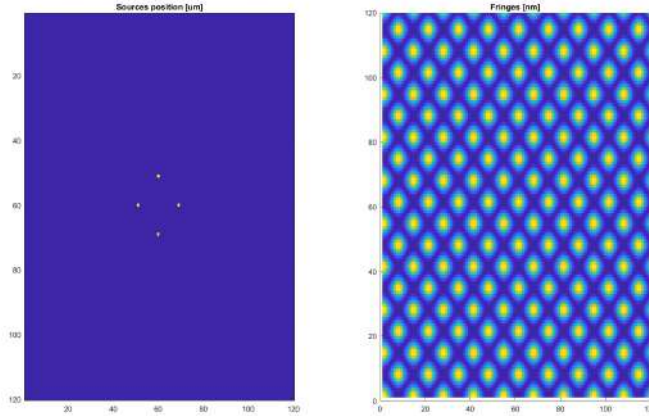


Figure 4.5: Pointing fringes obtained by 4 slits

These plots are obtained using the 2-D fast Fourier transform (fft2).

The brightening zones correspond to the constructive interference of the sources, while the dark zones are the destructive interference. As a consequence, a higher intensity of the field is present in the bright zone concerning the dark ones. As shown in the tables 4.1, 4.2 and 4.3, representing the module of the fields in each point of a screen, there is a high difference between areas with constructive interference and destructive interference. Using this difference, it is possible to induce only molecules under bright fringes to enter the hold state and enable the propagation of a logic state.

0,341056539	0,341056539	0,341056539	0,341056539	0,341056539	0,341056539	0,341056539	0,341056539	0,341056539
1,617706257	1,617706257	1,617706257	1,617706257	1,617706257	1,617706257	1,617706257	1,617706257	1,617706257
1,891134808	1,891134808	1,891134808	1,891134808	1,891134808	1,891134808	1,891134808	1,891134808	1,891134808
0,759280892	0,759280892	0,759280892	0,759280892	0,759280892	0,759280892	0,759280892	0,759280892	0,759280892
0,016831886	0,016831886	0,016831886	0,016831886	0,016831886	0,016831886	0,016831886	0,016831886	0,016831886
1,987823183	1,987823183	1,987823183	1,987823183	1,987823183	1,987823183	1,987823183	1,987823183	1,987823183
2,82674008	2,82674008	2,82674008	2,82674008	2,82674008	2,82674008	2,82674008	2,82674008	2,82674008
4,32216515	4,32216515	4,32216515	4,32216515	4,32216515	4,32216515	4,32216515	4,32216515	4,32216515
5,87419260	5,87419260	5,87419260	5,87419260	5,87419260	5,87419260	5,87419260	5,87419260	5,87419260
5,53982961	5,53982961	5,53982961	5,53982961	5,53982961	5,53982961	5,53982961	5,53982961	5,53982961
4,52573537	4,52573537	4,52573537	4,52573537	4,52573537	4,52573537	4,52573537	4,52573537	4,52573537
2,03288619	2,03288619	2,03288619	2,03288619	2,03288619	2,03288619	2,03288619	2,03288619	2,03288619
0,938548941	0,938548941	0,938548941	0,938548941	0,938548941	0,938548941	0,938548941	0,938548941	0,938548941
0,061274654	0,061274654	0,061274654	0,061274654	0,061274654	0,061274654	0,061274654	0,061274654	0,061274654
1,215642151	1,215642151	1,215642151	1,215642151	1,215642151	1,215642151	1,215642151	1,215642151	1,215642151
1,215642151	1,215642151	1,215642151	1,215642151	1,215642151	1,215642151	1,215642151	1,215642151	1,215642151
0,061274654	0,061274654	0,061274654	0,061274654	0,061274654	0,061274654	0,061274654	0,061274654	0,061274654
0,938548941	0,938548941	0,938548941	0,938548941	0,938548941	0,938548941	0,938548941	0,938548941	0,938548941
2,032886194	2,032886194	2,032886194	2,032886194	2,032886194	2,032886194	2,032886194	2,032886194	2,032886194
3,525735375	3,525735375	3,525735375	3,525735375	3,525735375	3,525735375	3,525735375	3,525735375	3,525735375
4,539829605	4,539829605	4,539829605	4,539829605	4,539829605	4,539829605	4,539829605	4,539829605	4,539829605
5,874192600	5,874192600	5,874192600	5,874192600	5,874192600	5,874192600	5,874192600	5,874192600	5,874192600
4,322165151	4,322165151	4,322165151	4,322165151	4,322165151	4,322165151	4,322165151	4,322165151	4,322165151
2,826740081	2,826740081	2,826740081	2,826740081	2,826740081	2,826740081	2,826740081	2,826740081	2,826740081
1,987823183	1,987823183	1,987823183	1,987823183	1,987823183	1,987823183	1,987823183	1,987823183	1,987823183
0,016831886	0,016831886	0,016831886	0,016831886	0,016831886	0,016831886	0,016831886	0,016831886	0,016831886
0,759280892	0,759280892	0,759280892	0,759280892	0,759280892	0,759280892	0,759280892	0,759280892	0,759280892
1,891134808	1,891134808	1,891134808	1,891134808	1,891134808	1,891134808	1,891134808	1,891134808	1,891134808
1,617706257	1,617706257	1,617706257	1,617706257	1,617706257	1,617706257	1,617706257	1,617706257	1,617706257
0,341056539	0,341056539	0,341056539	0,341056539	0,341056539	0,341056539	0,341056539	0,341056539	0,341056539

Table 4.1: Field values of horizontal fringes on a screen

0,016831886	1,987823183	2,82674008	4,32216515	5,87419260	5,53982961	4,52573537	2,03288619	0,938548941	0,061274654
0,016831886	1,987823183	2,82674008	4,32216515	5,87419260	5,53982961	4,52573537	2,03288619	0,938548941	0,061274654
0,016831886	1,987823183	2,82674008	4,32216515	5,87419260	5,53982961	4,52573537	2,03288619	0,938548941	0,061274654
0,016831886	1,987823183	2,82674008	4,32216515	5,87419260	5,53982961	4,52573537	2,03288619	0,938548941	0,061274654
0,016831886	1,987823183	2,82674008	4,32216515	5,87419260	5,53982961	4,52573537	2,03288619	0,938548941	0,061274654
0,016831886	1,987823183	2,82674008	4,32216515	5,87419260	5,53982961	4,52573537	2,03288619	0,938548941	0,061274654
0,016831886	1,987823183	2,82674008	4,32216515	5,87419260	5,53982961	4,52573537	2,03288619	0,938548941	0,061274654
0,016831886	1,987823183	2,82674008	4,32216515	5,87419260	5,53982961	4,52573537	2,03288619	0,938548941	0,061274654
0,016831886	1,987823183	2,82674008	4,32216515	5,87419260	5,53982961	4,52573537	2,03288619	0,938548941	0,061274654
0,016831886	1,987823183	2,82674008	4,32216515	5,87419260	5,53982961	4,52573537	2,03288619	0,938548941	0,061274654

Table 4.2: Field values of vertical fringes on a screen

0,113288865	0,296594099	2,797186337	2,0328862	2,62570793	2,497992629	2,728677089	2,776493431	0,140036639	0,181380462
0,296594099	0,776493431	2,826740081	4,3221652	5,87419260	5,539829605	4,525735375	2,032886194	0,36662068	0,474860215
2,079718634	2,82674008	4,290440549	8,3747647	13,02475227	10,807540069	9,475448564	4,400501610	2,334642806	2,728677089
3,032886194	4,32216515	8,374764749	9,4786626	17,11641702	14,824658955	31,019851731	8,933609260	2,512855525	3,254740336
3,625707928	5,87419260	13,024752273	18,1164170	20,85630866	20,896237740	19,065730612	11,996889873	3,245643899	4,203874043
3,497992629	5,53982961	10,807540069	18,8246590	19,89623774	18,080145643	18,116920262	10,121496187	3,087774710	3,999396223
2,728677089	4,52573537	9,475448564	10,0198517	14,06573061	28,116920262	16,377918818	9,848529035	2,136821917	2,767688160
2,776493431	2,03288619	4,400501610	8,9336093	13,99688987	10,121496187	9,848529035	4,221651514	2,959825402	2,243200184
0,140036639	0,36662068	2,334642806	2,5128555	3,24564390	3,087774710	2,136821917	2,959825402	0,173099627	0,224204827
0,043272496	0,000959273	2,113288865	7,41241582	8,77649343	4,002931184	2,954148280	2,660295892	0,296594099	0,003492129
0,181380462	0,474860215	2,728677089	3,25474034	4,20387404	3,999396223	2,767688160	3,243200184	0,224204827	0,290398109
0,296594099	0,776493431	2,826740081	5,32216515	6,87419260	6,539829605	4,525735375	2,032886194	0,666206802	0,474860215
0,181380462	0,474860215	2,728677089	3,25474034	4,20387404	3,999396223	2,767688160	2,243200184	0,224204827	0,290398109
0,140036639	0,36662068	2,334642806	2,51285552	3,24564390	3,087774710	2,136821917	2,959825402	0,173099627	0,224204827
2,076493431	2,032886194	7,400501610	11,93360926	17,99688987	17,121496187	11,848529035	5,322165151	2,959825402	2,243200184
2,728677089	3,525735375	10,475448564	11,01985173	10,06573061	18,116920262	16,377918818	7,848529035	2,136821917	2,767688160
3,497992629	4,539829605	13,807540069	34,82465896	17,89623774	19,080145643	38,116920262	10,121496187	3,087774710	3,999396223
3,625707928	5,874192600	25,024752273	37,11641702	20,85630866	20,896237740	20,065730612	11,996889873	3,245643899	4,203874043
3,032886194	4,322165151	9,374764749	26,47866263	17,11641702	19,824658955	11,019851731	9,933609260	2,512855525	3,254740336
2,079718634	2,826740081	4,290440549	19,37476475	15,02475227	13,807540069	6,475448564	7,400501610	2,334642806	2,728677089
0,296594099	0,776493431	8,267400812	13,22165151	6,87419260	6,539829605	4,525735375	2,032886194	0,36662068	0,474860215
0,002511409	0,006574955	2,393541162	2,04506541	2,058207201	2,055375984	2,038321648	2,017213457	0,003104359	0,004020877
0,113288865	0,296594099	2,079718634	2,03288619	2,625707928	2,497992629	2,728677089	2,776493431	0,140036639	0,181380462

Table 4.3: Field values of fringes grid on a screen combination of vertical and horizontal fringes)

## 4.2 Layout

The Reconfigurable FCN is a regular self-assembled monolayer (SAM), where the Bis-ferrocene molecules anchors on a gold surface [20]. Above the layer, a laser and perforated screens are located to realize the interference's patterns.

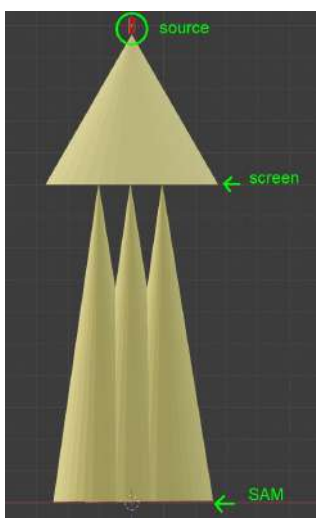


Figure 4.6: Schematic representation of the structure: the source, the perforated screen (3 slits) and the generated secondary sources that hit the SAM

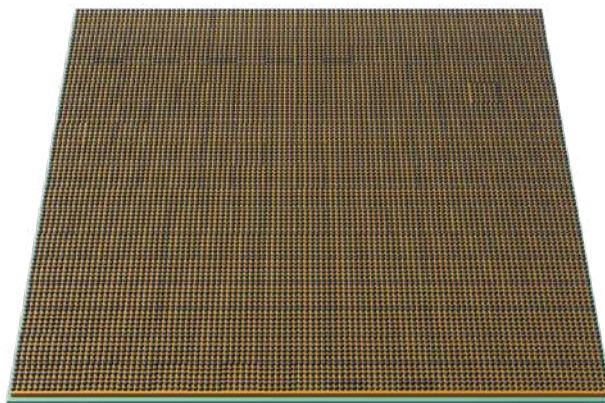


Figure 4.7: SAM representation with gold electrode and dielectric substrate  $SiO_2$

#### 4.2.1 Buried gold layer

As shown in tables 4.1, 4.2 and 4.3, even if in the dark zones of interference the module of the field is quasi zero, there are positive values in all the structure. This gives all the molecules the possibility to enter the hold state. Therefore, to enabling the propagation of the information only in the bright areas, a negative plane of ground (about  $-2V/nm$ ) is needed in the layer. For this reason, a "buried" layer of gold is inserted in the structure, using a dielectric  $SiO_2$  material as separation with the SAM: the negative ground operates as a difference contribution on the field generated by interference, inducing a reset in all the molecules that are in dark areas.

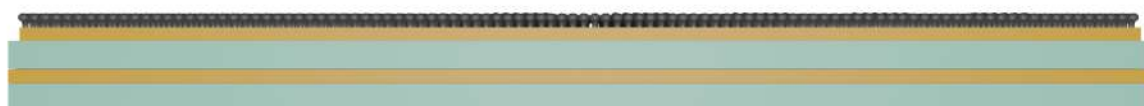


Figure 4.8: Buried gold layer in  $SiO_2$  dielectric

#### 4.2.2 Grid shape of SAM

The interference patterns that have proved most useful to realize the logic operations are the ones that produce horizontal, vertical and grid fringes. These patterns involves in work always the same molecules leaving the other fixes in RESET state.



Figure 4.9: Vertical and Horizontal fringes on SAM

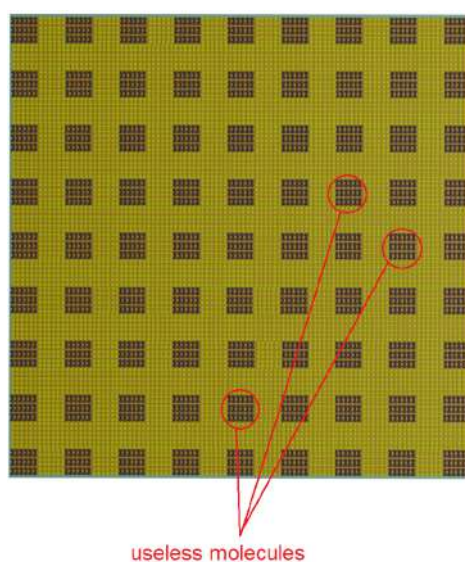


Figure 4.10: Useless molecules in chosen fringes configuration

The idea is the implementation of Electron-beam lithography (EBL) and plasma ashing techniques, to obtain a grid shape of the dielectric substrate [26], over which deposit the gold for the molecules, eliminating as consequence the useless molecules. The thickness of the lines of the grid must be around 6 nm, as the dimension of the bright fringes: the EBL technology allows the realization of a homogeneous pattern until 50 nm; below this thickness, there are problems in terms of reproducibility and throughput. Therefore, to reach the sub- 10 nm dimension is used the plasma ashing treatment where the plasma forms in vacuum and the free radicals hit the wafer substrate, creating the reduction of the lines' thickness.

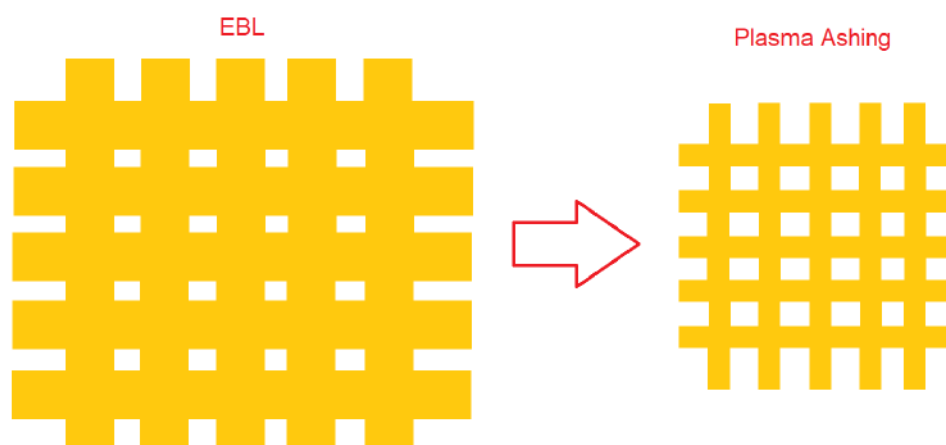


Figure 4.11: Electro beam lithography and plasma ashing processes

Over this substrate the SAM is created:



Figure 4.12: SAM representation

### 4.2.3 Electrodes

At the corners of the grid layer, nanoelectrodes have been positioned. They induce a field on the molecules at the intersections of the grid, needed to manage different situations:

- The field that reaches molecules is sinusoidal, varying between positive and negative values. When it is in the range between 0 and the positive peak, the HOLD state is verified. As soon as the wave moves toward negative values, the RESET condition is induced and the information is lost. When there is the necessity to maintain the data in a specific point of the layer, the electrodes are enabled and even if the wave became negative, the data is not lost.

- The data has to be maintained when the screen is changed to generate a different pattern of interference on the layer: the time needed to change the screen can be higher concerning the extinguish time of the previous interference field and the information can be lost.
- A reset state has to be induced on some molecules to allow the realization of an inverter: the inversion step is realized using a grid pattern, where all the molecules are under bright fringes and the hold state is enabled. In this case, there is the necessity to turn off the molecules at the intersection to allow the inversion step.

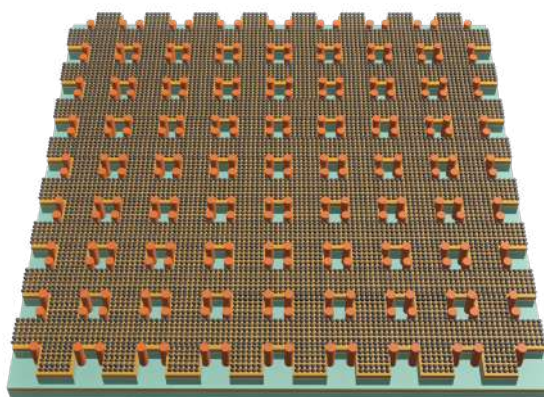


Figure 4.13: Complete layout of the structure

The voltage imposed on the electrodes depends on the field of the interference's pattern. Considering the previous tables (4.1, 4.2, 4.3) The higher values are obtained in the case of grid pattern, where the maximum module of the field in the intersection have the value of  $20 V$ . Imposing the general reset of  $-2 V/nm$  of the buried layer, the effective wave has the positive peak at  $+18 V$  and the negative at  $-22 V$ . So the electrodes, have to impose a HOLD of  $+18 V/nm$  and a RESET of  $-22 V$ , to ensure the correct operations.

Moreover, the electrodes are not all independent: the ones on the corners of the same intersection works simultaneously in order to induce the field in the intersection area.

Each time is possible to chose which group of electrodes, has to be tuned on to hold the data in a specific zone of the SAM.

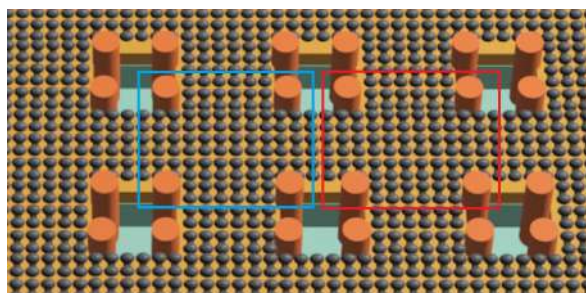


Figure 4.14: The electrodes on the corner of an intersection work together to maintain the information

## Chapter 5

# Logic operations simulation

The structure illustrated in the previous sections is here validate performing logic operations. As first assumption the same study on the molecule made for standard RFCN, through Molecular Simulator Quantum-Dot Cellular Automata Torino (MoSQuiTo)[11][20], has been considered (see section 2.5). As consequence, the simulation of the structure has been developed with a Self-Consistent Electrostatic Potential Algorithm (SCERPA)[12]

### 5.1 Simulation Structure

In order to use SCERPA for molecular behaviour simulations in different logic operations, some parameters have to be settled:

- Molecular distance:

The distance between molecules have been imposed in Angstrom ( $10^{-10}$  m)

```
5 % Molecules distance
6 - circuit.dist_z = 10;
7 - circuit.dist_y = 20;
```

Figure 5.1: Molecular distance settled on SCERPA

- Drivers:

The behaviour of driver molecules for all the steps of the simulation is a fundamental parameter. In the Figure 5.2, the behaviour of the drivers in a NAND simulation is reported: After the firsts steps, the drivers are not necessary.

```

circuit.Values_Dr = {
'Dr1' +4.5 +4.5 +4.5 0 0 0 0 0 'end'
'Dr2' -4.5 -4.5 -4.5 0 0 0 0 0 'end'
'Dr3' +4.5 +4.5 0 0 0 0 0 0 'end'
'Dr4' -4.5 -4.5 0 0 0 0 0 0 'end'
'Dr5' -4.5 -4.5 0 0 0 0 0 0 'end'
'Dr6' +4.5 +4.5 0 0 0 0 0 0 'end'
}

```

Figure 5.2: Drivers values over time for NAND simulation

- Molecular Structure:

By using SCERPA, it is possible to impose the circuit structure, in order to evaluate each molecule attitude. Plotting the code, the final structure is shown in Figure 5.4.

```

circuit.structure = {
0 0 0 0 0 0 0 0 0 'Dr3' 'Dr4' 'Dr3' 'Dr4' 'Dr3' 'Dr4' 0 0 0 0 0 0
0 0 0 0 0 0 0 0 0 '4' '4' '4' '4' '4' '4' 0 0 0 0 0 0
0 0 0 0 0 0 0 0 0 '4' '4' '4' '4' '4' '4' 0 0 0 0 0 0
0 0 0 0 0 0 0 0 0 '1' '1' '1' '1' '1' '1' 0 0 0 0 0 0
0 0 '2' '2' '2' '2' '2' '7' '5' '5' '5' '5' '5' '5' '7' '2' '2' '2' '2' '2'
0 0 '2' '2' '2' '2' '2' '7' '5' '5' '5' '5' '5' '5' '7' '2' '2' '2' '2' '2'
0 0 0 0 0 0 0 0 0 '1' '1' '1' '1' '1' '1' 0 0 0 0 0 0
0 0 0 0 0 0 0 0 0 '4' '4' '4' '4' '4' '4' 0 0 0 0 0 0
0 0 0 0 0 0 0 0 0 '6' '6' '6' '6' '6' '6' 0 0 0 0 0 0
'Dr1' 'Dr2' '2' '2' '2' '2' '2' '8' '3' '3' '3' '3' '3' '3' '8' '2' '2' '2' '2' '2'
'Dr1' 'Dr2' '2' '2' '2' '2' '2' '8' '3' '3' '3' '3' '3' '3' '8' '2' '2' '2' '2' '2'
'Dr1' 'Dr2' '2' '2' '2' '2' '2' '8' '3' '3' '3' '3' '3' '3' '8' '2' '2' '2' '2' '2'
0 0 0 0 0 0 0 0 0 '6' '6' '6' '6' '6' '6' 0 0 0 0 0 0
0 0 0 0 0 0 0 0 0 '4' '4' '4' '4' '4' '4' 0 0 0 0 0 0
0 0 0 0 0 0 0 0 0 '1' '1' '1' '1' '1' '1' 0 0 0 0 0 0
0 0 '2' '2' '2' '2' '2' '7' '5' '5' '5' '5' '5' '5' '7' '2' '2' '2' '2' '2'
0 0 '2' '2' '2' '2' '2' '7' '5' '5' '5' '5' '5' '5' '7' '2' '2' '2' '2' '2'
0 0 '2' '2' '2' '2' '2' '7' '5' '5' '5' '5' '5' '5' '7' '2' '2' '2' '2' '2'
0 0 0 0 0 0 0 0 0 '1' '1' '1' '1' '1' '1' 0 0 0 0 0 0
0 0 0 0 0 0 0 0 0 '4' '4' '4' '4' '4' '4' 0 0 0 0 0 0
0 0 0 0 0 0 0 0 0 '4' '4' '4' '4' '4' '4' 0 0 0 0 0 0
0 0 0 0 0 0 0 0 0 'Dr5' 'Dr6' 'Dr5' 'Dr6' 'Dr5' 'Dr6' 0 0 0 0 0 0
};

```

Figure 5.3: Molecular structure description with SCERPA

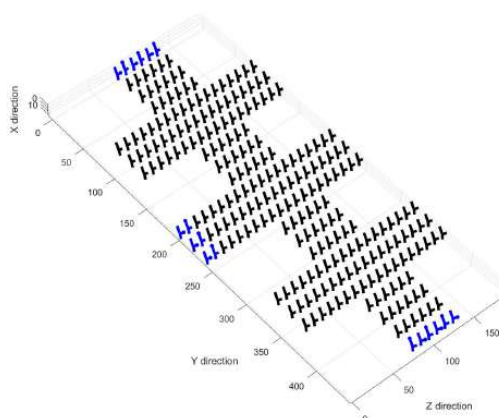


Figure 5.4: Plot of the Molecular description realized with SCERPA

- Clock evolution:

At each molecule, a clock evolution with time is associated: for each step of the simulation, the molecules are defined by the clock conditions.

```

circuit.stack_phase(1,:) = [rst hld hld hld rst hld hld hld];
circuit.stack_phase(2,:) = [rst rst rst hld rst rst rst hld];
circuit.stack_phase(3,:) = [rst hld rst hld hld hld rst rst];
circuit.stack_phase(4,:) = [rst hld rst hld rst hld rst hld];
circuit.stack_phase(5,:) = [rst hld hld hld rst hld hld hld];
circuit.stack_phase(6,:) = [rst hld rst hld hld hld rst rst];
circuit.stack_phase(7,:) = [rst rst hld hld rst rst hld rst];
circuit.stack_phase(8,:) = [rst rst rst hld hld rst rst rst];

```

Figure 5.5: Code of clock evolution

After the setting of all parameters, the simulation of Majority voter, Inverter, NAND, Half Adder and Full Adder have been carried out.

Note that, the simulation 3D plots will put beside the logic plots of the simulation to better understand the propagation. Moreover, to encourage the comprehension of propagation, the behaviors of all molecules will not be reported in the logic plots, but only those necessary for the correctness of the logic operation.

## 5.2 Majority Voter

The first logic operation realized is the Majority voter. It consists of three inputs that converge on a computing cell, which state is determined by the state of inputs [12].

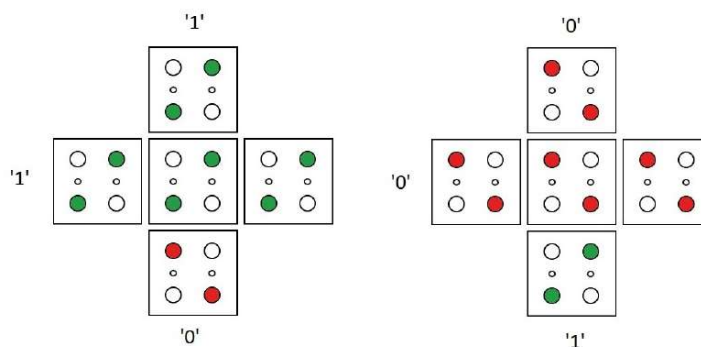


Figure 5.6: Majority voter FCN

Playing with the majority gate, it is possible to obtain both an AND gate and an OR gate, by fixing one of the three inputs respectively at 0 or 1.

A	B	C	Out
0	0	0	0
0	0	1	0
0	1	0	0
0	1	1	1
1	0	0	0
1	0	1	1
1	1	0	1
1	1	1	1

Figure 5.7: True table of Majority voter: by fixing  $A=0$  or  $A=1$ , it is possible obtain the AND or OR logic operations

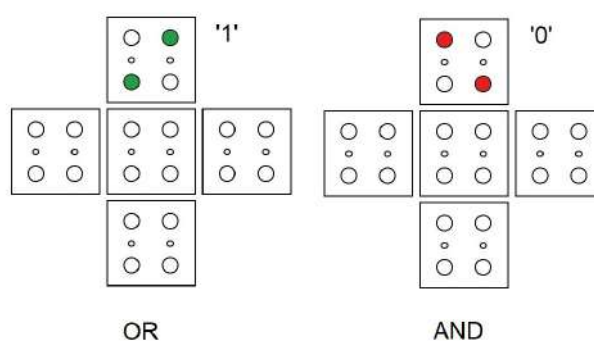


Figure 5.8: AND and OR implementation with Majority Voter

The simulation has been realized considering only one intersection of the SAM. Indeed, to realize the majority voter, it is necessary only to implement a grid fringes pattern and the electrodes to save the resulting data. The input data of the plotted simulation are  $A = 1, B = 1, C = 0$ , therefore the output of the operation is 1.

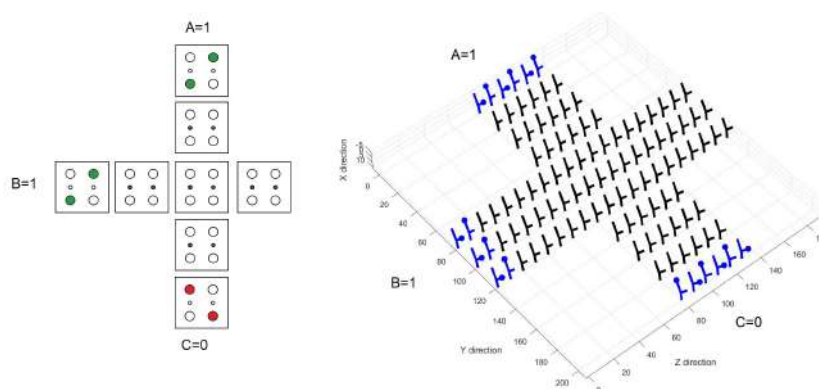


Figure 5.9: Majority voter in initial reset state

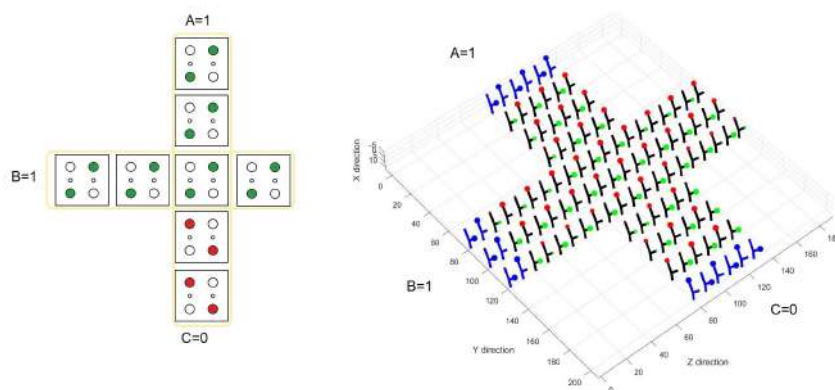


Figure 5.10: Majority voter simulation step 1: Grid fringes

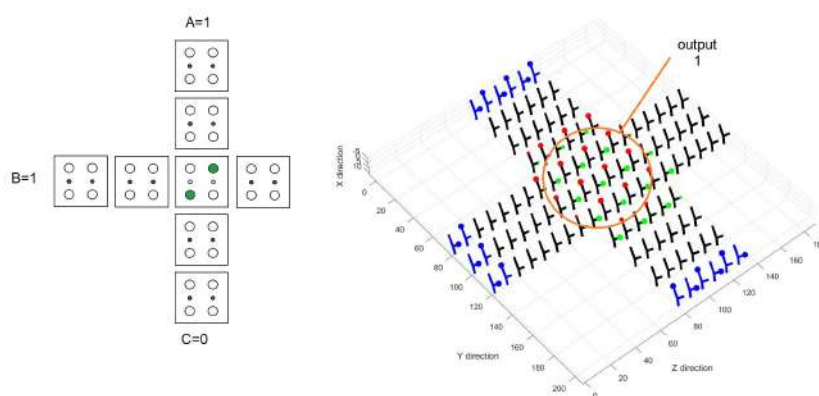


Figure 5.11: Majority voter simulation step 2: Electrodes activations

### 5.3 Inverter

The inverter operation has been realized firstly similarly to the classic FCN implementation.

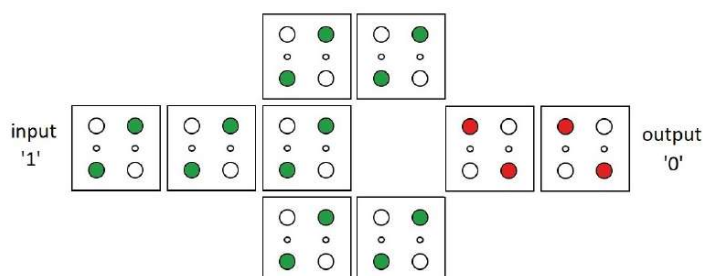


Figure 5.12: Inverter FCN

To realize the inversion the implementation of horizontal, vertical and grid fringes have been necessary: considering as input 0 with seven steps of operation, the inversion is obtained.

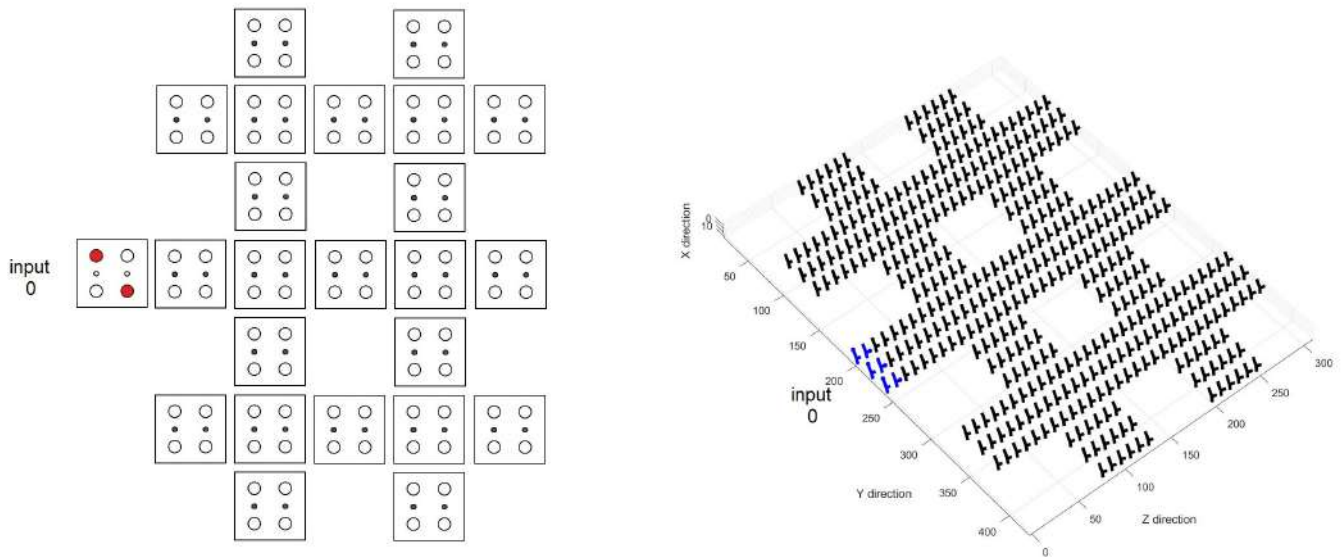


Figure 5.13: Inverter simulation in initial reset state

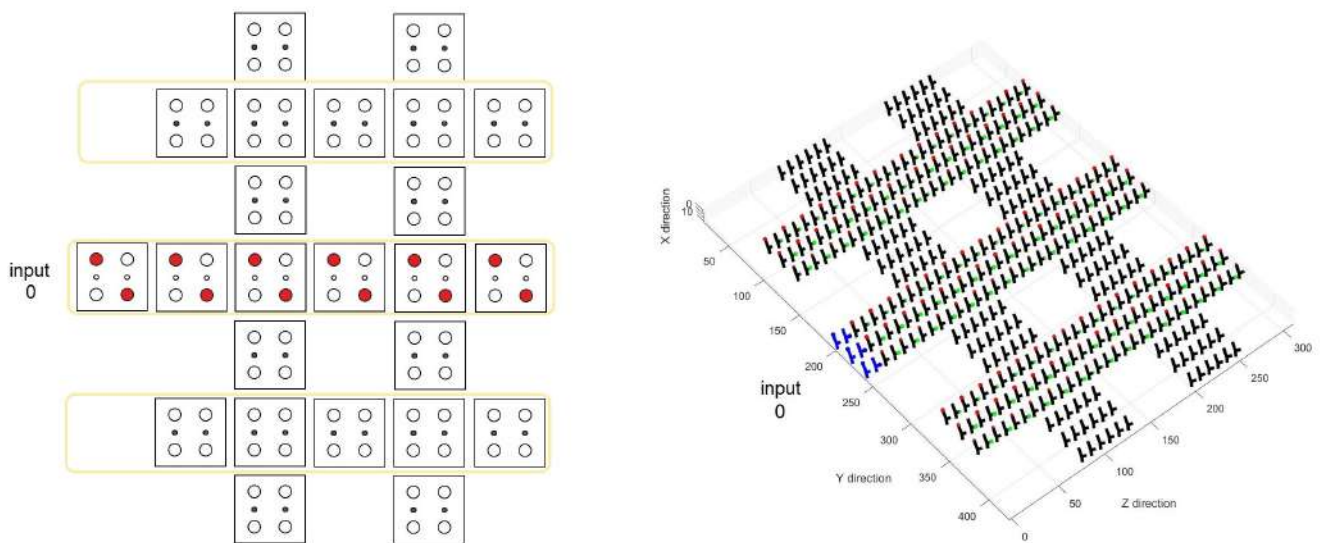


Figure 5.14: Inverter simulation step 1: Horizontal fringes

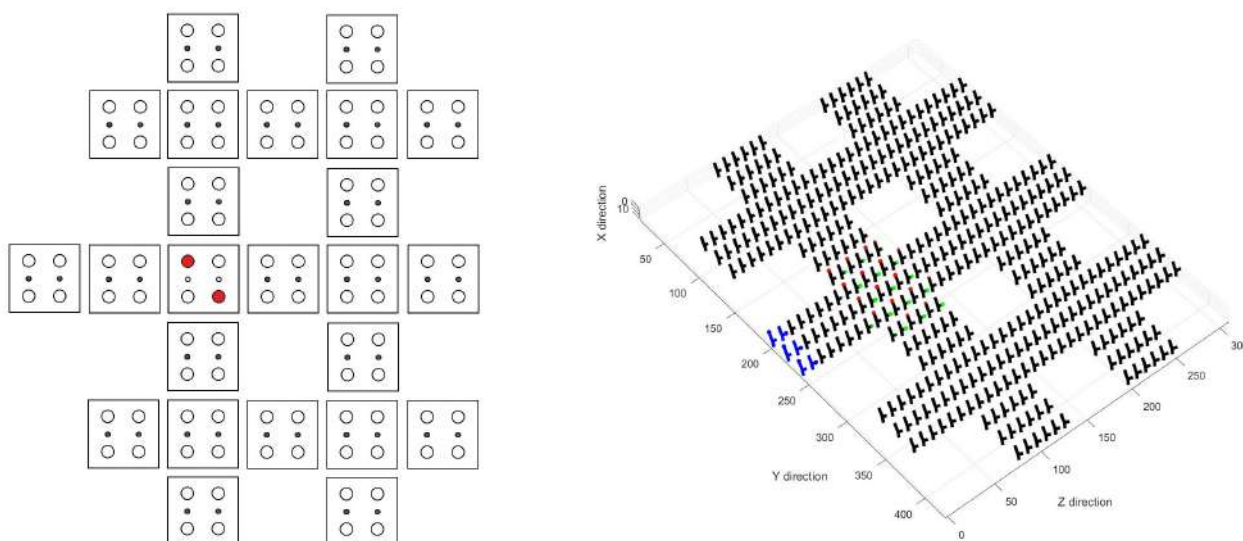


Figure 5.15: Inverter simulation step 2: Electrodes activation

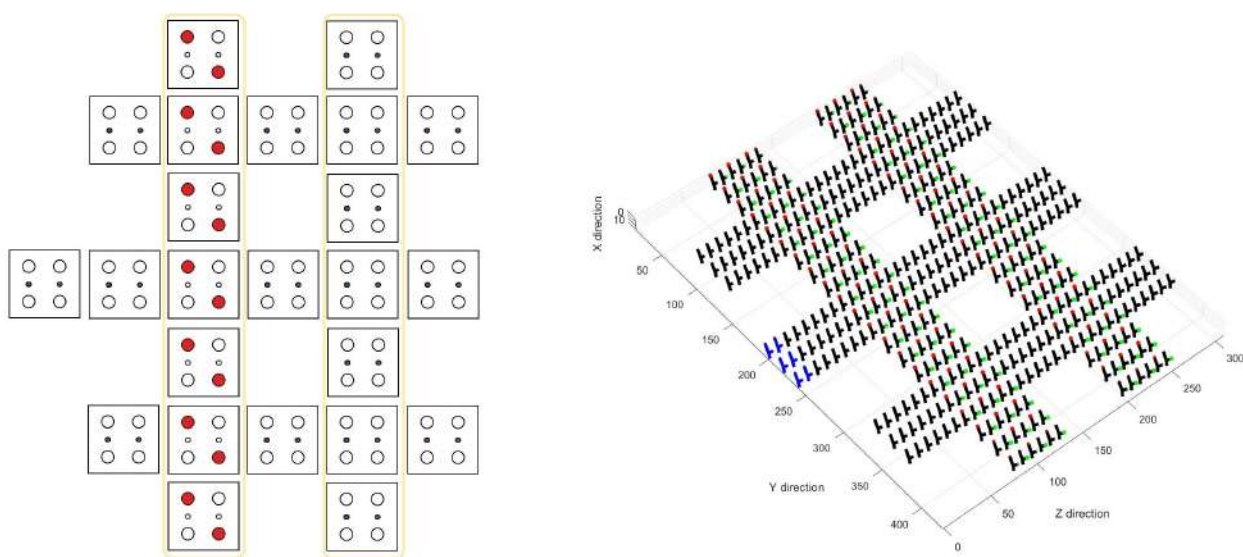


Figure 5.16: Inverter simulation step 3: Vertical fringes

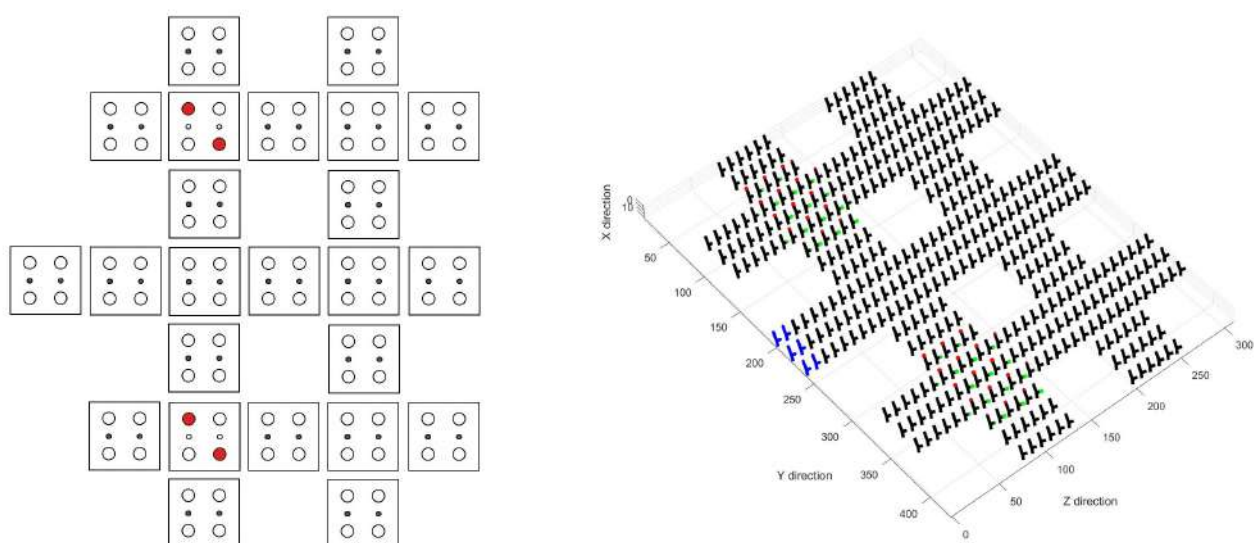


Figure 5.17: Inverter simulation step 4: Electrodes activation

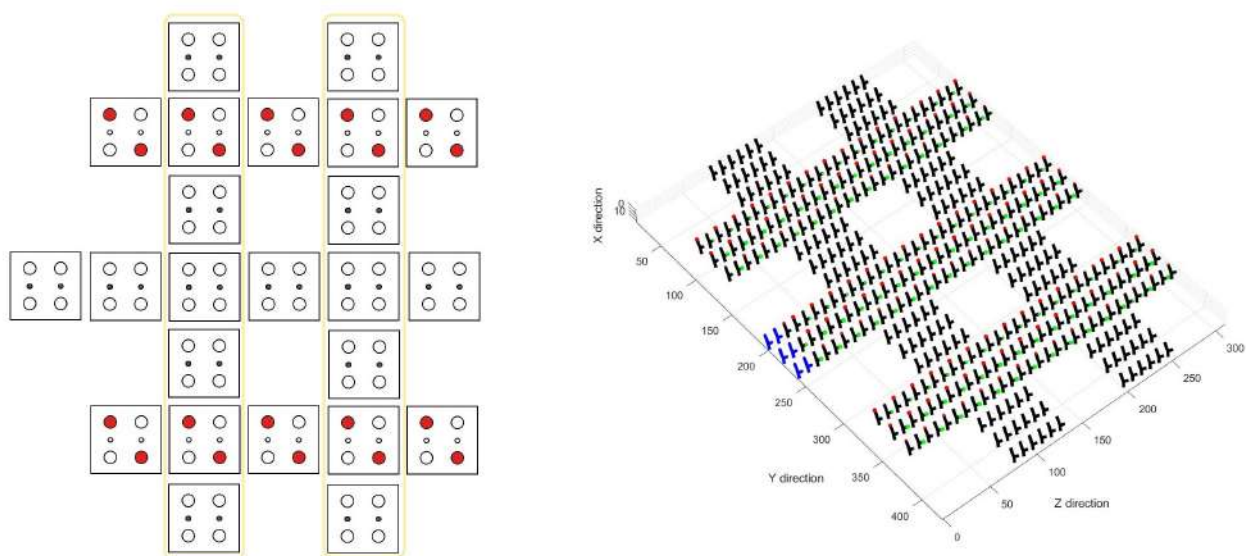


Figure 5.18: Inverter simulation step 5: Horizontal fringes

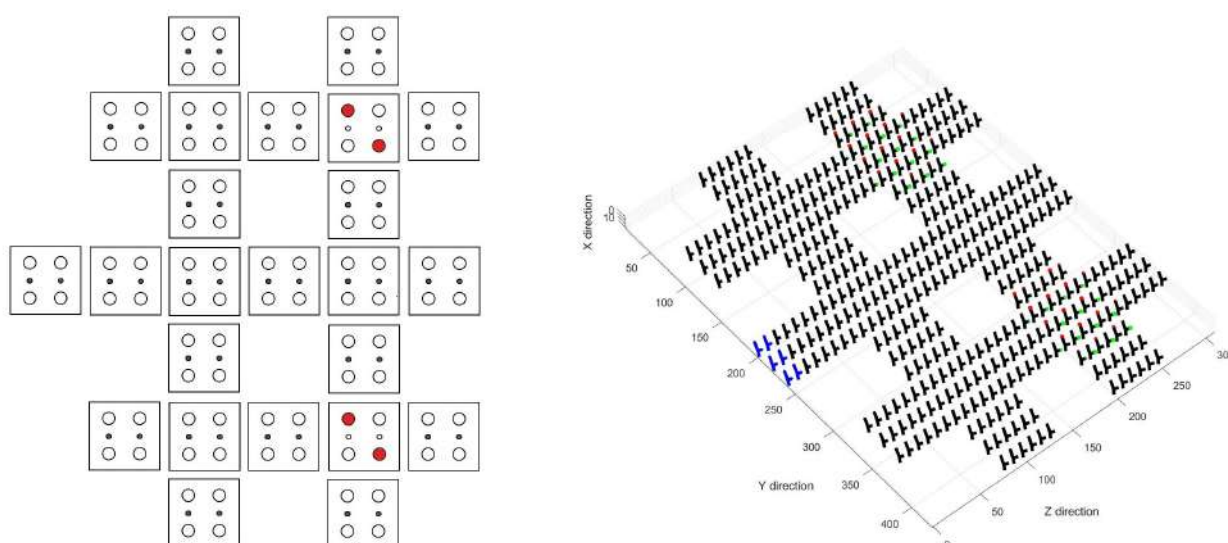


Figure 5.19: Inverter simulation step 6: Electrodes activation

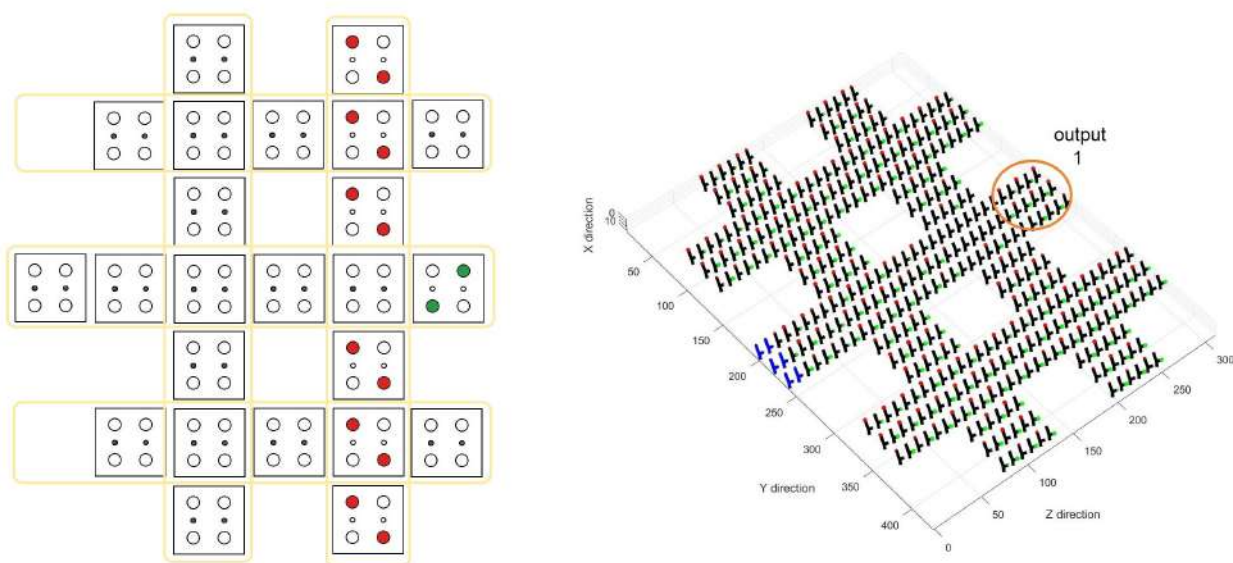


Figure 5.20: Inverter simulation step 7: Grid fringes and Electrode

Successively, it has been implemented employing fewer steps and less area. The structure has been reduced to only one vertical line of molecules and the simulation steps 5 and 6 have been eliminated. In this case, the simulation input chosen is 1

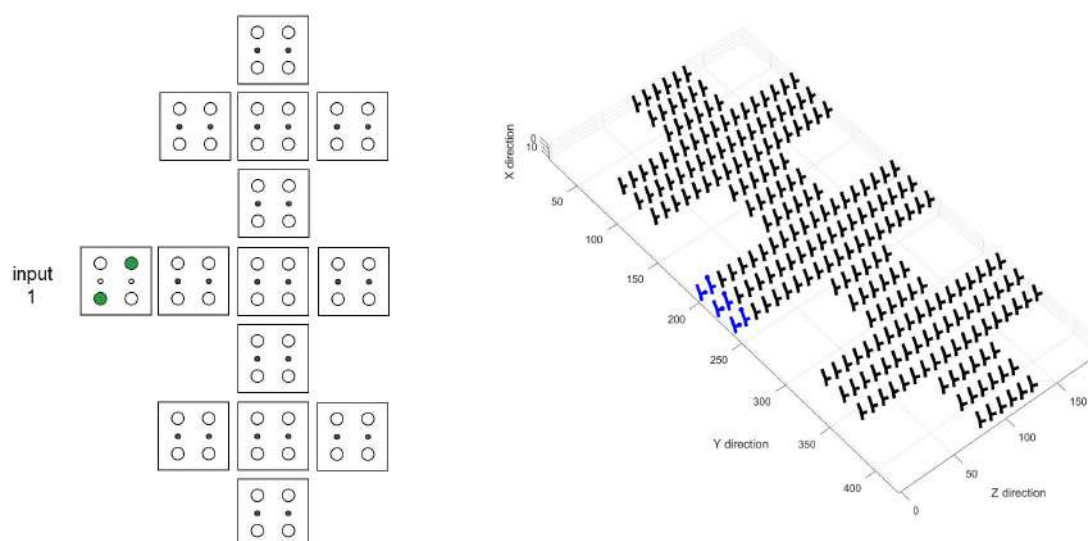


Figure 5.21: Initial reset state

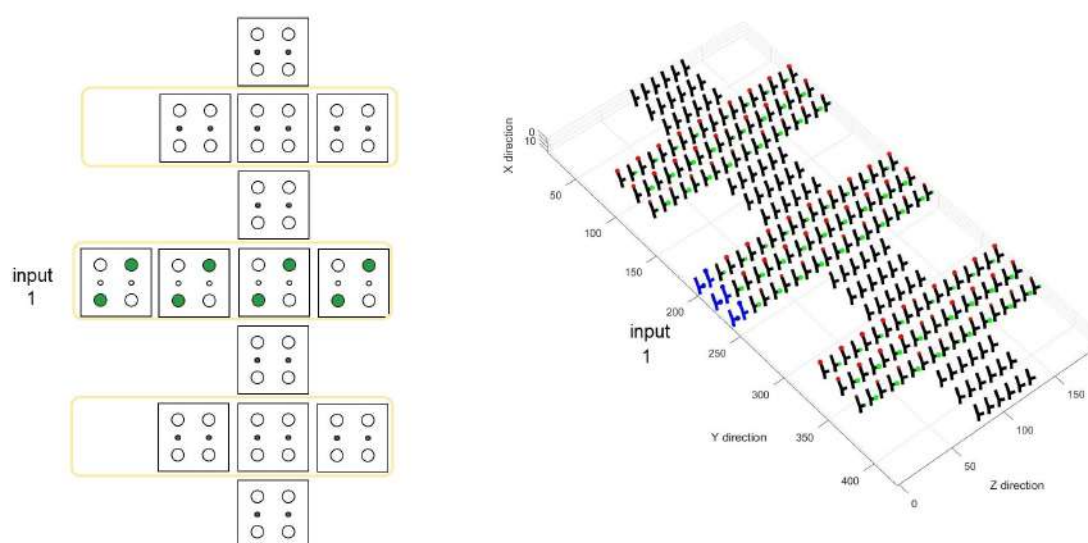


Figure 5.22: Simulation step 1: Horizontal fringes

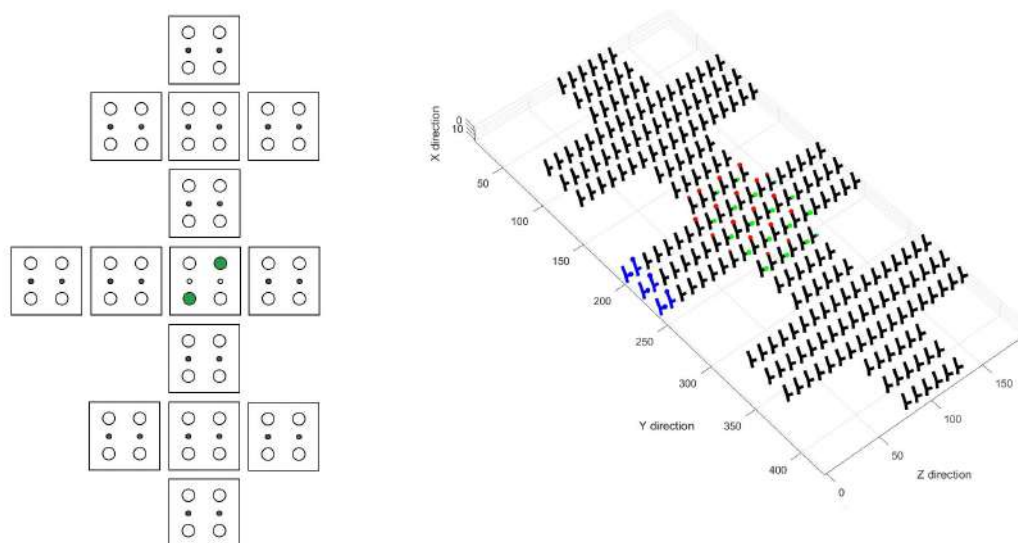


Figure 5.23: Simulation step 2: Electrodes activation

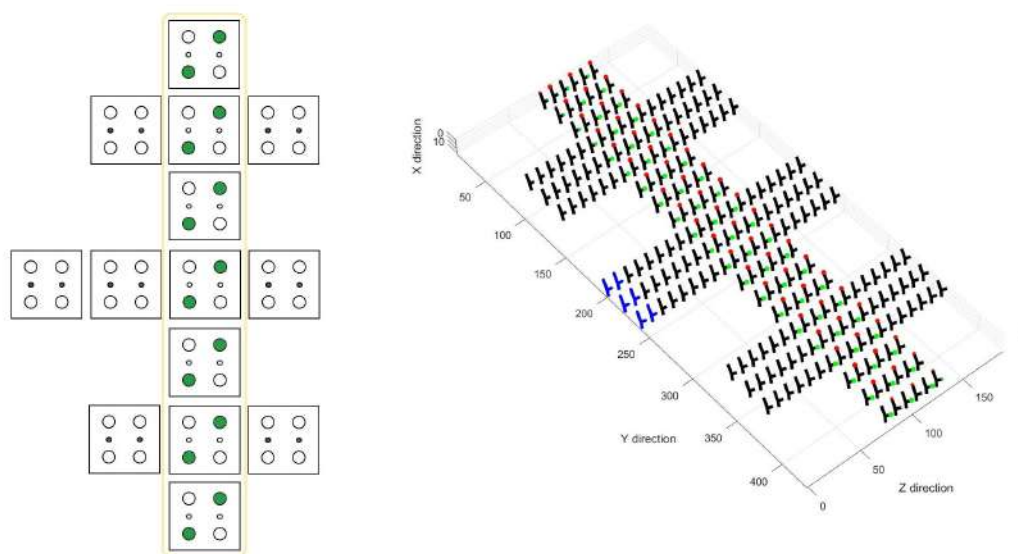


Figure 5.24: Simulation step 3: Vertical fringes

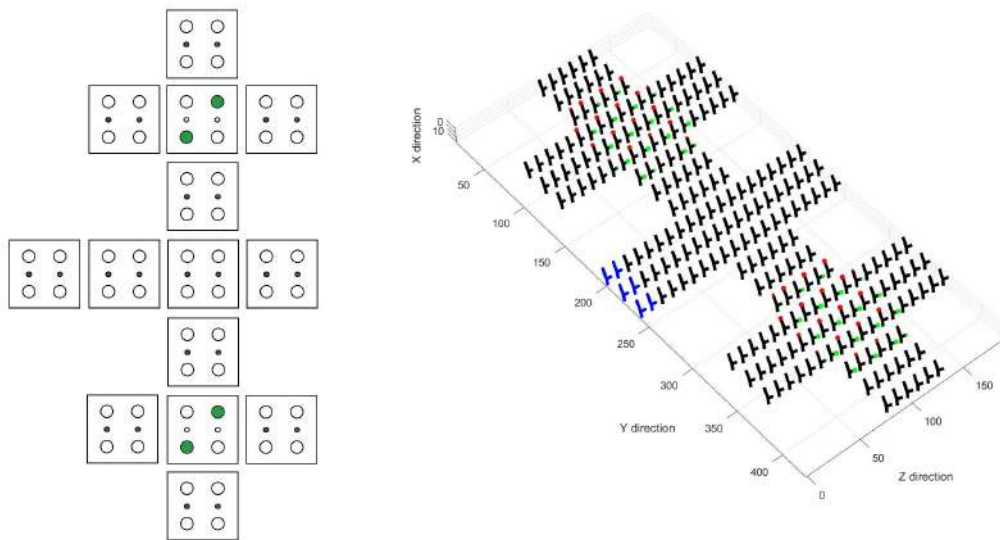


Figure 5.25: Simulation step 4: Electrodes activation

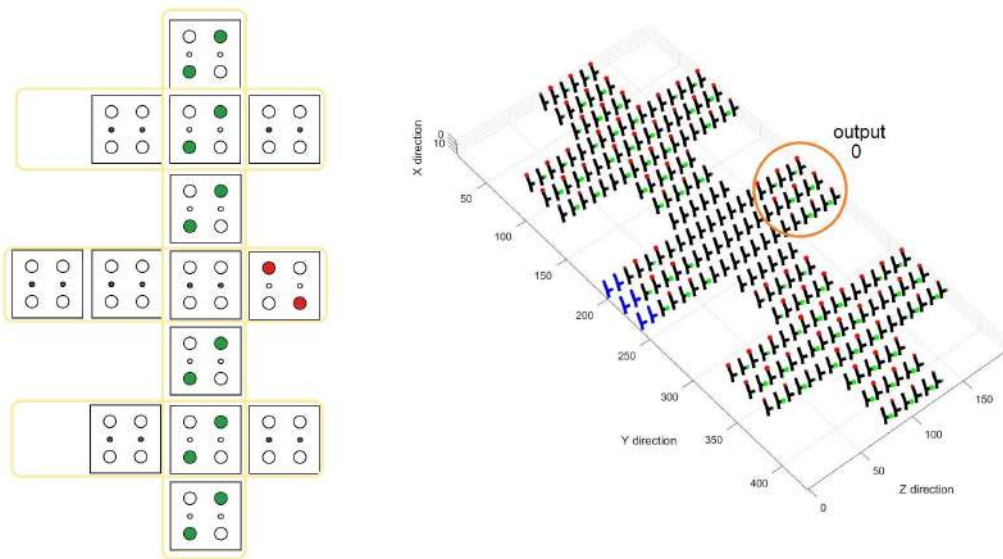


Figure 5.26: Simulation step 5: Grid fringes and Electrode

## 5.4 NAND

NAND logic operation has been simulated, considering both the Majority voter and Inverter simulations. The NAND consists into an AND operation with inverted result: to realize the simulation the input  $C$  has been fixed to 0, to ensure the AND operation, while  $A = 1$  and  $B = 1$ . As consequence the output of the NAND is 0.

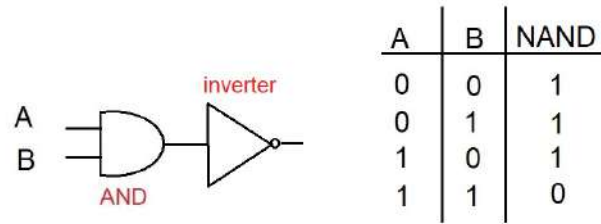


Figure 5.27: NAND logic gate and True table

To realize this operation, only vertical and grid fringes have been used, for a total number of simulation steps of 7.

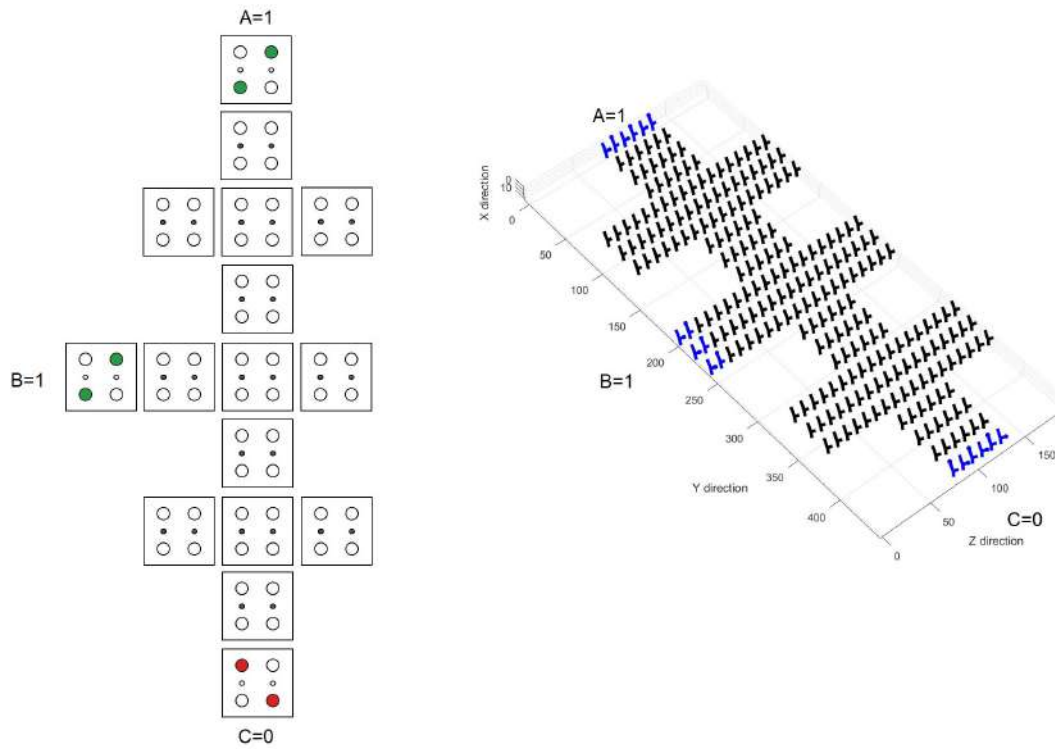


Figure 5.28: NAND in initial reset state

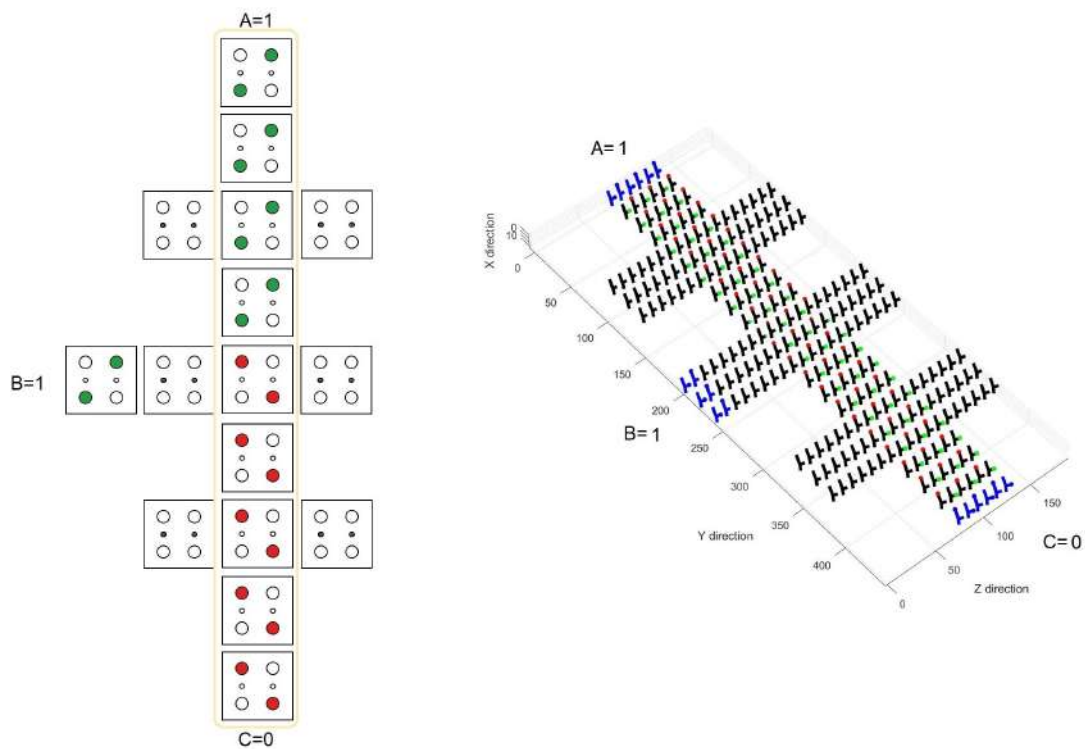


Figure 5.29: NAND simulation step 1: Vertical fringes

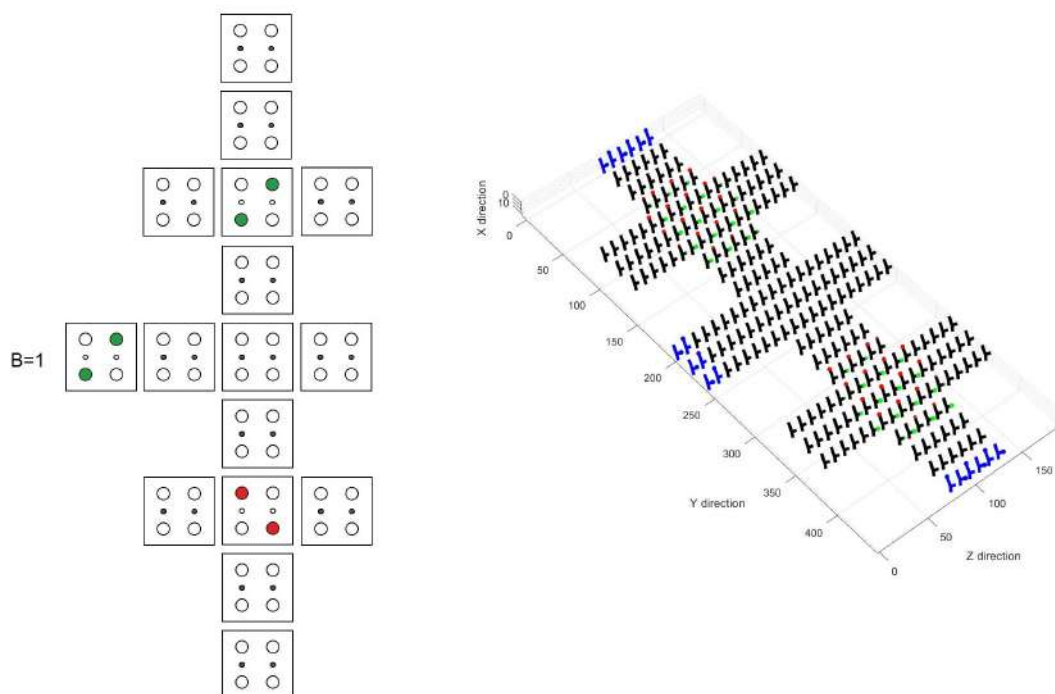


Figure 5.30: NAND simulation step 2: Electrodes activation

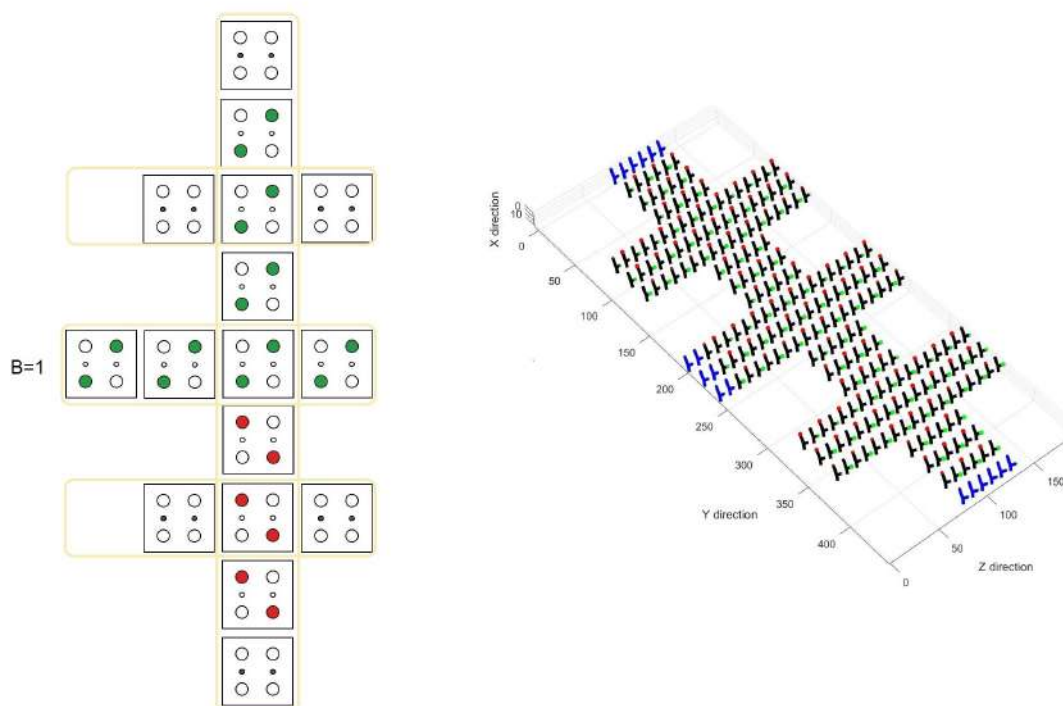


Figure 5.31: NAND simulation step 3: Grid fringes

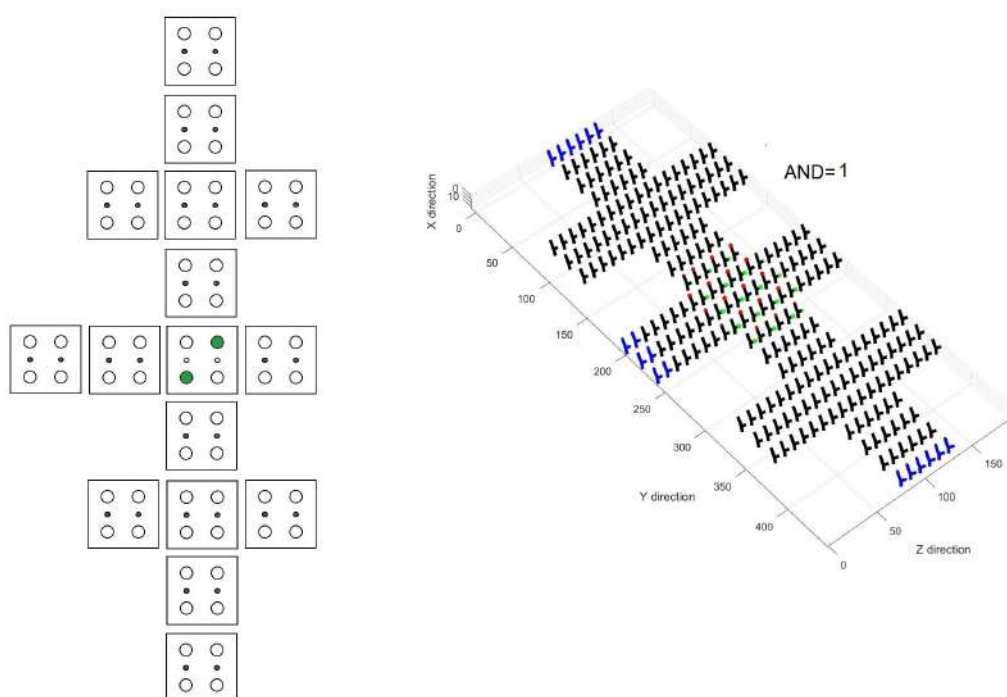


Figure 5.32: NAND simulation step 4: Electrodes activation

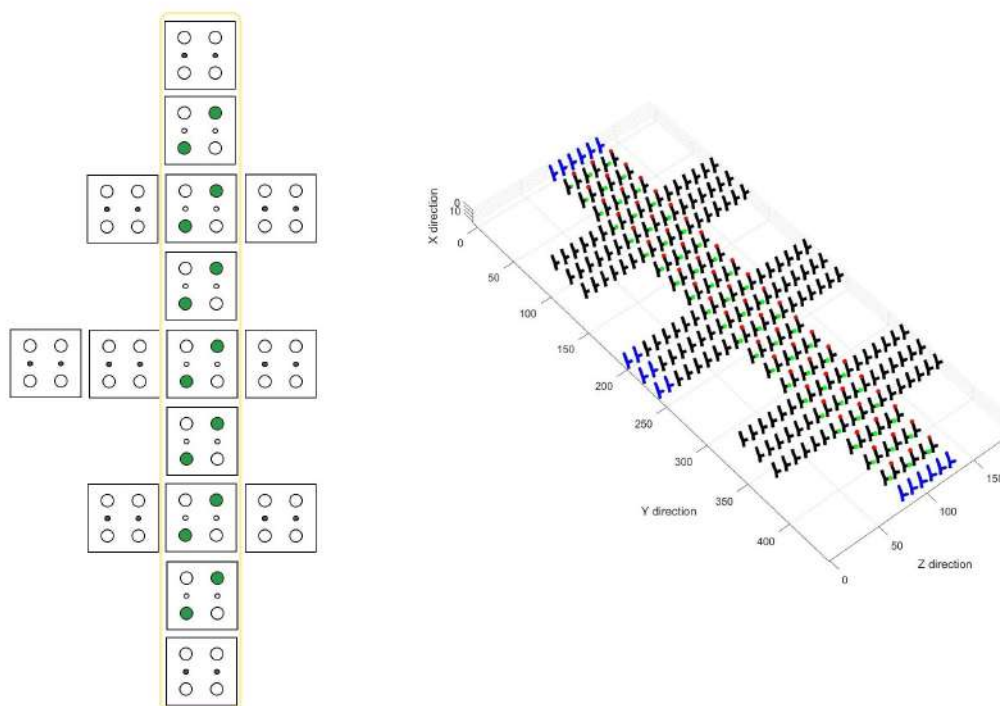


Figure 5.33: NAND simulation step 5: Vertical fringes

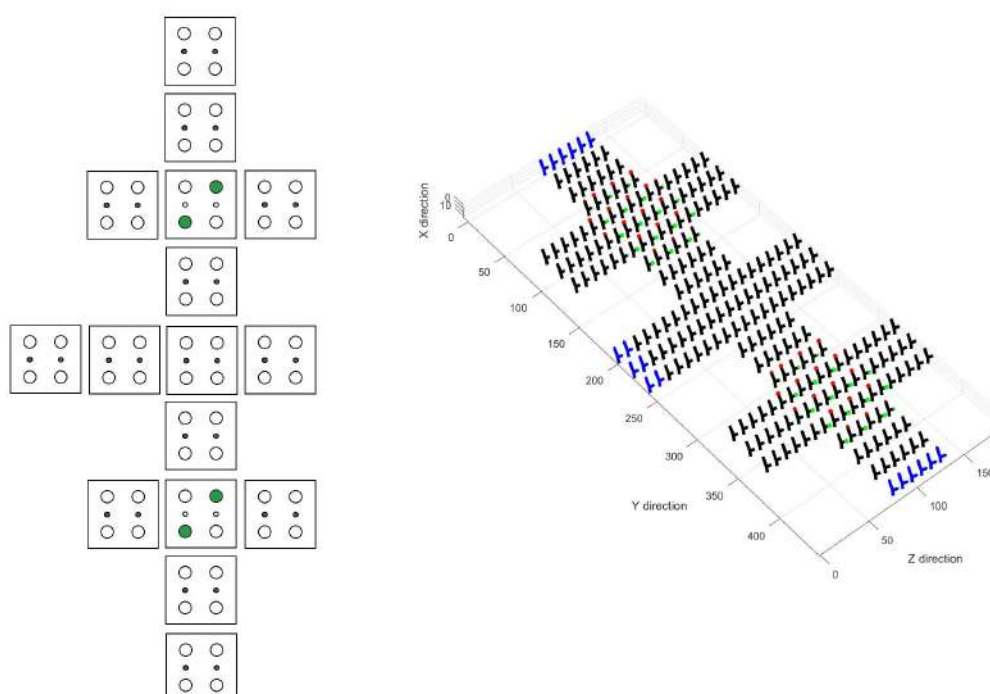


Figure 5.34: NAND simulation step 6: Electrodes activation

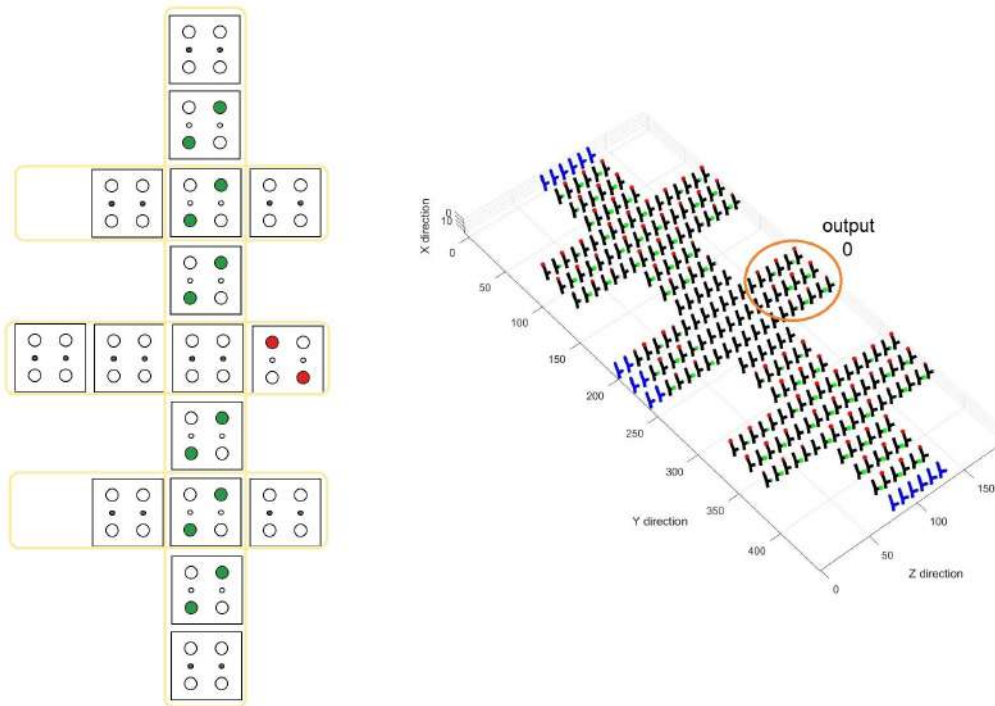


Figure 5.35: NAND simulation step 7: Grid fringes and Electrode

## 5.5 Half Adder

To observe the behaviour of the structure in more complex operations, the Half Adder simulation has been realized.

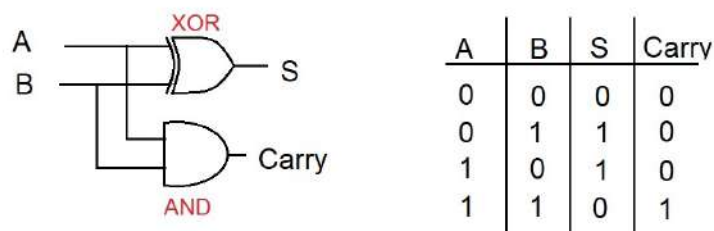


Figure 5.36: Half Adder logic gate and True table

The Half adder is based on XOR and AND logic operations, generating as results the sum and the carry. The simulation has inputs:  $A = 0, B = 1$ . Therefore, the results are  $S = 1$  and  $Carry = 0$ , as shown in figure 5.53.

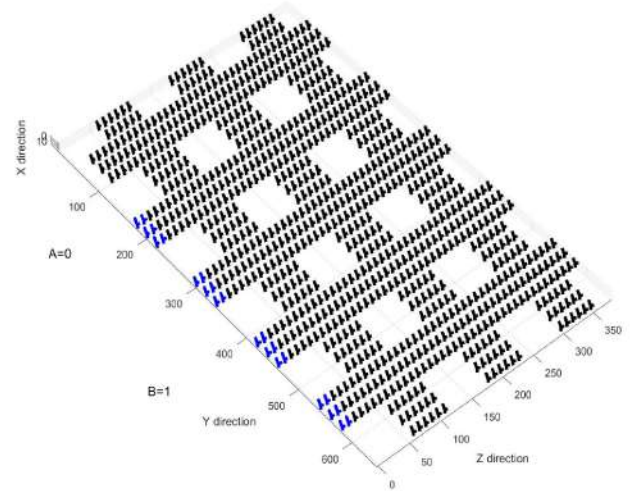
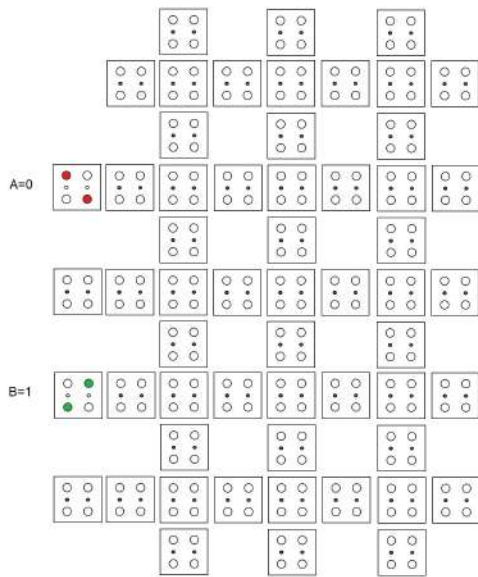


Figure 5.37: HALF ADDER in initial reset state

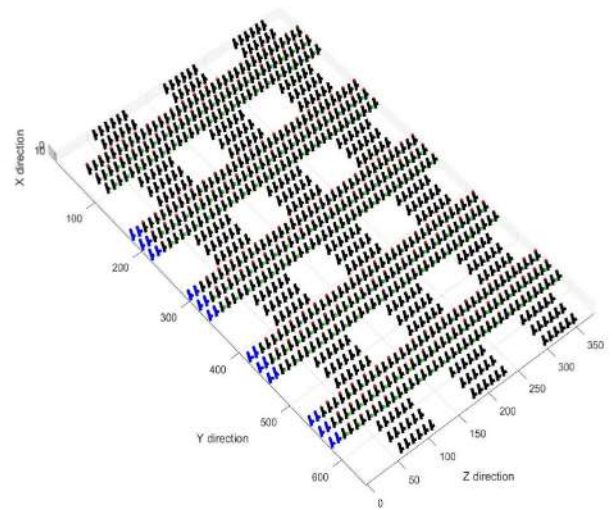
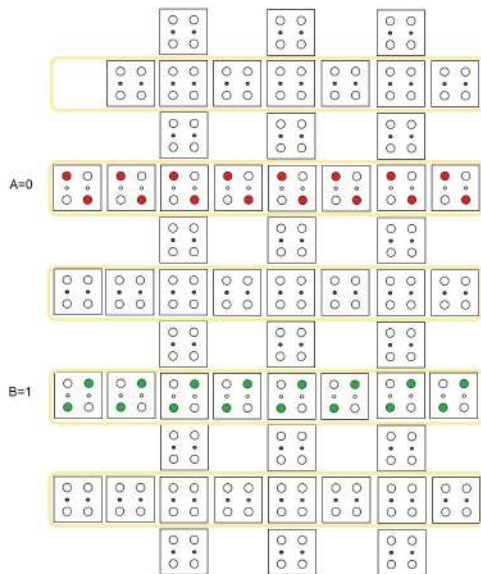


Figure 5.38: HALF ADDER simulation step 1

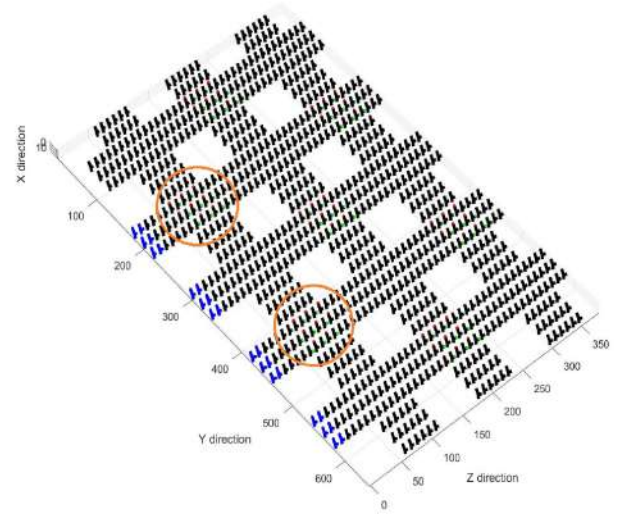
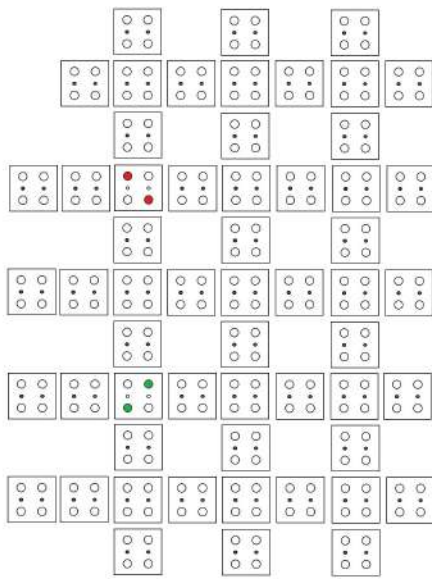


Figure 5.39: HALF ADDER simulation step 2

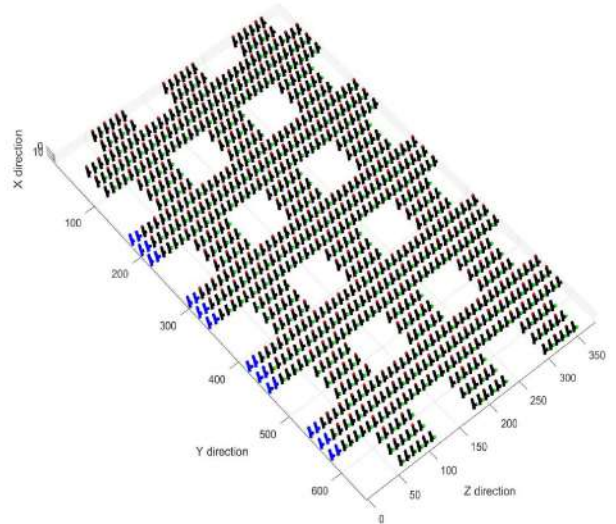
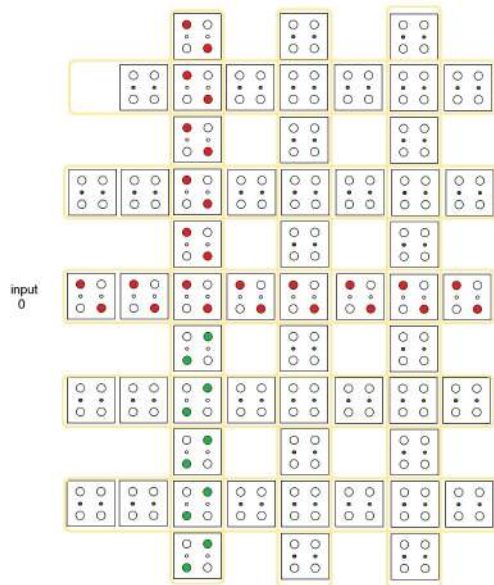


Figure 5.40: HALF ADDER simulation step 3

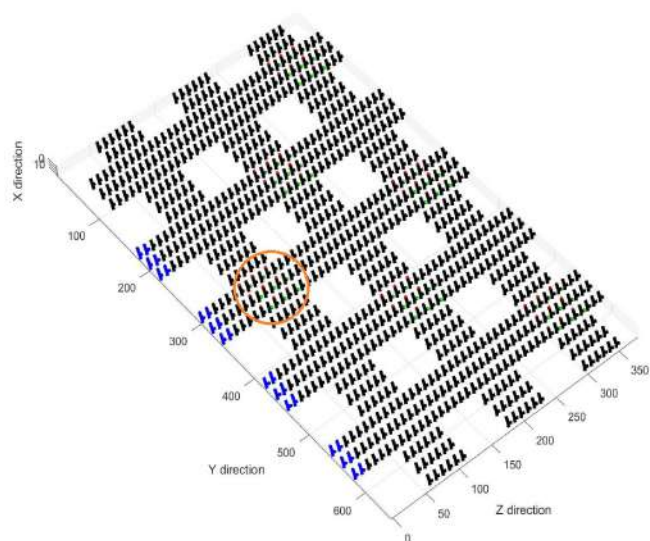
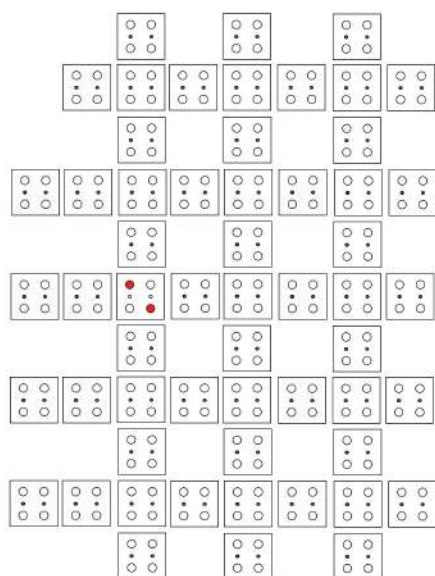


Figure 5.41: HALF ADDER simulation step 4

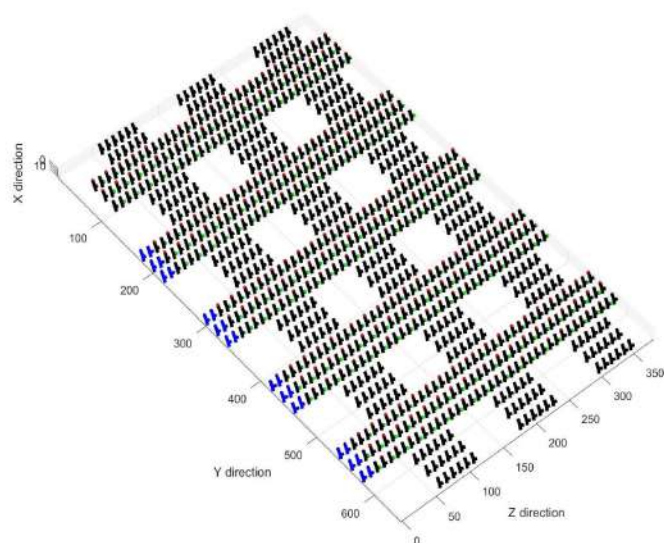


Figure 5.42: HALF ADDER simulation step 5

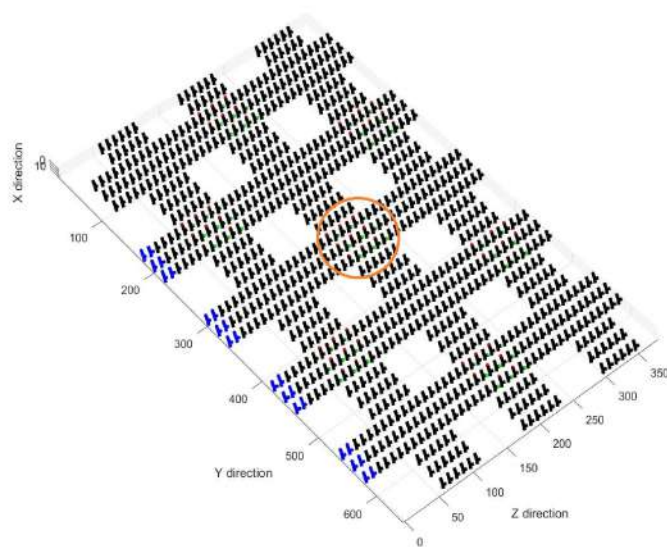


Figure 5.43: HALF ADDER simulation step 6

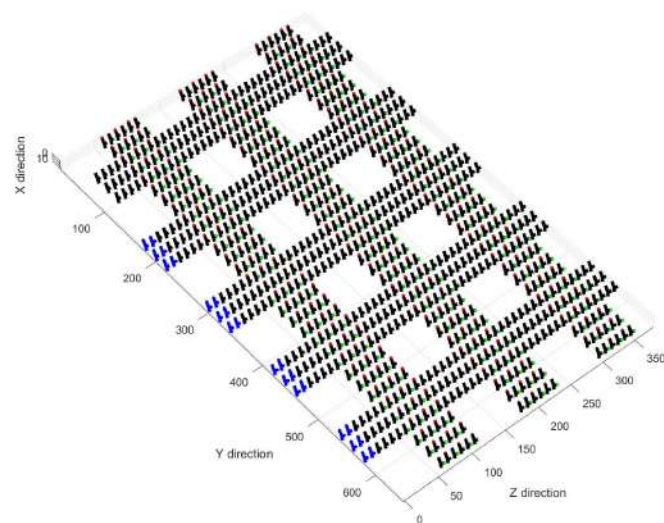
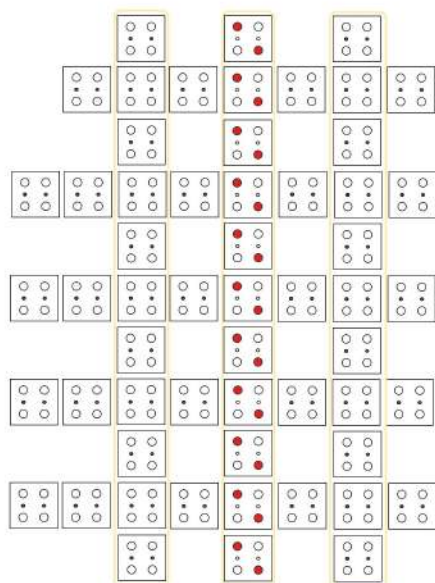


Figure 5.44: HALF ADDER simulation step 7

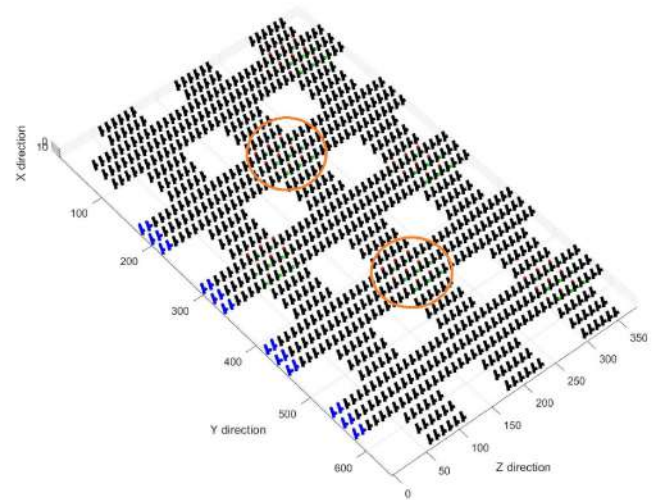
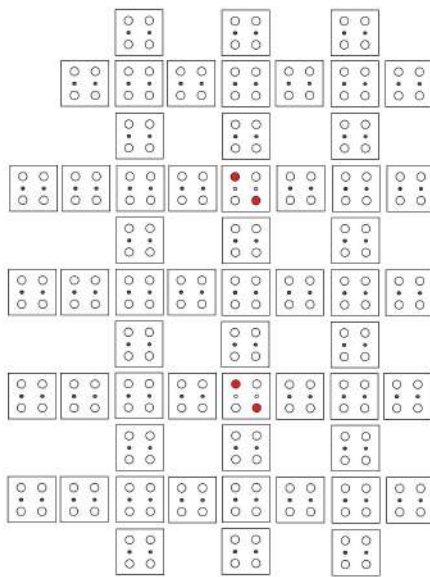


Figure 5.45: HALF ADDER simulation step 8

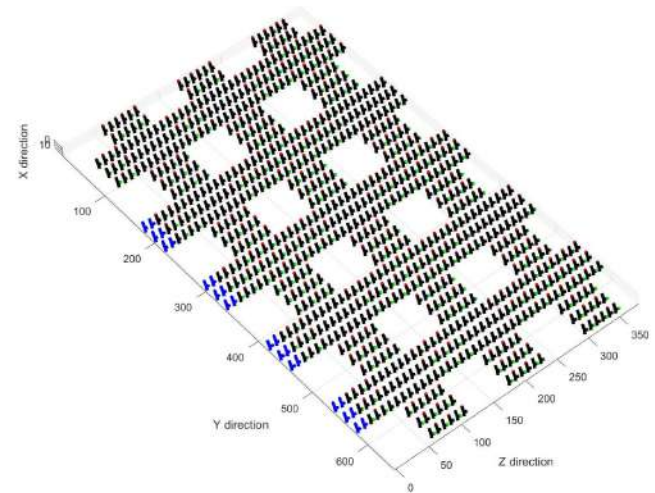


Figure 5.46: HALF ADDER simulation step 9

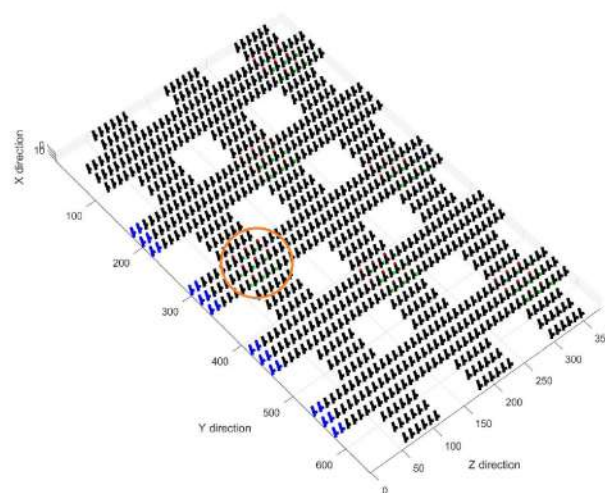
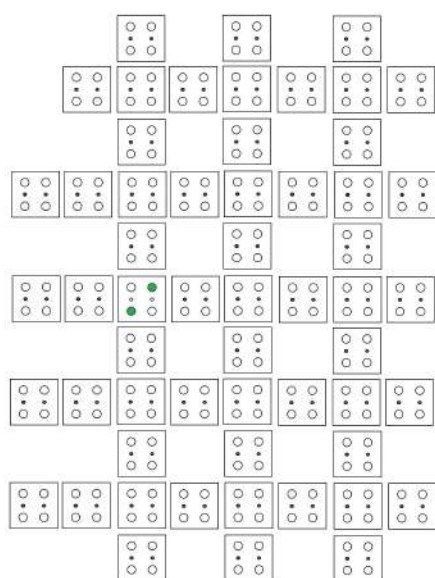


Figure 5.47: HALF ADDER simulation step 10

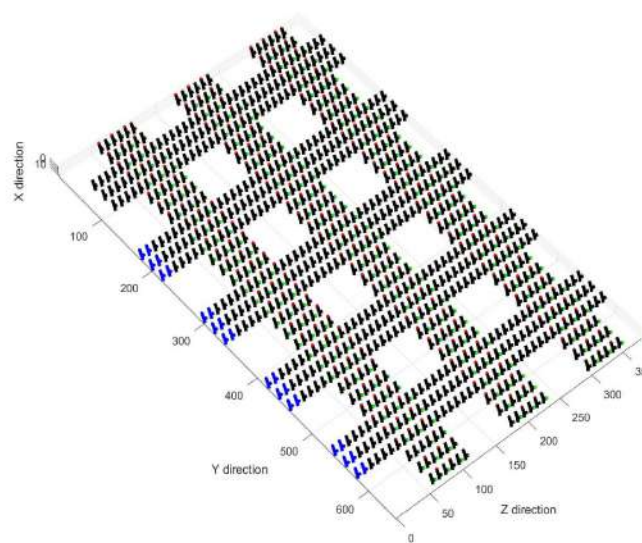
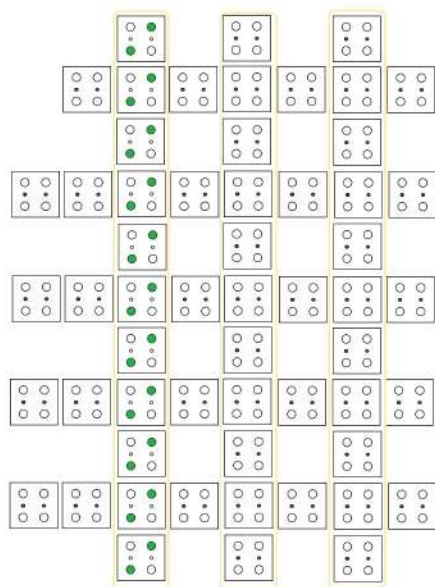


Figure 5.48: HALF ADDER simulation step 11

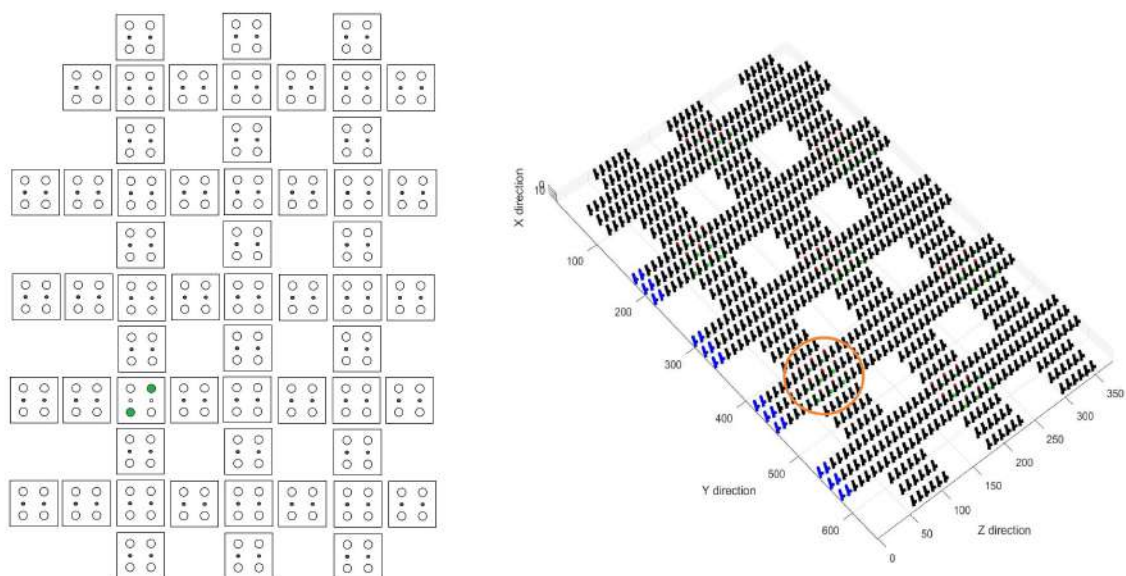


Figure 5.49: HALF ADDER simulation step 12

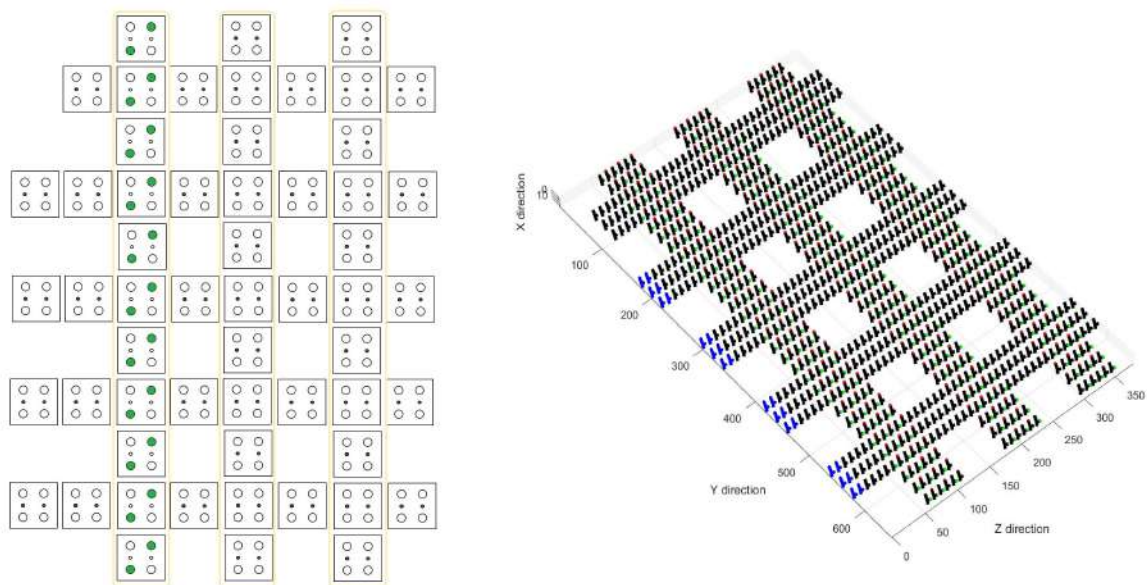


Figure 5.50: HALF ADDER simulation step 13

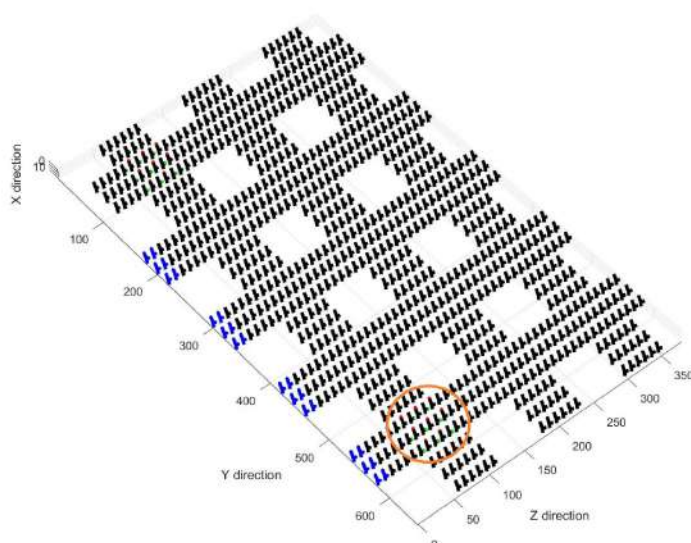


Figure 5.51: HALF ADDER simulation step 14

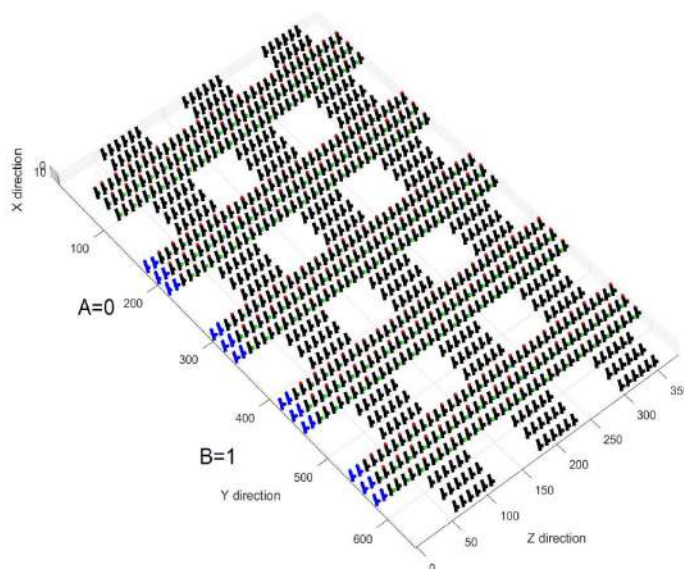
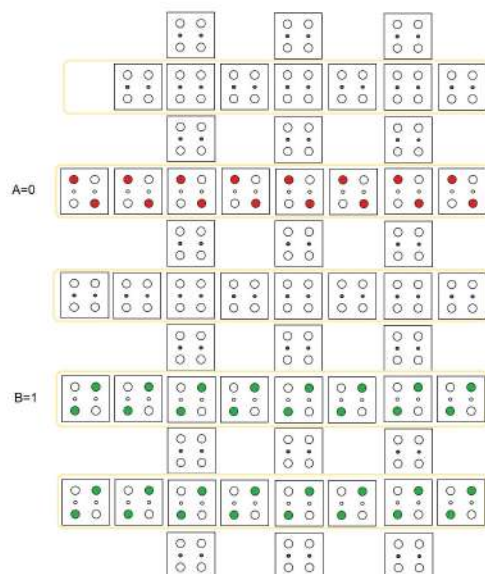


Figure 5.52: HALF ADDER simulation step 15



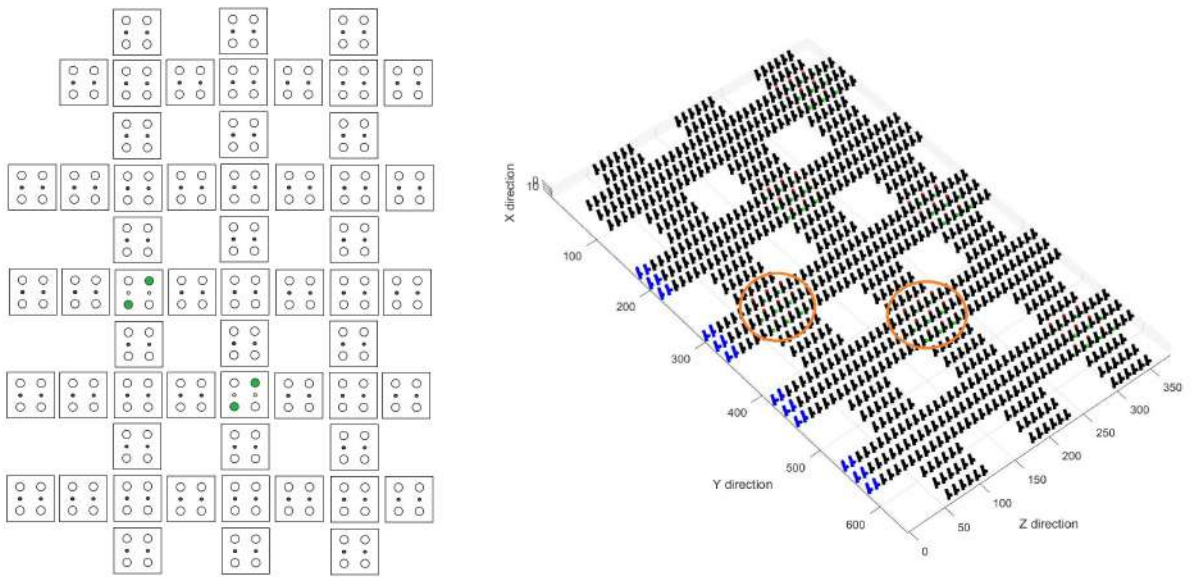


Figure 5.55: HALF ADDER simulation step 18

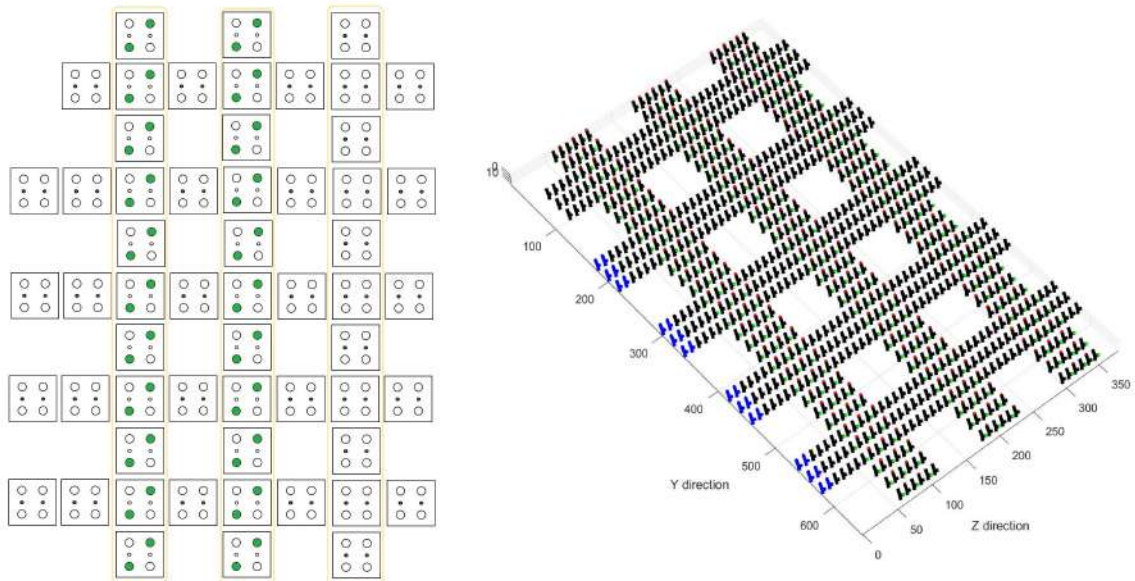


Figure 5.56: HALF ADDER simulation step 19

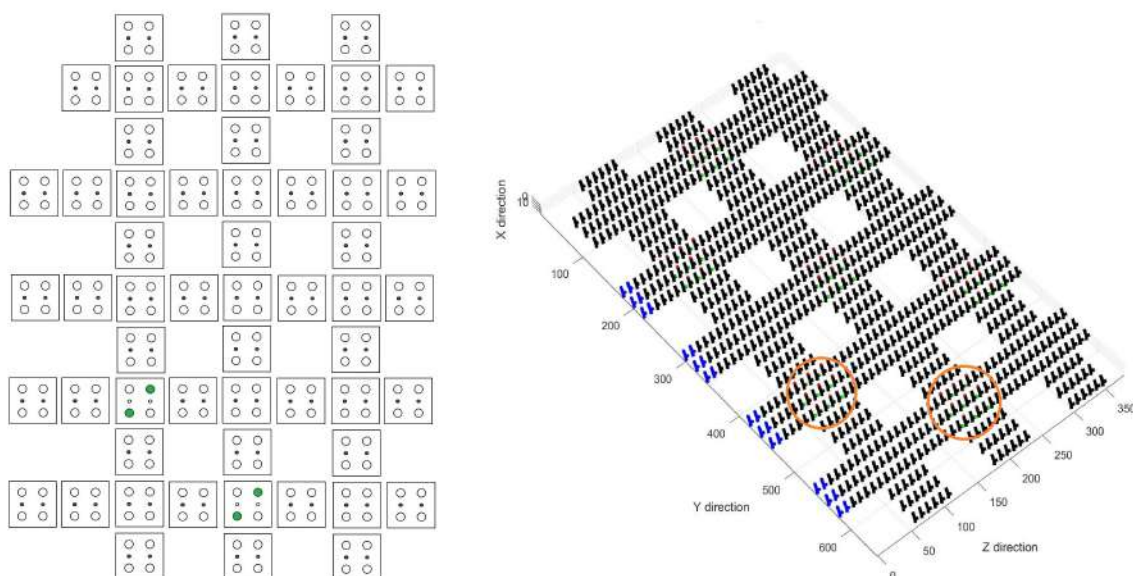


Figure 5.57: HALF ADDER simulation step 20

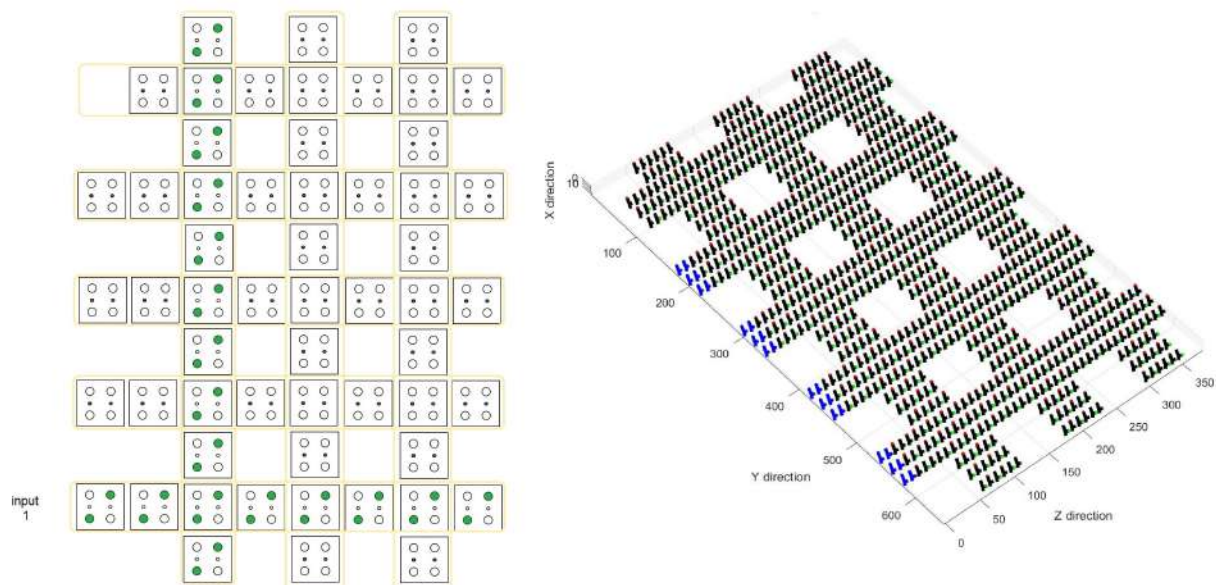


Figure 5.58: HALF ADDER simulation step 21

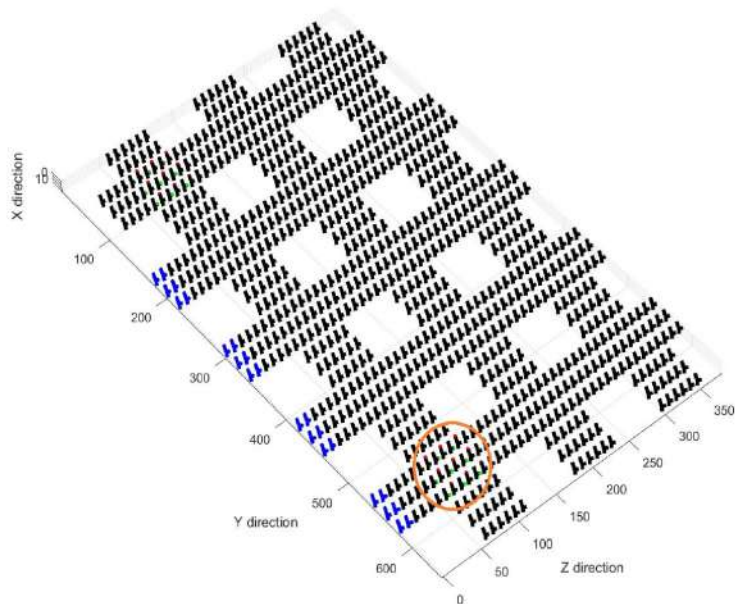
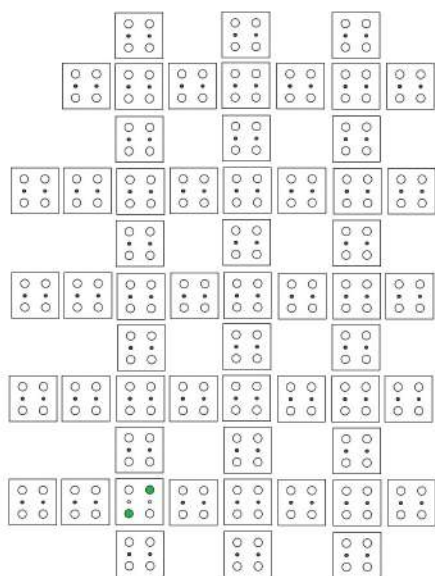


Figure 5.59: HALF ADDER simulation step 22

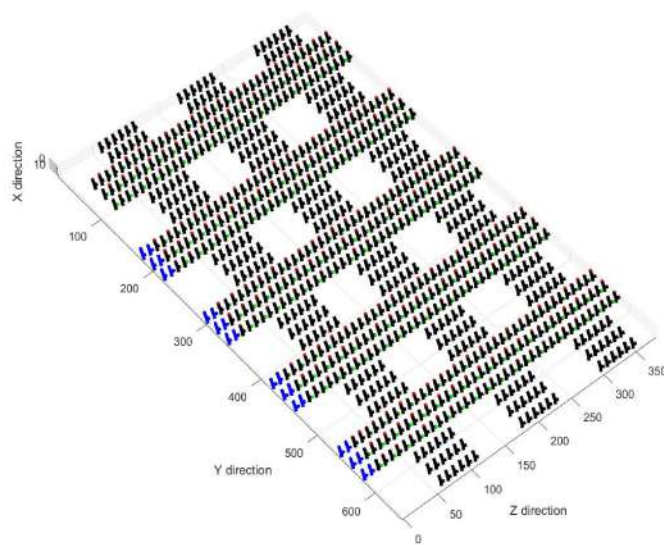
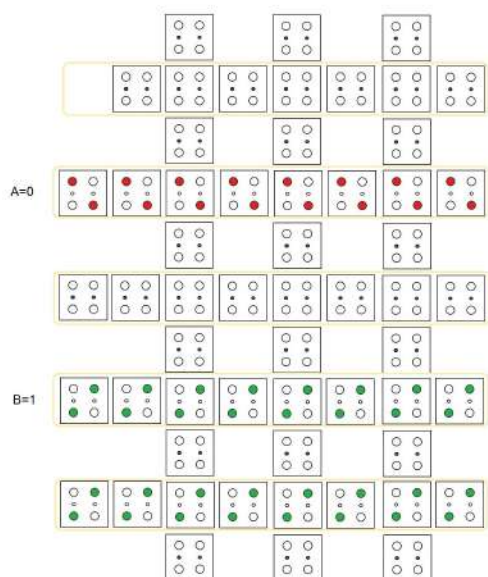


Figure 5.60: HALF ADDER simulation step 23

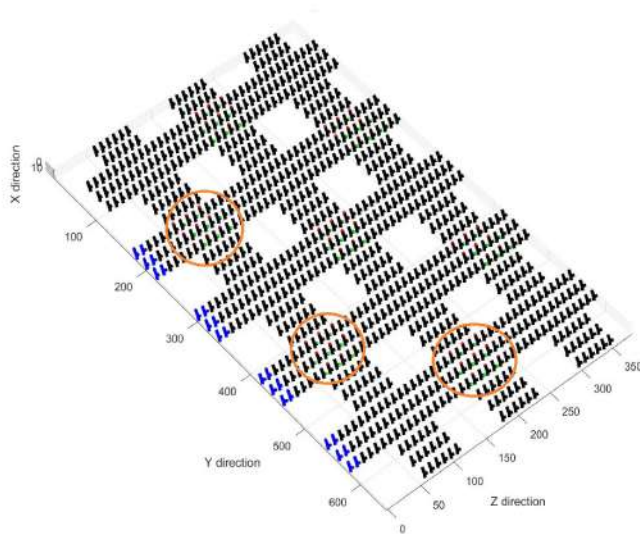
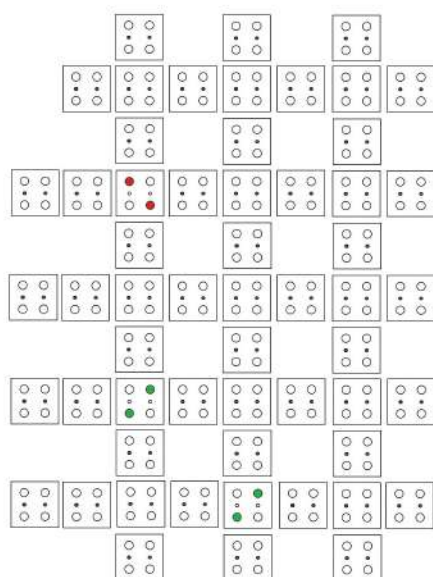


Figure 5.61: HALF ADDER simulation step 24

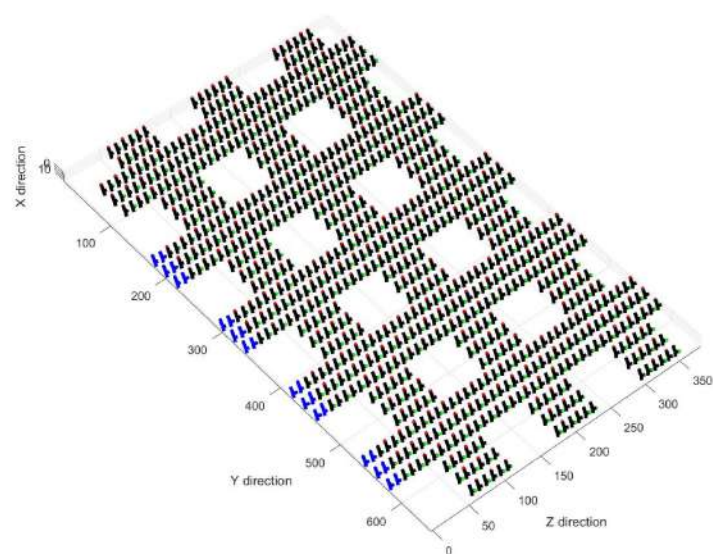
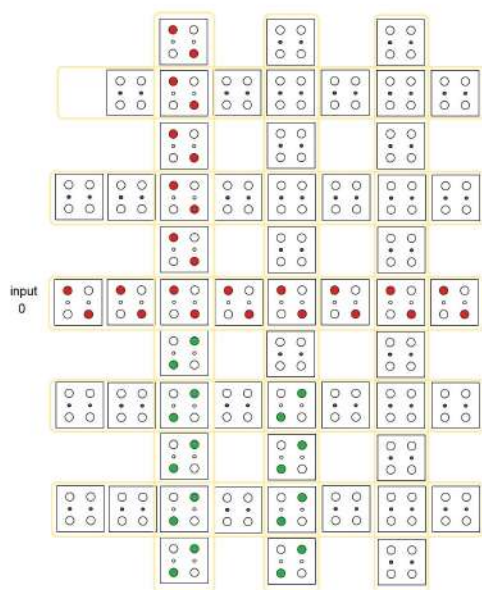


Figure 5.62: HALF ADDER simulation step 25

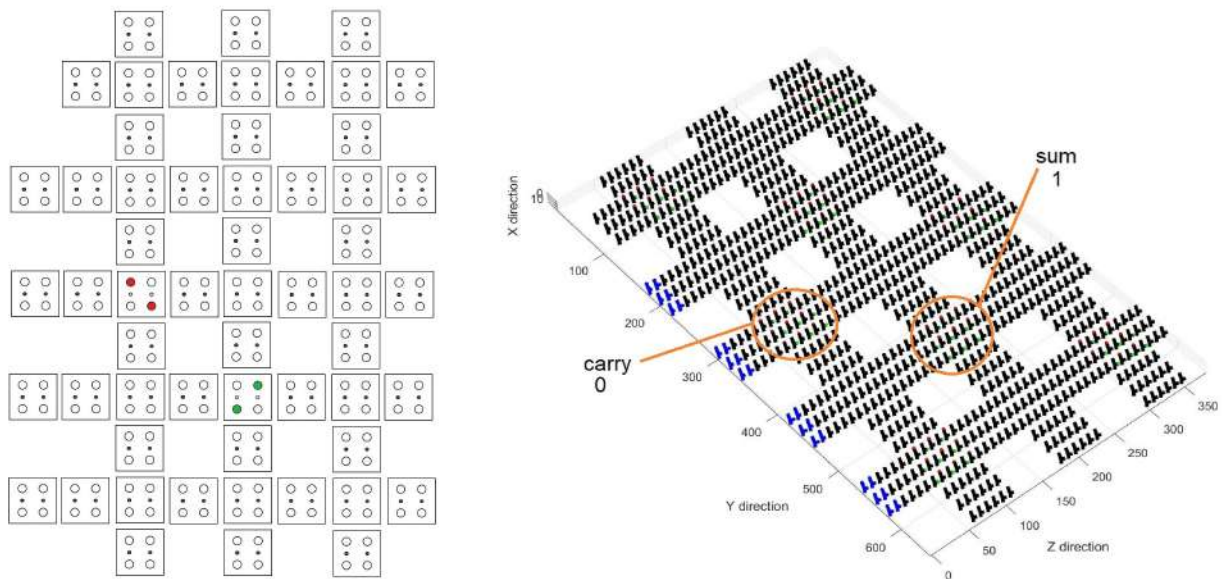


Figure 5.63: HALF ADDER simulation step 26

## 5.6 Full Adder

The last simulation realized is the Full Adder. This logic operation consists of two Half Adder, with carries as inputs of an OR operation.

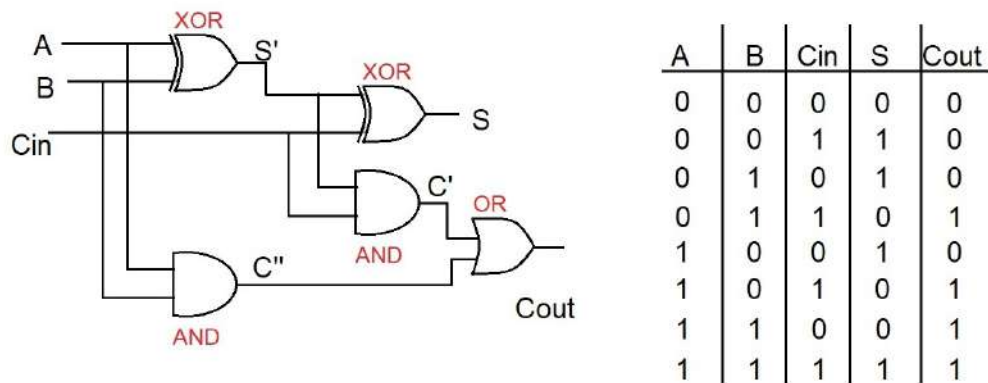


Figure 5.64: Full Adder logic gate and True table

The simulation has been realized with inputs  $A = 1, B = 0, Cin = 0$ . As results  $S = 1$  and  $Cout = 0$ . To better understand the propagation, it is possible to divide it into smaller logical operations. The first operation is the XOR, to obtain the first summation  $S'$ :

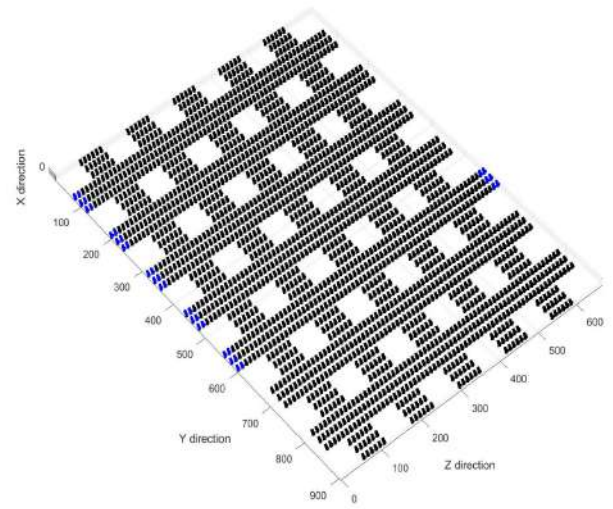
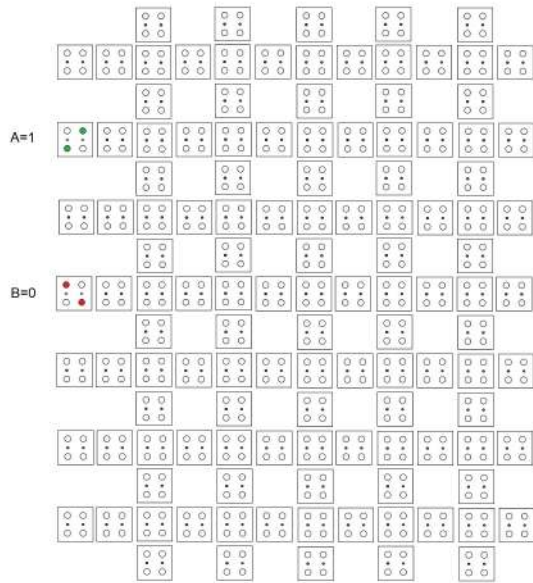


Figure 5.65: FULL ADDER in initial reset state

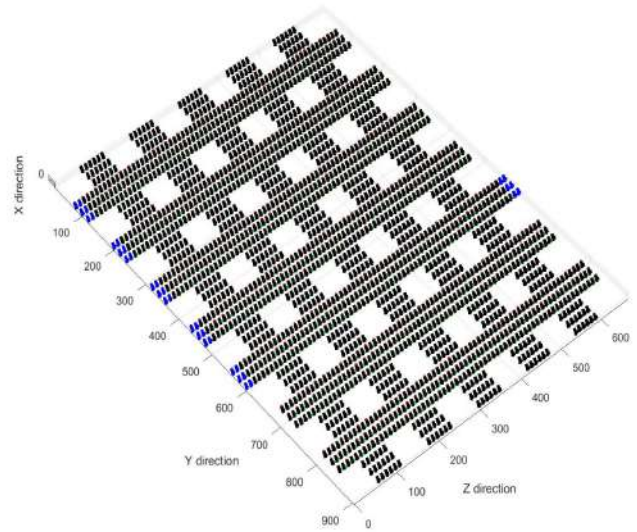
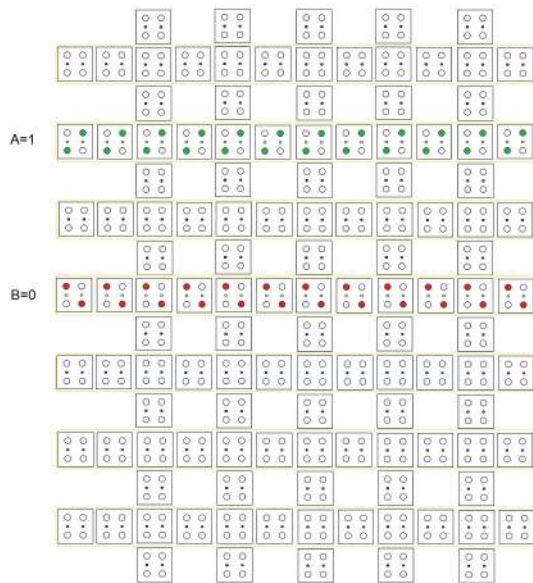


Figure 5.66: FULL ADDER simulation step 1

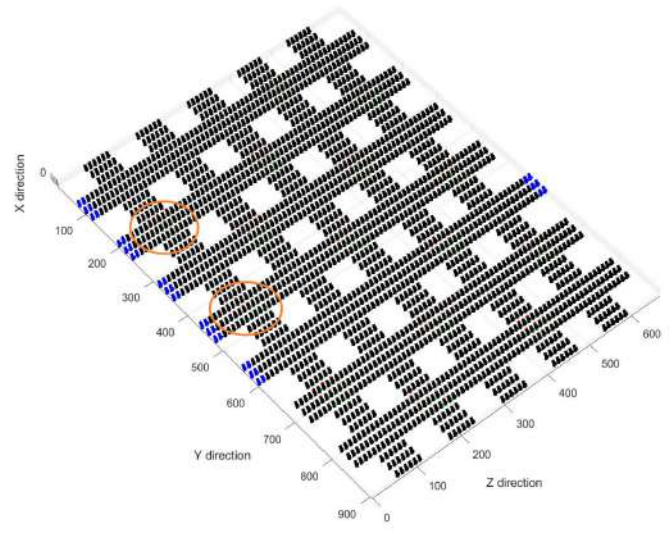
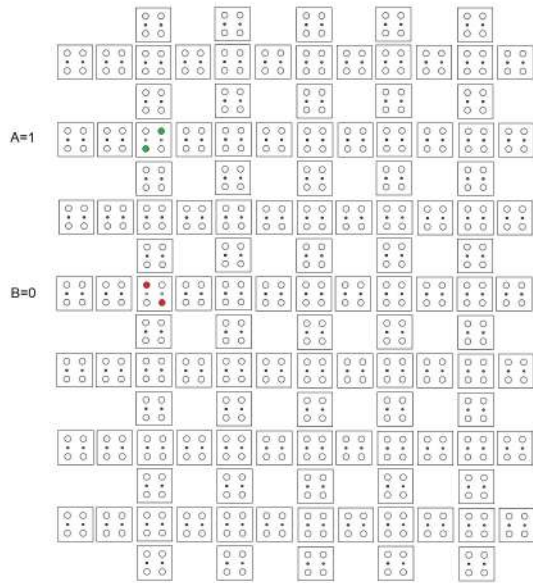


Figure 5.67: FULL ADDER simulation step 2

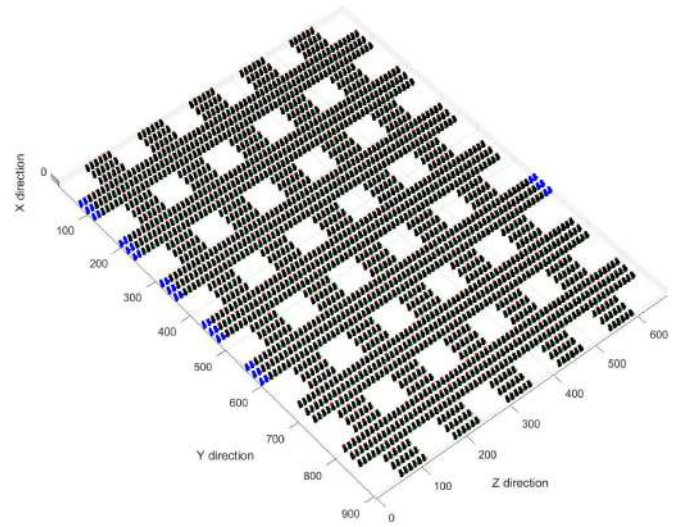
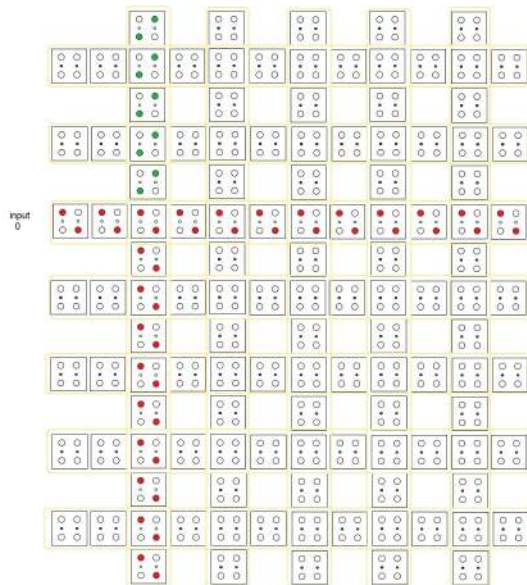


Figure 5.68: FULL ADDER simulation step 3

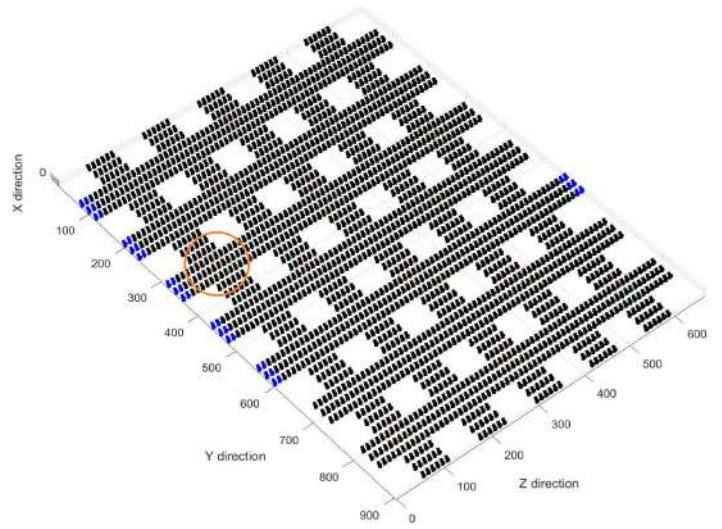
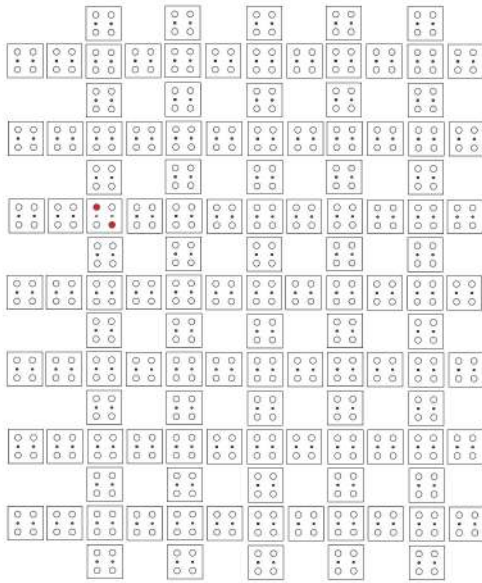


Figure 5.69: FULL ADDER simulation step 4

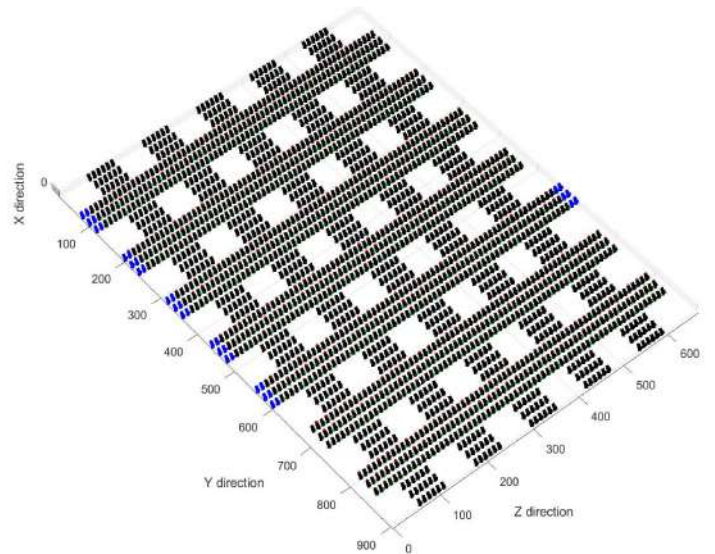
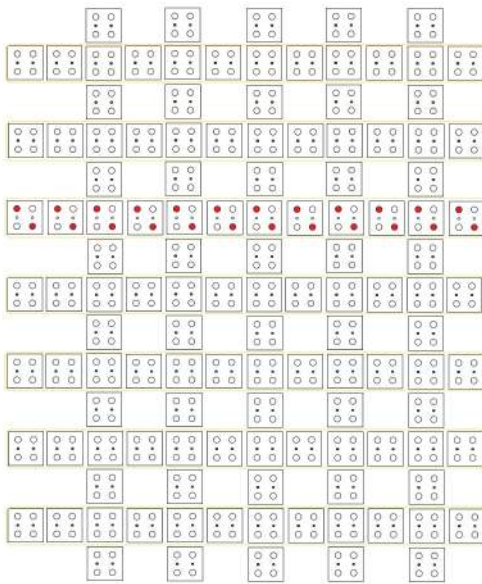


Figure 5.70: FULL ADDER simulation step 5

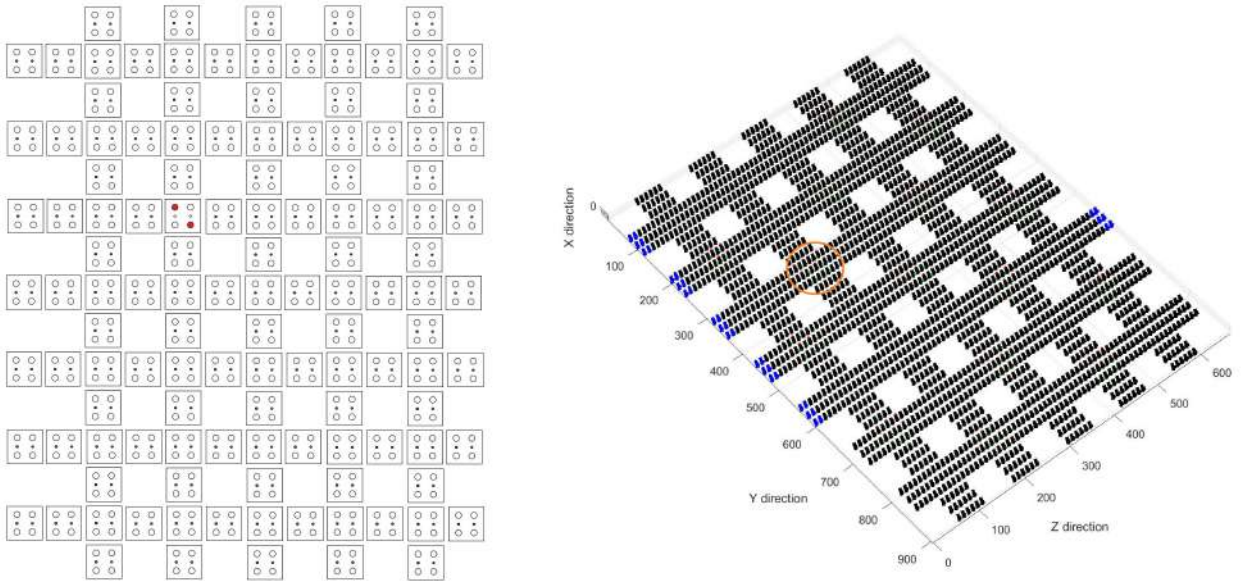


Figure 5.71: FULL ADDER simulation step 6

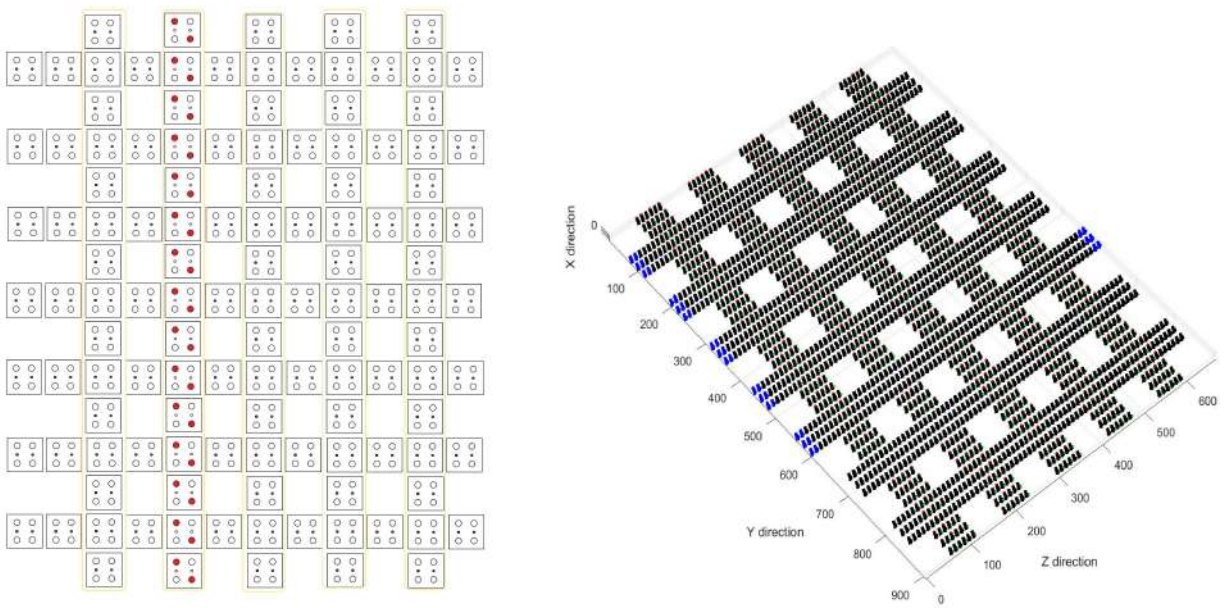


Figure 5.72: FULL ADDER simulation step 7

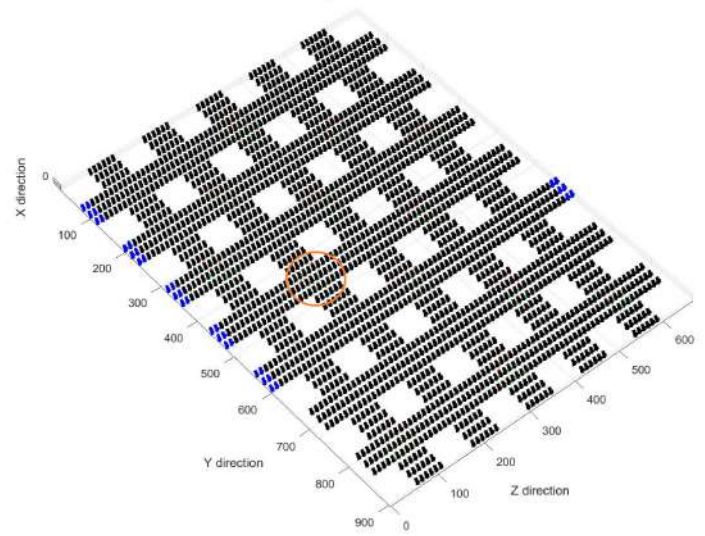
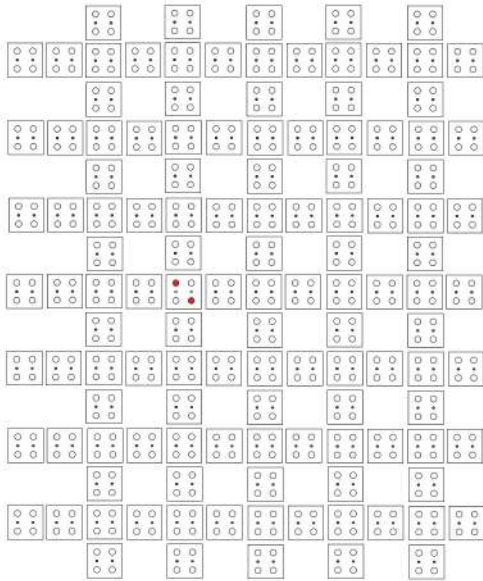


Figure 5.73: FULL ADDER simulation step 8

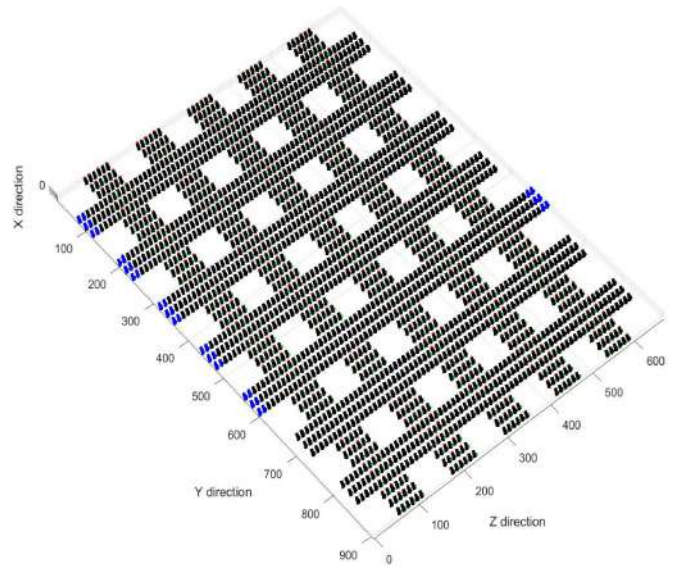
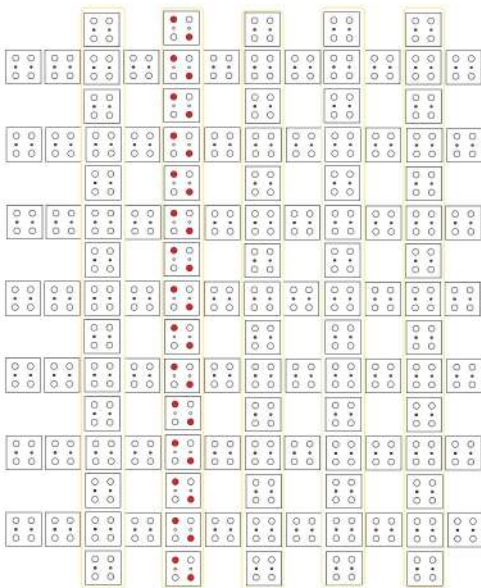


Figure 5.74: FULL ADDER simulation step 9

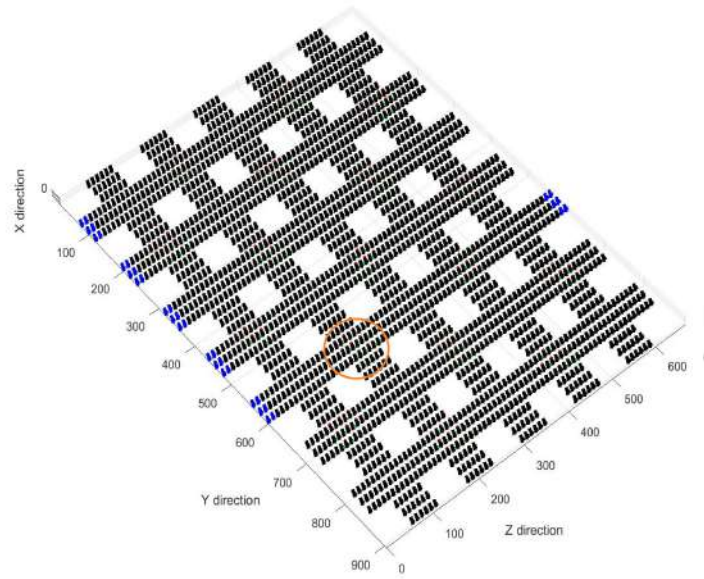
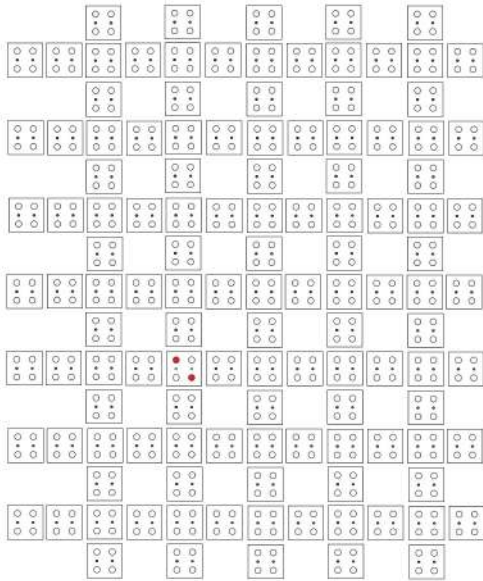


Figure 5.75: FULL ADDER simulation step 10

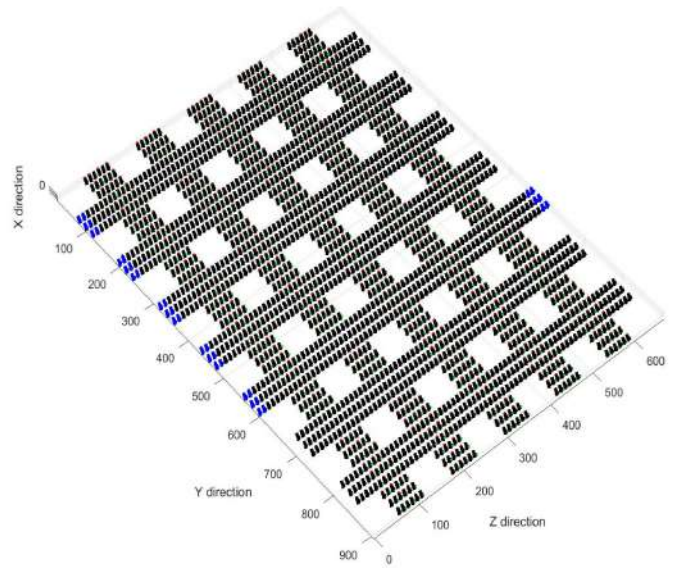
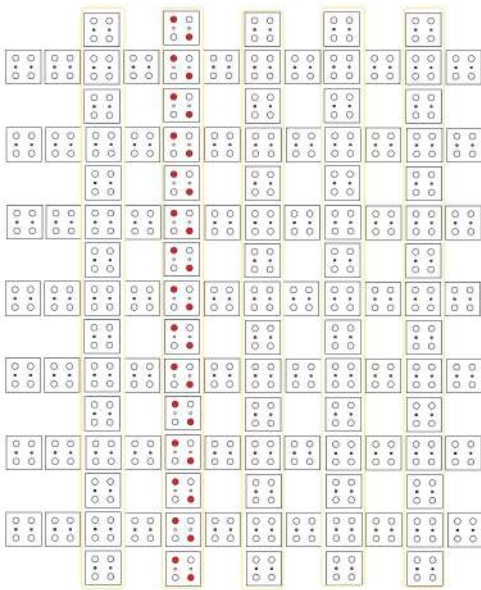


Figure 5.76: FULL ADDER simulation step 11

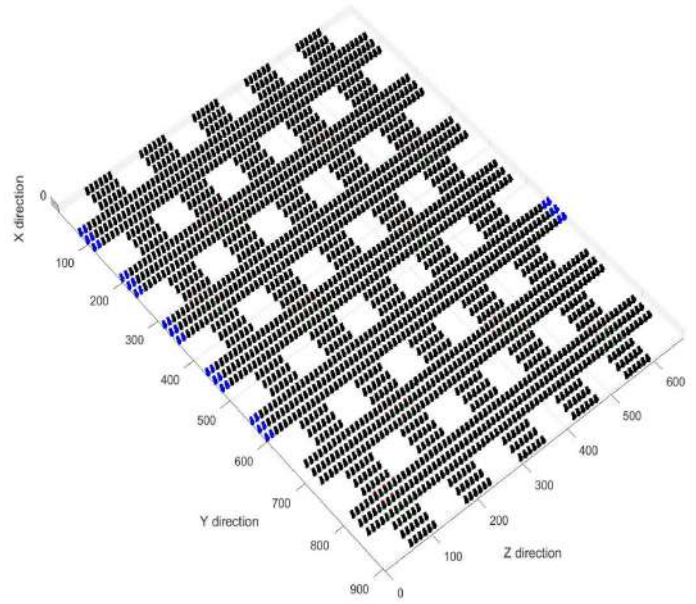
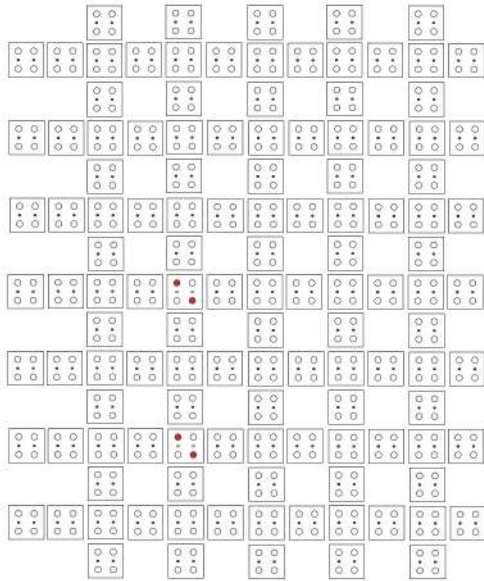


Figure 5.77: FULL ADDER simulation step 12

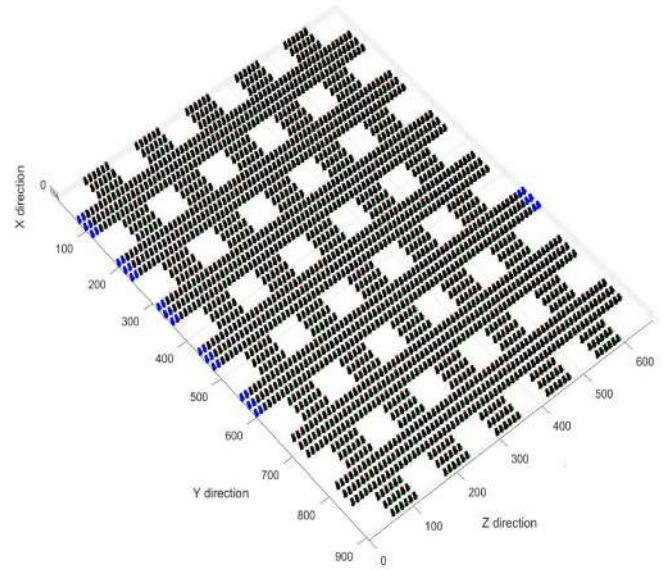
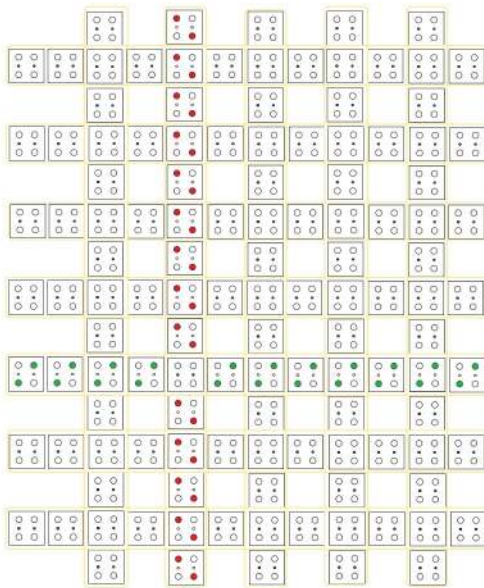


Figure 5.78: FULL ADDER simulation step 13

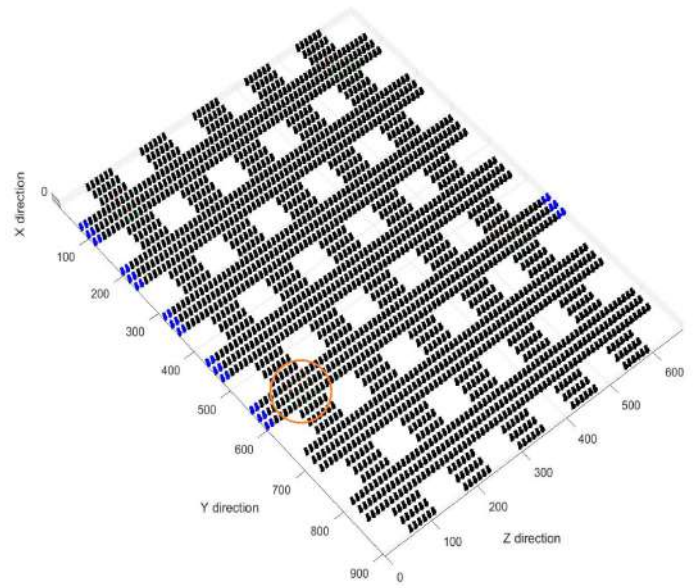
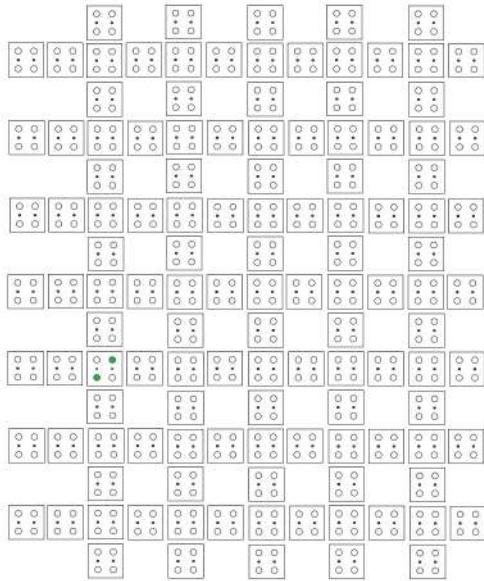


Figure 5.79: FULL ADDER simulation step 14

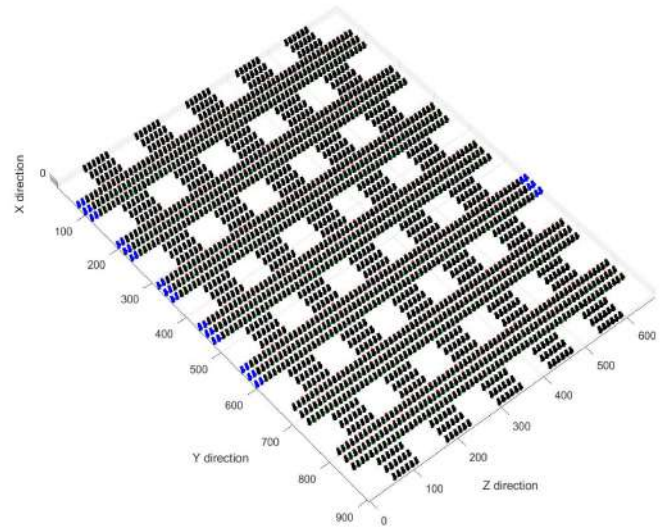
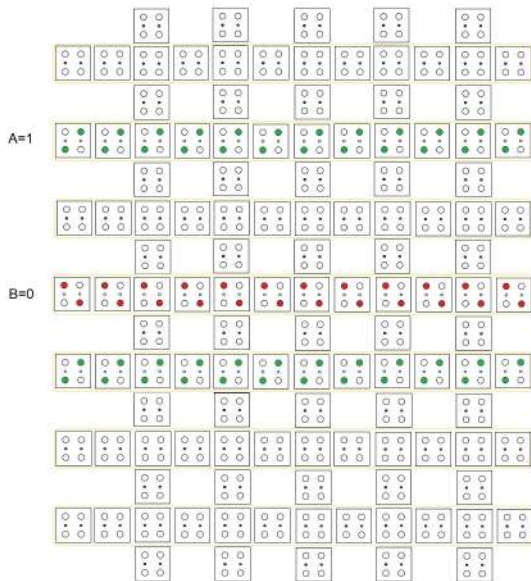


Figure 5.80: FULL ADDER simulation step 15

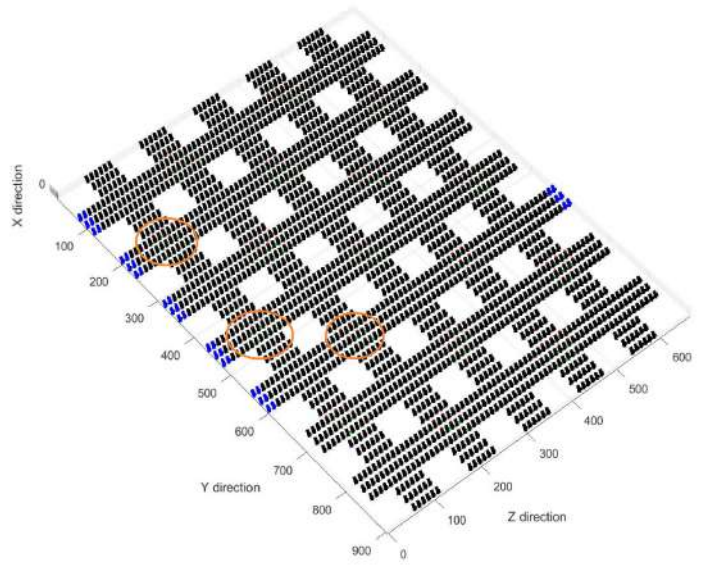
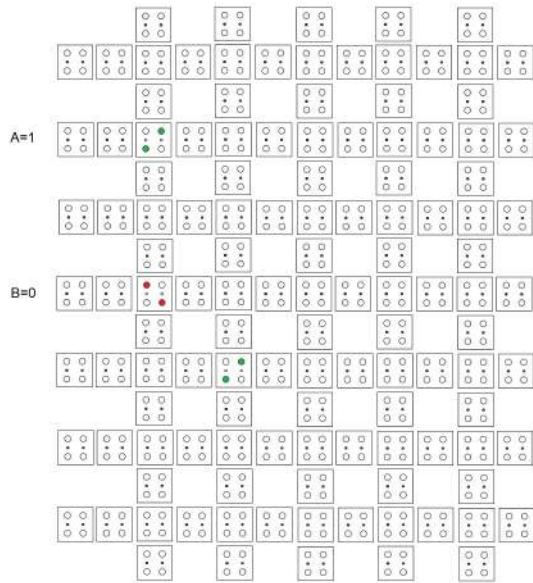


Figure 5.81: FULL ADDER simulation step 16

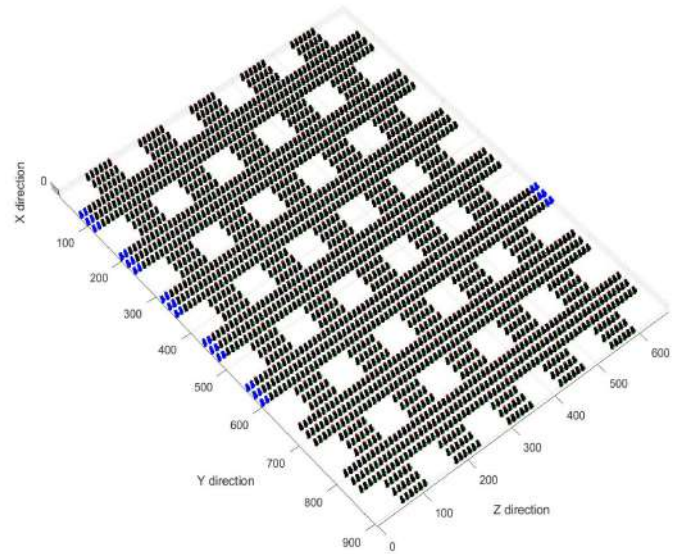
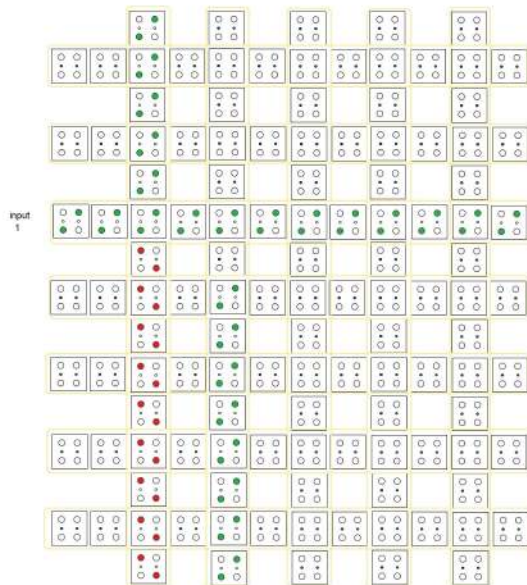


Figure 5.82: FULL ADDER simulation step 17

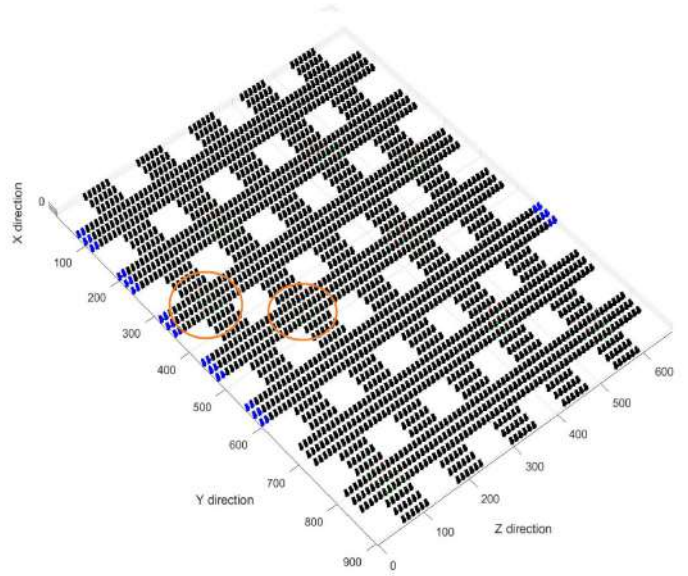
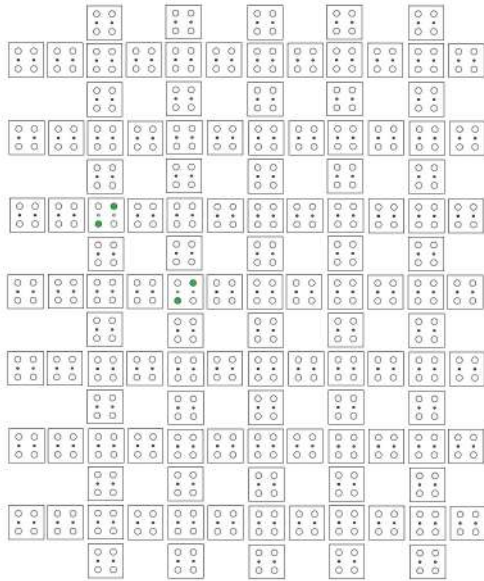


Figure 5.83: FULL ADDER simulation step 18

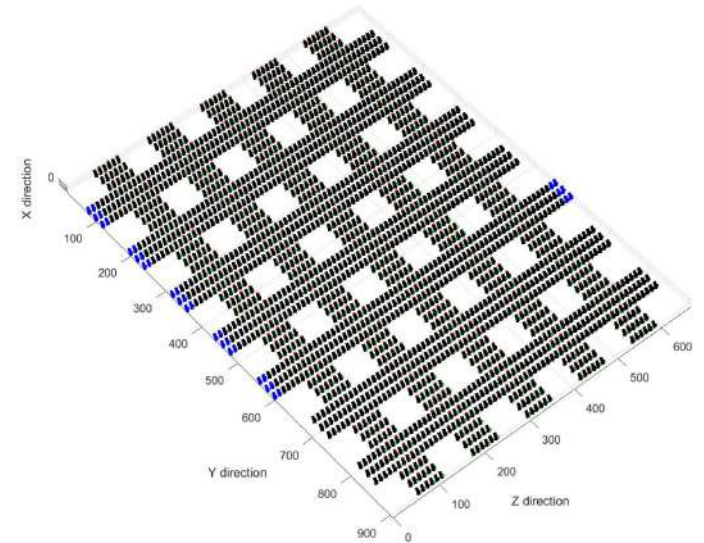
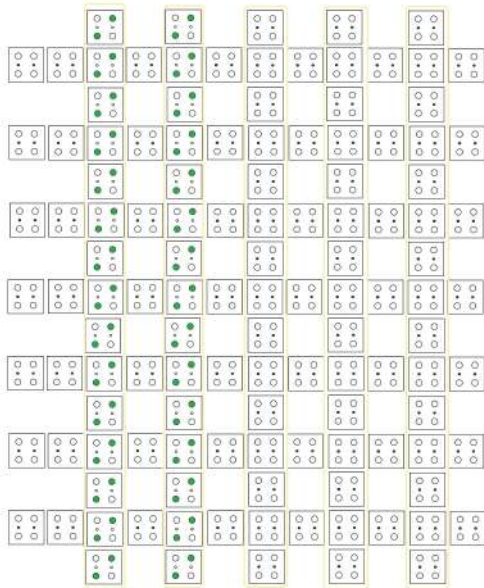


Figure 5.84: FULL ADDER simulation step 19

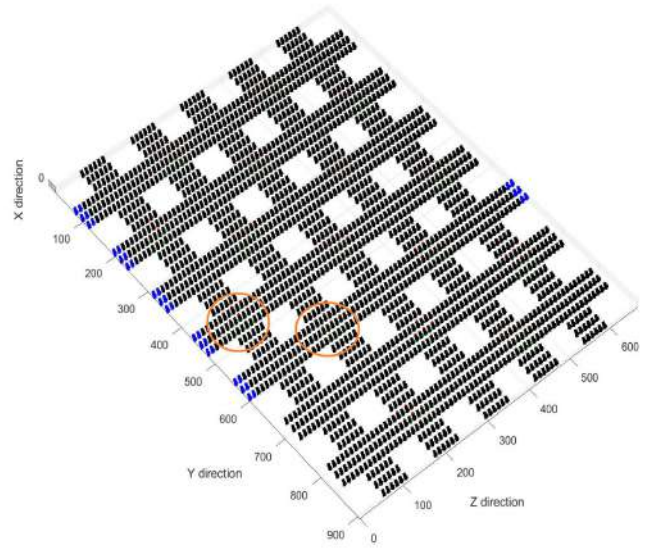
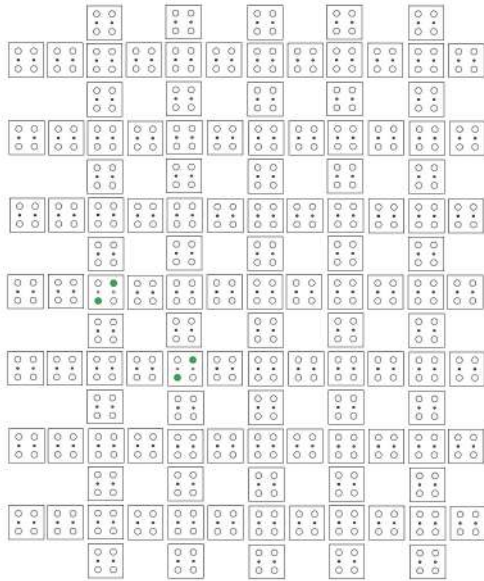


Figure 5.85: FULL ADDER simulation step 20

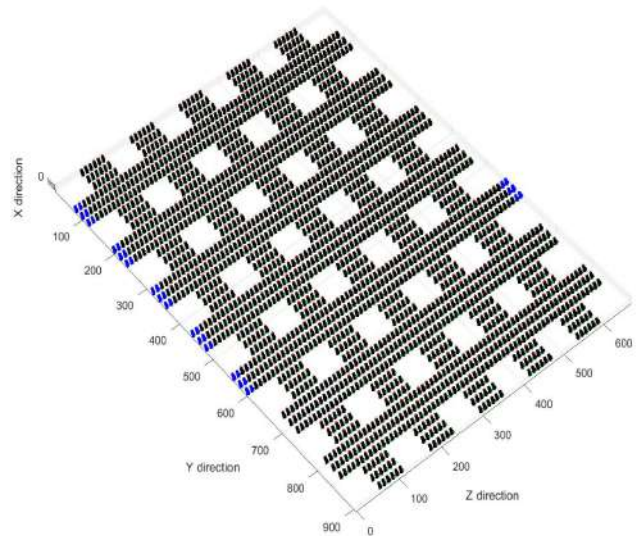
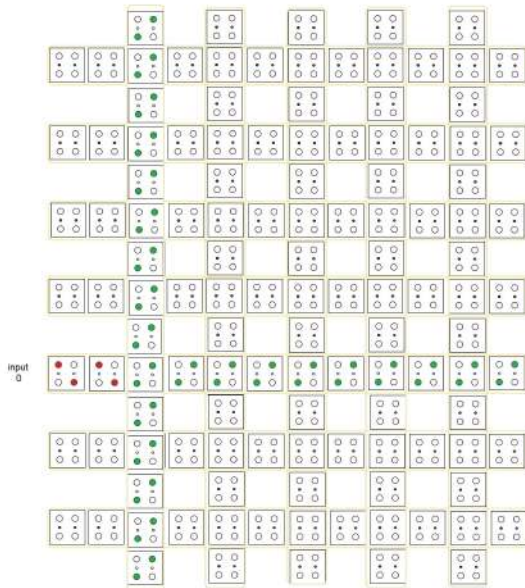


Figure 5.86: FULL ADDER simulation step 21

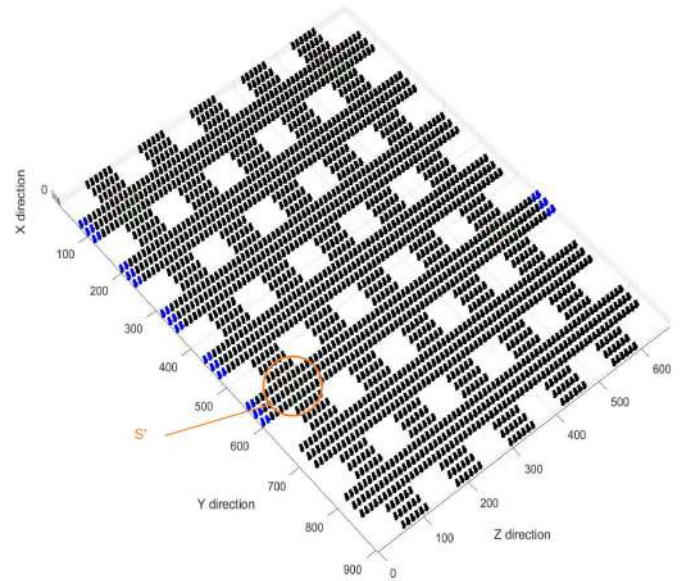
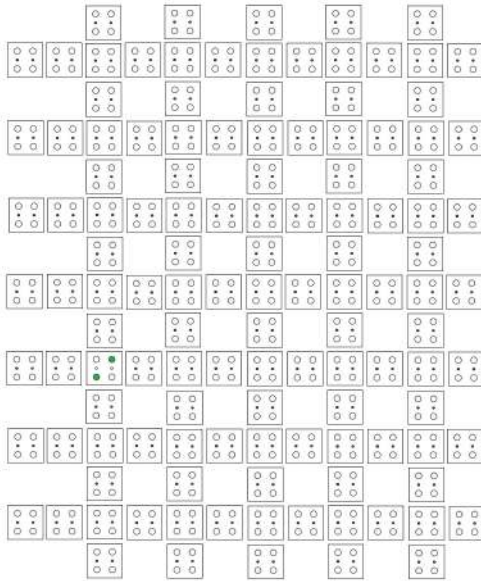


Figure 5.87: FULL ADDER simulation step 22

The value of  $S'$  find from the XOR is the input from the next parts of the operation: it is the input for the final summation and the Carry out. Moreover,  $S'$  will not be given by a driver, so it is necessary to create a copy of  $S'$  needed for the other operations.

To reduce the computational steps, the second logic operation realized is the ones needed to find the Carry out:

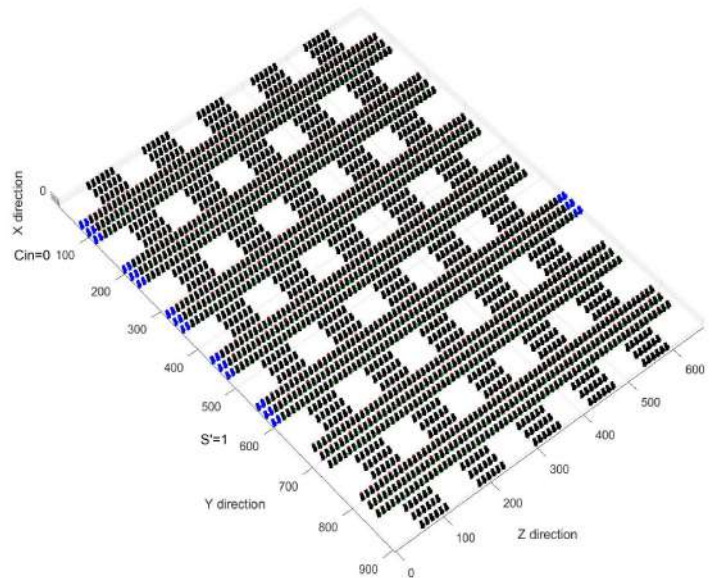
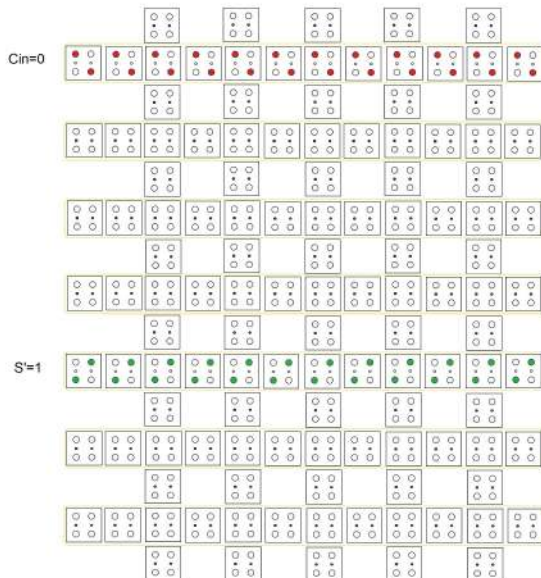


Figure 5.88: FULL ADDER simulation step 23

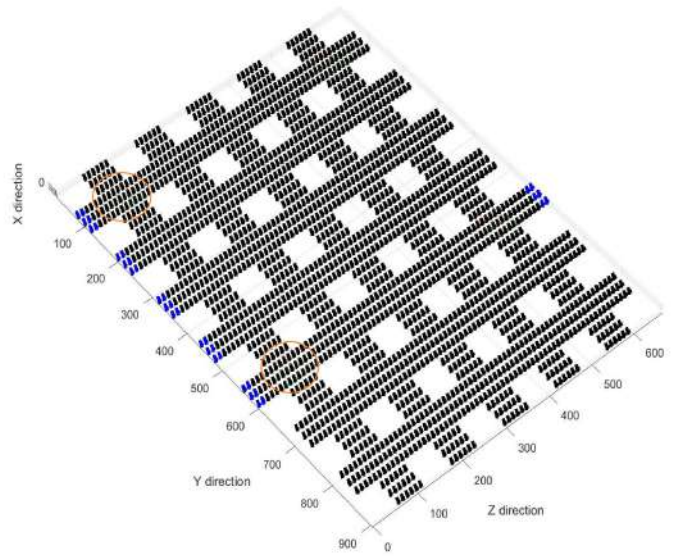
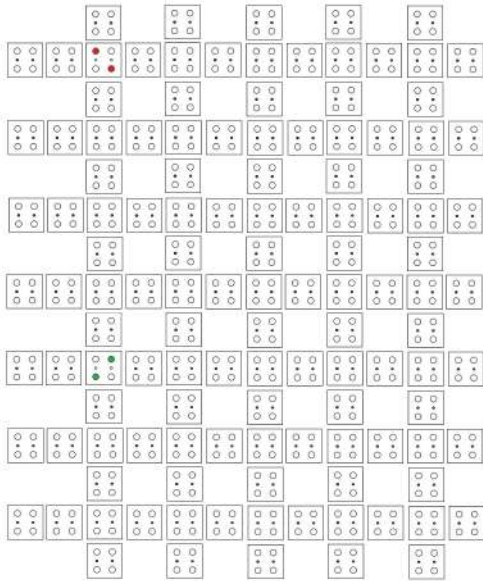


Figure 5.89: FULL ADDER simulation step 24

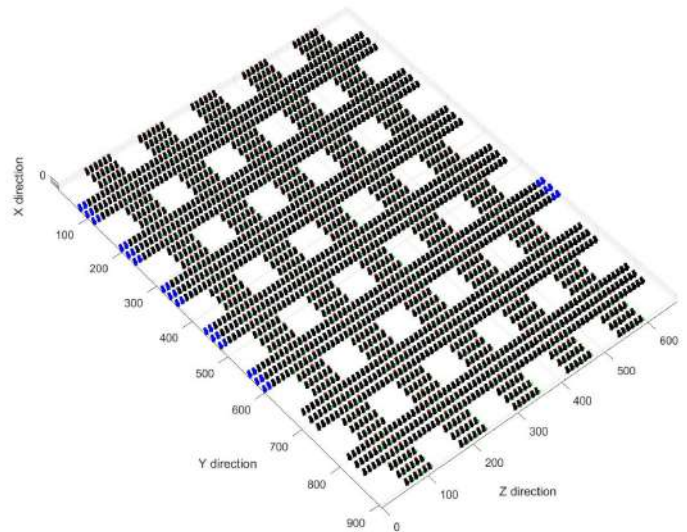
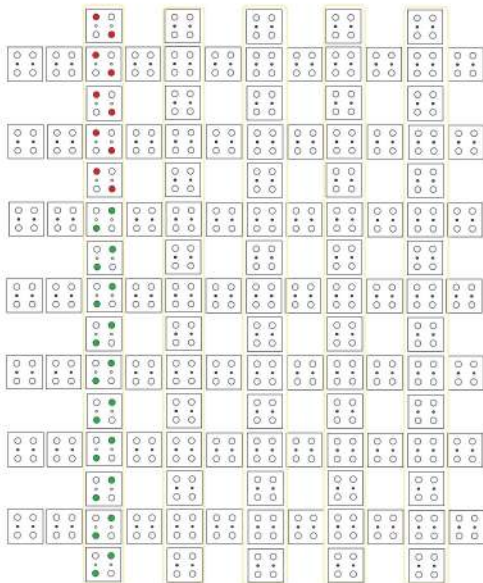


Figure 5.90: FULL ADDER simulation step 25

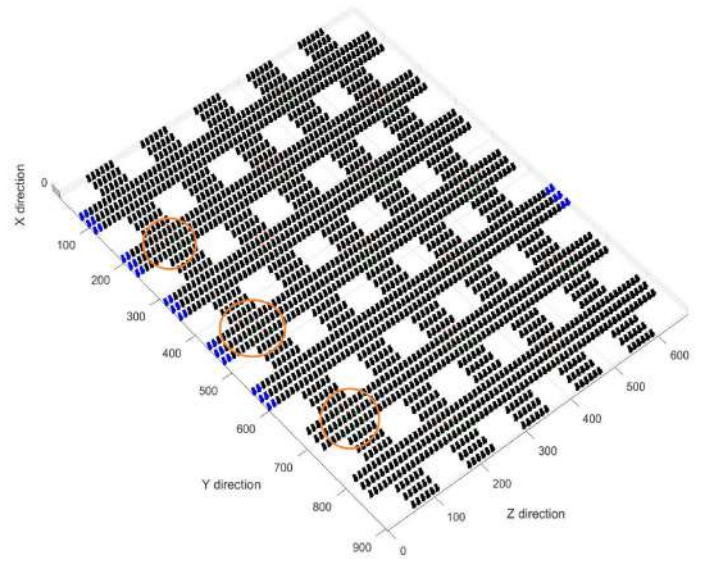
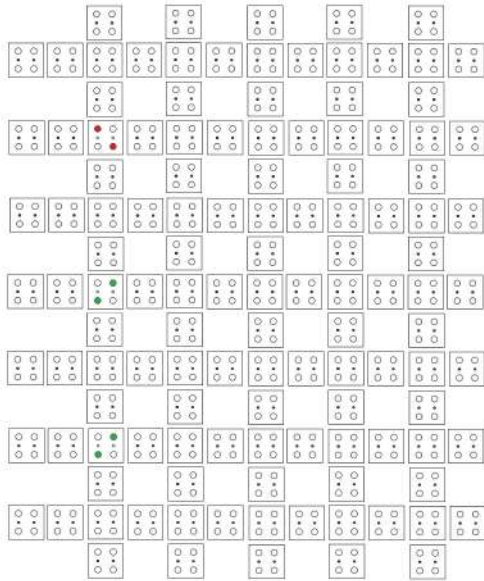


Figure 5.91: FULL ADDER simulation step 26

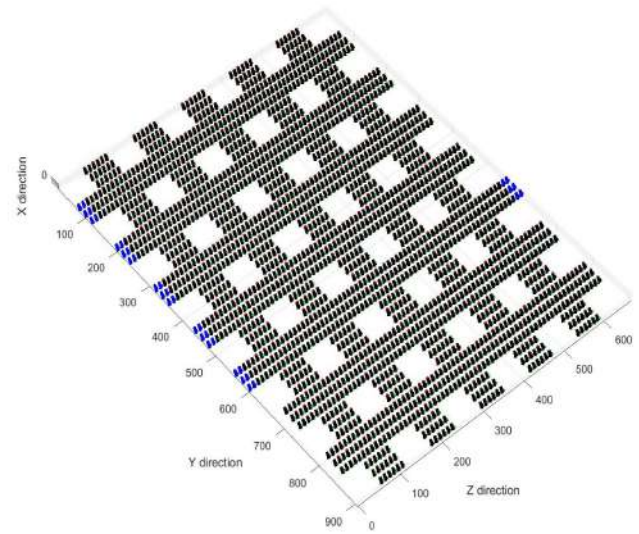
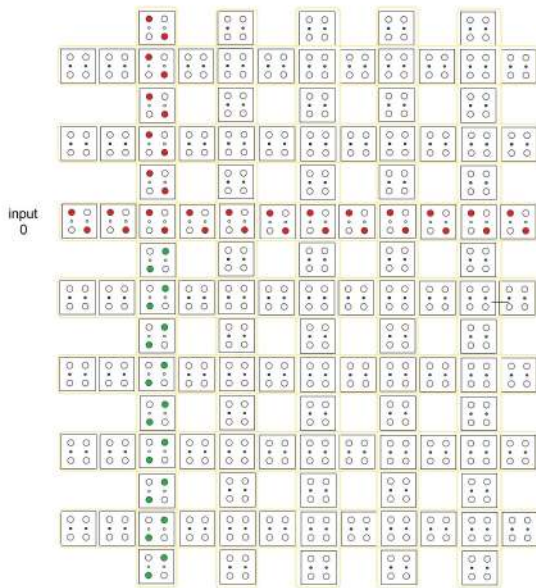


Figure 5.92: FULL ADDER simulation step 27

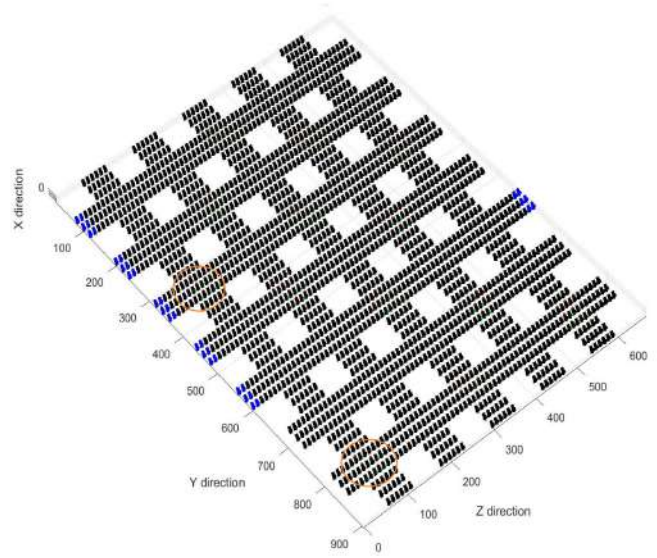
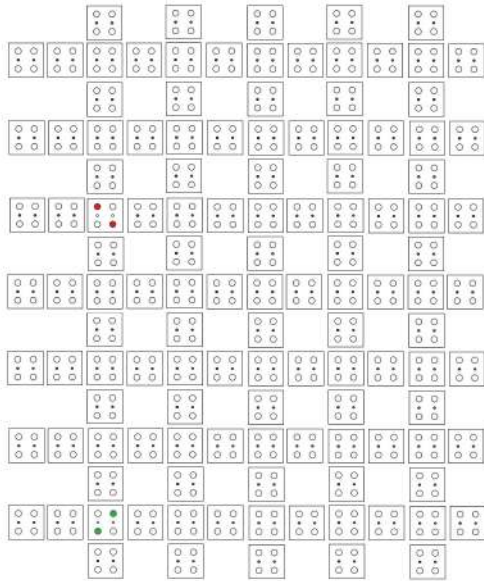


Figure 5.93: FULL ADDER simulation step 28

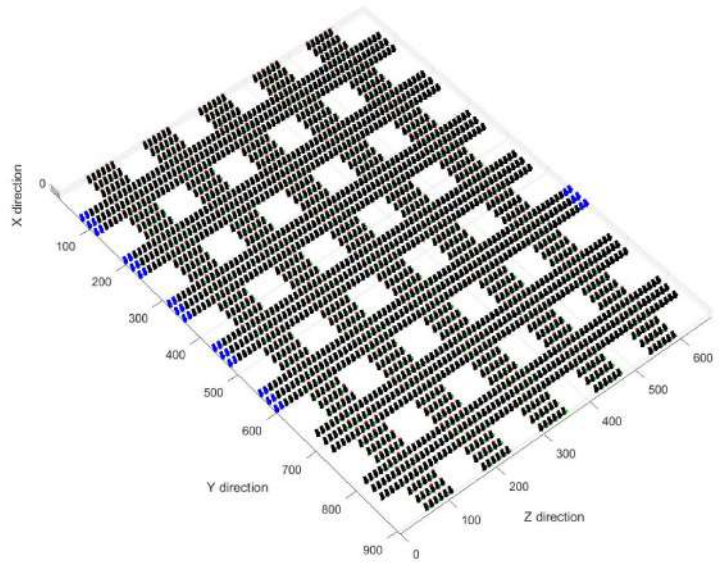
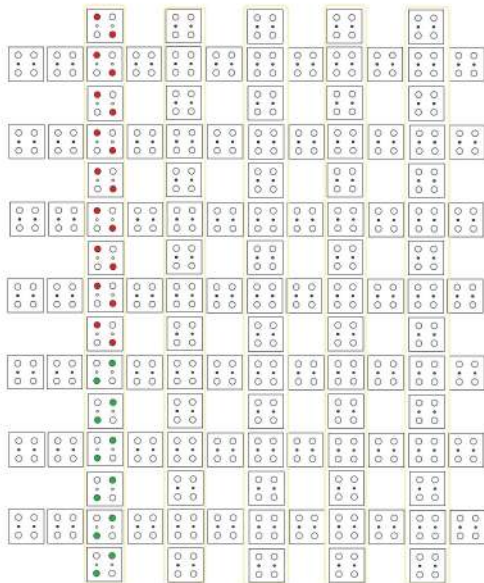


Figure 5.94: FULL ADDER simulation step 29

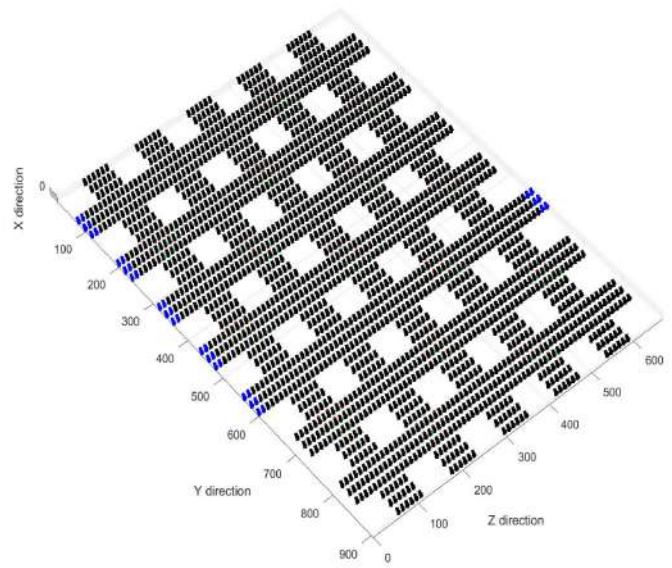
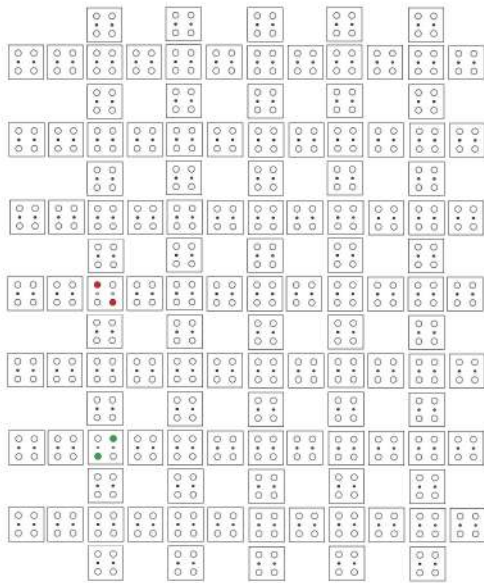


Figure 5.95: FULL ADDER simulation step 30

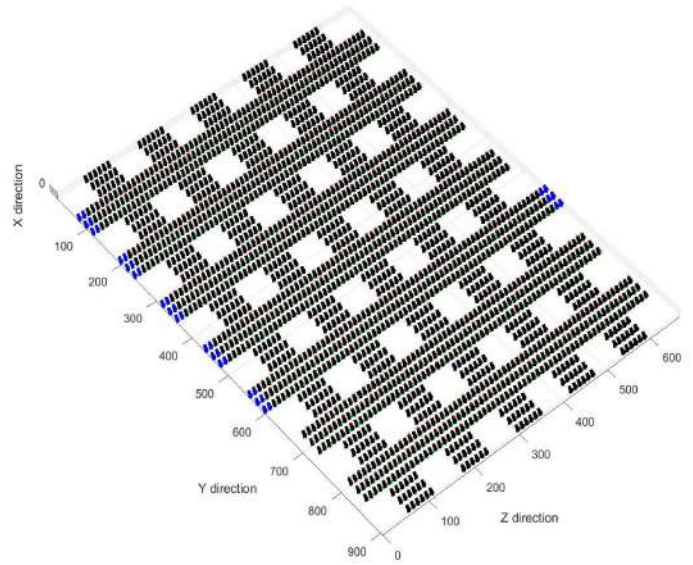
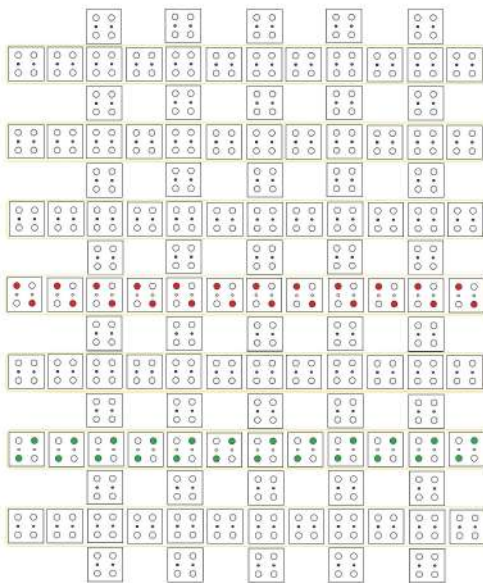


Figure 5.96: FULL ADDER simulation step 31

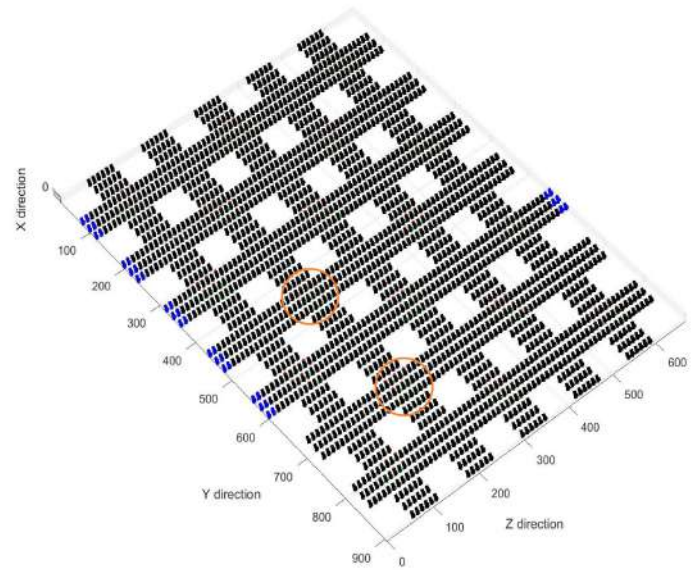
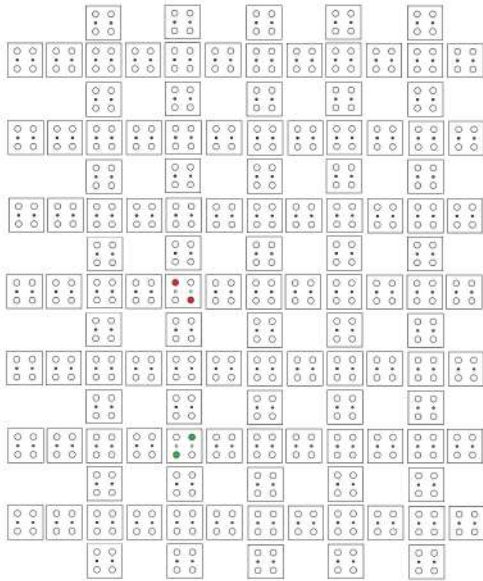


Figure 5.97: FULL ADDER simulation step 32

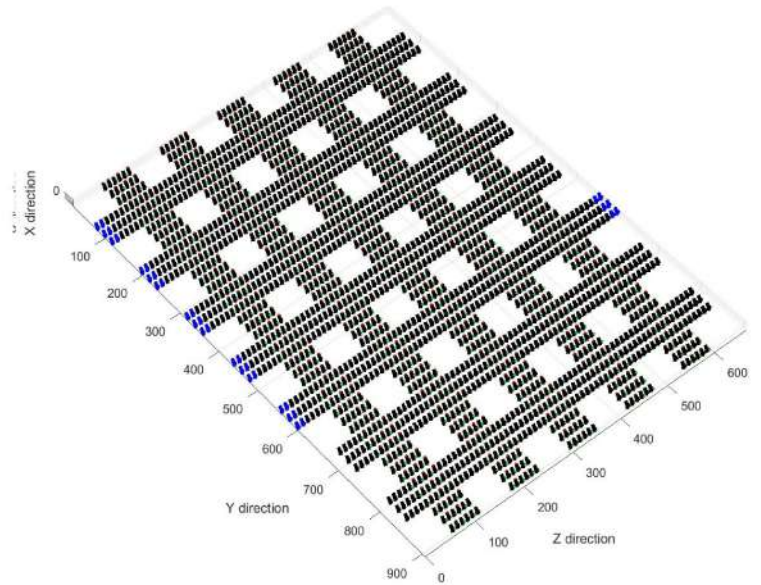
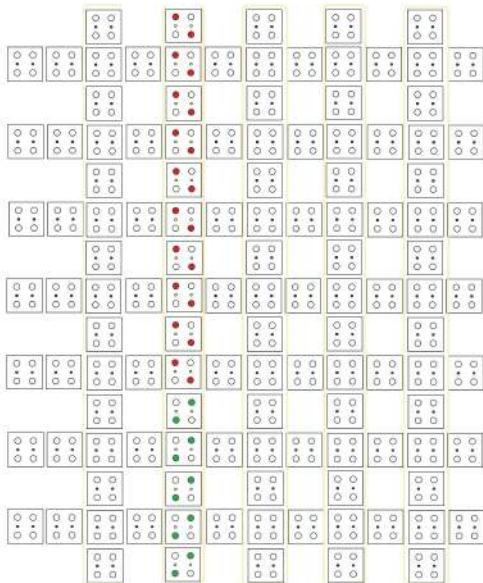


Figure 5.98: FULL ADDER simulation step 33

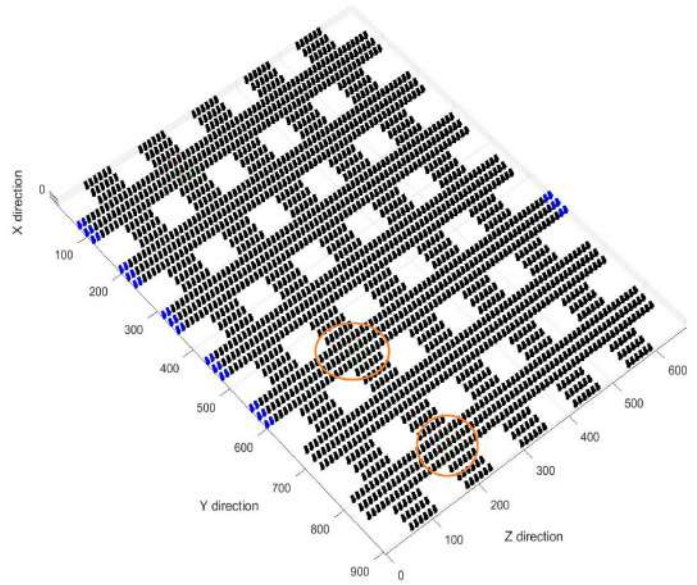
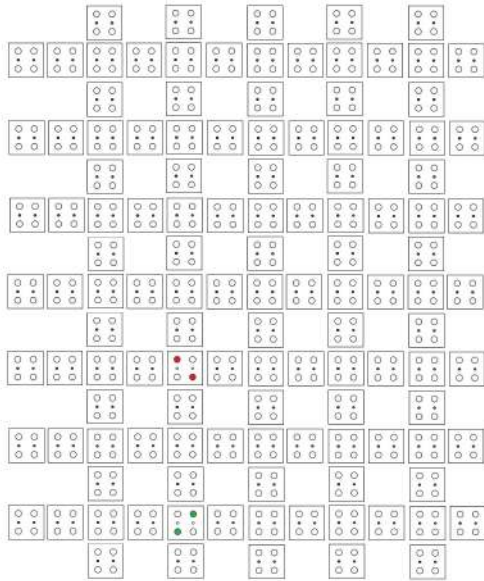


Figure 5.99: FULL ADDER simulation step 34

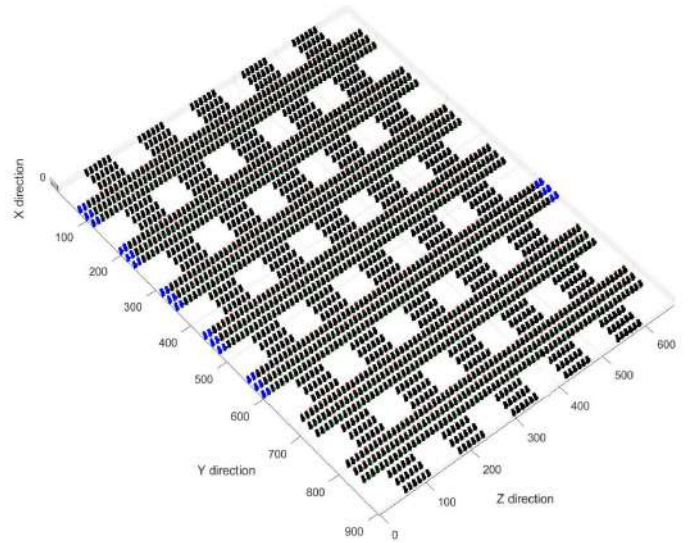
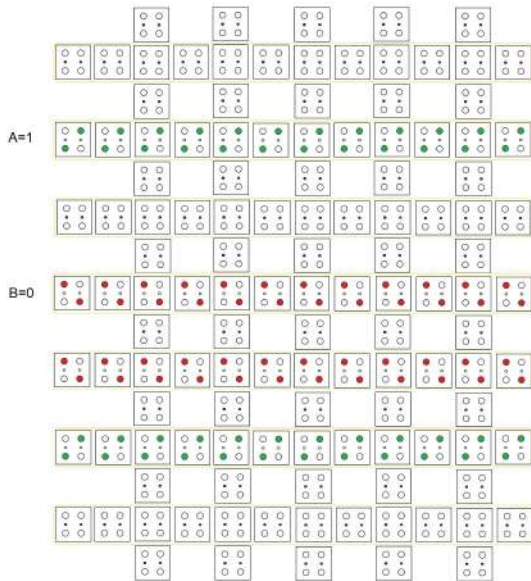


Figure 5.100: FULL ADDER simulation step 35

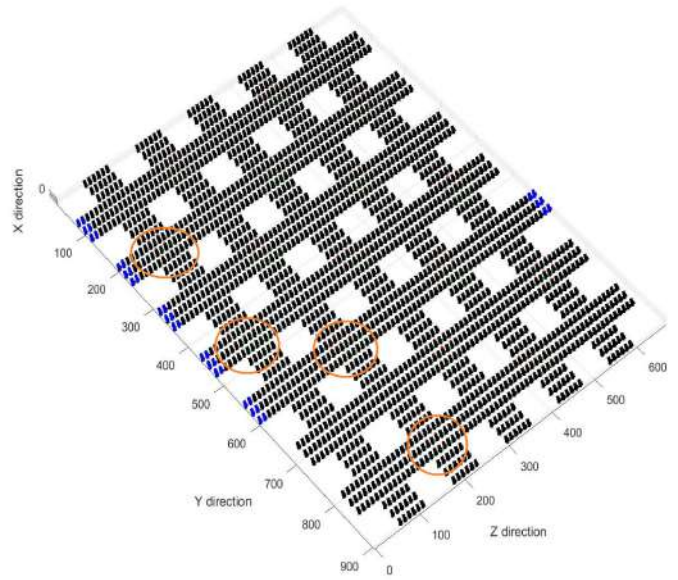


Figure 5.101: FULL ADDER simulation step 36

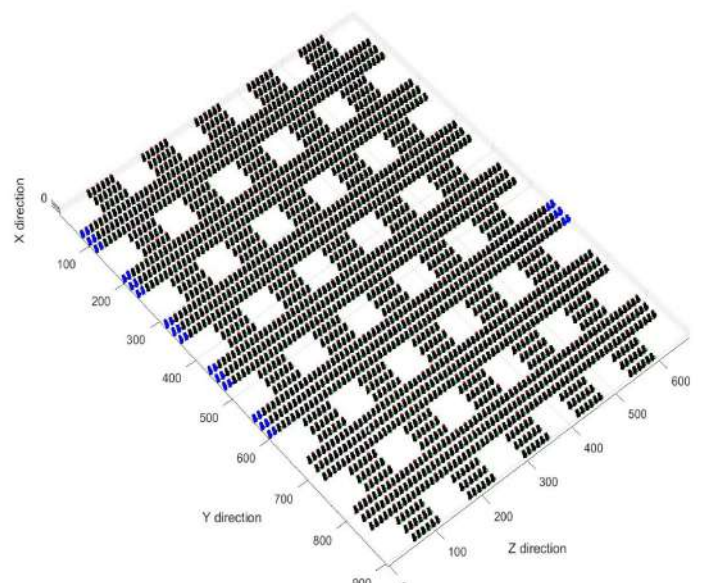
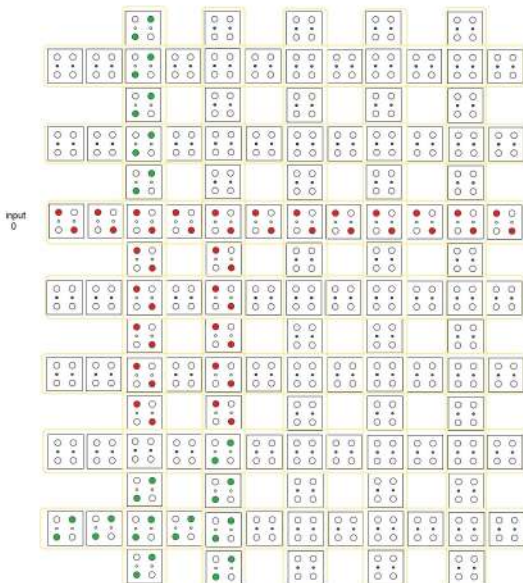


Figure 5.102: FULL ADDER simulation step 37

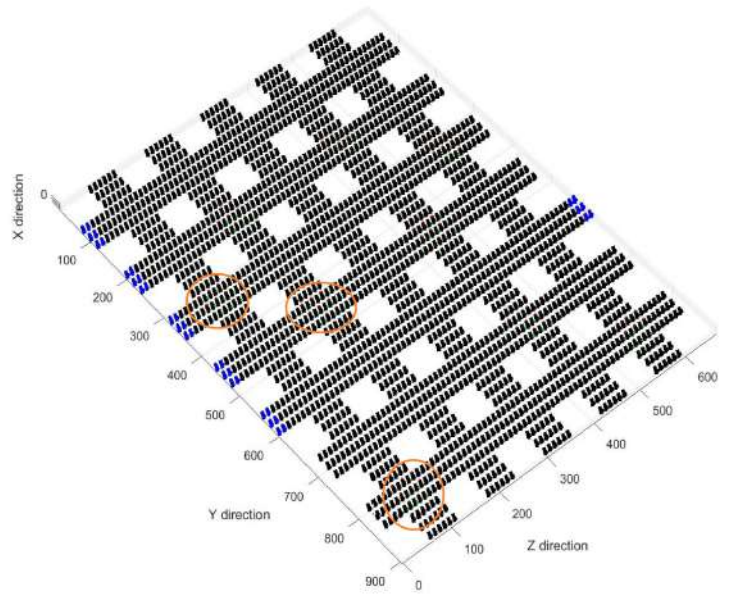
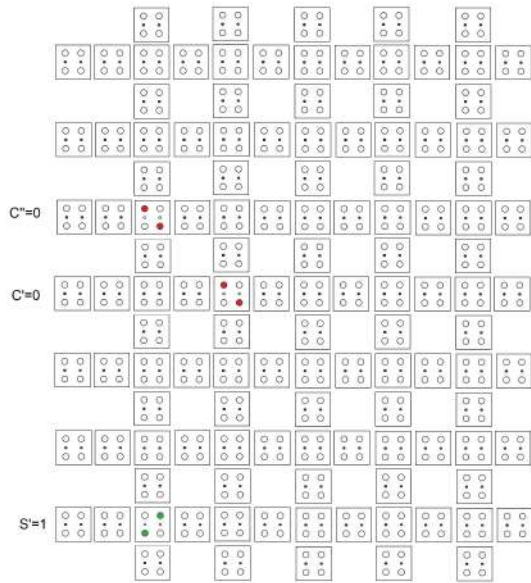


Figure 5.103: FULL ADDER simulation step 38

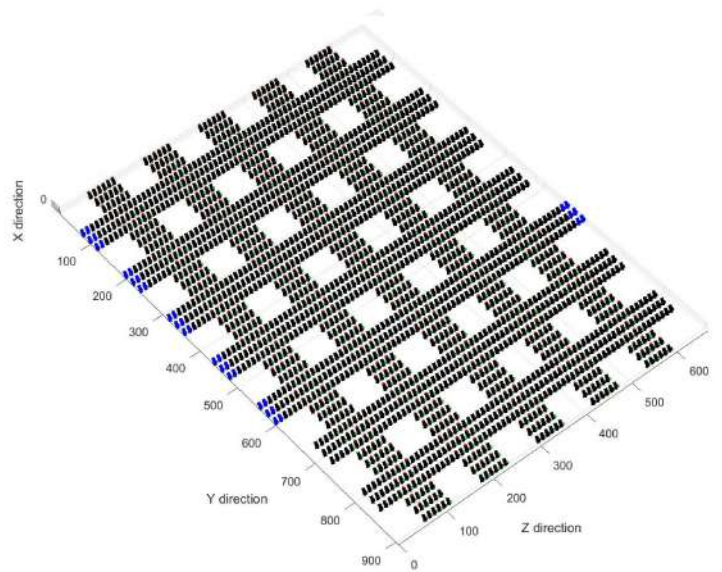
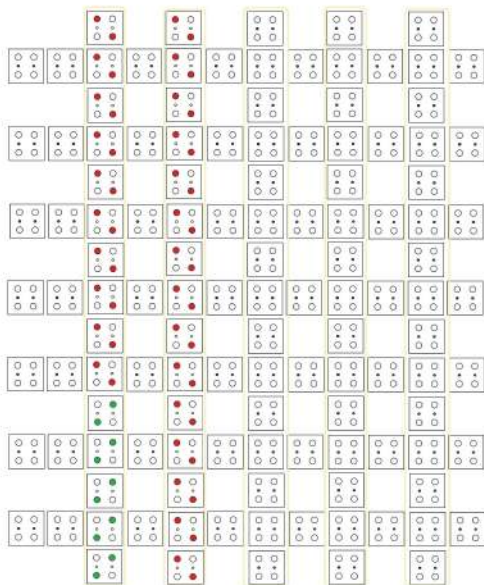


Figure 5.104: FULL ADDER simulation step 39

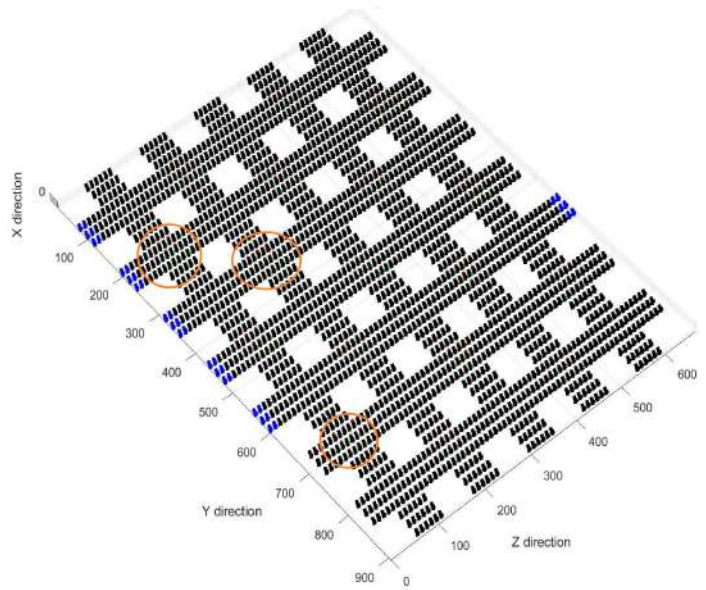
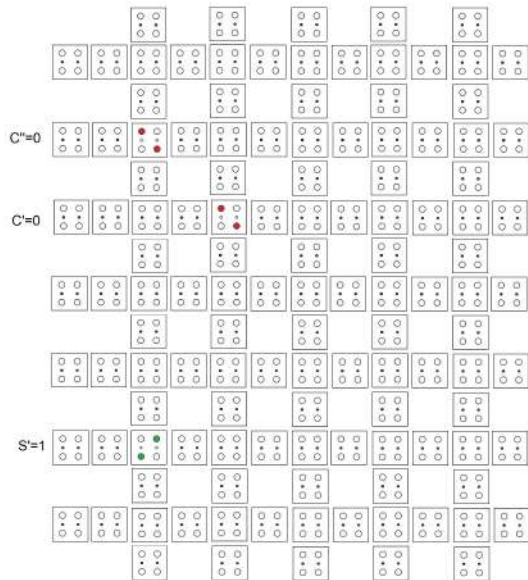


Figure 5.105: FULL ADDER simulation step 40

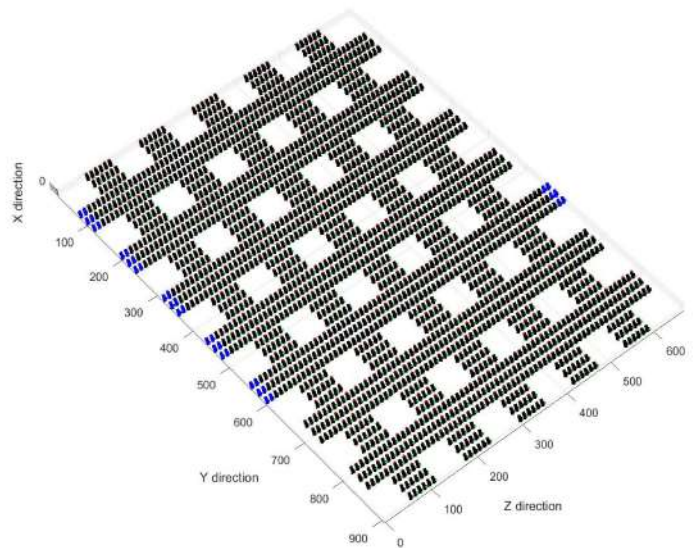
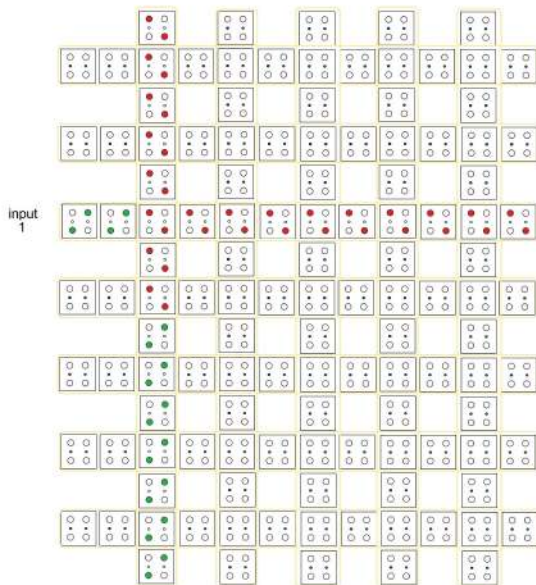


Figure 5.106: FULL ADDER simulation step 41

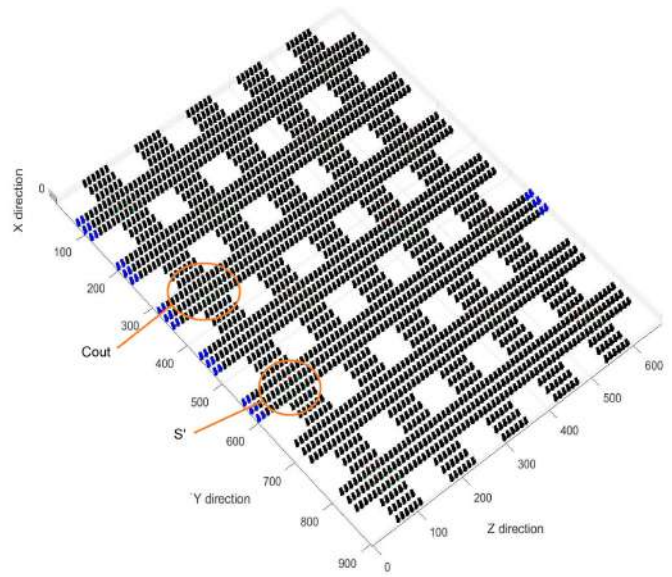
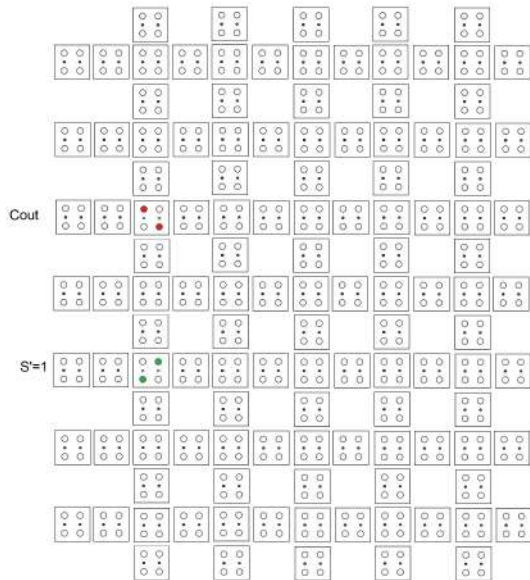


Figure 5.107: FULL ADDER simulation step 42

At this point the  $C_{out}$  result has been generated. The last part of the simulation consists of an XOR operation with inputs  $C_{in} = 0$  and  $S' = 1$ , to obtain the final result of the Full adder.

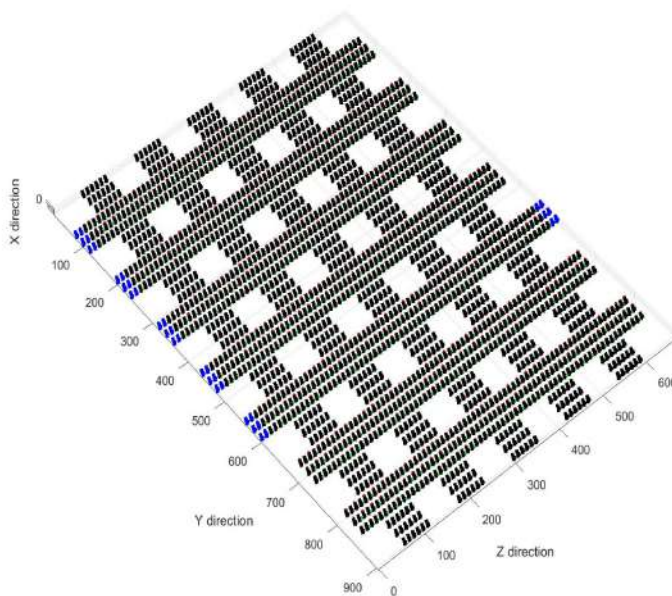
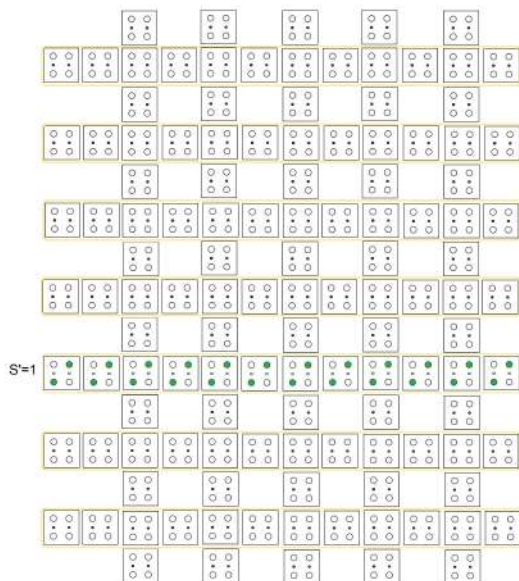


Figure 5.108: FULL ADDER simulation step 43

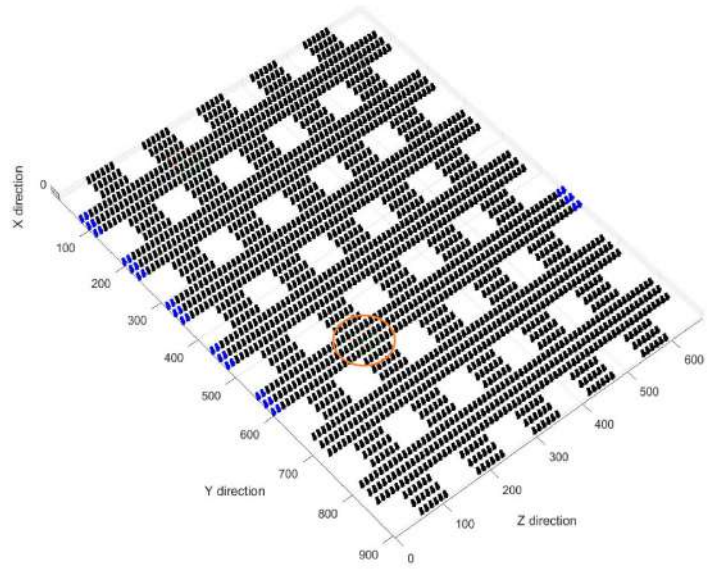
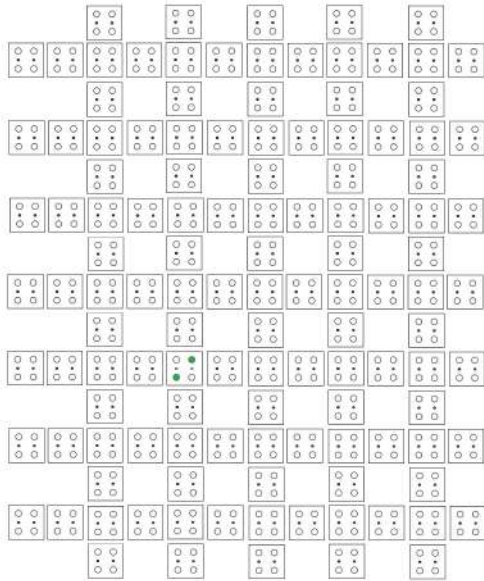


Figure 5.109: FULL ADDER simulation step 44

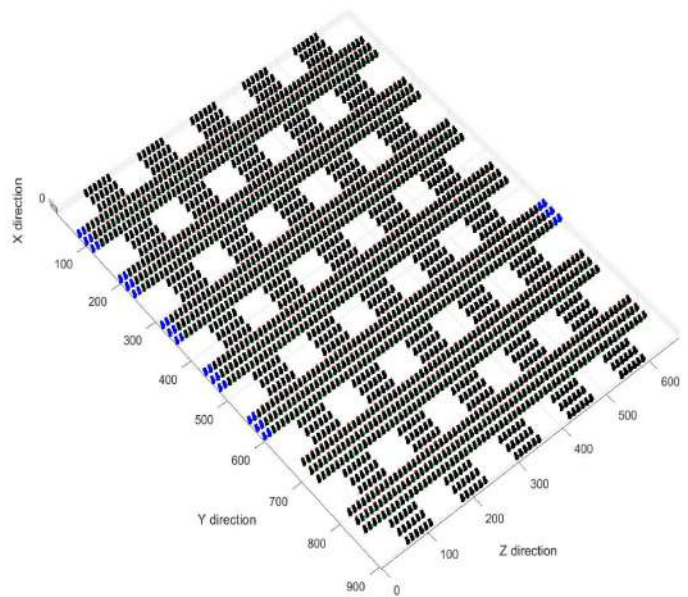
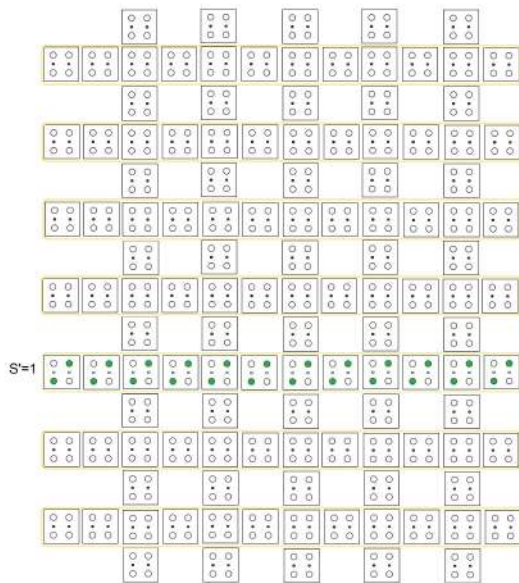


Figure 5.110: FULL ADDER simulation step 45

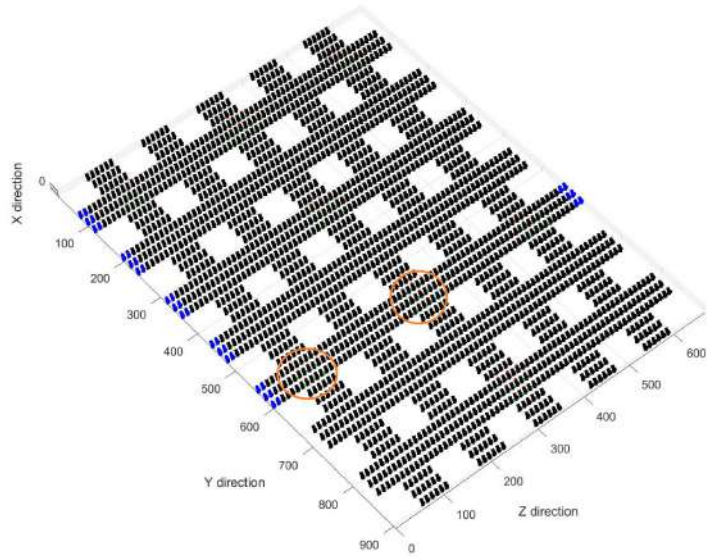
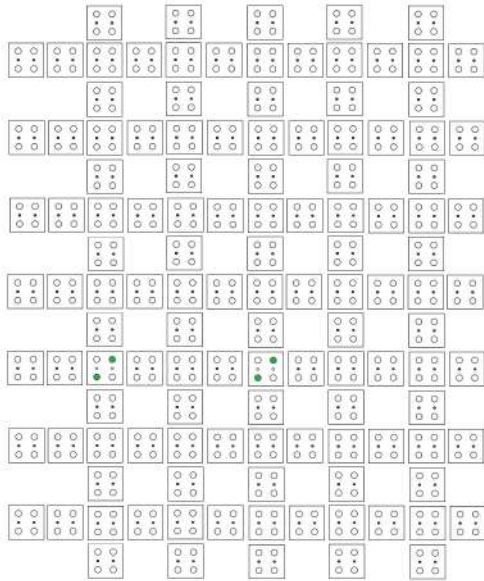


Figure 5.111: FULL ADDER simulation step 46

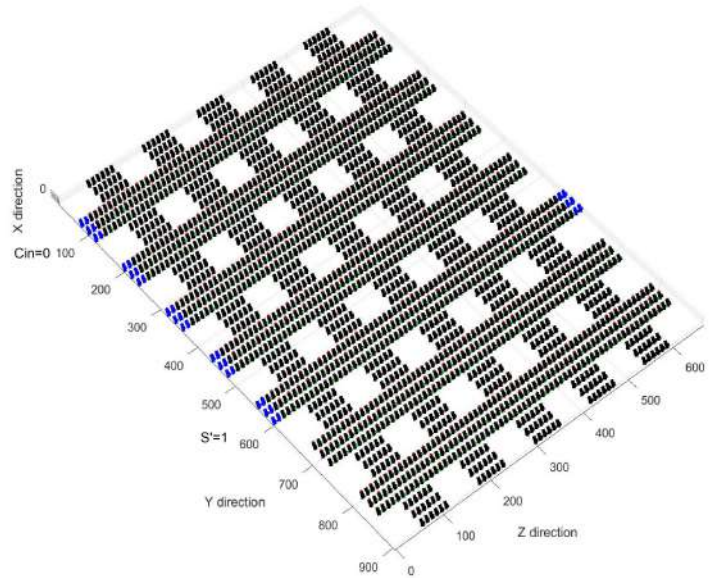
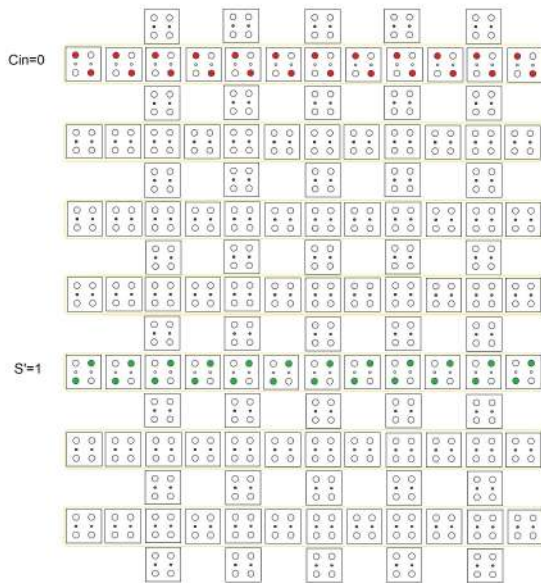


Figure 5.112: FULL ADDER simulation step 47

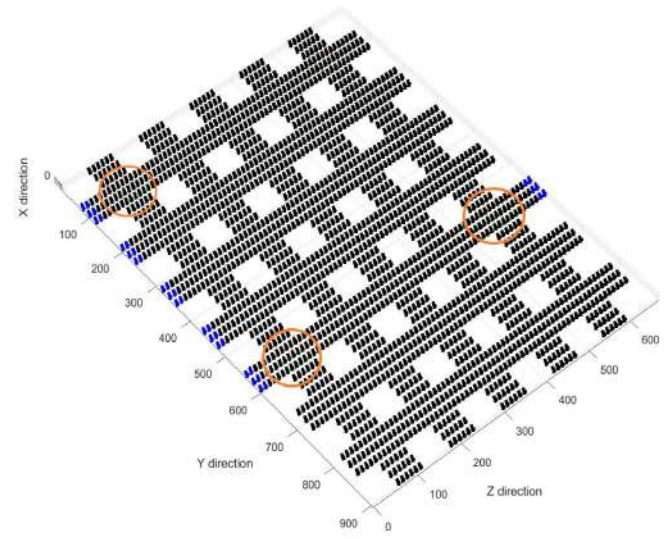
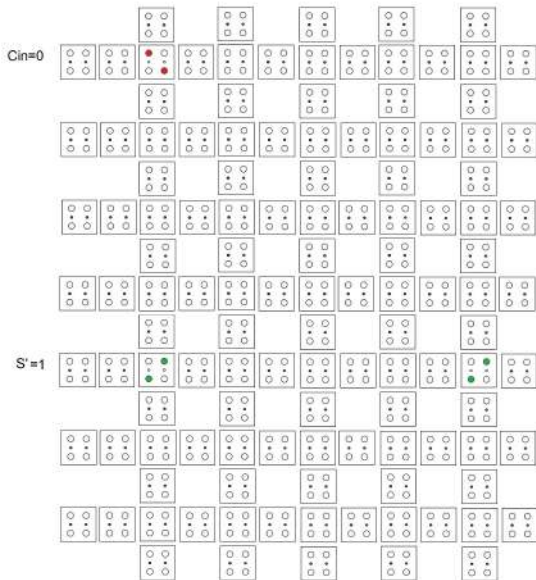


Figure 5.113: FULL ADDER simulation step 48

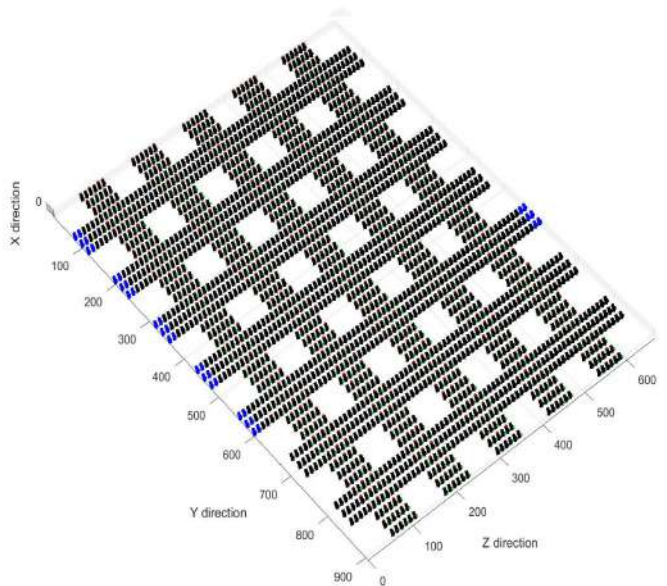
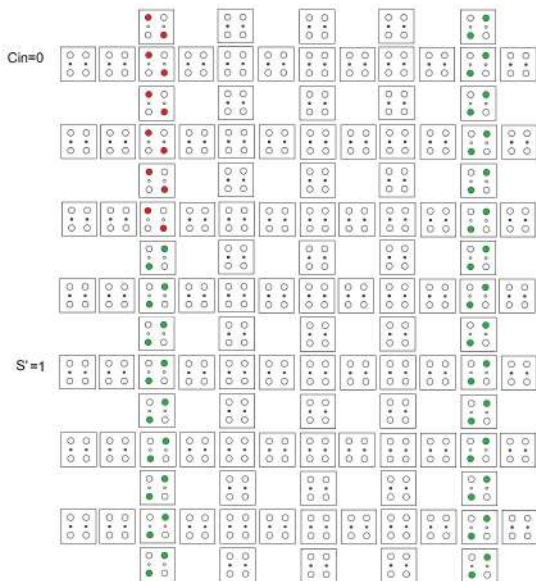


Figure 5.114: FULL ADDER simulation step 49

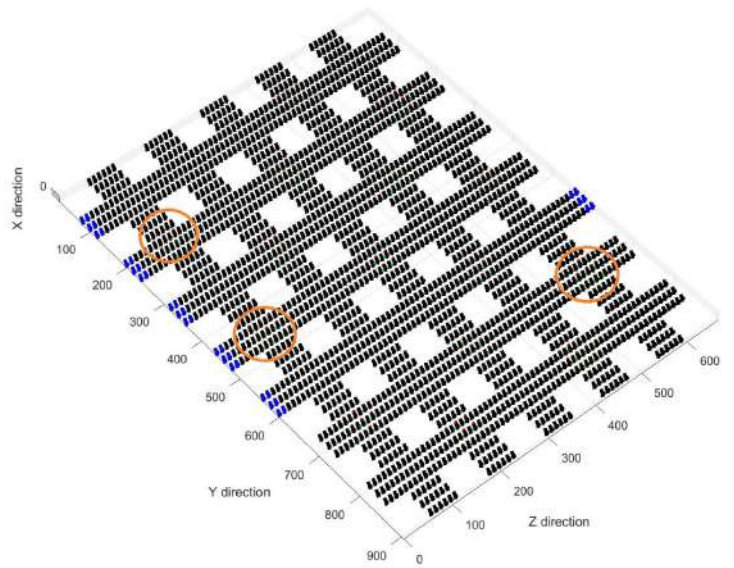
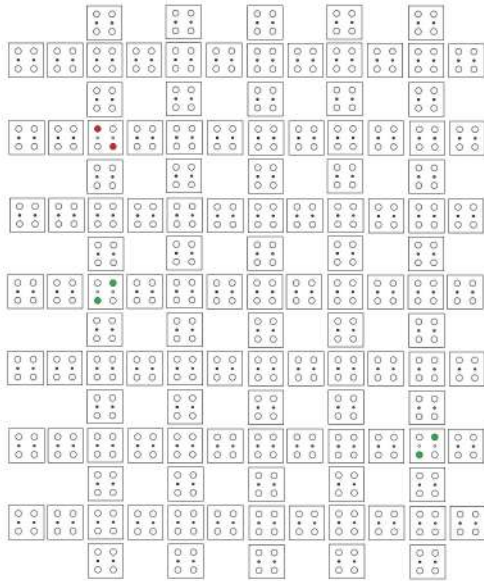


Figure 5.115: FULL ADDER simulation step 50

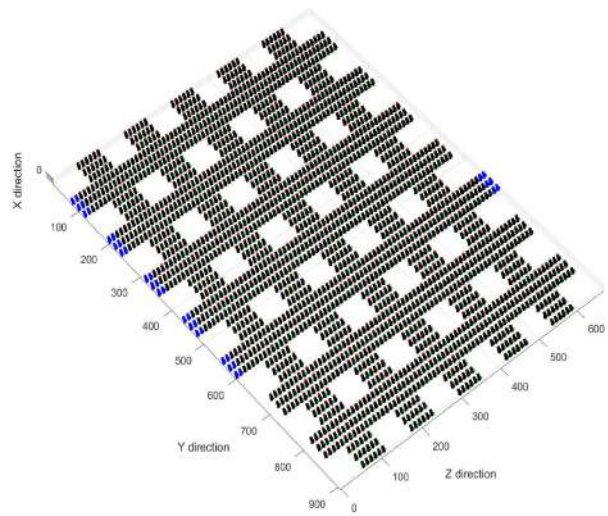
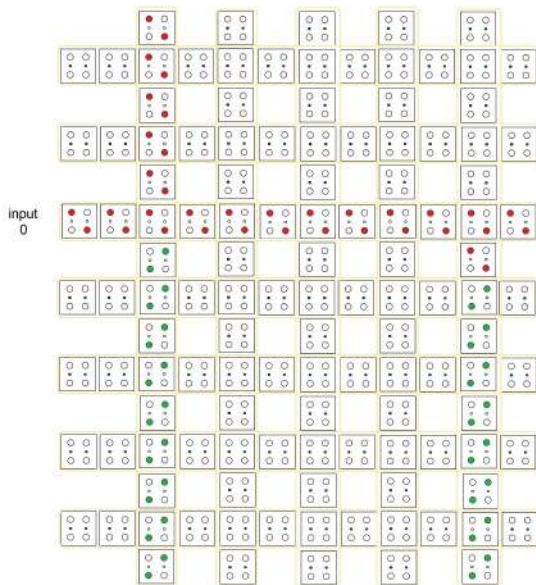


Figure 5.116: FULL ADDER simulation step 51

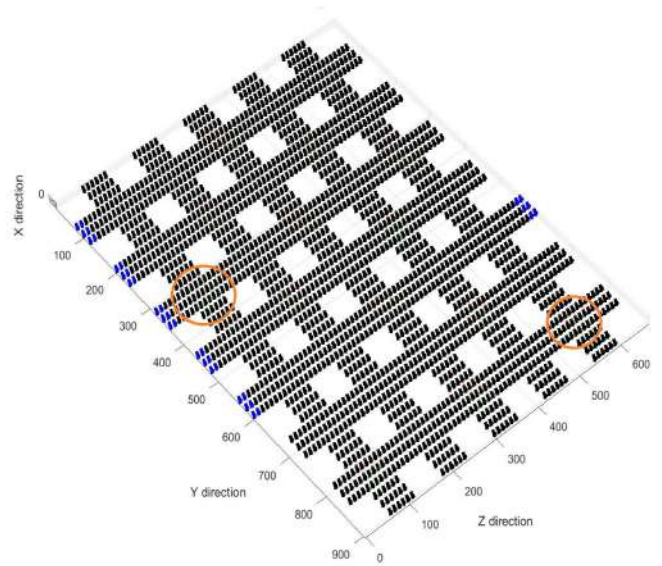
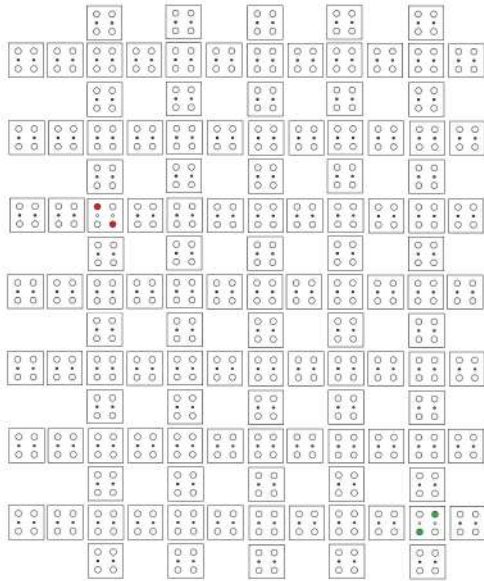


Figure 5.117: FULL ADDER simulation step 52

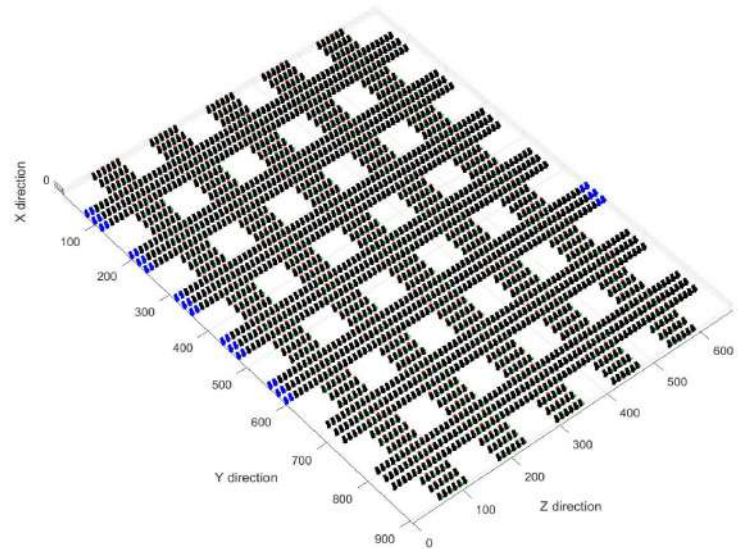
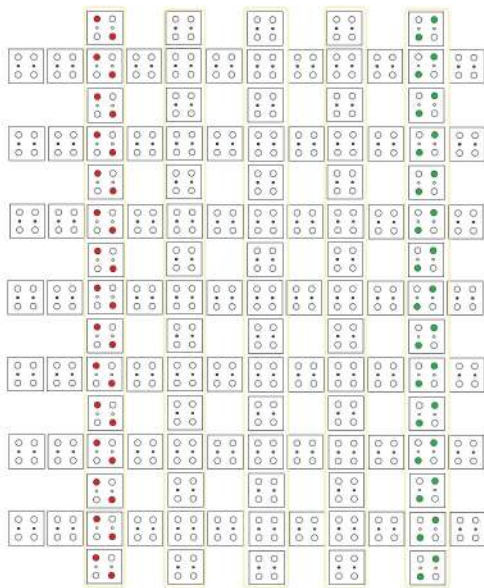


Figure 5.118: FULL ADDER simulation step 53

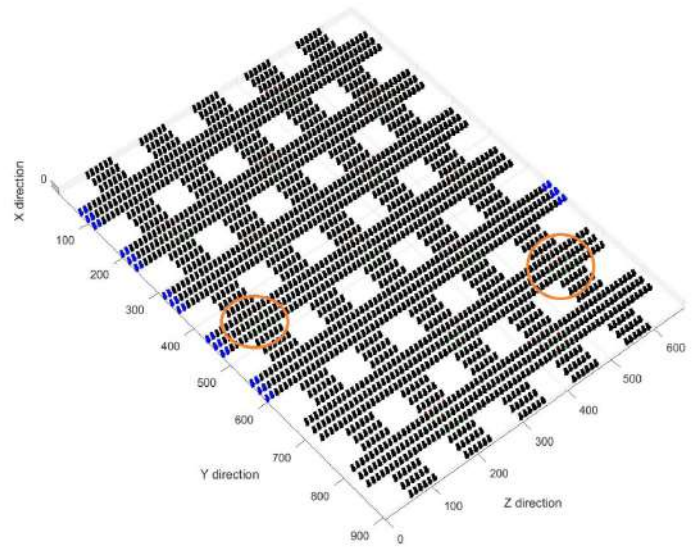
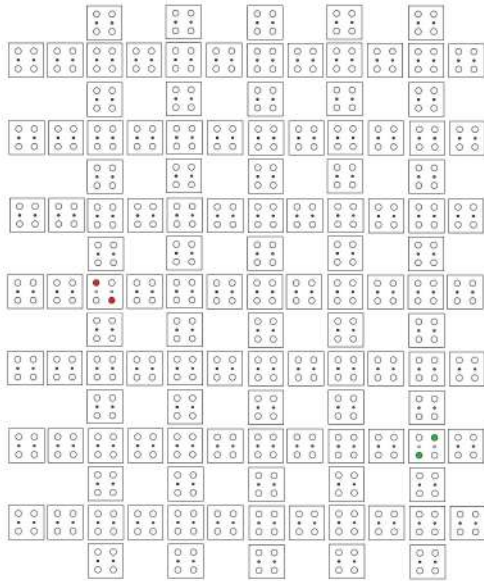


Figure 5.119: FULL ADDER simulation step 54

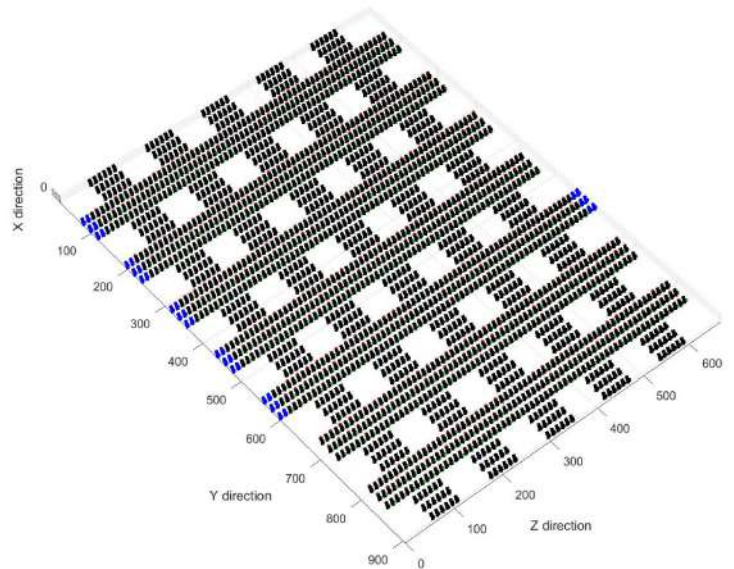
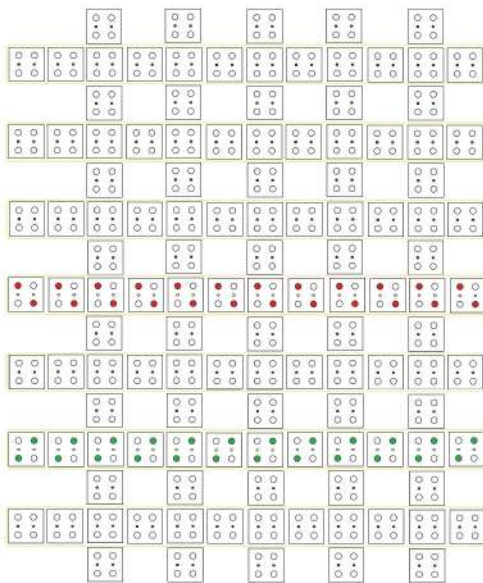


Figure 5.120: FULL ADDER simulation step 55

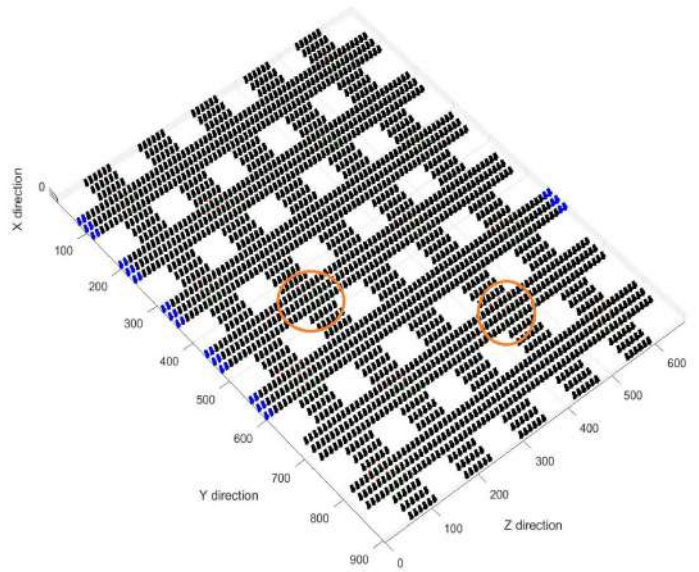
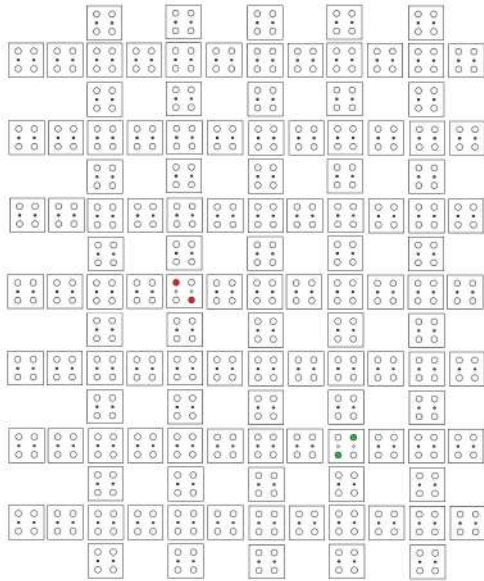


Figure 5.121: FULL ADDER simulation step 56

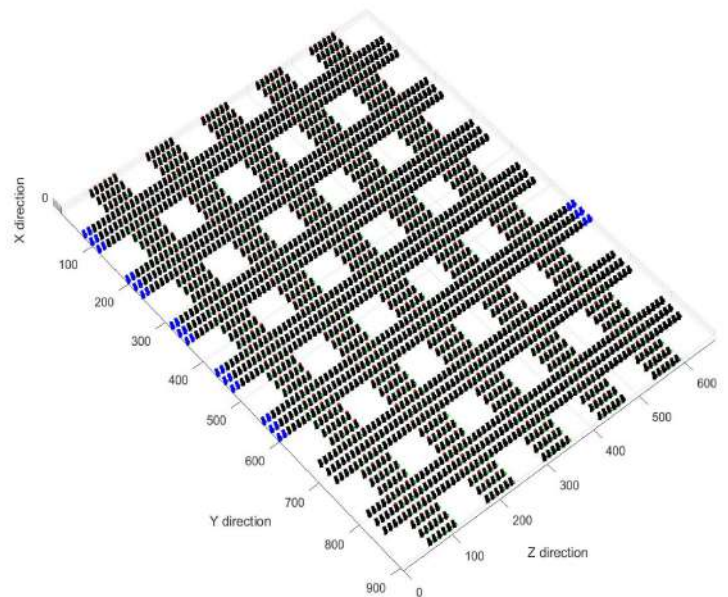
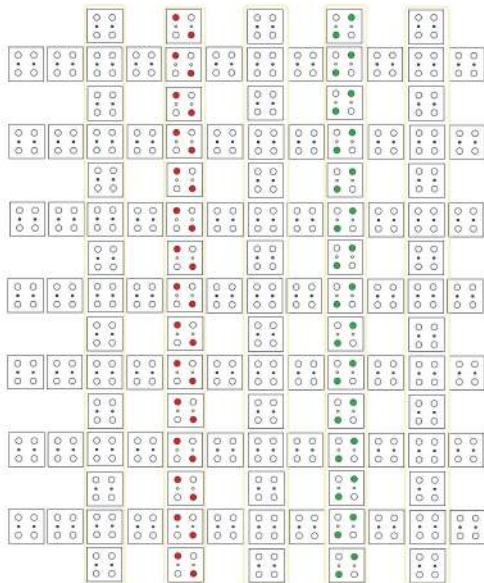


Figure 5.122: FULL ADDER simulation step 57

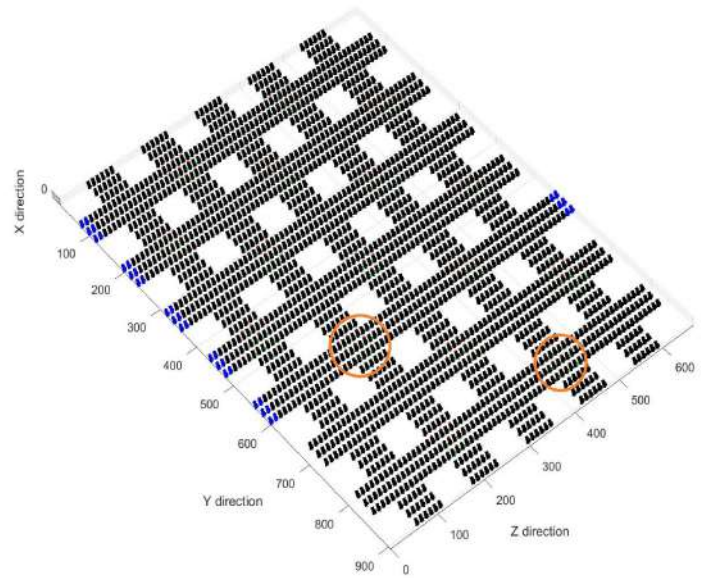
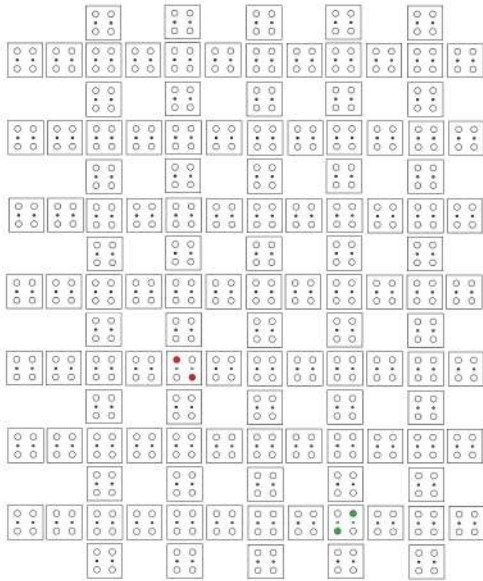


Figure 5.123: FULL ADDER simulation step 58

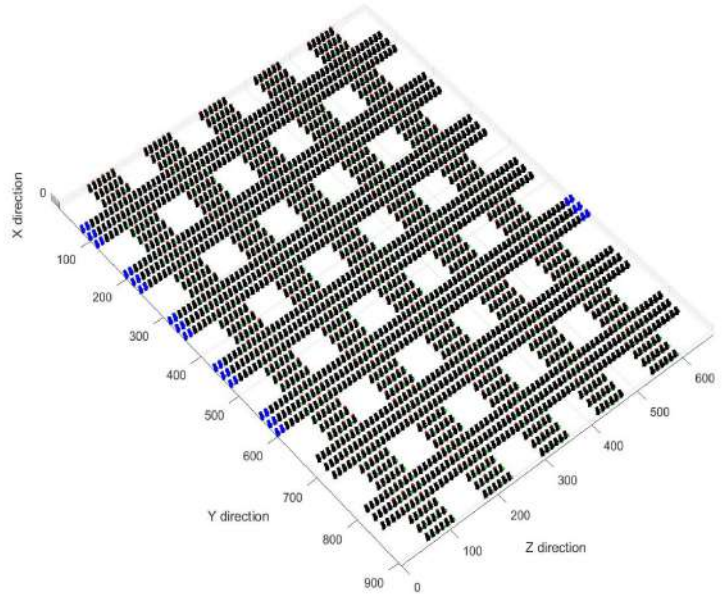
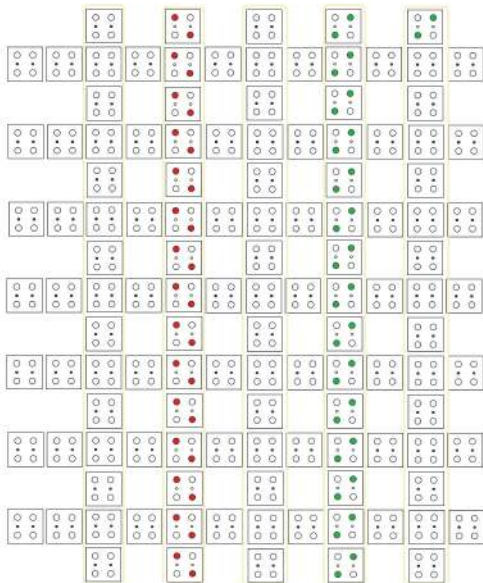


Figure 5.124: FULL ADDER simulation step 59

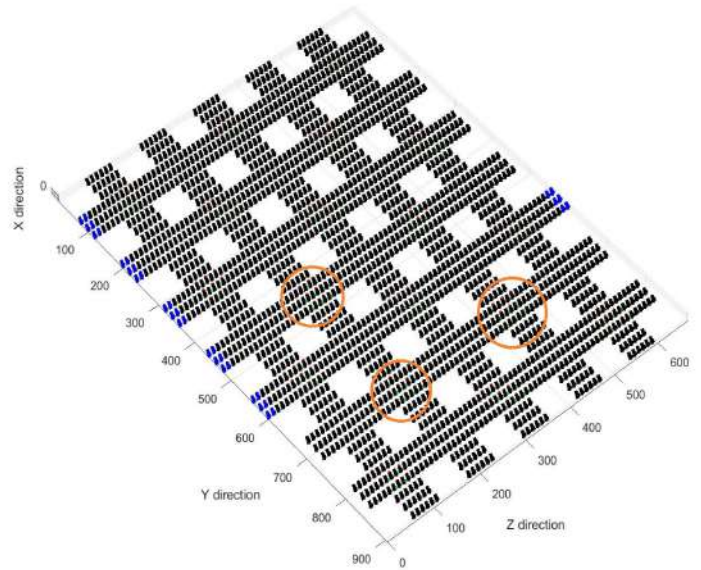
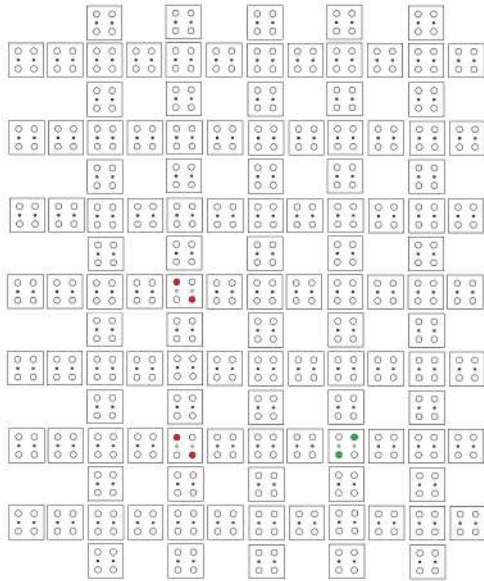


Figure 5.125: FULL ADDER simulation step 60

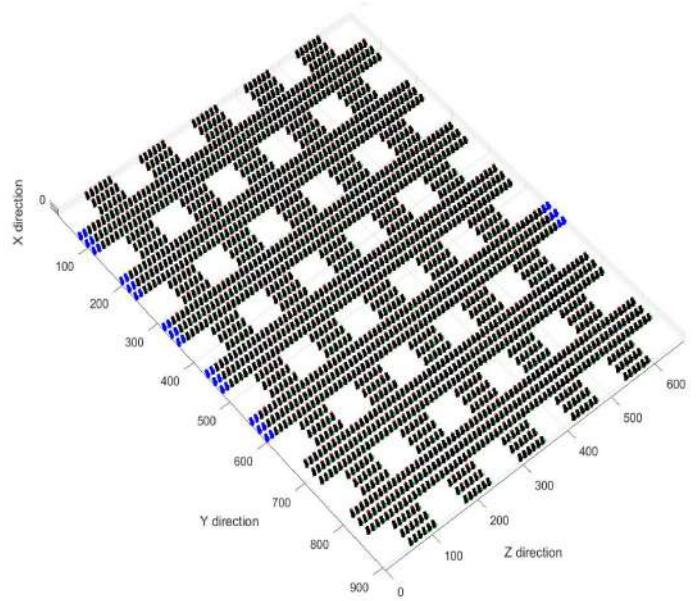
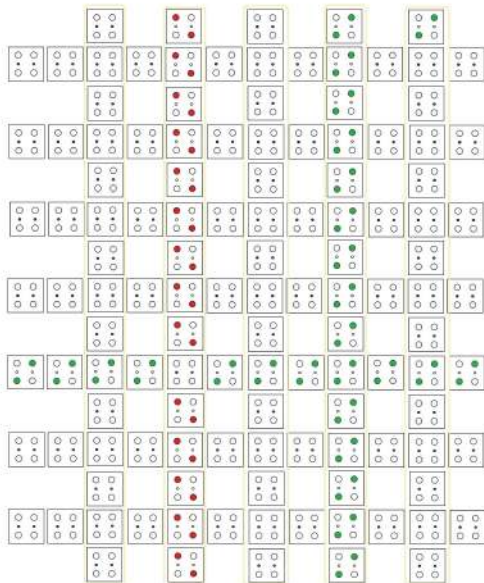


Figure 5.126: FULL ADDER simulation step 61

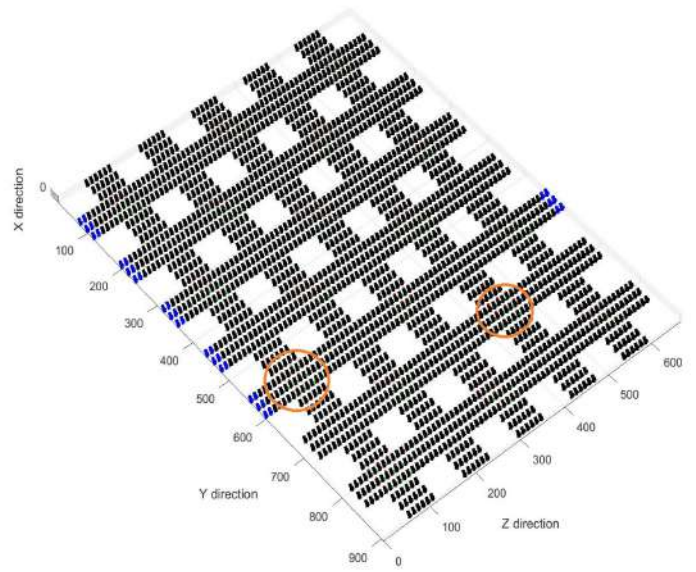
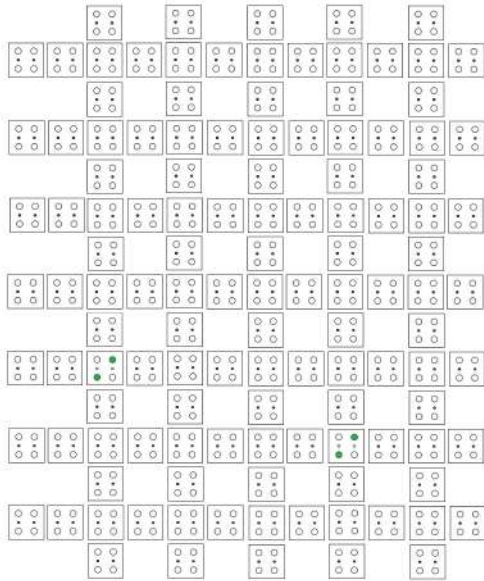


Figure 5.127: FULL ADDER simulation step 62

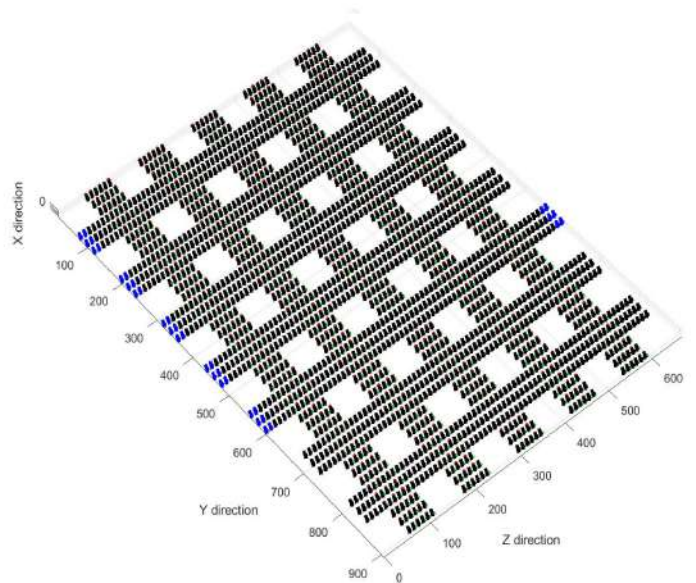
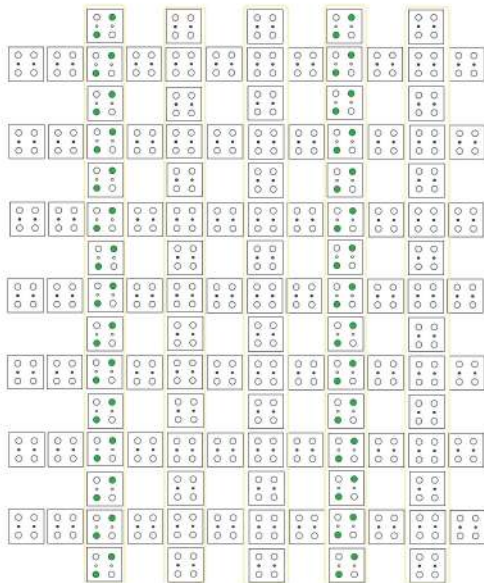


Figure 5.128: FULL ADDER simulation step 63

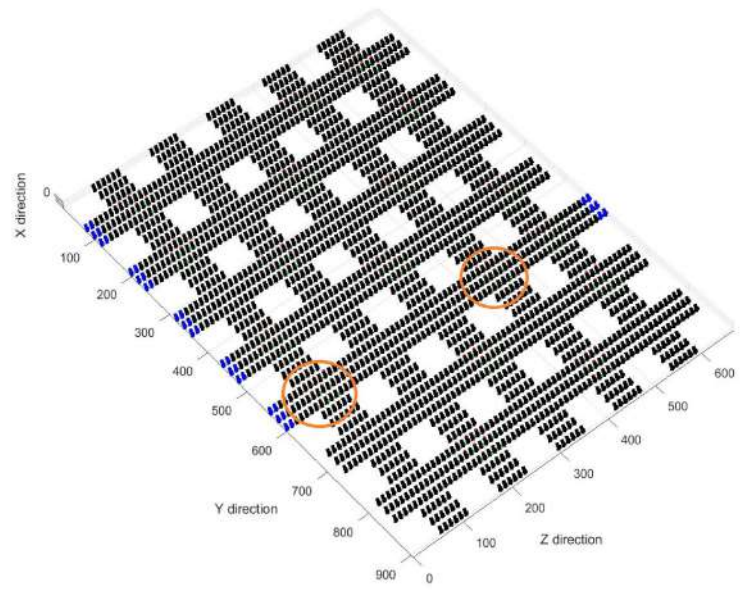
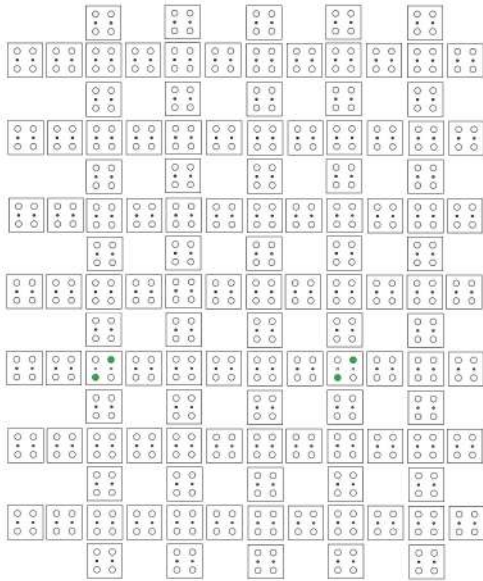


Figure 5.129: FULL ADDER simulation step 64

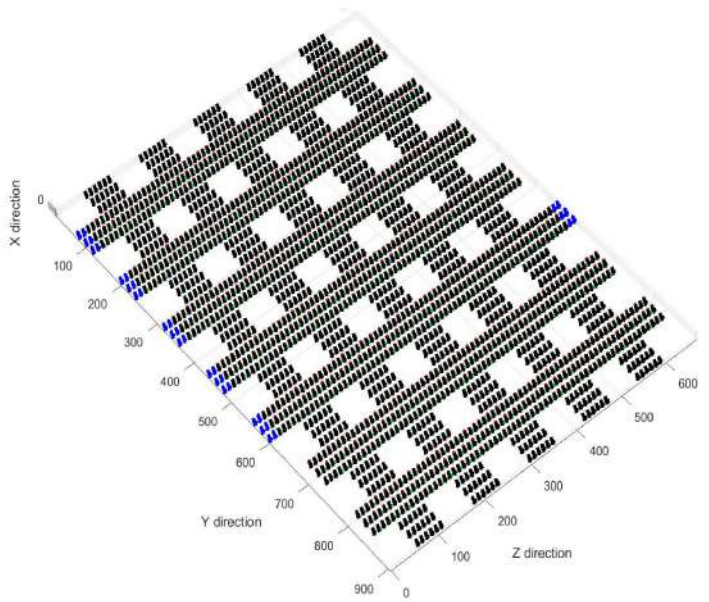
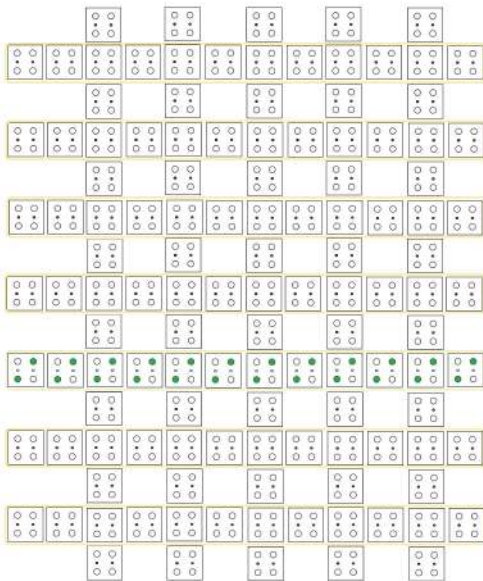


Figure 5.130: FULL ADDER simulation step 65

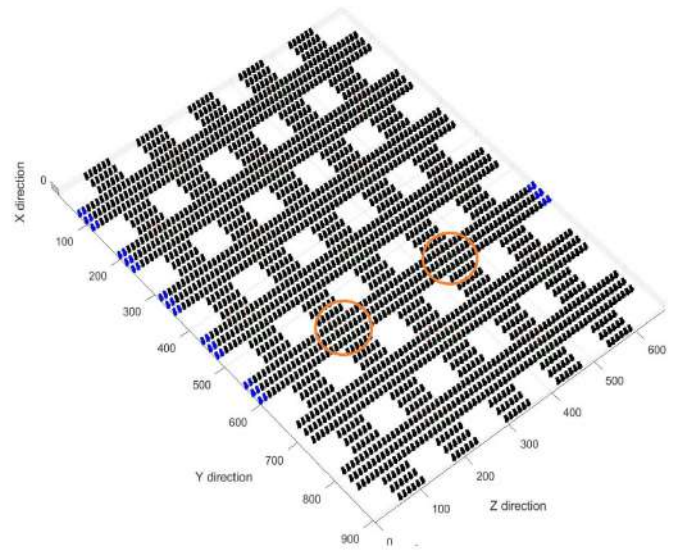
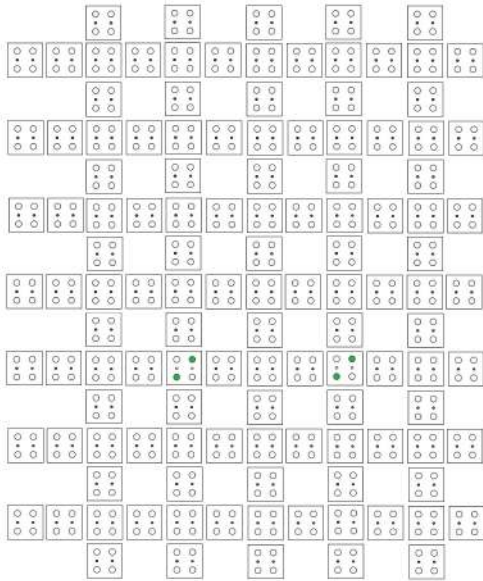


Figure 5.131: FULL ADDER simulation step 66

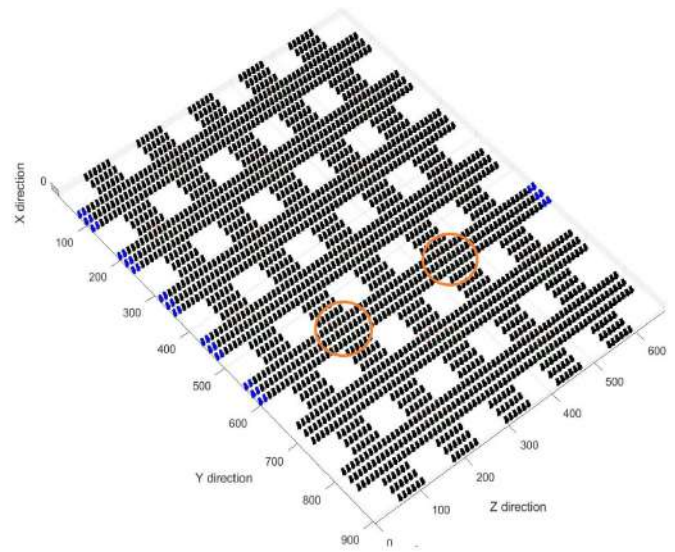
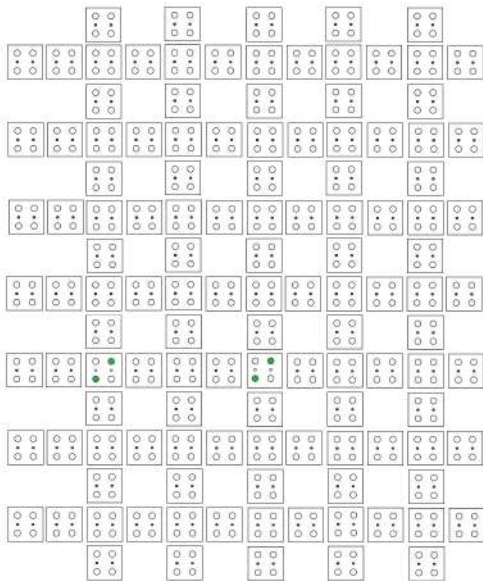


Figure 5.132: FULL ADDER simulation step 67

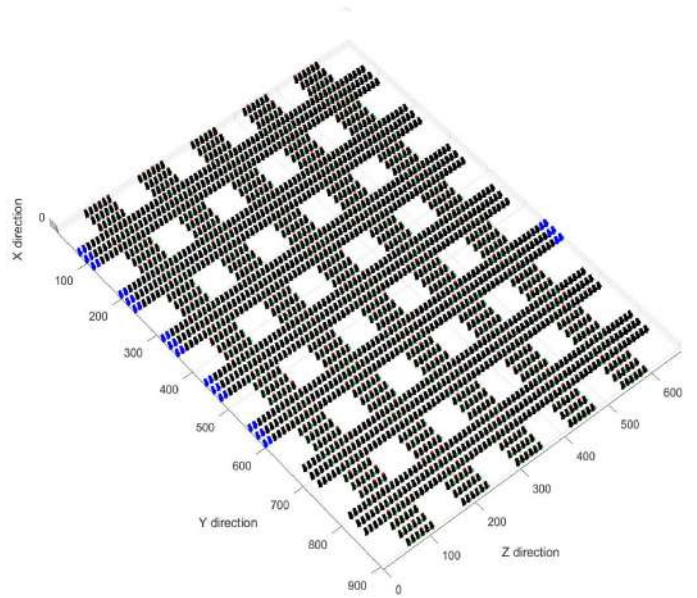
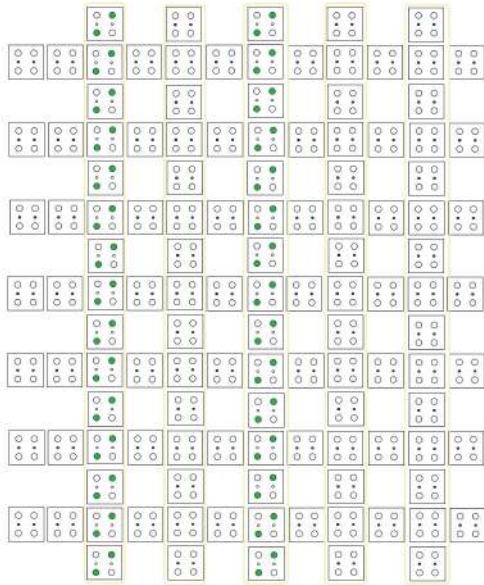


Figure 5.133: FULL ADDER simulation step 68

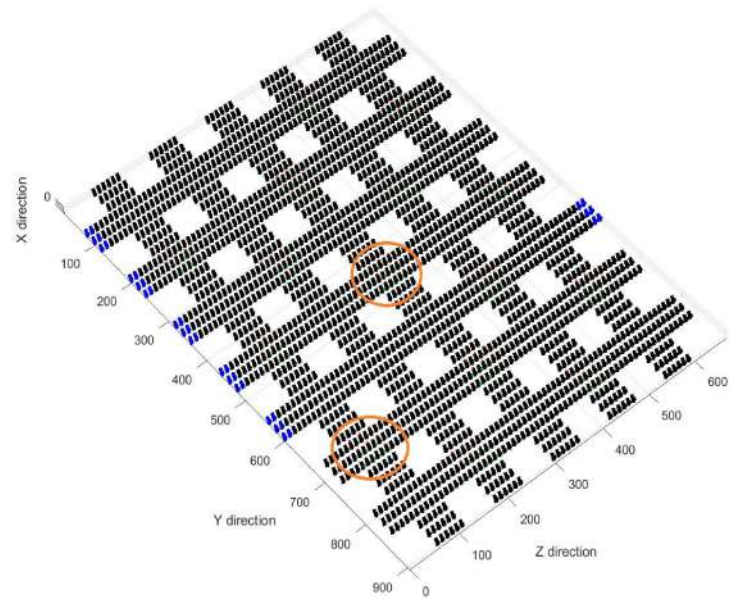
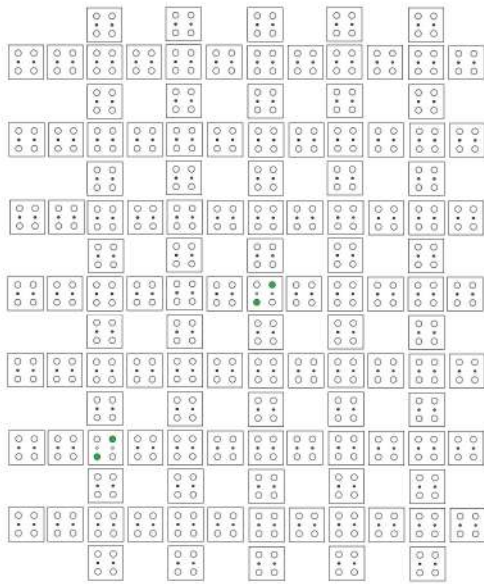


Figure 5.134: FULL ADDER simulation step 69

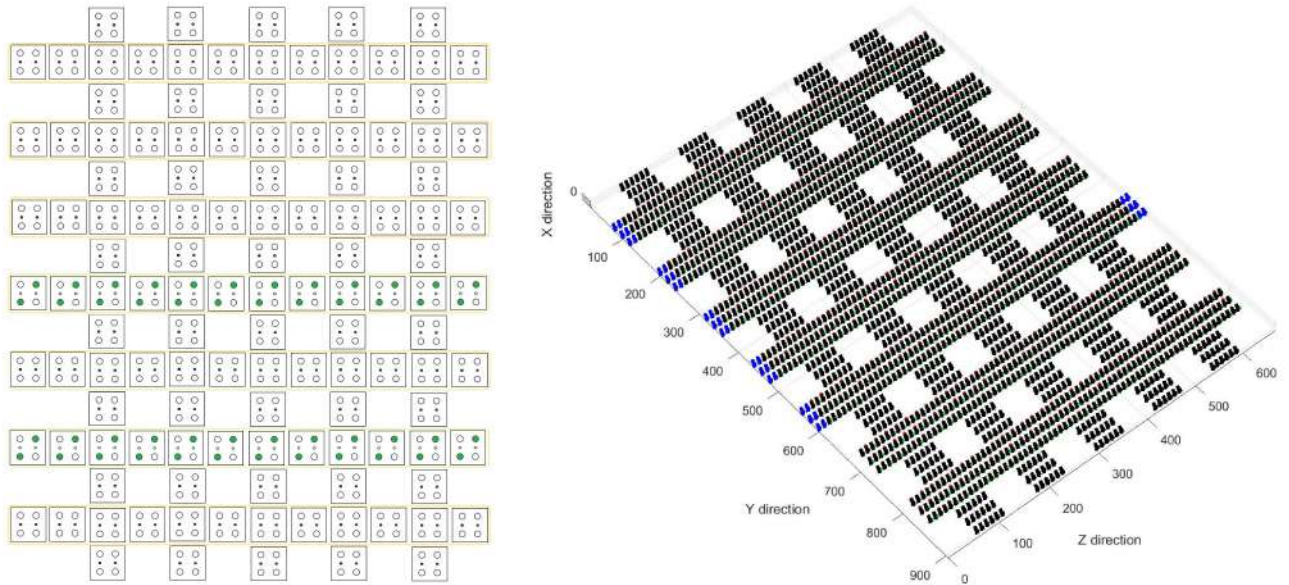


Figure 5.135: FULL ADDER simulation step 70

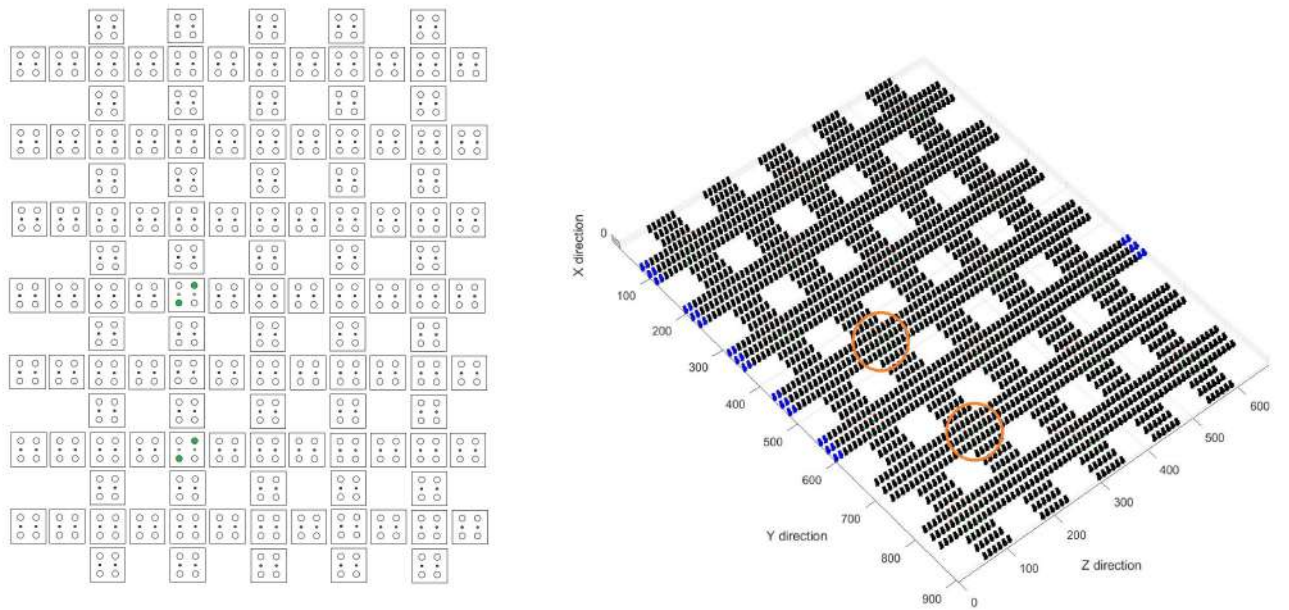


Figure 5.136: FULL ADDER simulation step 71

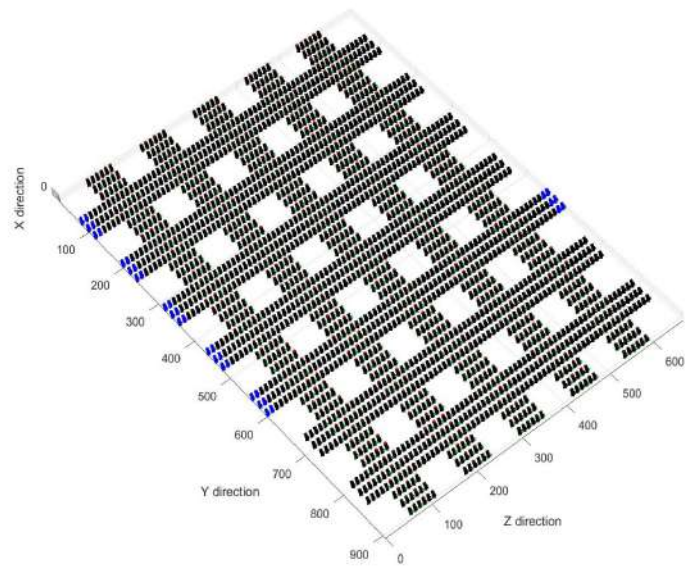
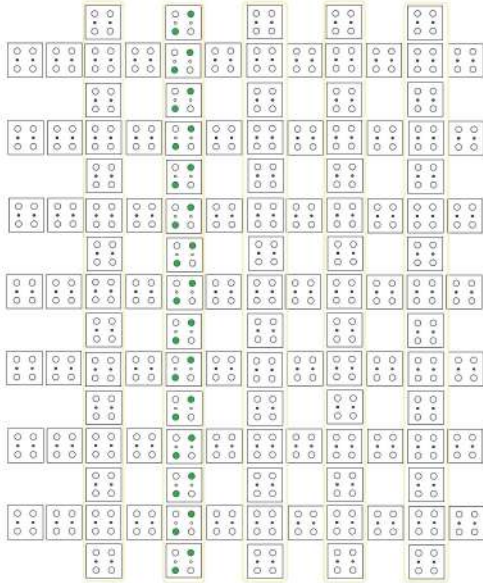


Figure 5.137: FULL ADDER simulation step 72

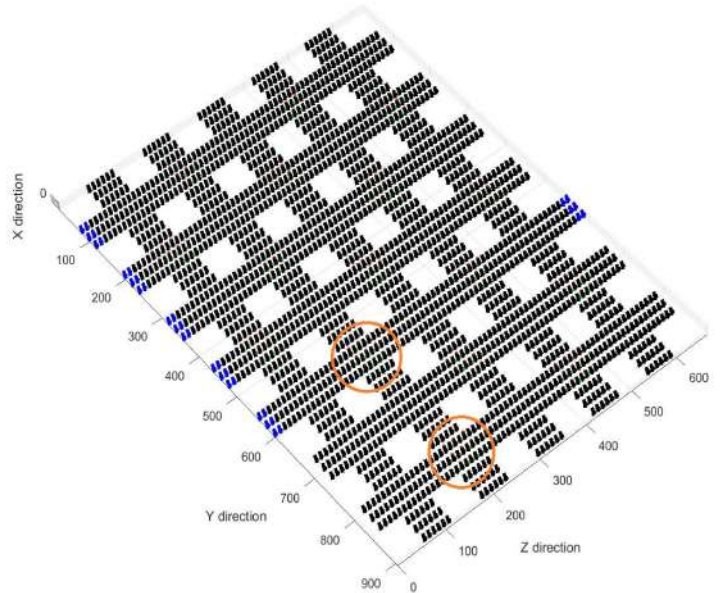
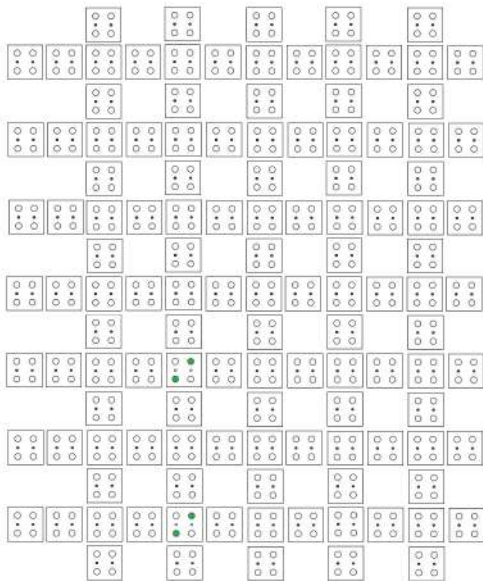


Figure 5.138: FULL ADDER simulation step 73

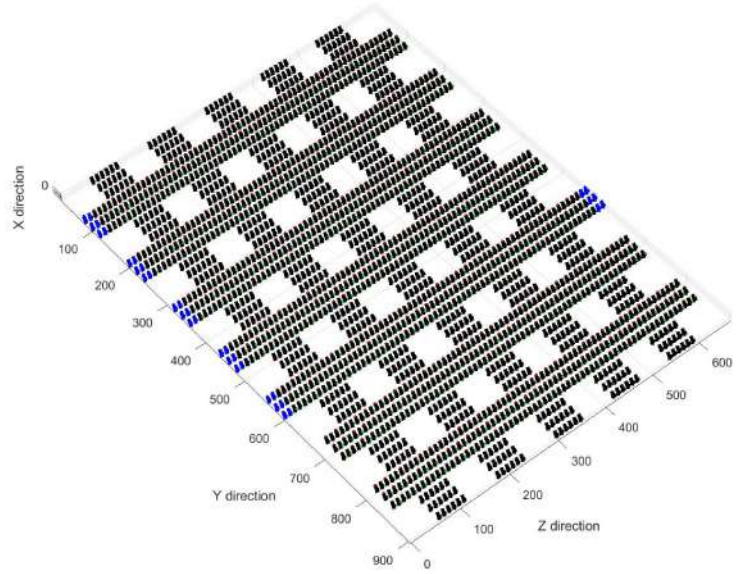
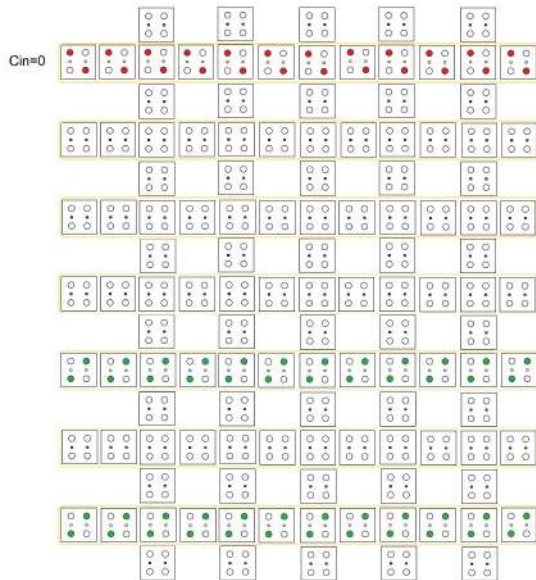


Figure 5.139: FULL ADDER simulation step 74

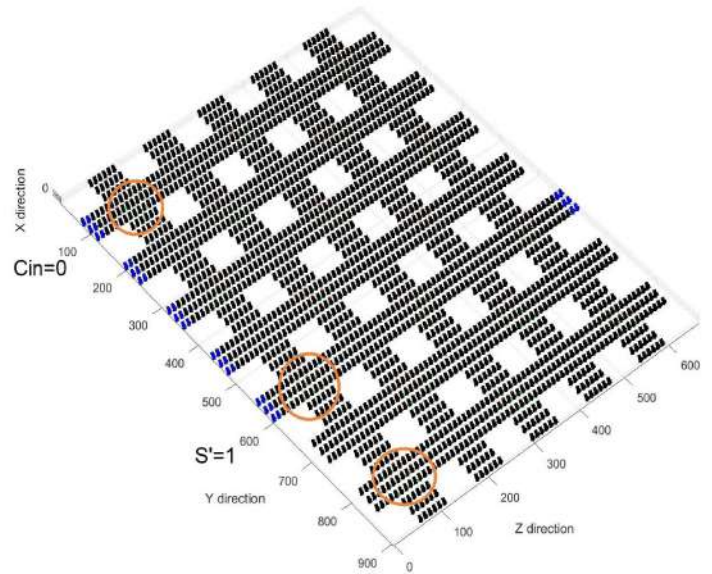
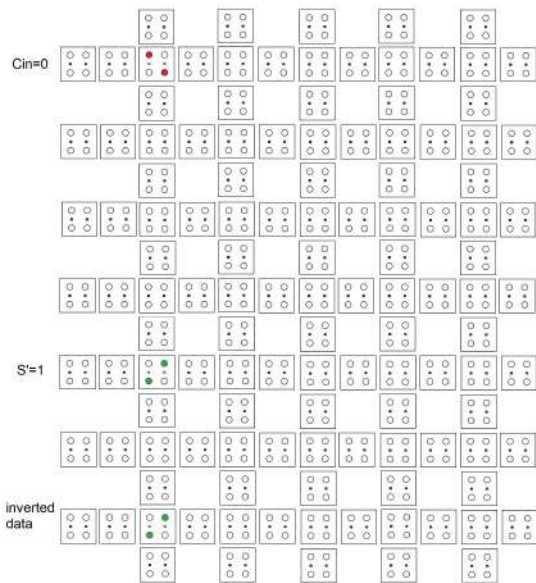


Figure 5.140: FULL ADDER simulation step 75

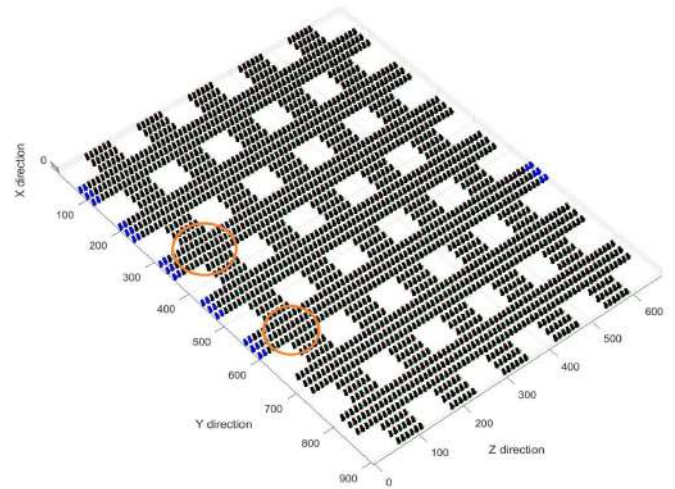
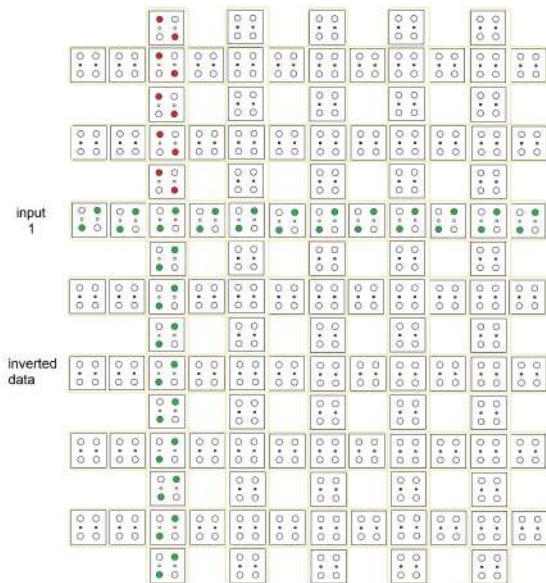


Figure 5.141: FULL ADDER simulation step 76

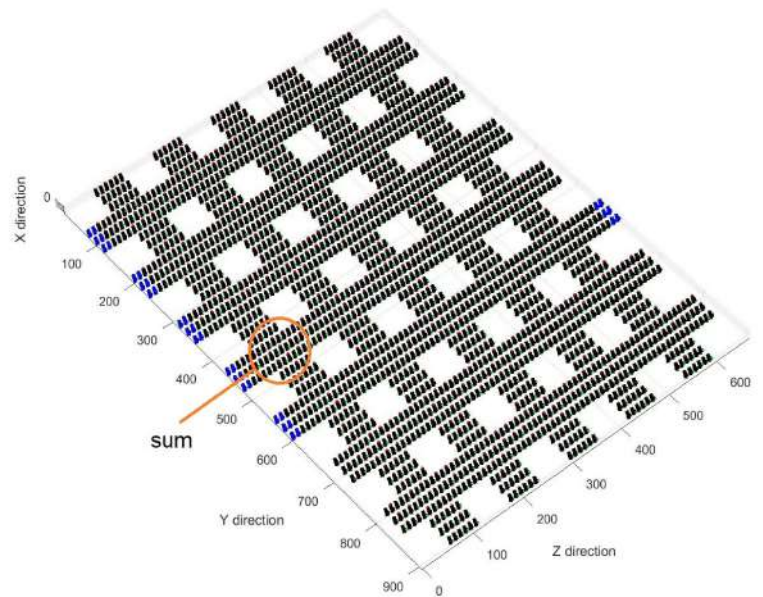
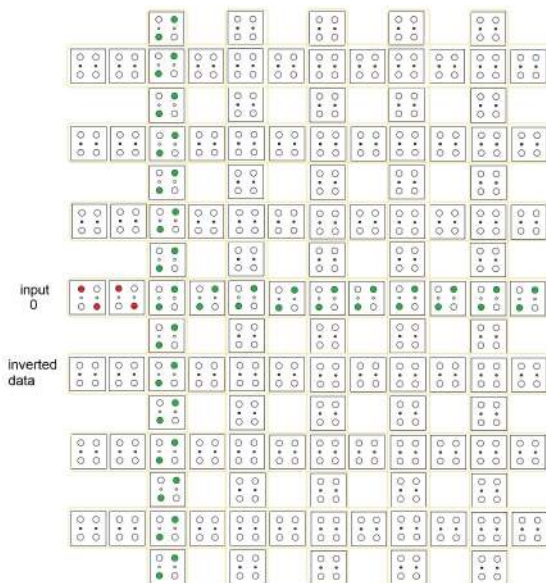


Figure 5.142: FULL ADDER simulation step 77

## 5.7 Summary

With the implementation of the previous simulations, the functionality of the realized structure was verified, even in the case of more complex operations such as half adder and full adder. Furthermore, comparing the standard NAND RFCN and the studied RFCN managed by interference, optimization in terms of area and clock have been observed.

### 5.7.1 Area

As shown in figure 5.143, the NAND logic operation is realized by standard RFCN with the implementation of 6 standard cells that gives a total Area of  $2000 \text{ nm}^2$ , as seen in equation 2.8 and here reported:

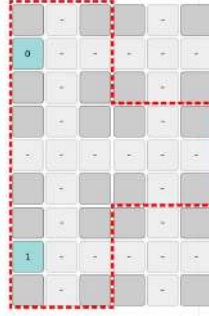


Figure 5.143: NAND RFCN: 6 standard cells, each made by 9 blocks

$$A_{stdNAND} = M \cdot A_{cell} = M \cdot \frac{9}{2} N^2 \cdot A_{base} \cong 2000 \text{ nm}^2 \quad (5.1)$$

On the other hand, with the implementation of the interference, the total area to perform the NAND operation turns out to be considerably smaller. Supposing to divide the NAND structure in blocks of the same dimension of the blocks defined in standard RFCN:

$$L_x \cong N \cdot d_x = 6 \text{ nm} \quad (5.2)$$

$$L_y \cong \frac{N}{2} \cdot d_y = 6 \text{ nm} \quad (5.3)$$

$$A_{block} = L_x \cdot L_y = \frac{N^2}{2} \cdot d_x \cdot d_y = 36 \text{ nm}^2 \quad (5.4)$$

The area needed to the realization of the NAND:

$$A_{NAND} = 13 \cdot A_{block} \cong 469 \text{ nm}^2 \quad (5.5)$$

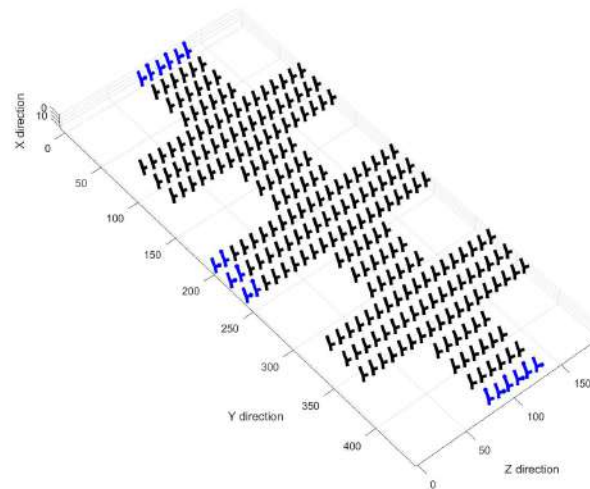


Figure 5.144: NAND layout in reset state. In evidence the block's dimension

It is observed a reduction of the 24% of the area.

### 5.7.2 Clock

Through the implementation of the interference, it is possible to have optimizations also in terms of clock. In fact, the time steps to carry out logic operations are less than the implementation of the standard RFCN. An example is the majority voter: in standar RFCN, the steps needed to obtain the output are 5, as shown in Figure 5.145; while with interference RFCN configuration, 2 steps are enough to obtain the result.

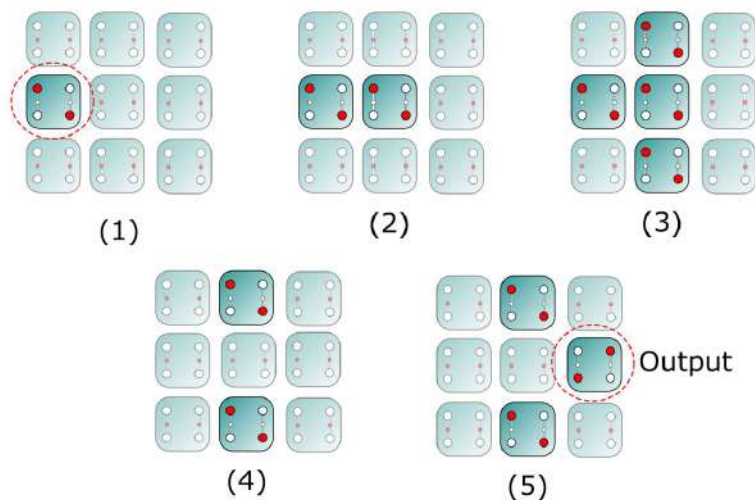


Figure 5.145: Majority Voter standard RFCN propagation steps [20]

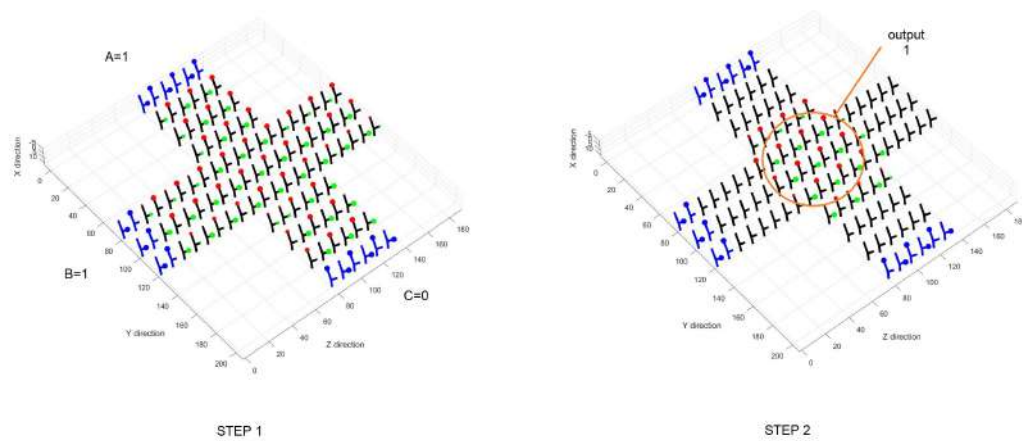


Figure 5.146: Majority Voter with interference propagation steps

The same happens in NAND logic operation: comparing with the standard RFCN (chapter 2, figures 2.17 to 2.22), a reduction of the steps needed for the realization of the operation is observed. The standard RFCN requires 12 clock's steps to realize the NAND operation, while through the implementation of interference, the steps necessary to obtain a correct result decrease to 7. This decreasing of time steps allows for a simpler and faster clock system: there are fewer micro-operations that have to be managed, respect the standard RFCN.

## Chapter 6

# Conclusions

The Reconfigurable Field-Coupled Nanocomputing is a new method of computation that seems to be promising for the future: its characteristic of being reconfigurable in terms of logic and datapath allows its possible application in the realization of new architectures.

The idea of using light interference was born with the needing for a way to improve the ease of manufacturing of the RFCN: the high number of independent and nanometric electrodes make it difficult the managing the clock configuration and the physical implementation.

The realization of the electromagnetic fields through the interference effect of coherent sources, allows the molecules to propagate information and realize logic operations, with a reduction of clock complexity with respect to the standard RFCN configuration. Moreover, as seen in the comparison of NAND logic operation, the interference implementation allows also a reduction of the operation area of about 24%.

On the other hand, the needing for electrodes continues to be inevitable: the propagation of data is managed by interference pattern, but to hold data in a specific zone of the layer, still the necessity of electrodes integration. Differently from standard RFCN, the electrodes are not all independent, so more easy to be managed.

In addition, the technologies necessary for the realization of this configuration are very advanced and expensive, which limit the possibility of the physical implementation of the structure.

Future studies on RFCN with interference could investigate the possibility of managing the operating frequencies, currently very high (in the order of  $10^{18}Hz$ ) or the deeper investigation in the electrodes: for example finding new methods for powering them, in order to remove the dependence on CMOS drivers and consequently reduce the energy consumption, or the total elimination of the electrodes using the interference for the all managing of the structure.

# Bibliography

- [1] C. S. Lent, P. D. Tougaw, W. Porod, and G. H. Bernstein, “Quantum cellular automata,” *Nanotechnology*,jan 1993.
- [2] Y. Lu and C. S. Lent, “Theoretical study of molecular quantum-dot cellular automata”, *Journal of Computational Electronics*, vol. 4.
- [3] C. S. Lent, M. Liu, and Y. Lu, “Bennett clocking of quantum-dot cellular automata and the limits to binary logic scaling”, *Nanotechnology*, vol. 17, Aug. 2006.
- [4] R.Jayalakshmi and R.Amutha. “A Theoretical Study on the Implementation of Quantum Dot Cellular Automata”. In: 4th International Conference on Advances in Electrical, Electronics, Information, Communication and BioInformatics (AEEICB-18)). Tamil Nadu, India, 2018.
- [5] Massimo Macucci. *Quantum Cellular Automata: Theory, Experimentation and Prospects*. Covent Garden, London: Imperial College Press, 2006.
- [6] Bernstein Gary H. Alexandra Imre V. Metlushko A. Orlov L. Zhou L. Ji György Csaba and Wolfgang Porod. “Magnetic QCA systems.” In: *Microelectronics Journal* vol. 36.no. 7 (2005).
- [7] Vacca, M.; Graziano, M.; Zamboni, M. *Nanomagnetic Logic Microprocessor: Hierarchical Power Model*. *IEEE Trans. VLSI Syst.*, 2012.
- [8] P. Douglas Tougaw and Craig S. Lent, ”Logical devices implemented using quantum cellular automata”, *Journal of Applied Physics*, 1994.
- [9] S. Srivastava, S. Sarkar, and S. Bhanja, “Estimation of upper bound of power dissipation in qca circuits”, *IEEE Transactions on Nanotechnology*, vol. 8, no. 1, Jan. 2009.
- [10] B. Hoeneisen and C. Mead, “Fundamental limitations in microelectronics—i. mos technology”, *Solid-State Electronics*, vol. 15, Jul. 1972.
- [11] Y. Ardesi, A. Pulimeno, M. Graziano, F. Riente, and G. Piccinini, “Effectiveness of molecules

---

for quantum cellular automata as computing devices”, *Journal of Low Power Electronics and Applications*, vol. 8, no. 24, Jul. 2018.

[12] Y. Ardesi, R. Wang, G. Turvani, G. Piccinini, and M. Graziano, “Scerpa: A selfconsistent algorithm for the evaluation of the information propagation in molecular field-coupled nanocomputing”, *IEEE Transactions on Computer-Aided Design of Integrated Circuits and Systems*, Dec. 2019.

[13] Zoli, L. *Active Bis-Ferrocene Molecules as Unit for Molecular Computation*. Ph.D. Thesis, Università di Bologna, Bologna, Italy, 2010.

[14] Lent, C.S.; Isaksen, B.; Lieberman, M. *Molecular quantum-dot cellular automata*. *J.Am. Chem. Soc.* 2003.

[15] A. Pulimeno, M. Graziano, D. Demarchi, and G. Piccinini, “Towards a molecular qca wire: Simulation of write-in and read-out systems”, *Solid-State Electronics*, Nov. 2012.

[16] Arima, V.; Iurlo, M.; Zoli, L.; Kumar, S.; Piacenza, M.; della Sala, F.; Martino, F.; Maruccio, G.; Rinaldi, R.; Paolucci, F.; et al. *Toward quantum-dot cellular automata units: Thiolated-carbazole linked bisferrocenes*. *Nanoscale* 2012.

[17] P.D. Tougaw C.S. Lent Bernstein and W. Porod. *Quantum cellular automata: the physics of computing with arrays of quantum dot molecules*. *PHYSCOMP 94 Proceedings*, 1994.

[18] G. Sanclemente, “Analysis and simulation of the sinusoidal clocking field in molecular fcn.” April 2019.

[19] R. Wang, A. Pulimeno, M. Ruo Roch, G. Turvani, G. Piccinini, and M. Graziano, “Effect of a clock system on bis-ferrocene molecular qca”, *IEEE Transactions on Nanotechnology*, Jul. 2016.

[20] E. P. Blair, “Quantum-dot cellular automata: A clocked architecture for highspeed, energy-efficient molecular computing”, in *Unconventional Computation and Natural Computation*, M. J. Patitz and M. Stannett, Eds., Cham: Springer International Publishing, 2017, isbn: 978-3-319-58187-3.

[21] Giuliana Beretta. *Study of Field-Coupled Nanocomputing based on molecules for neural systems*. Rel. Mariagrazia Graziano, Gianluca Piccinini, 2020

[22] C.Fabiano ”Reconfigurable standard-cell concept in Molecular Field-Coupled Nanocomputing”, 2020

[23] M.Born, E.Wolf, "Principles of Optics", 1999

[24] D.Morin "Interference and Diffraction", 2010

[25] Joseph Ivin Thomas. The Classical Double Slit Interference Experiment: A New Geometrical Approach. American Journal of Optics and Photonics. Vol. 7, No. 1, 2019, pp. 1-9. doi:10.11648/j.a.jop.20190701.11

[26] Jong Seob Choi, Hye Bin Park, Jonathan H. Tsui, Byungyou Hong, Deok-Ho Kim<sup>1</sup>, and Hyung Jin Kim, "Hybrid gold/DNA nanowire circuit with sub-10 nm nanostructure arrays"